# PLASMA INTERACTION WITH LOW – K SILSESQUIOXANE MATERIALS

Thesis submitted for the degree of

Doctor of Philosophy

by

**Jithin Francis Cherunilam, M.Eng. , B. Tech**.

School of Electronic Engineering

Dublin City University

Supervised by

**Dr. Stephen Daniels**

**Dr Andreas Heise**

June 2017

# DECLARATION

I hereby certify that this material, which I now submit for assessment on the programme of study leading to the award of Doctor of Philosophy is entirely my own work, and that I have exercised reasonable care to ensure that the work is original, and does not to the best of my knowledge breach any law of copyright, and has not been taken from the work of others save and to the extent that such work has been cited and acknowledged within the text of my work.

Signed:

ID No.: 57213011

Date: 08/06/2017

# ACKNOWLEDGEMENTS

# ABSTRACT

Low – κ dielectric materials play a very important role in the fabrication of integrated circuits (IC). Materials with a very low dielectric constant are necessary for use as inter layer dielectrics (ILDs), because they increase the efficiency of the ICs by reducing the resistance capacitance delays and power consumption of the circuits.

This thesis presents the deposition and characterisation of Silsesquioxane (SSQ) materials, particularly Methyl Silsesquioxane (MSQ) and Poly Phenyl Methyl Silsesquioxane (PMSQ) thin films by spin coating and subsequent annealing. The changes to the film post plasma exposure were studied using a wide range of characterisation techniques such as spectroscopic ellipsometry, stylus profilometry, FTIR, TGA, water contact angle measurement, XPS, AFM, SEM, EDX, AFM, dielectric constant measurement of the thin films, etc.

The study on MSQ films were carried out to have a better understanding of film deposition, processing, and characterisation techniques as these studies are widely reported in literature because of its use as an ILD material. The deposited MSQ thin films had a κ - value of ~ $2.6 \pm 0.1$. Significant increase in the κ - value was observed upon exposure of these films to $SF_6$ and $O_2$ plasmas due to the deteriorating effect of the plasma on the films. Deposited PMSQ thin films had a κ - value of ~ $2.7 \pm 0.1$ and they did not show any considerable variation in their κ - value upon exposure to $SF_6$ and $O_2$ plasmas, even though significant erosion of the PMSQ film was observed during the exposure of the film to $SF_6$ plasma.

Modern day electronics require materials with very low dielectric constants for optimal performance. Several approaches are used commercially to further reduce the κ – value of dielectric materials used for ILD applications. Porosity was introduced into the

PMSQ thin films by sacrificial porogen technique to further reduce the dielectric constant of the thin films using Heptakis (2,3,6-tri-O-methyl)-β-cyclodextrin (tCD) as the porogen material. Changes in the PMSQ films due to the introduction of porosity were studied which showed a reduction in the density and the $\kappa$ – value of the film. A reduction of ~ 25% in density was observed in the XRR measurements of the porous films and the $\kappa$ – value of the films were reduced by ~ 20% from $\kappa = 2.7 \pm 0.1$ to $\kappa = 2.2 \pm 0.1$ by the introduction of porosity. The effect of plasma exposure on the porous PMSQ films resulted in an increase in the dielectric constant of the porous material.

The thesis also analyses the expected variations in the film density and $\kappa$-value and compares it with the observed density and $\kappa$-value. It also calculates a rough estimate of the change in the surface area of the film as a result of porosity integration. Experimental demonstrations of a novel method to pattern the dielectric film surface namely Nano sphere Lithography is presented in the final section of this thesis.

# TABLE OF CONTENTS

xiii

# LIST OF FIGURES

for 1,2, 4, 6 &10 minutes). For thickness measurements see appendix 3.24.

seconds). For thickness measurements, capacitance measurements and 'k' – value calculations see appendix 4.22 & 4.23.

# LIST OF TABLES

# LIST OF ABBREVIATIONS

| | |
|---|---|
| **A** | Area of plates in a parallel plate capacitor |
| **AFM** | Atomic force microscopy |
| **BEOL** | Back-end-of-line |
| **C** | Capacitance |
| **CMP** | Chemical mechanical planarization |
| **CVD** | Chemical vapour deposition |
| **DLC** | Diamond – like carbon |
| **EDX** | Energy dispersive X - ray spectroscopy |
| **FDLC** | Fluorinated diamond-like carbon |
| **FO*x*®** | Flowable oxide |
| **FO*x*-1*x*®** | Flowable oxide |
| **FSG** | Flurosilicate glass |
| **FTIR** | Fourier transform infrared spectroscopy |
| **HOSP** | Hybrid organic siloxane polymer |
| **HSQ** | hydrogen silsesquioxane |
| **IC** | Integrated circuit |
| **ILDs** | Interlayer dielectrics |
| **MIBK** | Methyl isobutyl ketone |
| **MSQ** | Methyl silsesquioxane |
| **NSL** | Nanosphere lithography |
| **O2** | Oxygen (feed gas) |
| **PECVD** | Plasma enhanced chemical vapour deposition |
| **PhSSQ** | Phenyl silsesquioxane |

| | |
|---|---|
| **PMSQ** | Phenyl – Methyl silsesquioxane |
| **PTFE** | Polytetrafluoroethylene |
| **RC** | Resistance capacitance |
| **SCCM** | Standard cubic centimeter per minute (gas flow rate) |
| **SEM** | Scanning electron microscopy |
| **SF6** | Sulfur hexafluoride (feed gas) |
| **SiCOH** | silicon, carbon, oxygen and hydrogen |
| **SiO2** | Silicon dioxide |
| **SSQ** | silsesquioxane |
| **T** | Thickness of the insulator between the plates |
| **tCD** | Cyclodextrin - Heptakis(2,3,6-tri-O-methyl)-β-cyclodextrin |
| **TCE** | Trichloroethylene |
| **TGA** | Thermogravimetric analysis |
| **THF** | Tetrahydrofuran |
| **ULK** | ultra-low-k |
| **XLK** | Spin on dielectric from Dow Corning / Porous form of FO$x$ |
| **XPS** | X-ray photoelectron spectroscopy |
| **XRR** | X-ray reflectivity |
| **$\varepsilon_o$** | the permittivity of free space |
| **$\varepsilon_r$** | dielectric constant of the material |
| **$\kappa$** | dielectric constant |

**PUBLICATIONS**

1.  Investigation of $O_2$ and $SF_6$ plasma interactions on thermally stable damage resistant poly phenyl-methyl silsesquioxane low-k films.

   **Cherunilam, J.F.** et al. J. Phys. D. Appl. Phys. 47 (2014) 105204 (5pp)

2.  Interaction of $SF_6$ and $O_2$ plasma with porous poly phenyl methyl Silsesquioxane low – k films

   **Cherunilam, J.F.** et al. J. Phys. D. Appl. Phys. 48 (2015) 125201 (9pp)

**POSTERS PRESENTED**

1.  Deposition and characterisation of thermally stable porous poly phenyl methyl silsesquioxane low-k thin films,

   Intel Ireland Research Conference, Dublin 2014

2.  Development and investigation of ultra low-k PMSQ-tCD hybrid films and thermally stable, damage resistant PMSQ low-k films

   Plasma Nanoscience Conference, Ireland 2014

3.  Investigation of $O_2$ and $SF_6$ plasma interactions on thermally stable damage resistant poly phenyl methyl silsesquioxane low-k films and reduction in k value by addition of porosity.

   Intel Ireland Research Conference, Dublin 2013

4.  Deposition of Low - k dielectric films and patterning by Nanosphere Lithography, RINCE day 2013 .

   School of Electronic Engineering, Dublin City University

# CHAPTER 1
# INTRODUCTION

The last two decades has witnessed the unprecedented growth of Information and communication technologies creating a never-ending demand for high performance systems that require electronic hardware with superior computational capabilities. The integrated circuit (IC) chips that perform these computations are the key components of most high-end hardware. The performance of these chips is increased by improving the computing speed of these devices, reducing the power consumption and reducing the time delays associated with the operation of the ICs. The use of materials with very low dielectric constant as inter layer dielectrics (ILDs) play a critical role in improving device performance by reducing the power consumption and the associated time delays of the ICs. Implementation of organic materials with low dielectric constant as ILDs presents a wide variety of integration challenges in IC manufacturing. Plasma processing is widely used in semiconductor device fabrication for cleaning, surface treatment, deposition, etching etc. The damage induced in these materials during plasma processing, primarily in etching of the material and photoresist ashing, are major bottlenecks for the use of these materials as ILDs. Hence materials with the least variation in their dielectric properties during plasma processing are of great importance.

The following section of the thesis gives a brief history about the advent of ICs and the emergence of various processes and process changes brought forward in device manufacturing to improve device efficiency.

# 1.1. HISTORICAL OVERVIEW

The invention of the transistor by Bell laboratories [1] was a milestone in the history of electronics. Even though the initial interest was on germanium transistors [2], the focus soon shifted to silicon transistors when it was announced by Texas Instruments in 1954 [3] as it was easy to grow a silicon crystal which was to be used as the bulk material to fabricate these devices. The ease to grow stable native oxides on silicon was an added advantage. As years passed transistors became available in packaged forms, very different from their initial bulky prototypes and were good enough to be soldered onto circuit boards paving the way for the electronic revolution. But even then, there were lots of performance issues associated with these circuits. A bad solder or connection could render the whole circuit useless. Also as the system became more complex, the end product became more bulky and expensive and consumed huge quantities of power for their operation. The realisation of Integrated Circuits by Texas instruments came as a solution to the above-mentioned problems [4,5].

The ICs today are comprised of billions of transistors and thousands of meters of interconnect wiring in many levels. In an IC, chiefly in microprocessors, the number of devices on the chip has increased exponentially over the years. This is in agreement with the famous words of Intel Cofounder Gordon Moore which is known as Moore's Law. Moore suggested the number of components on an IC will increase by a factor of two every year [6]. This came to be the rule of thumb for the industry leader to set the pace for the industry itself.

The quest to increase device performance has led to miniaturisation of components within the IC and thereby leading to increased packaging densities. The advances that happened in tooling, process integration, lithography & photoresists and a whole range of other factors enabled the scaling down of component size. This increased the

operational speeds of transistors. ICs today have become more complex and faster than ever before. Even though the industry has succeeded in bringing out transistors that are smaller and faster, one of the limiting factors in increasing the computing speed of these advanced chips is the time delays associated with their operation.

There are two main factors that govern the speed of an electrical signal within an IC [7]. They are switching delays and interconnect delays. Switching delay is the time taken by an individual transistor to go from a non-conducting state to a conducting state when a voltage is applied at the gate of the transistor, also known as the gate delay of the transistor. Signal propagation delay is the time taken by a signal generated by one transistor to reach another through a conducting medium such as an interconnecting wire. This is also known as interconnect delay.

It was possible to improve transistor performance by scaling down gate length, gate dielectric thickness and junction depth [8]. Transistors today are smaller and work much faster than their predecessors. As the transistors became faster, signal propagation delays became the dominant factor dictating the performance of an IC. With the increase in complexity of interconnect wiring, crosstalk noise and power dissipation of the interconnect structures became key performance limiting factors.

# 1.2. INTERCONNECTS AND INTERCONNECT DELAYS

Interconnects are the network of conducting lines within an IC that is used to connect individual devices. They can be considered as the lifeline of the circuit. Their role is to carry power & ground to the various components and to carry signals between the components within the IC and also to the outside of the package. This is also referred to as the back-end-of-line [8] (BEOL) portion of the IC.

One of the best ways to characterise interconnect delays is to express them in terms of resistance - capacitance (RC) delays. Interconnections within an electrical circuit can be represented as a network of resistors and capacitors. The conductors in the circuit will possess some amount of resistance, which is a characteristic of the material from which they are made.

'RC delay' is dependent on two key factors. They are the size of the interconnect wiring and the placement of interconnects within the circuit. The reduced size of interconnecting wires inherently increases the resistance of interconnections. When the wires are placed close to each other, it increases the capacitance between the wires, which ultimately slows down the transmitted signal. The RC delay is roughly dependent on

$$RC = 2\rho\kappa\left(\frac{4L^2}{P^2} + \frac{L^2}{T^2}\right)$$
**Equation 1.1** [9]

Where $\rho$ is the metal resistivity, $\kappa$ is the dielectric constant of the insulator between the lines, L the line length, T the metal thickness and P the metal pitch.

The key factors that increase the RC delay can be easily identified from the equation 1.1. It is evident that replacing the interconnecting metal with a metal of lower resistivity can significantly reduce the associated RC time delay. Another approach is to reduce the capacitance of the interconnect material by reducing the parasitic capacitance.

Reduction in the parasitic capacitance helps to reduce power consumption of the circuit since the power consumption is directly proportional to capacitance as seen in equation 1.2.

$$Power = CV^2 f$$

We know that the energy stored in a parallel plate capacitor is $\frac{1}{2}CV^2 f$. Some energy is spent for charging the capacitor. The dissipated energy during the charging process is again is $\frac{1}{2}CV^2 f$. Whenever we use a capacitor, the stored energy is used for something productive. In the case of parasitic capacitance, as the name indicates, both the energy stored and the energy spent to create the charge is a waste. Hence the total energy wasted in this process can be quantified as $CV^2 f$.

# 1.3. METHODS TO REDUCE RC DELAYS

RC delays in ICs can be considerably reduced by change in the nature of materials used in the manufacturing of these circuit components. Resistance can be substantially reduced by using metals of lower resistivity as interconnects. The capacitance can be reduced by using materials with lower dielectric constants.

## 1.3.1. INTERCONNECTS WITH REDUCED RESISTANCE

Aluminium [10] was the metal widely used for interconnects in IC manufacturing because of the ease with which it could be etched during processing. As device dimensions shrunk the dimensions of interconnect wiring also went down proportionally. This led to significant increase in the resistance of the interconnect wiring. Higher heat generation within the circuits became a key issue as improved cooling techniques had to be employed. The increase in power consumption was also a downside. This led the industry to adopt copper as the 'interconnect metal of choice' from the traditional

aluminium. IBM was the first to use copper in a product in 1997[11]. By this one change, significant improvement [12] could be made as Cu had 30% lower resistivity than Al. Hence it was possible to reduce the line resistance of interconnects and thereby the RC delay. Even though gold had better conductivity when compared to copper it was not a cost effective solution to address the issue of RC delays and hence copper became the de facto standard for interconnects in the industry.

## 1.3.2. REDUCTION IN PARASITIC CAPACITANCE OF INTERCONNECTS

Capacitor is an electronic component used for charge storage. A schematic of a parallel plate capacitor is shown in figure 1.1. In the figure we can see the conductive plates of the capacitor separated by an insulating medium. The insulating medium is known as dielectric, a term coined by an Anglican priest scientist and philosopher William Whewell as requested by Michael Faraday to explain the charging process of a capacitor. Dielectrics are insulating materials and they can be polarised by the application of electrical fields.
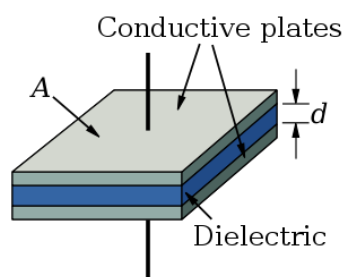


**Figure 1.1. Schematic of a parallel plate capacitor**

The ability of the device to store charge is termed as capacitance and is given by the equation 1.3.

$$C = \frac{\varepsilon_r \, \varepsilon_o \, A}{T}$$  **Equation 1.3**

Where C is the capacitance

T is the thickness of the insulator / between the plates

A is the area of the parallel plates

$\varepsilon_o$ is the permittivity of free space, 8.85 x 10E-12 F/m

and $\varepsilon_r$ is the dielectric constant of the material.

Dielectric constant is the ratio of the permittivity of a substance to the permittivity of free space and is a property of the material.

In the microelectronics context the dielectric constant $\varepsilon_r$ of the material is denoted by the lower case Greek alphabet $\kappa$. Even if the Greek letter '$\kappa$ - *kappa*' is used to denote the dielectric constant, it is pronounced as the letter 'k' of the English alphabet when we talk about this value in the microelectronics context.

Rearranging equation 1.3 we get the expression for dielectric constant $\kappa$.

$$\kappa = \frac{CT}{\varepsilon_o \, A}$$  **Equation 1.4**

From equation 1.4 we can see that there is a proportional relation between the capacitance and dielectric constant of the insulating material. Hence the capacitance can be reduced by reducing the dielectric constant of the insulating medium and vice versa.

Silicon dioxide ($SiO_2$) was the material that was used as dielectric for more than four decades with a dielectric constant of $\sim 4$ ($3.9 - 4.2$) [13,14]. Based on the $\kappa$-value of $SiO_2$ as reference, materials with a dielectric constant $> \kappa$-$SiO_2$ are referred to as high-$\kappa$ dielectric materials and are fundamentally used as gate insulators in MOSFETs [15].

Materials with $\kappa < \kappa$-$SiO_2$ are classified as low-$\kappa$ materials and are used as Inter – layer dielectrics (ILDs) in microelectronic fabrication. Materials with $\kappa < 2.2 – 2.4$ are considered as ultralow-$\kappa$ (ULK) materials [16].

Use of materials with lower $\kappa$-value significantly improves device performance [16 - 20]. Two main factors that affect the dielectric value of a material are its density and polarisability. To further reduce the $\kappa$-value lower than that of $SiO_2$, we have to explore materials with density lower than that of $SiO_2$ or materials in which the chemical bonds are of lower polarisability than that of $SiO_2$ or both.

## 1.4. METHODS TO REDUCE K VALUE OF MATERIALS

$\kappa$-value of materials can be reduced by many different techniques as seen in figure 1.2. The first approach is to reduce the polarisability of the dielectric material. This can be realised by the use of materials with chemical bonds that are less polar than Si – O
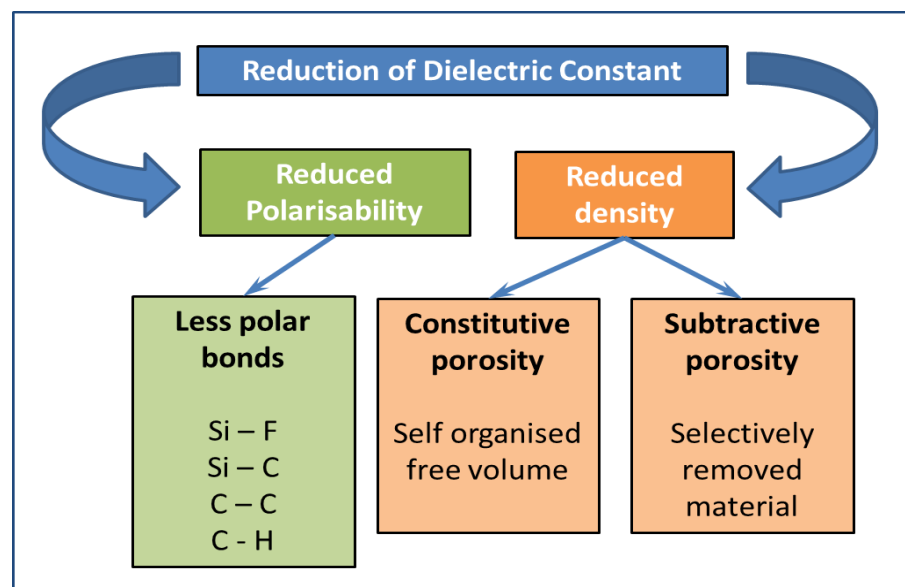


**Figure 1.2. Different approaches to reduce the dielectric constant of the material**

bonds by substituting the Si – O bonds with bonds like Si – F [21]. Another way is to use non polar bonds like C – C or C – H which are present in organic polymers [20].

The second approach is to reduce the density of the dielectric material and thereby bring down the dielectric constant of the bulk of the material. Materials with self-organised free volume [13,20] will have lower density, when compared to a similar material that is tightly packed in its naturally existing state. The free volume is usually a property of the material and is termed as constitutive porosity of the material.

Another method that is widely pursued is the introduction of porosity into an existing material by use of subtractive porogens. Porogens are thermally labile materials that decompose when heated. Porogens are introduced into the material during the deposition phase. The material together with the porogen forms a hybrid material which is deposited as the thin film. Once heated to the right temperature porogens vaporize creating pores within the material and thereby reducing their density. Hence they are also known as 'sacrificial porogens'. This technique is widely used to further reduce the κ value of materials that are identified as good candidates for ILD applications to the ULK range [22]. The reduction in κ-value the material is a result of the pores filled with air ($\kappa = 1$) [23], thereby reducing the κ-value of the bulk of the material.

# 1.5.  OVERVIEW OF THE EVOLUTION OF DIELECTRIC MATERIALS FOR INTER LAYER DIELECTRIC (ILD) APPLICATIONS

Silicon is the primary substrate material for IC manufacturing. A key property of silicon is its ability to grow good quality oxides. $SiO_2$ could be grown over silicon substrates by thermal oxidation. A variety of deposition techniques such as chemical

vapour deposition (CVD) and Plasma enhanced CVD (PECVD) are also available to deposit oxide layers that have good adherence [24].

Silicon dioxide [13] is a very dense material (2.2-2.3 $g/cm^3$) with exceptional thermal stability with decomposition temperature above 1500°C and a high breakdown voltage of 10 MV/cm. A very good network bonding imparts an elastic modulus between 72 and 74 Gpa and has a very low coefficient of thermal expansion of only 0.5 ppm/K. The fact that it could be processed and patterned by wet etching with buffered HF or dry etched by fluorine containing plasmas was highly advantageous. Hence $SiO_2$ (Glass), with a dielectric constant of 4.2, was the traditional dielectric insulator used by the industry because of its many advantages and compatibility with silicon substrate.

Introduction of copper into the manufacturing process addressed the problem associated with the RC delay to a great extent, but additional measures were required with the advancement of this technology node. It necessitated dielectric materials with lower dielectric constants to further reduce C values and hence the RC delay. The 180 nm technology node in the year 2000 saw the introduction of Fluorosilicate glass (FSG) to replace $SiO_2$ as dielectric material in high volume manufacturing. FSG is also known as fluorine doped oxide and has a κ-value of 3.8. Doping of glass with fluorine introduces Si – F bonds into the material [25]. Fluorine is highly electronegative with a value of 4.0 on the Pauli scale. Hence the electron pairs in the bond are held strongly by fluorine thereby reducing the polarisability of the bond. This lower polarisability of Si-F bonds when compared to that of Si –O bonds reduces the dielectric constant of the material. FSG with an even lower κ-value, κ=3.6, was used in the 130 nm technology node in the year 2002. The introduction of new materials as dielectrics by IBM over the years is shown in figure 1.3.[26].
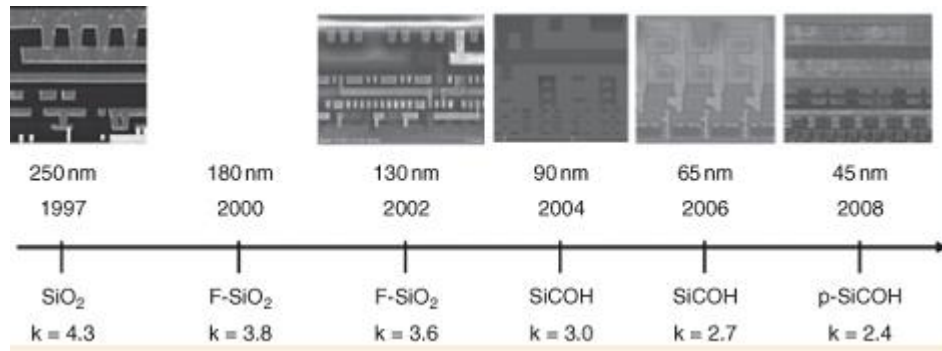
**Figure 1.3. Timeline showing the introduction of new materials as dielectrics [26]**

Continued efforts were made to find materials with lower κ-values to use as ILD in manufacturing. Many materials were investigated over the years by different research groups around the world. Materials that arouse interest include organic amorphous carbon materials like Diamond – like carbon (DLC) with k ~3.3. Attempts were made to further reduce the k value of this material by the incorporation of fluorine to create fluorinated diamond-like carbon (FDLC). But the fluorine in the material was found to have effects on tantalum/tantalum nitride used as adhesion linear between copper and BEOL insulator, leading to the formation of tantalum fluoride. This led to adhesion failure between copper and the BEOL insulator.

Films composed of silicon, carbon, oxygen and hydrogen (SiCOH[*]) deposited by PECVD was another class of materials that was studied. The integration of these materials into the interconnect structures was easy since they had similar chemical composition to that of $SiO_2$. SiCOH films with κ = 3.0 was used in the 90 nm technology node in the year 2004 and films with κ = 2.7 in the 65 nm technology node in 2006. These films have organic groups introduced into the $SiO_2$ based matrix to integrate free volume into the material and thereby decrease their dielectric constant.

---

[*] Does not represent the stoichiometry. Description only represents the elements present in the film.

11

Later technology nodes adopted porous SiCOH (p-SiCOH) films with $\kappa = 2.4$ in the 45 nm technology node in 2008 and also for the later 32 nm technology node [13].

PECVD is the technique most widely used for the deposition of dielectric layers. Spin coating is another viable technique that can be used for the deposition of dielectric materials. A wide variety of organic and inorganic materials are available, that can be made into a solution, which can be spin coated to obtain thin dielectric films. Polyimides, polybenzoxazoles, polyarylene ethers, polyarylenes etc., are some organic materials that can be applied by spin coating. Inorganic materials ideal for application by spin coating are generally classified as silicates and organosilicates. They are applied either in their original form or in the form of copolymers, derived from orthosilicate, silsesquioxane and siloxane based monomers. Extensive studies were conducted over the years on spin coatable materials for the development of a good material with low-$\kappa$ value. SiLK [27] is an example for a commercially available, organic polyarylene thermosetting polymer from Dow Chemical. Films of much lower $\kappa$ values can be attained with porous SiLK yet another formulation from Dow Chemical.  Aerogels and Xerogels are also materials studied for application as dielectric materials. Nanoglass K2.2-A10B [28] is a xerogel based material from Allied Signal which is commercially available.

# 1.6. INTEGRATION CHALLENGES

Although a wide range of materials are available today that can be considered to be used as a dielectric material, most of them fail to meet all the desired specifications for successful integration. Moreover the introduction of new materials has created new integration challenges, especially when integrating dielectrics into the manufacturing process. This is principally as the result of trying to adapt the processes perfected around the traditional $SiO_2$ to the new carbon containing low – k materials.

Inferior mechanical properties [29] are a major issue in integrating low-k materials into fabrication. The ideal material for low-k application will have to withstand the high amounts of mechanical forces acting on the material during chemical mechanical planarization (CMP). Degradation of mechanical integrity can also lead to lower adhesion, crack propagation through the film during high stress process and during packaging and lifetime testing. The need of the number of layers of dielectric material will increase as the number of metal layers on which the circuit is fabricated increases. Reliable performance of the material when integrated into a multilayer structure is also of key importance from a mechanical perspective.

The dielectric material heats up in a number of ways [30] when incorporated into a fabricated structure. The main sources of heating of the material are the resistive heating that happens when an electric current passes through a conductor. The substrate heats up because of the components fabricated on the substrate and the generated heat dissipates onto the dielectric layers. This heat generation within a circuit can have serious implications on its performance as heat will increase line resistance and reduce electron migration lifetimes. When high current flows through a conductor, the resulting stress leads to a mass transport mechanism within the metal by means of momentum transfer between lattice atoms and conduction electrons due to collisions [31]. This phenomenon

is termed as electromigration and can result in the breakdown of the conductor after extended periods of use. Device breakdown due to electromigration is factored in when estimating the lifetime of circuits in their design phase. But extended overheating can accelerate the electromigration process creating open circuits and render the IC useless before it reaches its life expectancy. Hence the dissipation of heat generated within the circuit is of prime importance.

When the κ- value of the dielectric material is reduced by the addition of porosity, it reduces the thermal conductivity of the material and thus makes the heat transport within the fabricated structure more challenging. Also the material has to withstand the high temperatures at which many of the fabrication steps take place. Absorption of processing agents into pores at one fabrication stage and desorption of the same at a later stage can lead to contamination to the process step itself. Diffusion of materials through pores is another issue. [32]

Another major challenge that the industry faces today is the damage and subsequent degradation of the dielectric materials during plasma processing [33]. Plasma induced damage during dielectric processing is a major objective of this study and will be addressed in more detail in the following sections.

# 1.7. PLASMA PROCESSING IN IC MANUFACTURING

Plasma processing has a major role in IC manufacturing [34]. One of the most important use of plasma is to deposit materials using PECVD and by sputtering. Other major areas of use are ion implantation and for growing of layers in manufacturing. Plasma treatments are used to promote adhesion between layers, surface cleaning and for pore sealing. Plasmas are used for etching and patterning surfaces and also for the removal of photoresists (ashing) after photolithography processes.

When aluminium was used for interconnects, initially the metal was deposited, etched in the required wiring pattern and the space in between was filled with dielectric. This was possible since aluminium had a key advantage over copper, as it was very easy to etch aluminium using plasmas since it gave gaseous by-products. It was not possible to etch copper in a similar fashion since the by-products were not volatile. But by the arrival of the dual damascene technique it was possible to create copper patterns in the desired way and hence copper could be used for interconnect wiring within the IC. In the dual damascene technique [35], the dielectric is deposited first. This is followed by the creation of the required vias and trenches by plasma etching, through which connections are made. These vias are then filled with copper creating the required contacts and then planarised using CMP. The transfer to copper led to a drastic change in the integration sequence from dielectric filling after metal patterning, to metal filling after dielectric patterning as seen in figure 1.4.

The major challenge involved in the plasma processing of organic low-k polymers is to minimise the damage caused by the interaction of the material with plasmas [36 - 38]. Plasma interaction will modify the low-k material surface and alter their key properties.

15

This can lead to defect formation, charge accumulation followed by physical and chemical changes thereby creating extensive damage to the film.
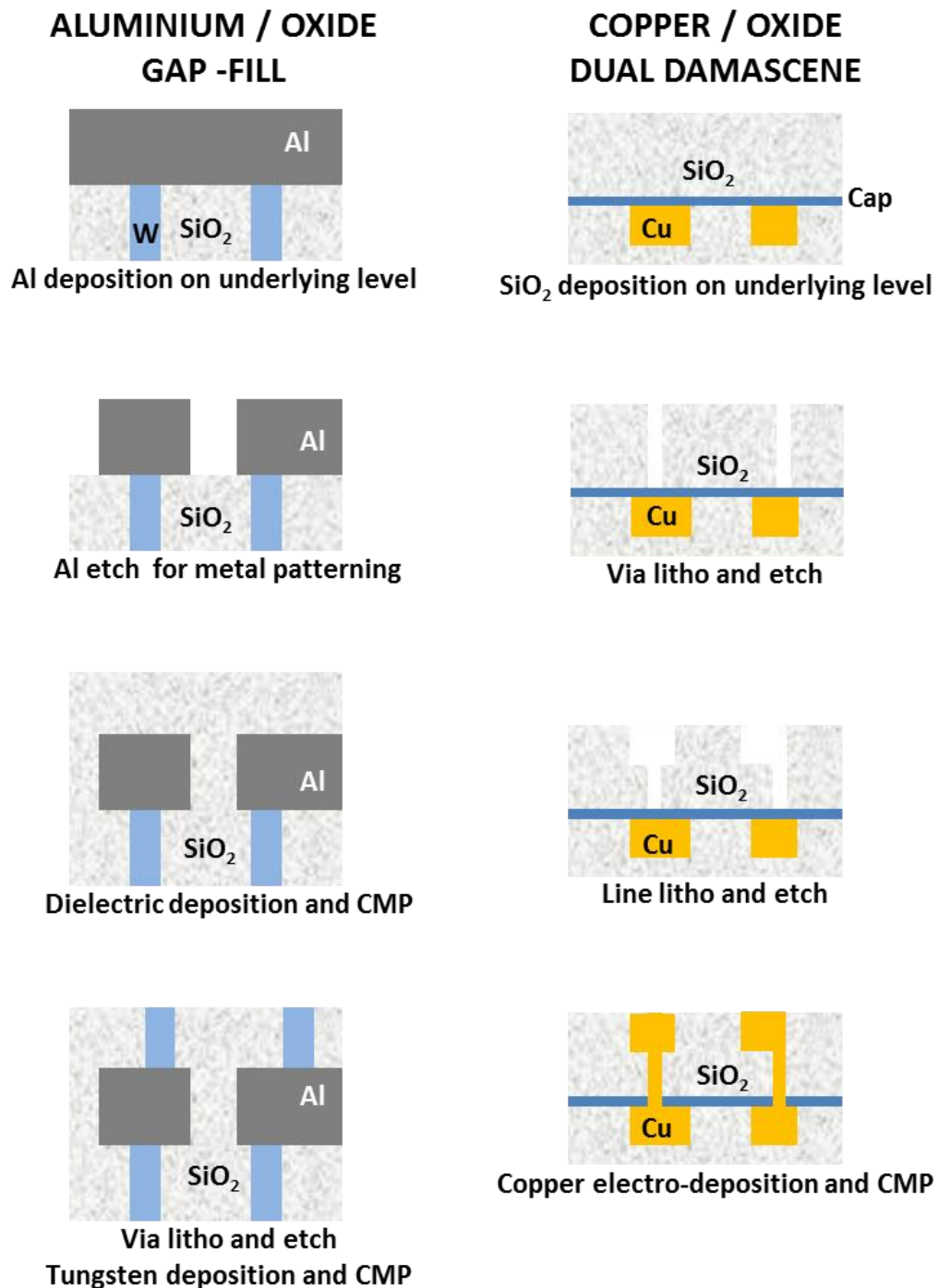


**Figure 1.4. Simplified schematic representation of aluminium / oxide gap – fill approach and the copper / oxide dual damascene process.**

# 1.8.  SILSESQUIOXANES

Compounds with empirical formula RSiO are called Siloxanes [39,40]. They contain silicon, oxygen and 'R' can either be hydrogen atom or a hydrocarbon. The name Siloxane is coined with letters from these three constituting components namely Silicon (**Sil**), Oxygen (**ox**) and Alkane (**ane**). Polymer materials with siloxanes as their monomers are usually called polysiloxanes. 'Sesqui' is a term that denotes the stoichiometry 1 to 1.5. Hence polysilsequioxane (SSQs) are materials with empirical formula $RSiO_{1.5}$ where Silicon and oxygen are in the ratio 1:1.5. SSQs find widespread applications in chemical catalysis, antimicrobial coatings. In microelectronics they are used as ILDs, as resist for e – beam lithography, as capping layer in device fabrication etc.

SSQs can exist in a variety of structures such as closed cages, partially open cages, ladder chains or as random network structures. A good knowledge of the structure in which the material exists is very important to understand the properties of the material. Some of the common structures are random, ladder, cage and partial cage structures as seen in figure 1.5 [39].

When the substituent R is a methyl group the SSQ is known as Methyl Silsesquioxane (MSQ) [41] and if the substituent R is a phenolic group then it is a Phenyl Silsesquioxane (PhSSQ) [42,43]. Hydrogen silsesquioxane (HSQ) [44] is another member of the family with hydrogen as the substituent group.

HSQ [$(HSiO_{1.5})_n$] is extensively studied for application in microelectronic manufacturing. HSQ is used as ILD in microelectronic applications [45]. It is also a widely used resist for e-beam lithography [46,47] . FO$x$® - Flowable oxide is a commercial product available from Dow Corning. FO$x$-1$x$® is a HSQ solution in methyl – isobutyl ketone (MIBK) which is used for spin coating applications. XLK [48] is another HSQ based spin coatable dielectric material from the same company. MSQ

[($CH_3SiO_{1.5})_n$] is also widely studied because of its dielectric properties for ILD applications.

Phenyl – Methyl silsesquioxane (PMSQ) is yet another SSQ material and was used as barrier layers in copper chloride based device fabrication [49,50]. It has the empirical formula [($C_6H_5SiO_{1.5})_m$ ($CH_3SiO_{1.5})_n$] and the particular material used in these experiments is of the ratio 90% Phenyl – 10 % Methyl in composition.



(a) Random structure

(b) Ladder structure

(c) (T$_8$)   (d) (T$_{10}$)   (e) (T$_{12}$)

Cage structures

(f) Partial cage structure
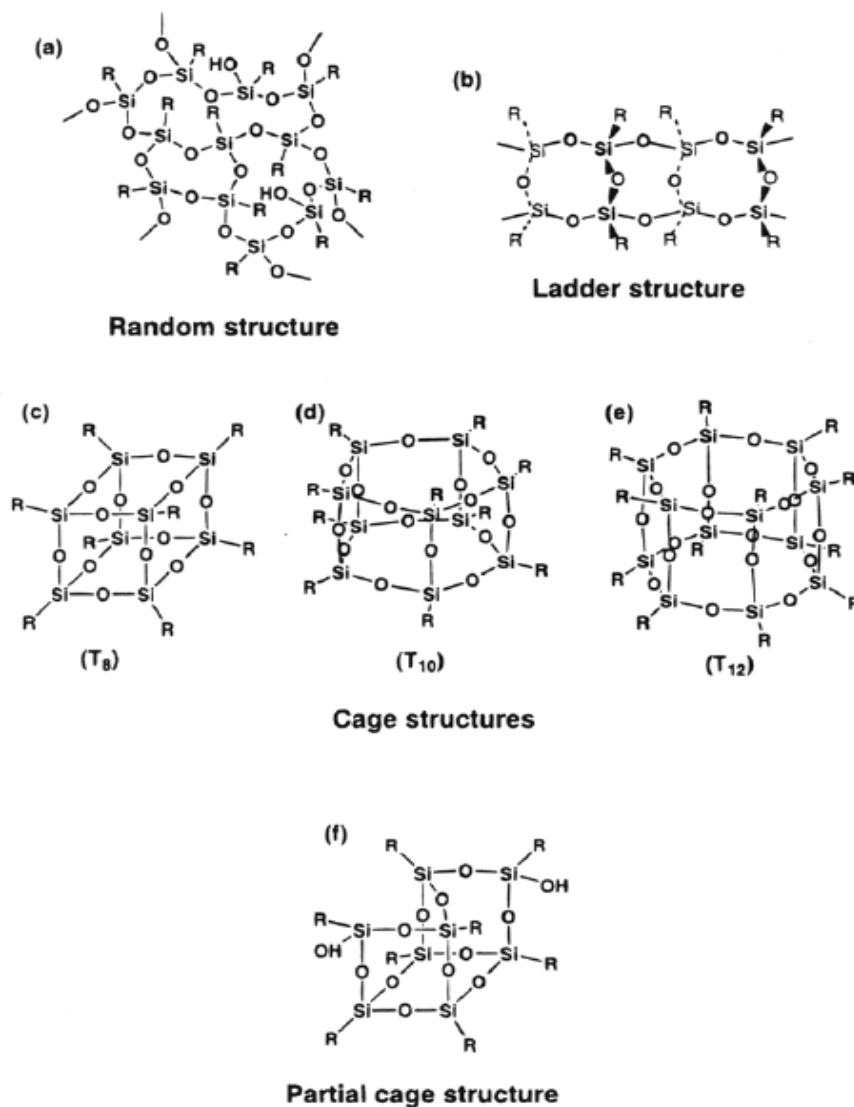
**Figure 1.5. Structures of Silsesquioxanes [39]**

# 1.9. PLASMA DAMAGE STUDIES ON SSQ AND SIMILAR MATERIALS.

Plasma exposure creates significant modification on dielectric materials Considerable variations in the κ- values of materials with chemical composition similar to SSQ materials Hybrid organic siloxane polymers (HOSP) have shown variation in its κ – value from ~ 2.6 to ~6.0 in studies by Chang et al when the material was subjected to oxygen plasma treatment [51]. κ variation from 2.9 to 3.2 was noticed for SiCOH films during oxygen plasma treatment as reported by Yonekura et al [52].

Considerable variation in the κ values of SSQ materials such as HSQ and MSQ has been reported as a result of oxygen plasma ashing experiments [52 - 54]. Chang et al reported a variation in κ-value from ~ 2.6 to ~6.0 for MSQ films [55] as a result of oxygen plasma exposure.

The dielectric properties of the material change due to a wide variety of reasons post plasma treatment. The main reason reported is the moisture absorption that takes place into the material post plasma treatment, which significantly increases the κ-value of the material. Further the damage to the chemical structure of the material resulting from plasma exposure increases the dielectric constant of the material.

# 1.10. OBJECTIVES OF THIS THESIS

With this brief introduction we were able to understand the need for low-κ materials as ILDs, the need for plasma processing and the resulting degradation of the low-κ material during processing. To conduct a study on the effects of plasma processing on low-κ SSQ materials this thesis has sought to address many scientific questions, mainly the questions mentioned below.

1. Is it possible to develop and perfect a deposition technique that gives good quality films?

2. Will this process developed ensure repeatability and can the developed process be adopted to deposit other materials of the same class?

3. How do some of the plasmas frequently used in IC manufacturing such as $SF_6$ and $O_2$ plasmas affect the low-$\kappa$ films?

4. Is it possible to further reduce the $\kappa$-value of the films by the incorporation of air volume within the deposited thin films by subtle modifications in the deposition process?

5. What sort changes does the incorporation of porosity bring about in the low-$\kappa$ films? and lastly

6. Is the resulting damage from plasma interaction the same for normal films and porous films?

# 1.11. THESIS ORGANISATION

The thesis is organised as follows

**Chapter 1** so far presented a brief literature review highlighting the importance of ILDs in IC manufacturing and the need for materials with low dielectric constants for efficient devices. It discussed in brief the historical evolution of materials used for ILD applications, integration challenges and need for plasma processing in IC fabrication. Further the chapter examined SSQs, which are widely used in ILD applications and reviewed studies elucidating plasma damage, with key focus on the variation of $\kappa$-value of SSQs and similar materials

**Chapter 2** details the deposition technique used to deposit metal and dielectric thin films in this study. It also looks at plasma processing of the films and the various techniques used to characterise the films to have an understanding of the changes happening to the films as a result of plasma exposure.

**Chapter 3** discusses the deposition and characterisation of MSQ thin films and the changes to the film post plasma exposure. The study on MSQ films were carried out to have a good understanding of the film deposition, processing and characterisation techniques as these studies are widely reported in literature. Similar experiments were carried out on PMSQ thin films basing the studies done on the MSQ films as a baseline for comparison.

**Chapter 4** shows the introduction of porosity into the PMSQ thin films by sacrificial porogen approach and studies the changes in the PMSQ films due to the introduction of porosity. The chapter looks at the variation in the density of the film, the change in $\kappa$ – value and also the changes happening to the film as result of plasma exposure of the porous PMSQ films.

**Chapter 5** consists of a more detailed analysis of the expected variations in the film density and $\kappa$-value and compares it with the observed density and $\kappa$-value. It also gives a rough estimate about the change in the surface area of the film as a result of porosity integration. It also explains experiment done by a novel method to pattern the dielectric films.

**Chapter 6** gives an overall conclusion of the thesis and suggests some ideas to take this work forward.

# CHAPTER 2

# THIN FILM DEPOSITION, PROCESSING AND CHARACTERISATION TECHNIQUES

Various characterisation techniques were used to optimise the deposition parameters to produce repeatable films with consistent chemical, physical and electrical properties. The characterisation was done after the films were subjected to plasma exposure to understand the changes happened to the films during the exposure. The film deposition technique, plasma processing of the films and characterisation techniques used for the experiments are discussed in this chapter.

## 2.1. THIN FILM DEPOSITION TECHNIQUES

Films of thicknesses ranging from a few nanometres to tens of micrometres are categorised as thin films. The deposition and manipulation of thin films is an integral part of integrated circuit manufacturing [56]. Thin films are used in the industry for the production of electronic components, electronic displays, for creating optical coatings, antistatic coatings, hard surface coatings, in the production of data storage components including magnetic and optical components and many other similar applications. There exist a large number of methods for the deposition of thin films. They can be classified as evaporative methods, glow – discharge processes such as sputtering and plasma processes, gas –phase chemical processes such as CVD and thermal forming processes

and liquid – phase chemical techniques including electro processes and mechanical techniques [57].

Different deposition techniques were used to deposit different materials throughout this project. We will take a detailed look at these techniques in this section.

### 2.1.1. WAFER PREPARATION FOR FILM DEPOSITION

The silicon wafers (n type, Phosphorus doped, Virginia Semiconductor Inc.) were cut into pieces of approximately 1.5 cm x 1.5 cm. The pieces were then cleaned by blowing with pressurised clean dry air to get rid of the silicon particles sticking on to the surface. They were then rinsed in DI water (obtained from a Millipore filtration system) and Piranha etched to remove any organic residue on the silicon. A base piranha etch was used to clean the wafers prior to spin coating. The base piranha etch solution is a mixture of 3 parts ammonium hydroxide ($NH_4OH$) and 1 part hydrogen peroxide ($H_2O_2$). The mixture will oxidise the materials present on the surface leaving behind a clean surface. The reaction is not self-initiating under normal conditions; hence it is necessary to heat the mixture to start the reaction. The silicon pieces are immersed in the mixture for 45 minutes to complete the cleaning process. The pieces are then removed from the etch solution and rinsed thoroughly with DI water. The pieces are left in a clean container immersed in DI water to avoid any contamination, and are blow dried using clean compressed air just before spin coating.

### 2.1.2. SOLUTION PREPARATION

The solution is a mixture of a solvent, which is the volatile part and solute, which is the non – volatile part [58]. The function of the solvent is to act as a carrier for the solute and to help the solute disperse uniformly on the surface to be coated after which it is removed by evaporation. The various solutions for the experiments in this project were

custom made in the lab in a fume hood seen in figure 2.1.(a), to avoid risks of fume inhalation and necessary personal protection equipment such as gloves, lab coat and goggles were used at all times to reduce any risks involved in the handling of chemicals.

The solute and solvent were measured in the required quantities using a weighing scale and mixed together in glass bottles. The mixture was then stirred over time using a magnetic stirring technique. This technique uses PTFE capsules which are resistant to most solvents with magnetic material inside. The pellets are dropped into the bottles along with the mixture and placed on a magnetic stirrer. The stirrer has a rotating magnetic component within it. When it rotates it causes the pellet to move inside the bottle stirring the solution. Figure 2.1.(b) shows a magnetic stirrer in operation.



(a)                                                                    (b)

**Figure 2.1.(a)Fume hood in which chemical handling, piranha etch and spin coating of films were done to avoid risks of fume inhalation. (b) Magnetic stirrer in operation**

### 2.1.3. SPIN COATING

Spin coating is a mechanical technique, where a motor drives a chuck that holds the substrate onto which the material is to be deposited. The material is applied in the liquid phase also known as the solution.

## 2.1.3.1. THEORY OF SPIN COATING

One of the easiest methods to obtain a thin film, from a solution is to form it by spin coating on the required surface. Figure 2.2 shows the various stages in the spin coating process.
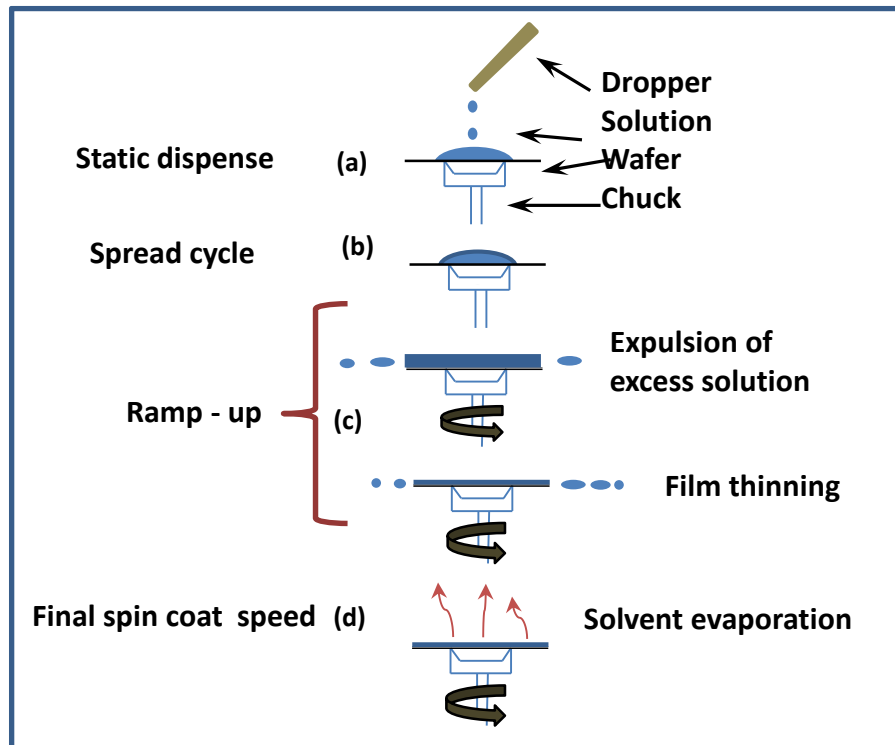


**Figure 2.2. Formation of thin film during spin coating**

In the initial static dispense phase, a small quantity of the viscous solution is put on the surface where the film is to be formed while it is immobile. The substrate is then set to spin at high spin speeds, typically around 3000 rpm. The next step is the spread cycle where the substrate starts to spin. Centripetal forces acting on the liquid cause the solution to spread radially and skinning of the film occurs at this stage. As the speed ramps up, the excess solution is expelled from beneath the skin surface which in turn will be thrown off the edges of the substrate. The rate of elimination of the fluid decreases as the film thins down. This is because during the thinning process the resistance to the flow increases as the viscosity of the liquid on the surface increases as a result of fluid

expulsion and evaporation of the solvent. As the spin process continues it eventually leaves behind a thin film of the non – volatile component of the solution in a highly viscous state on the spinning surface.

Figure 2.3 shows WS-400A-6NPP spin coater from Laurell technologies used to deposit films for this project.



**Figure 2.3. WS-400A-6NPP spin coater from Laurell technologies**

### 2.1.3.2. ADVANTAGES OF SPIN COATING

Spin coating is a very simple yet effective technique for film deposition. It is a cost - effective technique in terms of equipment cost and requires only very little deposition time. The technique can be mastered easily and the deposition process can be optimised quickly. It also gives uniform coverage and good gap - filling during film deposition.

## 2.1.4. PHYSICAL VAPOUR DEPOSITION

Deposition of metal by thermal evaporation is an age old technique widely used in laboratories and in the industry for the deposition of metals and alloys. Figure 2.4 shows the schematic of a metal evaporator.
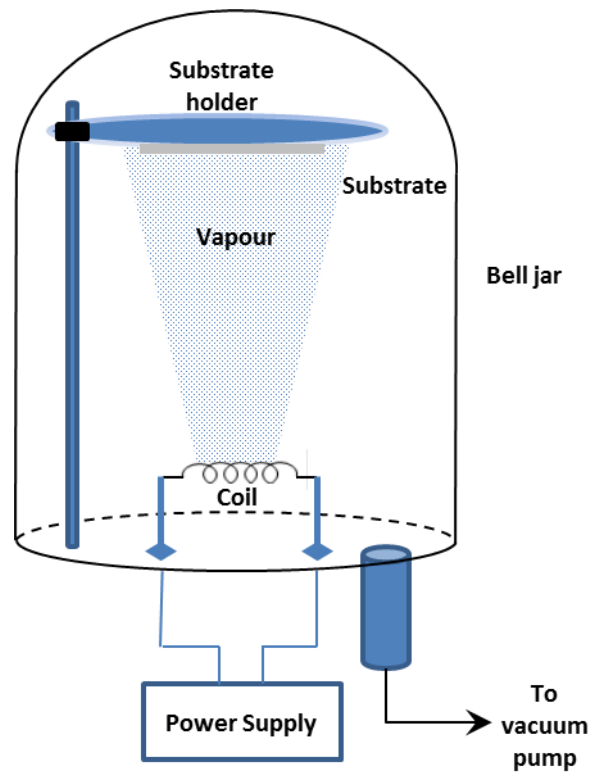
**Figure 2.4. Schematic of a metal evaporator**

In this deposition technique, the vapour phase of the metal to be deposited is generated by heating the material to its evaporation point. This is done by placing the material to be sublimed in a boat or coil made of materials like tungsten that can be heated to extremely high temperatures by resistive heating. The vapour generated is then transported to the substrate that is to be coated held in place by a substrate holder, where it condenses to form a solid film on the substrate surface. Specialised power supplies are required for the system to generate the high currents needed to heat the coils. High vacuum is another important factor needed to ensure good quality deposition. The absence of ambient atmosphere prevents the formation of oxides when the metal is heated to high temperatures. It also aides in the efficient transport of the generated vapour from the

source to the substrate for deposition. Hence the whole setup is enclosed in a bell jar which is pumped down to extremely low pressure.

Edwards E306 coater was used for the deposition of aluminium films in this project, for the fabrication of metal – insulator – metal (MIM) structures to make capacitance measurements Custom made tungsten coils were used as the evaporation source for the deposition process.

## 2.1.5. ANNEALING OF DIELECTRIC FILMS

The deposited polymer films need to be annealed at high temperatures to complete the cross linking of the material. The normal dielectric films were annealed in Gero F-A-100-1000/13-3 tube furnace. Shown in figure 2.5.(a). The films are placed on a graphite boat and then placed in the tube furnace as shown in figure 2.5.(b). The heating temperature, heating ramp and anneal duration are programmed in the furnace automatic controller shown in figure 2.5.(c). The annealing was done in ambient atmosphere. The hybrid films containing porogen material and polymer for the development of porous films were processed in a Lenton thermal designs limited tube furnace seen in figure 2.5.(d), which has the option to circulate inert gasses through the furnace tube to maintain an inert atmosphere. The system is connected to mass flow controllers to regulate the amount of gas flow through the furnace tube. The hybrid films were annealed in argon atmosphere.
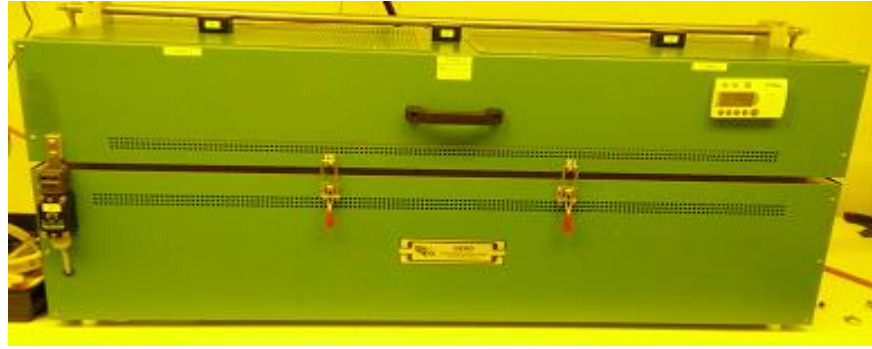
(a)
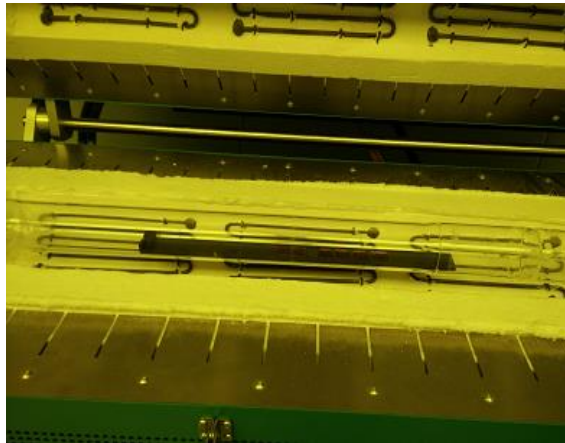


(b)



(c)
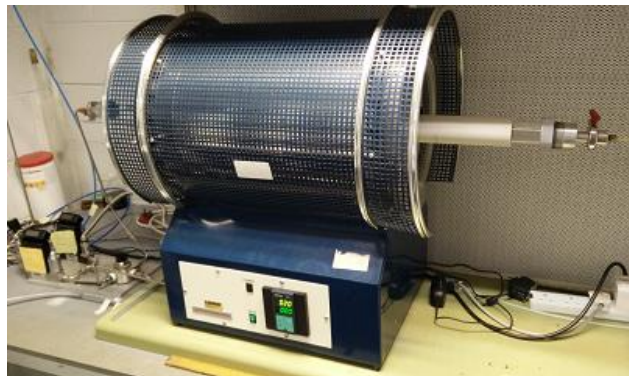


(d)

**Figure 2.5. (a) Gero high temperature tube furnace (b) samples on graphite boat placed inside tube furnace for high temperature anneal (c) Programmable automatic control for the Gero furnace (d) Lenton tube furnace with gas flow mechanism and mass flow controllers to regulate gas flow**

# 2.2. PLASMA PROCESSING OF DIELECTRIC FILMS

Plasma is the fourth state of matter where gases exist in an ionised state. In a plasma the charged particles move in random directions and on average are electrically neutral. Most of the matter in the universe exists as plasma. We can strike a plasma by applying a strong electric field between two electrodes and thereby ionising the gas in between the electrodes. Figure 2.6 shows the formation of plasma sheaths. The extent of ionisation will be very small when compared to the bulk of the gas and hence they are usually known as weakly ionised plasmas.

The presence of large number of charge carriers makes plasma an electrically conductive medium. Charge diffusion to walls is a common phenomenon in plasmas as the fast moving electrons gets lost to the walls of the chamber. This loss and recombination of ionised species at boundary surfaces can create charge depletion in the
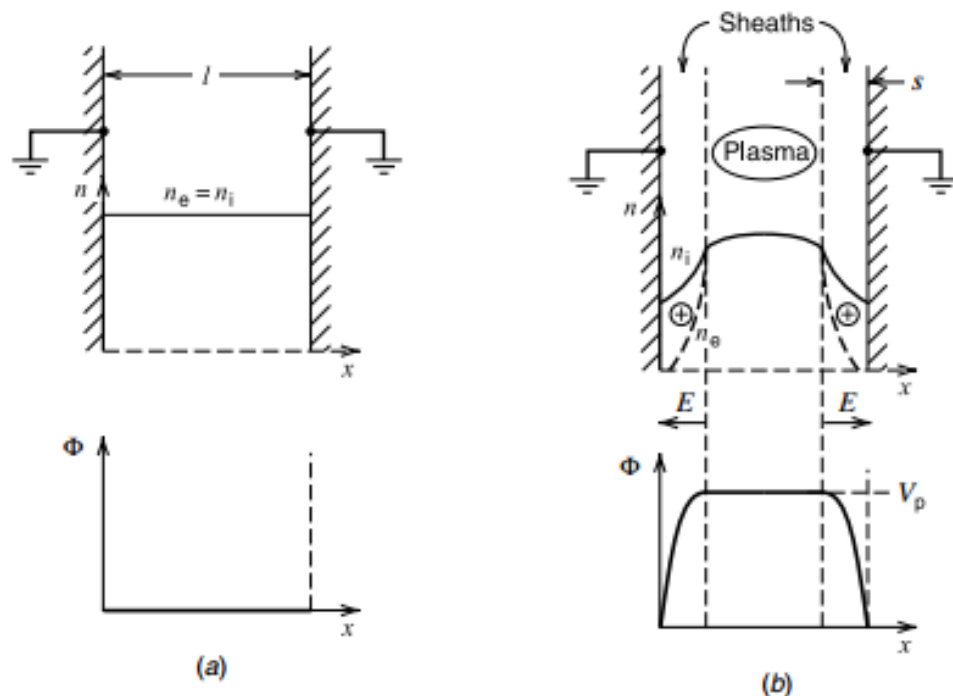


**Figure 2.6. Formation of plasma sheaths: (a) initial ion (ni) and electron (ne) densities and potential (ϕ); (b) densities, electric field (E) and potential (Vp) after formation of the sheath such that sheath (s) << width of plasma (l) [33]**

nearby gas phase forming a positively charged region called sheath. The sheath can be considered as a thin boundary layer between the plasma and the surrounding gas phase. Here we can say that the plasma is in a quasi-neutral state as some of the electrons have been lost to the walls.

When electric field is applied to sustain the discharge they preferentially heat the mobile electrons. So even though the ions and electrons usually are at an electrical equilibrium they are not at a thermal equilibrium between themselves or with their surroundings.

Plasma discharges are used for materials processing and are usually capacitively driven radio frequency discharges. Figure 2.7 shows a plasma chamber containing two electrodes. The substrate to be processed is kept at the bottom electrode and the gases are introduced through the shower head on the top electrode. The nature of the reaction that happens within the chamber depends on the nature of the gases introduced. The feed gas determines the plasma chemistry. They are also affected by the applied power and chamber pressure. The effluent gasses are pumped out of the chamber through a pumping mechanism, which also maintains the vacuum inside the chamber.

Many mechanisms can happen when the charged particles of the plasma hit a surface [59]. Energetic ions crossing the sheath can fall on the surface causing transfer of large quantities of energy and momentum to the substrate and physically remove material from the surface. This removal mechanism termed sputtering, is also widely used as a deposition technique.

Etching usually refers to removal of material and is a critical step in micro fabrication. Sputter etching requires high energy particles and is not a good method for selective etching. Another common form of etching mechanism employed is a reactive etching. Here the reactive chemicals / ions in the plasma react with the material on the substrate giving out volatile products, which are then removed as exhaust by the pumping mechanism. This is a more refined method where the selectivity of the etch can be controlled. The purpose of the plasma in this kind of etcher is to make the reactive etchant species. This is done by the dissociation of the feed gas, which dissociates into ions and electrons because of the applied potential. The nature of the ionic species determines the nature of the reaction.
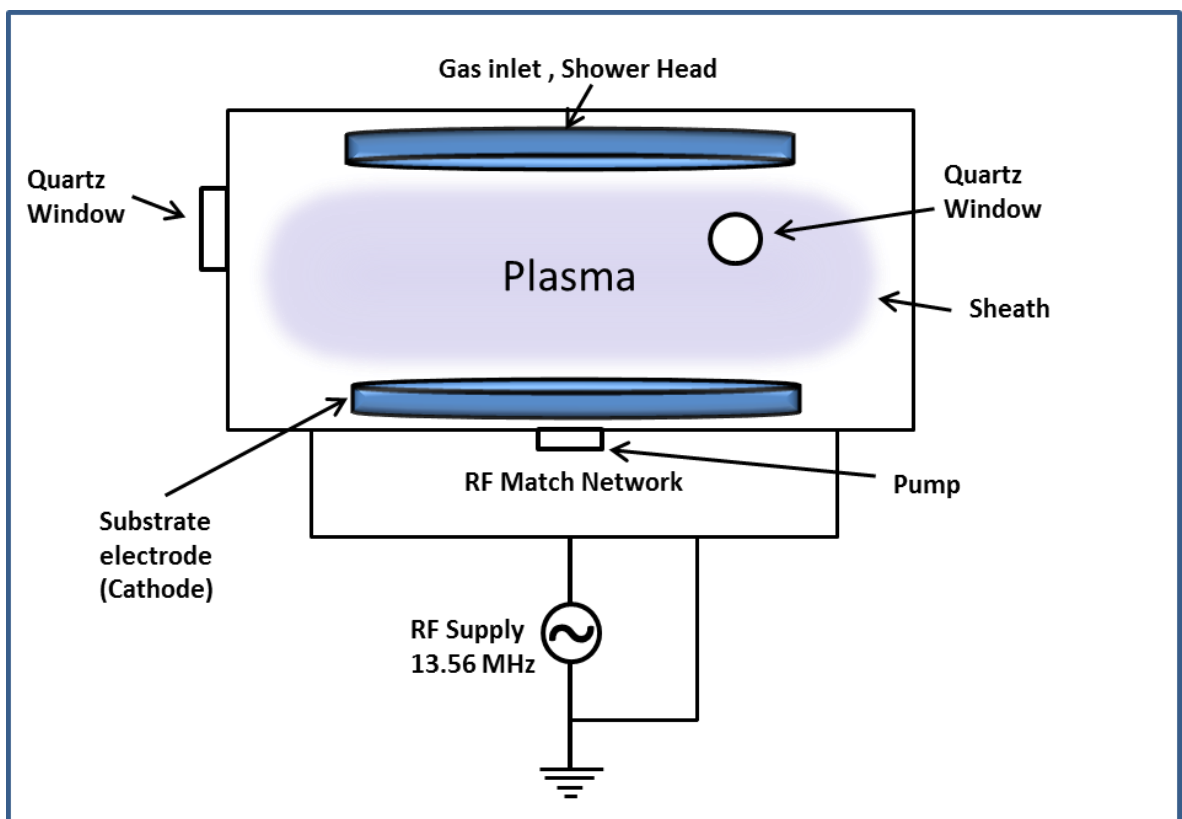


**Figure 2.7. Schematic of a plasma etching chamber.**

The intensity of reaction can be adjusted by regulating the amount of gas feed, thereby reducing the number of reactive species formed. The reaction can also be controlled by regulating the applied power which regulates the amount of energy associated with the reactive species.

Oxford Instruments 80 plus chamber shown in figure 2.8.(a) was used for the reactive ion etching (RIE) experiments. The Oxford Instruments Plasmalab 80 Plus RIE chamber has a 13.56 MHz driven parallel plate reactor with a 240 mm substrate electrode and an optimised shower head gas inlet. The feed gas flow rate, chamber pressure and applied forward power were varied during experiments. Figure 2.8.(b) the chuck which acts as the substrate electrode. The substrate to be processed is placed on the chuck. The chuck has concentric circles marked on it to help position the sample. In our experiments the samples were always placed at the centre of the chuck as shown in figure 2.8.(b).



(a)
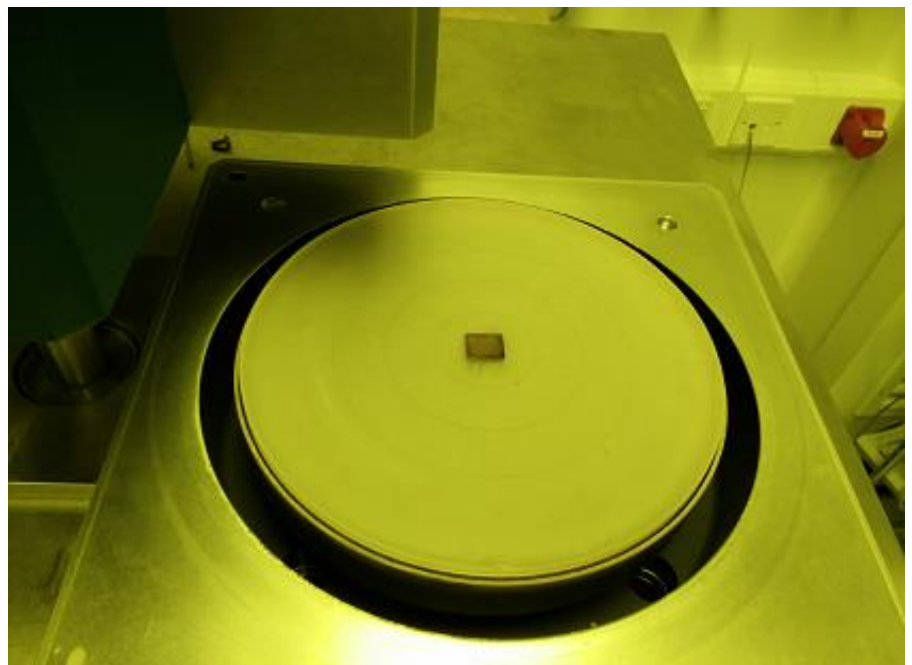
(b)

**Figure 2.8.(a) Oxford Instruments Plasmalab 80 Plus RIE chamber (b) placement of the sample at the centre of the chuck for processing**

Figure 2.9 shows the exposure of samples to $O_2$, $SF_6$ and Ar plasmas as seen from the view port of the chamber.



(a)          (b)          (c)
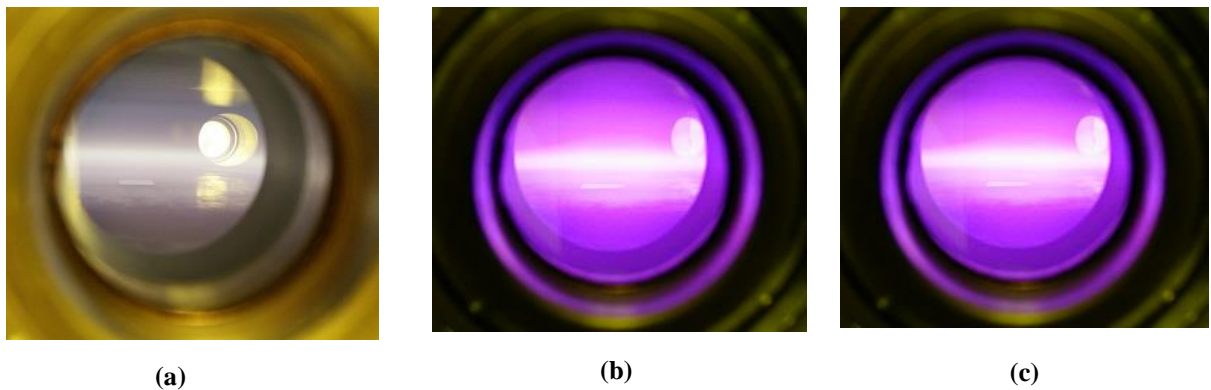
**Figure 2.9. Exposure of samples to (a) O₂ plasma (b) SF₆ plasms and (c) Argon plasma**

# 2.3.  THIN FILM CHARACTERISATION

## 2.3.1.  SPECTROSCOPIC ELLIPSOMETRY

Ellipsometry is an optical technique employed in measuring thickness and optical properties of films with wide application in microelectronics, semiconductor industry and biology. The technique works on the principal of the change in polarisation of reflected light from the film whose thickness is being measured.

Reflection is important to measure thicknesses of films using this technique. Consider a thin film coated on a silicon substrate. When light falls on the surface of the film, light is reflected off the surface of the film. This can be considered as the 1st interface (interface between air and the film). The light is also after travelling through the bulk of the film and reflected from the bottom substrate on which the film is deposited. (2nd interface between the film and the underlying reflecting surface, which is the Si substrate in our case). There is a phase delay between the light reflected from 1st interface and from the light reflected 2nd interface, leading to interference oscillations. The delay is related to

the index of refraction and also to the physical thickness of the film. Based on the position

of the interference peaks and number of interference oscillations, the thickness data is

provided by Spectroscopic Ellipsometry. This data is then fitted with the model that is

supplied to the software, and hence the use of a precise model is very important for

accurate thickness measurements with this technique. Figure 2.10 shows the schematic of

an ellipsometer.

$$\tan \Psi \, e^{j\Delta} = \frac{R^P}{R^S} \qquad \text{Equation 2.1. [60]}$$
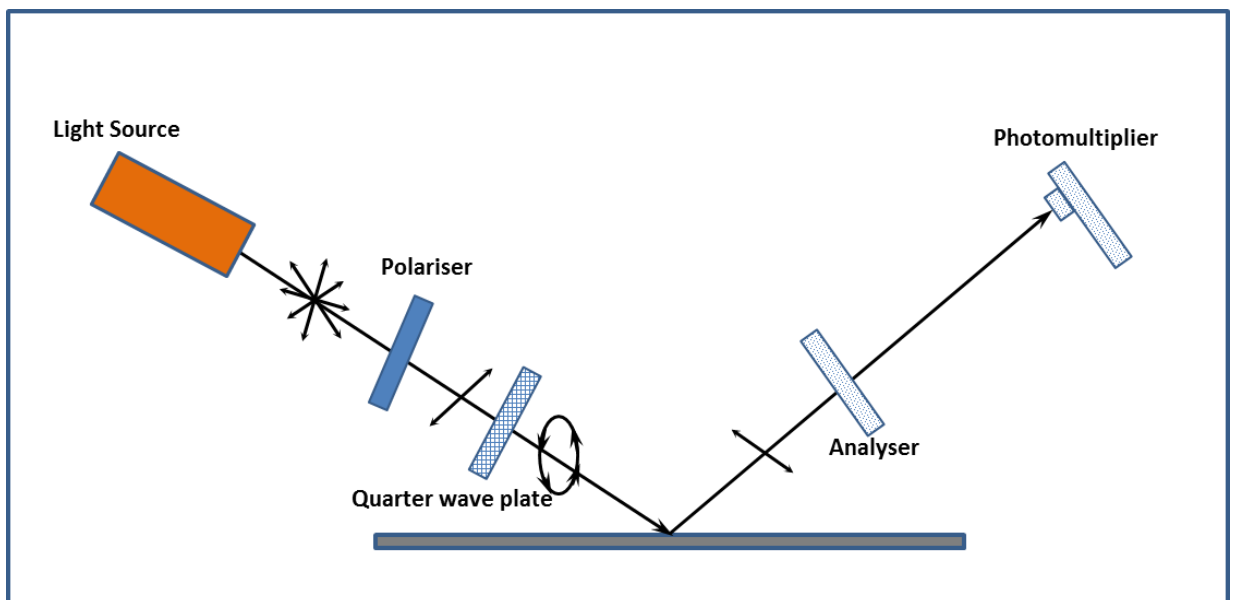


**Figure 2.10. Schematic of an ellipsometer**

Equation 2.1 is the fundamental equation for ellipsometry where $\Delta = \delta 1 - \delta 2$. $\delta 1$ is

the phase difference between the parallel component and the perpendicular component of

the incoming wave and $\delta 2$ of the outgoing wave and $\Psi$ is the angle whose tangent is the

ratio of the magnitude of the reflection coefficients. $R^p$ and $R^s$ are the parallel and

perpendicular components of light that may change upon reflection.

Standard models are not available for all materials. For the particular material under

investigation a new model had to be created. This was achieved by using the Cauchy

dispersion model available within the software. Cauchy model describes the dispersion index of refraction of materials in the spectral ranges in which the given material is transparent and is given by

$$n(\lambda) = A + \frac{B}{\lambda^2} + \frac{C}{\lambda^4} + \cdots$$

**Equation 2.2[60]**

Here $\lambda$ is the wavelength in microns and A, B and C are fit parameters. This is a very effective model for describing the index of refraction of dielectric materials and semiconductors in the spectral regions where they are transparent (where the extinction coefficient is zero)

The software interface has the option to auto fit certain parameters. During standard operation an accurate model is fed into the software. Once a scan is complete, the software will try to fit the measured parameters to the model by adjusting the thickness (set to auto fit). There will be a mismatch between the data generated by the model chosen in the software and the data measured by the system from the sample. This mismatch between the theoretical model and the actual measurement is the quantified error. The error is least when the data read by the system matches exactly with that of the model. One important thing to note is that the parameters A, B and C for standard models are available within the system and cannot be changed. To create a model for the material under investigation, a thin sample was created and the sample thickness was measured using X –ray reflectivity (XRR). This thickness was then fed into the Cauchy model. Since we were sure of this thickness as it closely matching with the profilometer measurements it was kept constant parameter in the Cauchy model. The fit parameters A, B and C were set to auto fit. Now the software had to match the measured values to the Cauchy model to reduce the error. Error could only be reduced by adjusting the fit parameters rather than adjusting the thickness films as in the case of standard operation. The model was validated

with another set of samples. The measured thickness was compared to thickness data obtained from stylus profilometry measurements and they closely matched.

Thickness measurements were made with Spectroscopic Ellipsometer Base- 160 from J. A. Woollam Co., Inc.

## 2.3.2. STYLUS PROFILOMETRY

Profilometry as the name suggests is a technique that is used to study surface profiles of samples. It is a widely used direct and surface independent technique and requires no modelling. Stylus profilometry is a contact technique in which the stylus is made to move laterally across the surface to be profiled in a straight line. As it moves along the surface, the system measures the variations on the surface of the sample scanned and by taking into account the signal generated by the relative displacement of the stylus. Figure 2.11 shows the generation of a signal by the sample surface when probed by the stylus.

Veeco Dektak 150 contact profilometer was used for profilometry measurements.
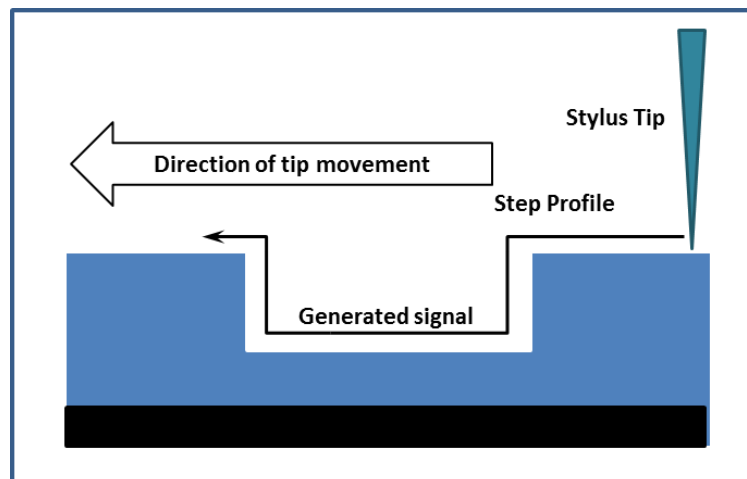


**Figure 2.11. Signal generation based on the surface feature of the scanned sample in stylus profilometer**

### 2.3.3. FOURIER TRANSFORM INFRARED SPECTROSCOPY

Fourier Transform Infrared spectroscopy (FTIR) is an important tool for analytical and preparative applications because of the ease with which it is able to identify the chemical species in the spectrum. Figure 2.12 shows a block level representation of a typical FTIR spectroscopy system.
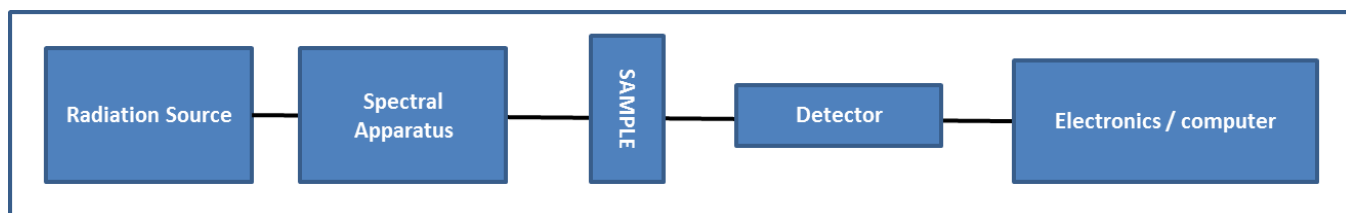


**Figure 2.12. Block level representation of an FTIR**

The IR radiation from the source is incident on the sample by the help of the spectral apparatus. Depending on the nature of the sample some part of the incident IR radiation is absorbed and some is passed through onto the detector. The resulting spectrum reaching the detector will have details regarding the molecular structure of the sample; essentially a fingerprint of the sample. The absorption peaks will correspond to the frequencies of vibrations of the chemical bonds within the material [61]. As materials differ in their chemical composition their absorption spectrum will also be different. It is also possible to identify the change in bonding structure of the material with this technique.

FTIR studies on low-k samples were done on Perkin Elmer, Spectrum GX. The FTIR spectrum was obtained in a ratio scan at resolution of 8 $cm^{-1}$ with 1 $cm^{-1}$ interval, averaged over 20 scans with Si spectrum as the background.

## 2.3.4. CONTACT ANGLE MEASUREMENT

A setup as shown in the figure 2.13 is used to measure contact angle, by which the wettability of a film can be determined. A drop of water is made to fall on the surface of an illuminated sample using a motor driven syringe. The motor driven stage and the illumination by the light source can be controlled from the user interface within the computer. Pictures of the droplet from the sample surface are taken by the camera and the water contact angle measurements are calculated by using the software. Water contact angle is the angle that a water droplet makes at the interface between the film and the water droplet. Based on the angle that the droplet makes at the interface, we can identify the wettability of the film and thereby its hydrophilicity or hydrophobicity. Variations happening at the surface level can lead to change in wettability of the material which can be easily identified using this technique.
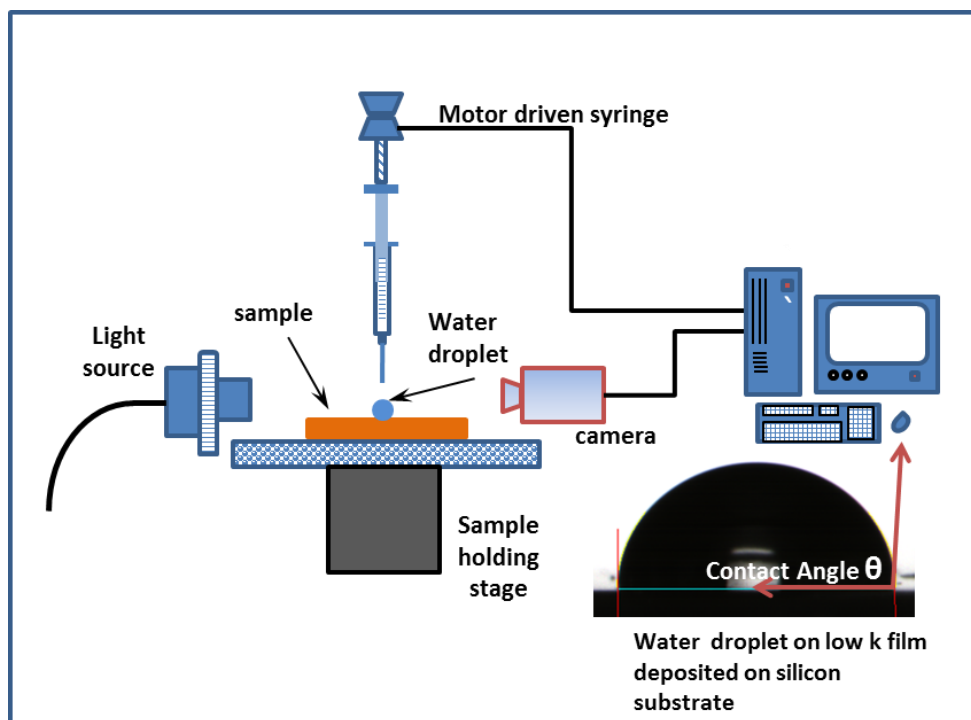


**Figure 2.13. Goniometer setup for water contact angle measurement**

Contact angles were measured with a First Ten Angstroms FTA200 goniometer using a high purity HPLC grade water (Sigma Aldrich) as the probe liquid.

### 2.3.5. THERMAL GRAVIMETRIC ANALYSIS

Thermal gravimetric analysis (TGA) is a simple way to observe the change in the properties of a material with respect to temperature over time. The system is used to study vaporisation of materials and sublimation or desorption of species from the material when it is heated. Figure 2.14 shows the schematic of a TGA system. The material to be investigated is kept in a crucible and then heated. We can identify the decomposition pattern of materials by observing the weight loss happening to the material over time, as the crucible is heated in the tube furnace.
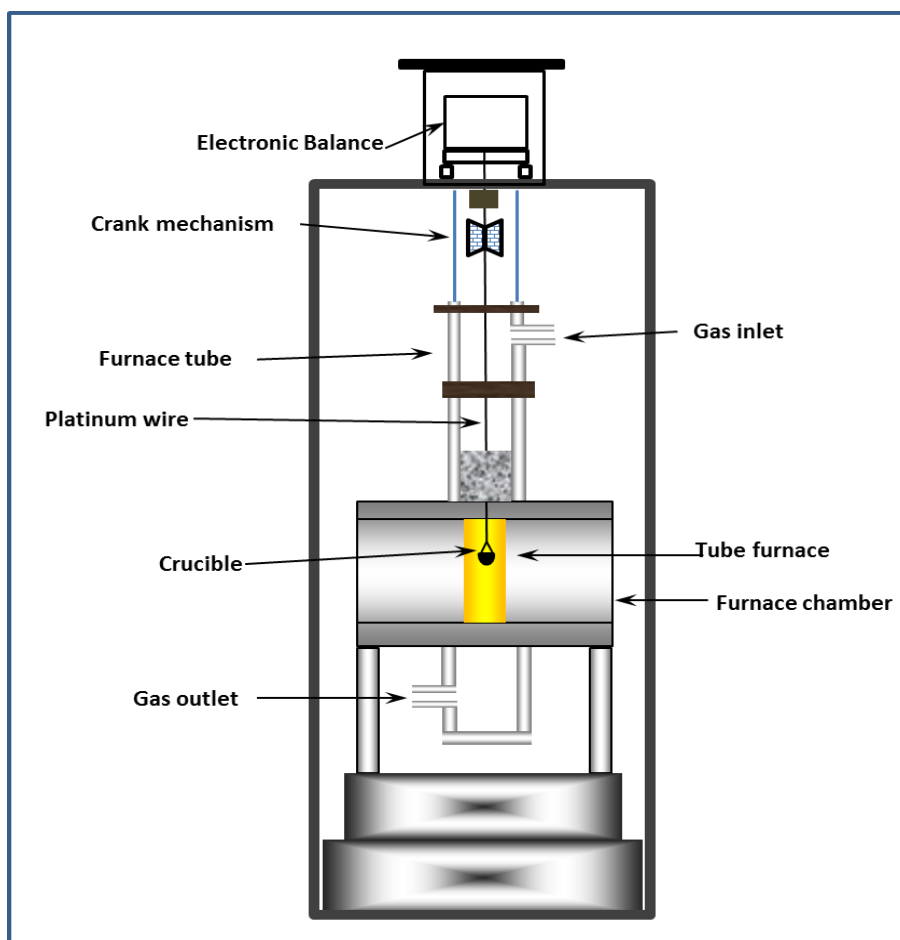


**Figure 2.14. Schematic of a TGA system**

Two materials were considered for use as high temperature porogens in this work namely styrene-b-butadiene-b-styrene (SBS) and Heptakis (2,3,6-tri-O-methyl)-β-cyclodextrin (tCD). TGA was used to study the decomposition temperature of these materials and the temperature at which the majority weight loss happened to the material. Studies were also conducted on porogen - polymer hybrid films as a function of temperature.

The studies were done on TA Instruments, TGA Q50.

## 2.3.6. X RAY PHOTOELECTRON SPECTROSCOPY

Techniques that involve the detection of electrons emitted or scattered from a surface are known as electron spectroscopies. The energy of the detected electrons can range from 5 – 2000 eV depending on the technique being used. These electrons are used to gain information about the electronic energy levels in the surface region namely core levels and valence levels. Core energy levels are those associated with the electron states localised within a single atom and thereby it is a characteristic of the atomic species. Valence energy level comprises of the electronic energy levels of the surface with lower binding energies and also the bonding orbitals associated with adsorbed molecules. As they are not well localised these levels are very sensitive to the local chemical environment.

Photoelectron spectroscopy is a technique that involves the analysis of electrons emitted from a surface that has been irradiated with photons. Depending on the nature of the photon source the technique can be again classified into Ultraviolet Photoelectron Spectroscopy (UPS), that typically makes use of gas discharge lamps with fixed photon energy ($hv$) in the range of 10 – 40 eV or X – ray Photoelectron Spectroscopy (XPS) which uses soft X – ray sources with $hv$ in the range of 1200 -1400 eV [62]. XPS is a core

level spectroscopy technique and UPS is used to investigate valence levels. XPS is also known as electron spectroscopy for chemical analysis (ECSA).

Figure 2.15 helps us to understand the XPS process. XPS uses focused X - ray beams of around 1.5 kV, which are allowed to fall on the sample to be scanned. This leads to photo emission of electrons from top few nanometres of the sample, which is collected by a lens system and is fed into the electron analyser. The analyser measures the kinetic energy of the electrons. Following this they are counted in an electron detector to get the signal. The binding energy of the electrons and photoelectron peak intensity are analysed from which the elemental identity, its quantity and chemical state are determined [63].
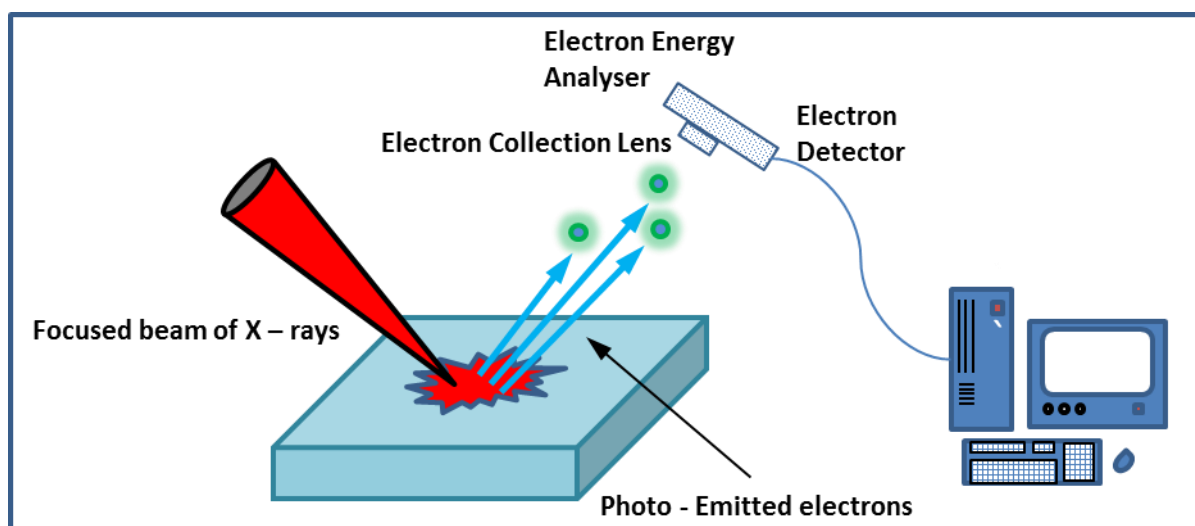


**Figure 2.15. Schematic of an XPS system**

Let us look at some of the phenomenon that takes place at the atomic level when a surface is irradiated with photons [64]. These phenomena are shown in figure 2.16. and is as follows

a. The photon can pass through the atom without disturbing it.

b. The photon can lose part of its energy as it gets scattered by an orbital electron within the atom

c. The photon can transfer the whole of its energy to an orbital electron leading to the emission of that electron from within the atom.

The photon in the first case is of no significance as it passed through the atom without any interaction with the atom, thereby leaving the atom in its initial state itself. The second case is the phenomenon known as 'Compton scattering'. The third case is the photoemission process which is the basis of ECSA.
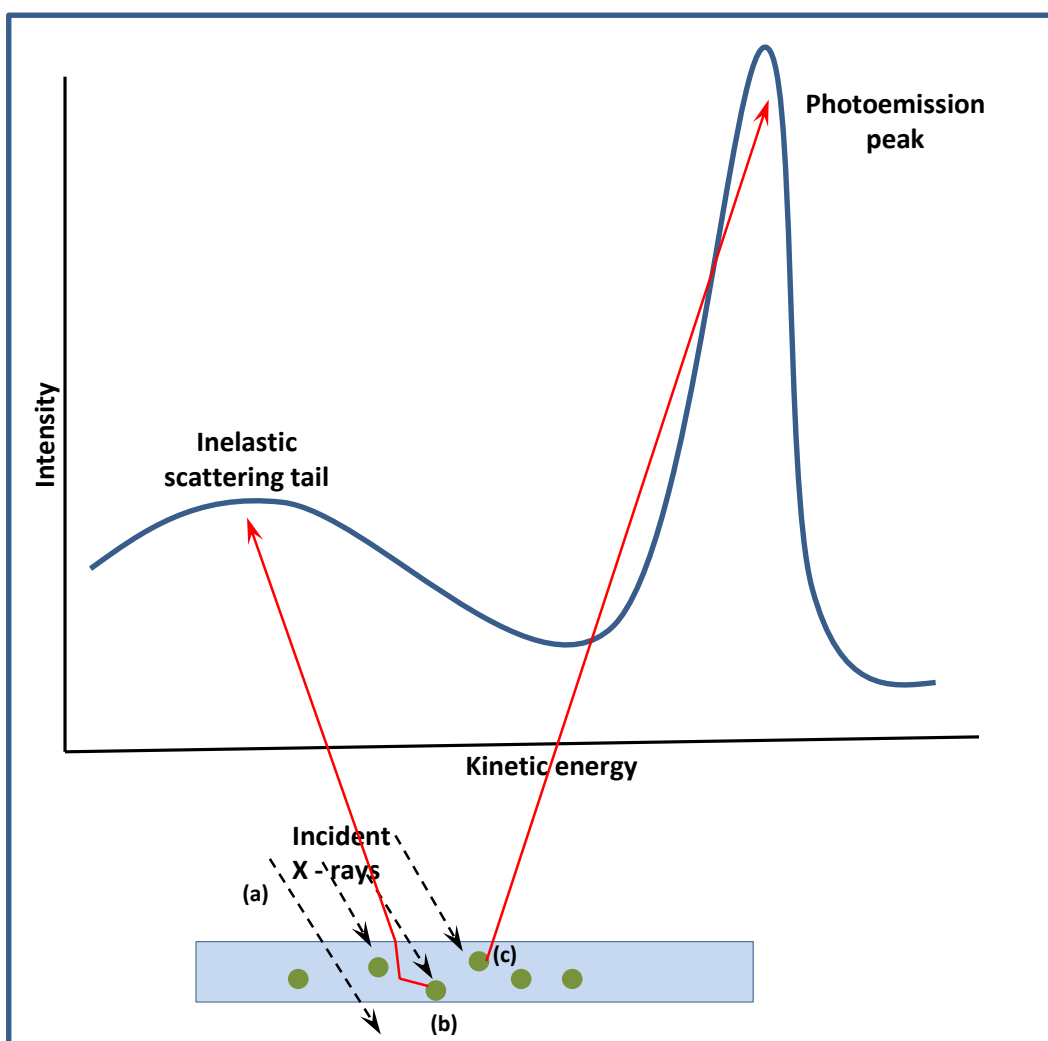


**Figure 2.16. Diagram showing paths of various electron emissions during photoemission process**

The energy of the X - rays we use for XPS are of the order of approximately 1 keV. A beam of photons with such high energy is capable of penetrating several microns into

irradiated sample. There is a high probability that the electrons photoexcited deeper in the material undergo inelastic scattering. Hence the electrons emitted as a result of these collisions do not provide any useful information about the electronic structure of the solid. As a result, the XPS sampling depth is essentially less than 10 nm from the surface of the sample, because it is in this depth where most of the elastic collisions occur

## 2.3.6.1. PRINCIPLE OF PHOTOEMISSION SPECTROSCOPY

When the surface is irradiated with photons of energy $h\upsilon$, it penetrates the surface of the material being irradiated. The photon gets absorbed by an electron with binding energy $E_b$ if the energy of the photon is greater than the work function $\phi$ of the material. This leads to photo excitation of the atoms in the material leading to emission of electrons from within the material. The photoemission process is shown in figure 2.17.

The photoionization leading to the photoelectron formation takes place as follows.

$$A + h\upsilon \rightarrow A^+ + e^- \qquad\qquad \textbf{Equation 2.3}$$

Where A is the atom that was excited by the photon with energy $h\upsilon$ which led to the emission of and electron ($e^-$) and thereby leaving behind the atom in an ionised state ($A^+$).

For the energy to be conserved

$$E(A) + h\upsilon = E(A^+) + E\ (e^-) \qquad\qquad \textbf{Equation 2.4}$$

Since the electron was emitted from the atom let us assume that the energy of the electron is purely kinetic ($E_{kin}(e^-)$), and equation 2.4 can be rewritten as follows
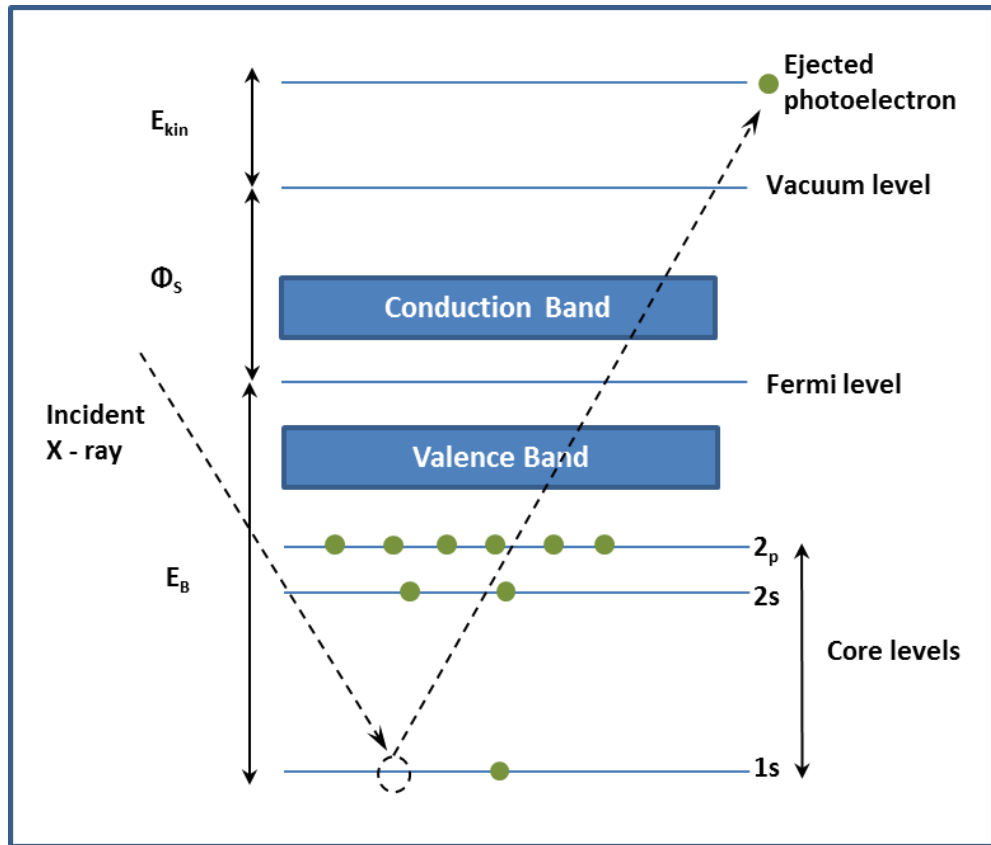
**Figure 2.17.The photoemission process**

$$E_{kin}(e^-) = h\upsilon \ - [E(A^+) - E(A)] \qquad \text{Equation 2.5}$$

But $[E(A^+) - E(A)]$ is the difference in energies between the ionised atom and the neutral atom which is the binding energy ($E_B$) of the electrons. Hence the above kinetic energy equation becomes

$$E_{kin}(e^-) = \ h\upsilon - E_B \qquad \text{Equation 2.6}$$

From equation 2.6 we can see that the kinetic energy of the photoelectron is directly proportional to the photon energy. Since the energy of the photon source is known, the binding energy can be calculated by measuring the kinetic energy of the emitted electron.

$$E_B = \ h\upsilon - E_{kin}(e^-) \qquad \text{Equation 2.7}$$

Equation 2.7 is known as the Einstein equation which explains the basic physics of the photoemission process. $E_B$ gives us valuable information about the type of atom that undergoes photoemission as it is a function of the atom and its chemical environment.

XPS spectra can be obtained from solids, liquids or gasses. For gasses the energy of an electron in a particular orbital is the same as the ionization energy of that electron. This is also known as the first ionization potential of that electron. The influence of the surface is felt in the case of solids and thereby we have to factor in an additional energy component while calculating the binding energy of electron.

$$E_B = \ h\upsilon - E_{kin}(e^-) - \Phi_s \qquad\qquad \text{Equation 2.8}$$

Equation 2.8 displays the binding energy of electrons for solids, where $\Phi_s$ is the work function of the material. As it can be seen from figure 2.15, $\Phi_c$ is the difference in energy between the vacuum level and Fermi level of the sample material.

Another important aspect is that the core level energy of an atom depends on the chemical state of the atom. Formation of chemical bonds can result in a change in the local charge density around the atom thereby creating a change in the binding energy of the atom, when compared to the binding energy in its neutral state. Observing this shift in the binding energies in XPS spectra will give us valuable information about the chemical state of the atoms in the near surface region

The XPS analysis was carried out using a VG Microtech electron spectrometer at a base pressure of $1 \times 10$-9 mbar. The photoelectrons were excited with a conventional Mg K$\alpha$ (h$\upsilon$ = 1253.6 eV) x-ray source and an electron energy analyser operating at a 20 eV pass energy, yielding an overall resolution of 1.2 eV.

## 2.3.7. SCANNING ELECTRON MICROSCOPY

Scanning Electron Microscopy (SEM) are microscopes with very high magnification (>100,000X) which are extensively used for investigating microstructure and chemical composition of materials. They employ electron beams for imaging rather than visible light as used in conventional optical microscopes and because of this they have very high resolutions when compared to optical microscopes. Schematic of an SEM system is shown in figure 2.18.
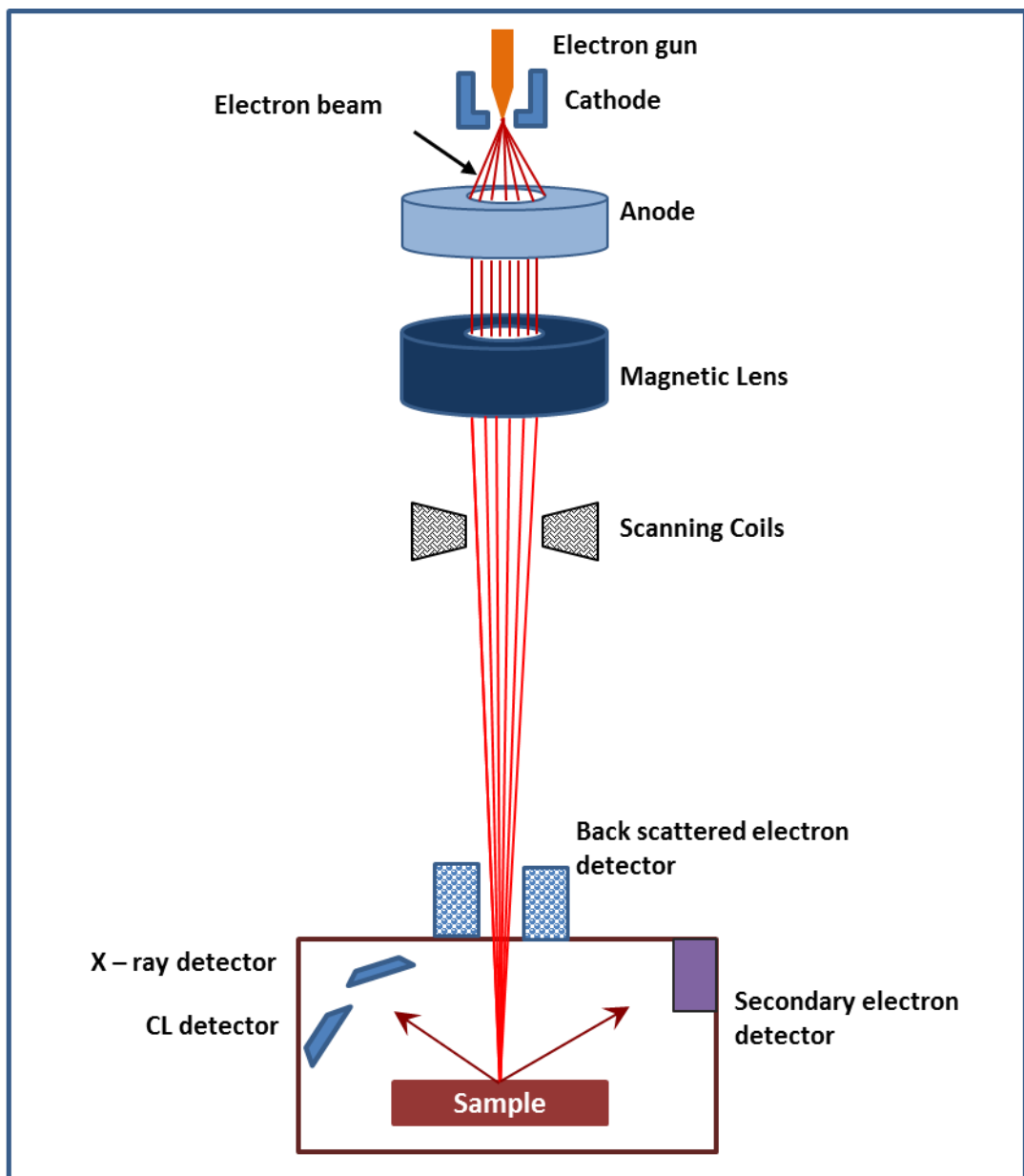


**Figure 2.18. Schematic of an SEM**

Electrons from a thermionic, Schottky or field emission source [65] are accelerated with the help of an accelerating voltage between the cathode and the anode. The beam is monochromated by the magnetic lenses. A raster scan is performed using this fine focused beam to probe the sample surface. The interaction of the beam with the surface is analysed by software to obtain an image of the sample surface. Figure 2.19 shows some of the interactions that occur when the beam hits the specimen.
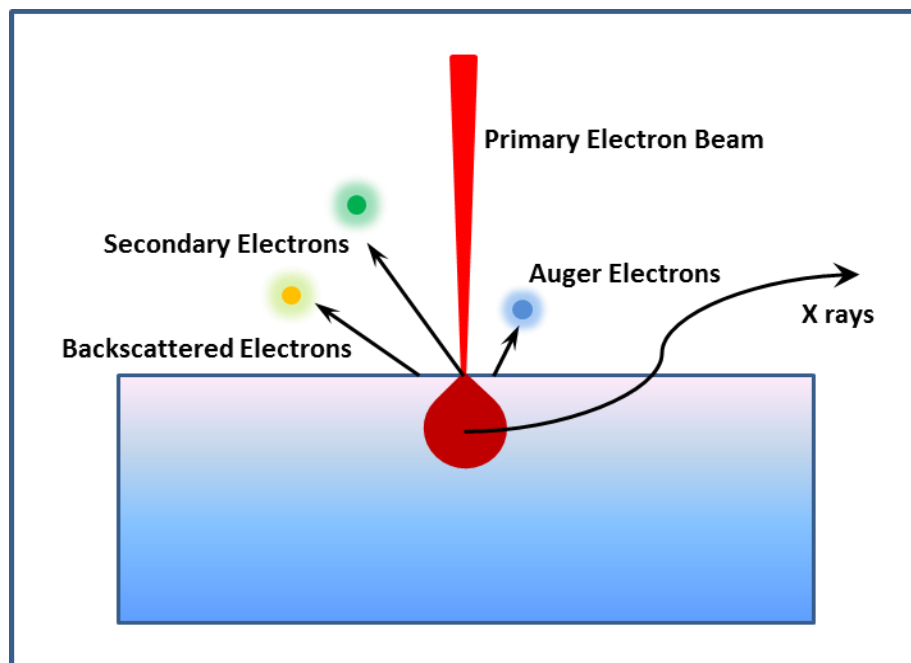


**Figure 2.19.Surface mechanism after the primary electron beam hits the surface**

When the primary electron beam hits the surface of the specimen elastic and inelastic scattering occurs. Electron diffusion into the specimen leads to the loss of electron energy and also the lateral spreading of the electrons occurs by multiple elastic large angle scattering. These weak and scattered electrons are detected and they are used to form the surface image by the system software. The spectrum contains contributions from secondary electrons, backscattered electrons, auger electrons, X –rays and heat. The generation of secondary electrons are influenced by the topography of the material and

the creation of the backscattered electrons is affected by the atomic number of the atomic species present on the sample surface.

ZEISS EVO LS-15 SEM system was used to study the patterned low-k film surfaces.

## 2.3.8. ENERGY DISPERSIVE X-RAY ANALYSIS

When a sample surface is bombarded with primary electrons, electrons in the inner shell of the sample atoms are ejected. To fill up the vacancies thus created, the electrons from the outer shell transfer to the inner shell and generate X – rays. The X –rays generated during the SEM analysis of a sample surface give a clear idea of the elemental composition of the sample being investigated. The Energy Dispersive X-ray (EDX) spectrometer analyses the X –rays generated during the electron beam probing of the surface and provides information about the elemental composition of the surface being scanned using the X-ray peak intensity and position information by software analysis.

The elemental analysis of the low-k samples was investigated using an INCAx-act detector attached to a Zeiss EVO LS-15 scanning electron microscope

## 2.3.9. ATOMIC FORCE MICROSCOPY

Atomic force microscopy (AFM) is a powerful imaging technique that helps us to investigate the surface structure of substrates or films. Powerful AFM systems are capable of even imaging individual atoms or molecules on surfaces. One major difference of an AFM system from a conventional optical or electron microscope is that it does not form an image by focusing light or electrons on a surface [66]. Hence it can be used to image a variety of materials including glass, ceramics, polymers and biological samples. An AFM system probes the surface with a cantilever head and creates a height map of the surface of the sample under investigation, and hence is different from a 2D image obtained from other imaging systems.

A typical AFM system consists of a microscope stage, control electronics and a computer. The stage contains a sample holder, the tip to probe the sample and a video microscope to observe the sample and the tip as seen in figure 2.20. The video microscope outputs the image of the sample and tip onto a screen to make adjustments and operations easier. The control electronics is usually an interface between the stage and the computer. It handles the signals required to drive the components in the stage and digitizes and feeds the signals coming from the AFM into the software interface on the computer. The software in the computer takes the parameters for the scan from the user and communicates it with the stage via the control electronics. Apart from the control software the system also has imaging software that can be used for detailed analysis of the image data obtained from the AFM system.

The AFM tips used to probe the sample surface are usually made from silicon or silicon nitride.
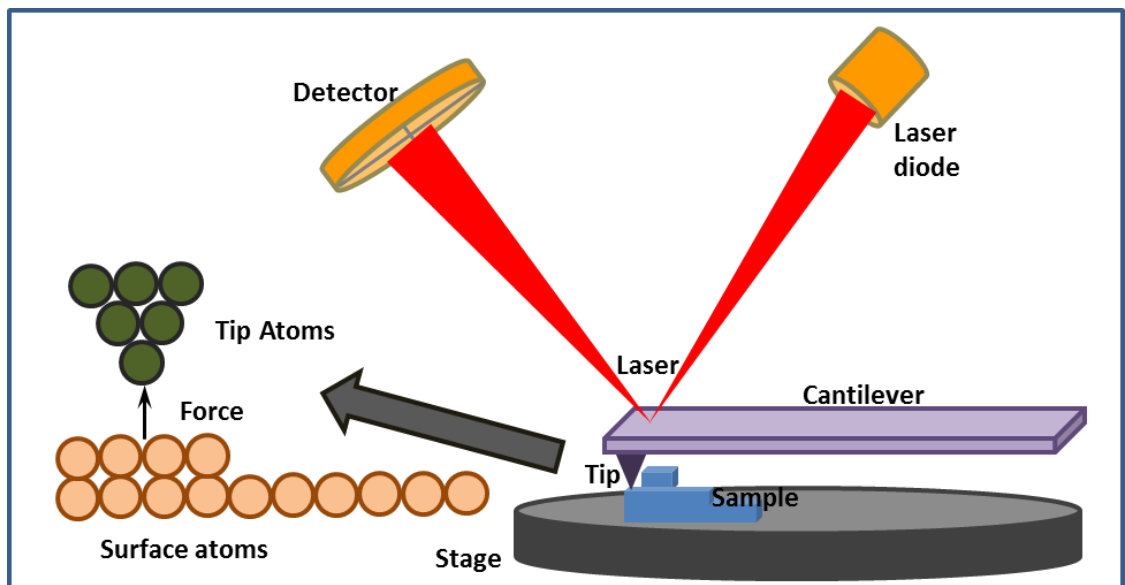


**Figure 2.20.Schematic showing the cantilever and sample holder of an AFM system**

The movement of the tip is controlled by a piezoelectric transducer. Force transducers are usually employed to measure the force between the tip and the surface of the sample. A feedback control monitors the force on the tip and depending on this the control electronics drives the piezoelectric components to maintain a constant probe – sample distance. If the tip experiences an increase in force the control electronics will move the tip further away from the surface and vice versa. Hence this apparent shift happening in the position of the tip is a direct map of the topography of the surface being investigated. A 3D image of the surface is created by monitoring the deflection of the tip during the movement of the probe, using an optical lever detection system.

Three common imaging modes are available in most AFM systems and they are contact mode, non-contact mode and tapping mode [67]. The contact mode of operation is used to get high resolution images of small areas on the sample. As the name suggests the tip makes physical contact with the sample under investigation. This can damage the sample, and in some instances the tip as well. In the non-contact mode of operation the tip moves over the sample surface without making a physical contact with the sample, and measures the van der Waals forces between the tip and the sample.

In tapping mode, the probe taps the sample surface rather than probe on it. During the tapping mode operation, the tip oscillates at 50- 100 kHz with amplitude of 20-200 nm with the help of a piezoelectric crystal.

Nanoscope Dimension 3100 AFM was used to obtain images of the film surface.

## 2.3.10. X RAY REFLECTOMETRY

X –ray reflectometry is a non contact and non – destructive technique that can be used to determine the roughness, density and thickness of thin films with very high level of precision. This charcaterisation technique can be used on crystalline as well amorphous materials. It makes use of the X – ray beams reflected off the sample surface at grazing angles. The grazing incidence X – ray scattering process and the arrangement for X – ray reflectometry measurements are shown in figure 2.21.

When X –rays fall on a surface the beam can either reflect or propogate along the sample surface or penetrate into the material by defraction, depending on the angle of incidence ($\theta$) of the x- ray beam and the value of the total reflection critical angle ($\theta_c$). If the $\theta = \theta_c$, then the X – rays will propogate along the sample surface. When $\theta < \theta_c$ all X – rays are reflected and when $\theta > \theta_c$ the X –rays penetrate into the material by refraction.
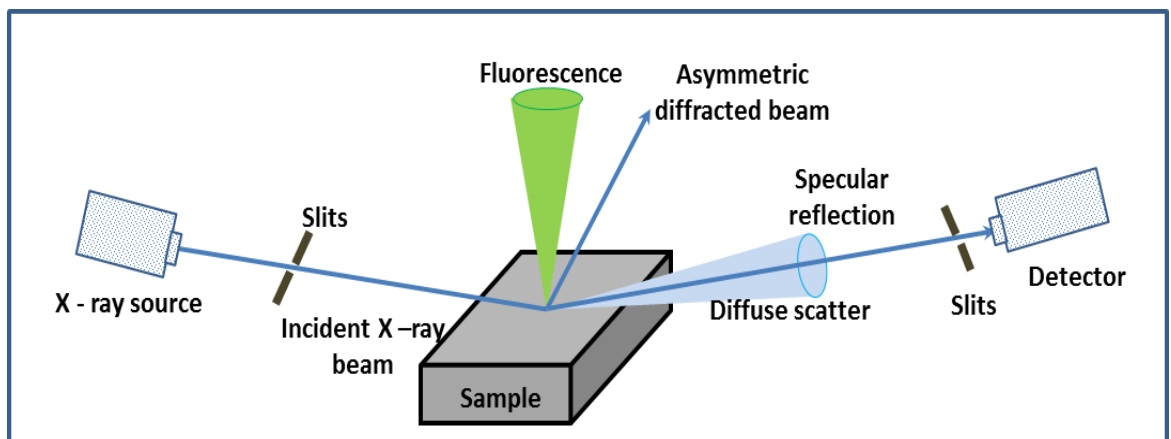


**Figure 2.21. Grazing incidence X – ray scattering process and arrangement for X – ray reflectometry**

When $\theta > \theta_c$ the beam passes into the film casuing the reflections to happen from the top and bottom of the film. The rays thus reflected from multiple locations intefere leading to the formation of interference fringes. We get a multitue of data from these

inteference fringes obtained from XRR as seen in figure 2.22. The density of the material can be deduced from the critical angle. The thickness of the layer can be found from the period of the interfernce fringes whereas the fall in intensity or slope gives an understanding about the roughness of the layer.
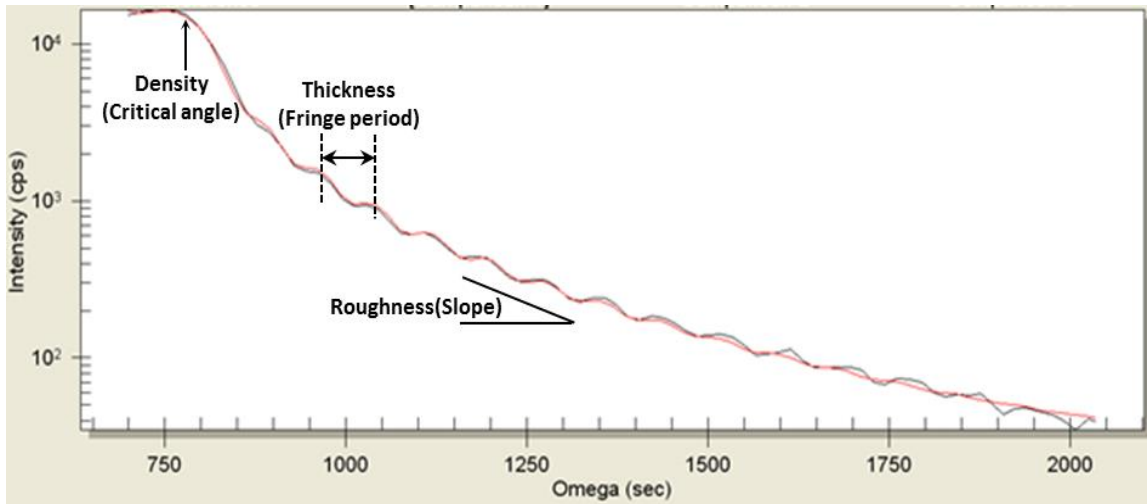


**Figure 2.22. Interference fringes obtained during XRR measurements on PMSQ thin films**

XRR measurements were carried out on the films using a triple-axis Jordan Valley Bede-D1 X-ray system using a monochromatic Cu-K$\alpha$1 ($\lambda$ = 1.5405Å) radiation source operated at 45 kV and 40 mA. The obtained fringes are fitted onto a model by the system software making use of a neural network bases algorithm to get an optimum fit between the model and the measured fringes.

## 2.3.11. CAPACITANCE MEASUREMENTS ON FABRICATED MIM STRUCTURES

A vital measurement in this work is the measurement of $\kappa$ – value of the deposited films and plasma processed films. The $\kappa$ – value of the films are calculated from capacitance measurements made on specially fabricated MIM structures [68] with the dielectric material sandwiched in between.

Silicon wafers were initially cut into the required size and were cleaned using piranha etch. The samples were blow dried and then were loaded in the aluminium evaporator, to deposit a layer of Aluminium on the Silicon surface which was used as the bottom contact. A good and uniform coating is required for it to act as a good conducting layer. Conductivity of the layer was checked using multi meter at multiple points on the surface. Dielectric films were deposited on these specially prepared substrates. A small portion of the polymer film at one edge of the substrate was wiped off to make connection to the bottom aluminium contact. Conductivity was checked on this cleaned area with a multi meter to ensure proper removal of the insulating films. The substrates were then annealed to cure the films. Aluminium dots (2 mm diameter) were deposited on the top of the dielectric films by thermal evaporation to act as the top contact using a metal hard mask. Figure 2.23 shows a schematic of the measurement process.
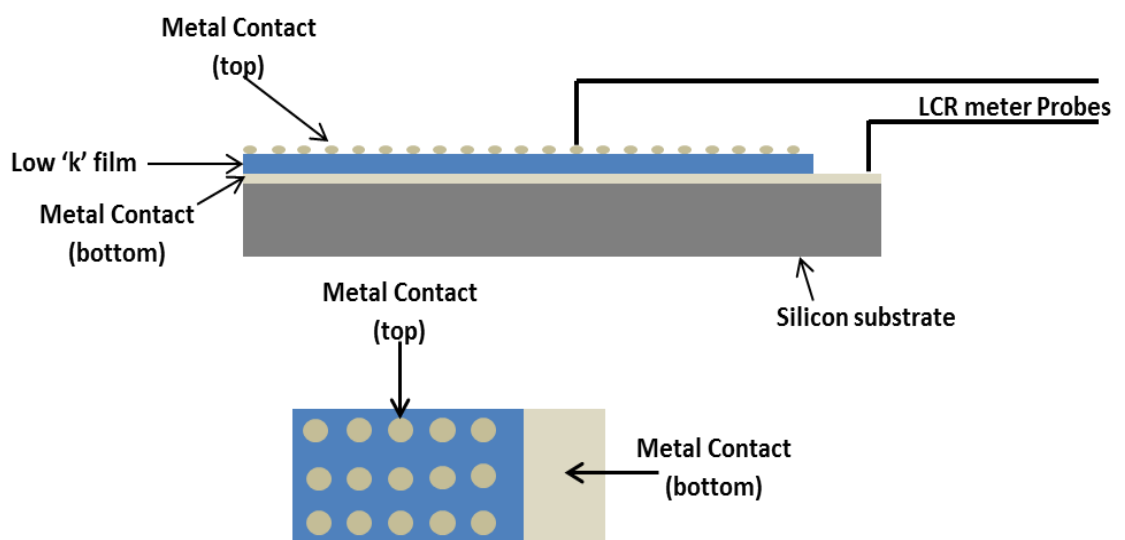


**Figure 2.23. Schematic detailing the capacitance measurements of fabricated MIM structures**

Figure 2.24.(a) shows a sample with multiple MIM structures fabricated These were the kind of samples created for one time measurement of capacitances, like in the case to measure the $\kappa$ - value of a MSQ film. Samples on which measurements were to be made pre and post plasma treatment were fabricated in a different way. Figure 2.24(b) shows a sample used to study the change in $\kappa$ – value of the film pre and post treatment. The picture also shows the custom made metal mask used to deposit top metal contacts by Al evaporation. As we can see in the picture, contacts were deposited on one half of the sample after annealing and measurements were made to determine the $\kappa$ – value of the as – deposited film. The sample was then exposed to plasma and contacts were deposited on the exposed region with no top contacts, so that the new MIM structures fabricated contain the plasma processed film inside. Measurements performed on these newly fabricated structures provide the capacitance and hence the $\kappa$ – value of the plasma treated film. Thus we can detect any change in these values post plasma treatment.



Bottom contact to make electrical contact during measurements

Area to fabricate MIM structures post plasma exposure

Metal dots deposited to act as top contact for capacitance measurements

(a)

(b)
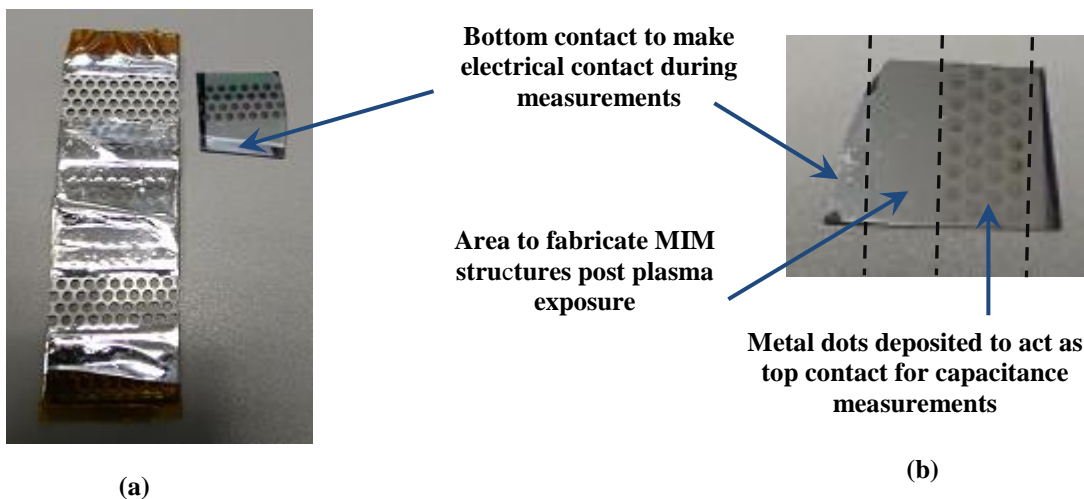
**Figure 2.24. (a) Sample made to facilitate $\kappa$ – value measurement with the mask used to deposit top contacts (b) sample used to measure $\kappa$ – value of films pre and post plasma exposure**

Figure 2.25(a) shows the HP4263A LCR meter that was used to measure capacitances (Measurement parameters, frequency: 100 KHz, voltage 1 $V_{rms}$, series connection as suggested in the manual for measurement of small capacitances). Figure 2.25.(b) shows the custom built probe station on which the measurements were performed. The accuracy of values measured by the meter was verified by measuring the capacitance values of commercially available capacitors before each set of measurements.



**(a)**



**(b)**

**Figure 2.25 (a) LCR meter used to measure capacitance (b) probe station used to make the measurements**

# CHAPTER 3

# DEPOSITION, CHARACTERISATION AND PLASMA INTERACTION OF LOW K PMSQ FILMS

## 3.1. INTRODUCTION

It is essential to have good quality low-k films to investigate the plasma interaction and the plasma induced damage on low-k films. Development of a repeatable deposition process and characterisation of the deposited films were essential for this project. Spin coating was used as the deposition technique because it was a simple and cost effective deposition technique. An added advantage of spin coating deposition is that porogen integration can be implemented with ease making small changes in the spin coating solution chemistry. SSQ was selected as the deposition material as it was easy to create spin coatable solutions and existing literature indicated that this material possessed many key attributes which should be possessed by a good dielectric material.

MSQ is a widely studied SSQ material. MSQ films were spin coated, annealed and characterised as control experiments for benchmarking purposes. PMSQ material even though used in certain studies [49,50], their dielectric properties and the interaction of the films with plasmas is not reported in literature. The objective of this chapter is to elucidate the deposition, characterisation and investigation of plasma interaction with PMSQ thin films with $SF_6$ and $O_2$ plasmas, and their comparison with MSQ thin films.

# 3.2. DEPOSITION OF LOW-K PMSQ FILMS

## 3.2.1. SOLUTION PREPARATION

MSQ and PMSQ flakes are commercially available and readily form solutions with a variety of organic solvents. MSQ is reported to be soluble in a wide variety of solvents. The solvent for the experiments was chosen by considering the solubility of both the dielectric polymer and the porogen material. Two porogen materials considered were Heptakis (2,3,6-tri-O-methyl)-β-cyclodextrin (tCD) [69] and polystyrene – block – polybutadiene – block – polystyrene (SBS) [70]. The following table will give a general idea about the solubility of the low-k and porogen materials in various organic solvents.

From the possible choice of solvents it was found that both the PMSQ and SBS were soluble in Butanone, THF, MIBK and TCE as seen table.3.1. Trials were carried out with all the four solvents to obtain a concentration to thickness matrix.

| Solvent used | PMSQ | SBS | tCD |
|---|---|---|---|
| **Butanone** | Y | Y | Y |
| **1 – Methoxy – 2- Propanol** | Y | N | Y |
| **Acetone** | Y | N | Y |
| **Tetrahydrofuran (THF)** | Y | Y | Y |
| **Propylene glycol monomethyl ether acetate** | Y | N | Y |
| **Methyl Isobutyl Ketone (MIBK)** | Y | Y | Y |
| **Tricholoroethylene (TCE)** | Y | Y | Y |

**Table 3.1. Solubility of PMSQ, poly(styrene-block-butadiene-block- styrene) SBS and Heptakis (2,3,6-tri-O-methyl)-β-cyclodextrin in various solvents**

PMSQ mixed with MIBK were left aside for dissolution for one hour in a glass bottle. As the solvents used for the experiment can dissolve plastic containers, glassware was used all throughout the experiments.

## 3.2.2. DEPOSITION OF DIELECTRIC FILMS BY SPIN COATING

The material was deposited on the silicon substrate by spin coating the PMSQ solution. Spin speed, spin time and acceleration are the main factors that can affect the thickness and uniformity of a spin coated film. The magnitude of the centrifugal force and the velocity & characteristic turbulence of the air immediately above the spinning medium are determined by the spin speed. Rapid solvent evaporation is a problem in the case of many of the solutions used for spin coating. Hence accelerating the substrate from rest to the final spinning rpm is of prime importance. Another major factor that can affect the whole process is the viscosity of the spin coating solution. A change in any of the above mentioned parameters can cause changes in the quality of the final film.

Upon spin coating the films needs to be annealed at 400°C to obtain a cured film. The need for high temperature curing is detailed later in the report.

Trials were carried out with PMSQ solutions with all of the four identified solvents to study the impact of various spin parameters like spin speed; acceleration and spin time on the thickness of the deposited films. Experiments were carried out to identify the optimum spin parameter set. Two approaches were considered to fix the optimum parameters.

## 3.2.2.1. SPIN COATING USING SOLUTION OF FIXED CONCENTRATION AND VARIABLE SPIN SPEED

PSSQ solutions were made with THF, MIBK, Butanone and TCE and samples were made from each of the solutions. In each case 0.5 gm of the solute (PMSQ) was mixed with 5 gm of the corresponding solvent to obtain the required solution. Figure 3.1 shows the thicknesses of samples created PMSQ solution in THF. Samples were spin coated at different spin speeds. The initial sample in each case was spin coated at 2500 rpm. The speed was increased for each sample in steps of 1000 rpm and samples were made for 2500, 3500, 4500, and 5500 rpm spin speeds for each of the different solutions. The thicknesses of the deposited films were measured using spectroscopic ellipsometry after annealing. The figure shows the average of the thicknesses plotted with the deviation from the mean value as the error bar. It can be seen from figure 3.1, that the thickness of the films obtained was ~ 350 nm.
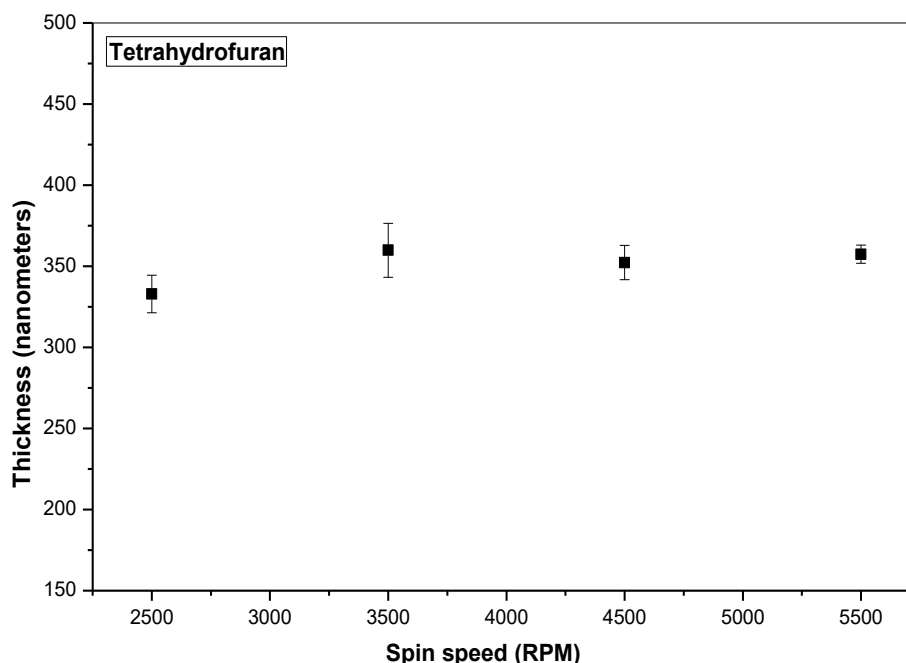


**Figure 3.1. Figure showing thickness vs spin speed plots for PMSQ - THF solution. Concentration 0.5 gm of PMSQ in 5 gm of THF. Spin speed increased in steps of 1000 RPM. For thickness measurements see appendix 3.1.**

60

Figure 3.2 shows the thicknesses of films obtained from PMSQ – MIBK solution. The same steps as discussed in the previous experiment were repeated here as well to obtain deposited films thickness of ~ 130 nm.
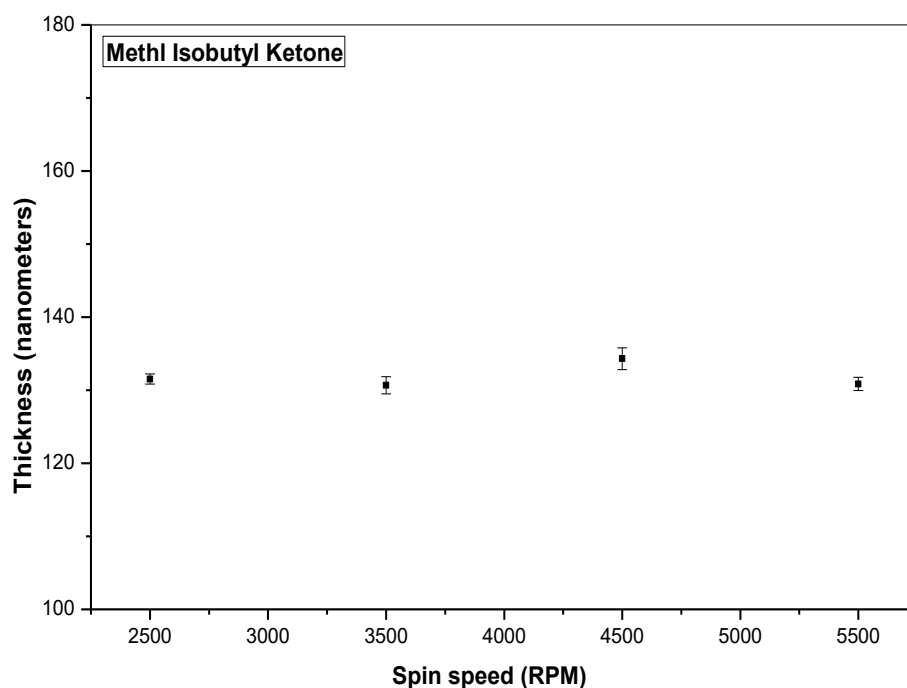


**Figure 3.2. Figure showing thickness vs spin speed plots for PMSQ - MIBK solution. Concentration 0.5 gm of PMSQ in 5 gm of MIBK. Spin speed increased in steps of 1000 RPM. For thickness measurements see appendix 3.2.**

Figure 3.3 shows the thicknesses of PMSQ films deposited from its solution in butanone with average thickness around ~ 230 nm and figure 3.4 shows the thicknesses of films from PMSQ - TCE solution with thicknesses averaging around ~ 350 nm.
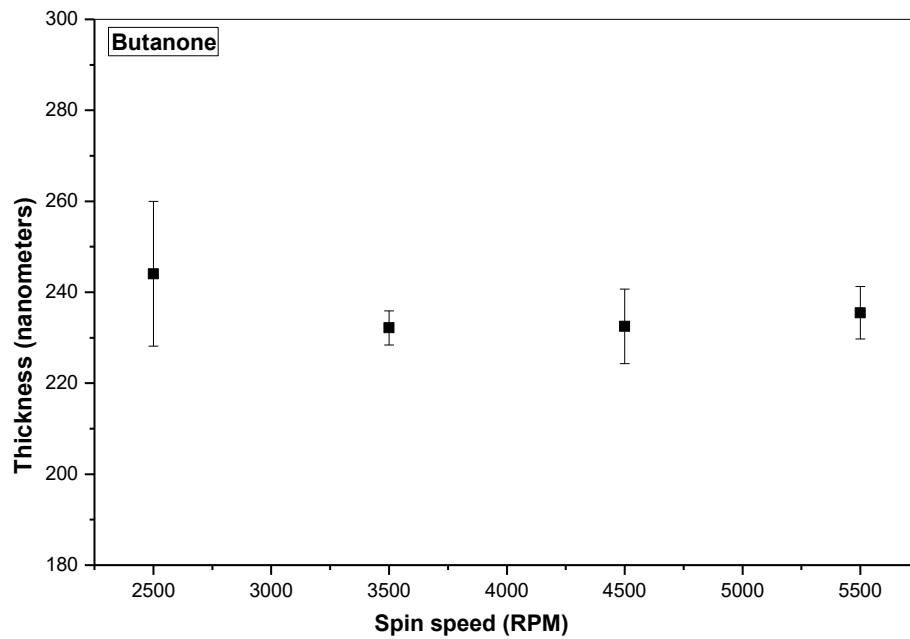
**Figure 3.3. Figure showing thickness vs spin speed plots for PMSQ - Butanone solution. Concentration 0.5 gm of PMSQ in 5 gm of Butanone. Spin speed increased in steps of 1000 RPM. For thickness measurements see appendix 3.3.**
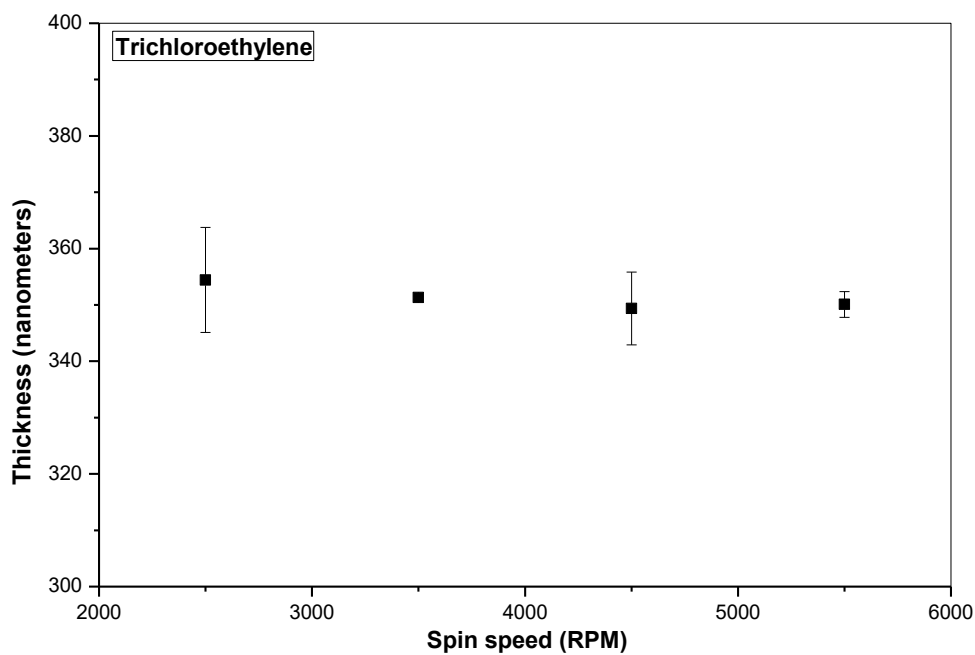


**Figure 3. 4. Figure showing thickness vs spin speed plots for PMSQ - TCE solution. Concentration 0.5 gm of PMSQ in 5 gm of TCE. Spin speed increased in steps of 1000 RPM. For thickness measurements see appendix 3.4.**

From the graphs it is very evident that even though the spin speeds were varied during the experiment, it did not have much effect in our particular case. This is because the viscosity of the solution, at the concentration levels selected for our experiments, were too low for the spin parameters to have any significant effect on the thicknesses of the spun films, hence a second approach was attempted to control the thicknesses of the deposited films.

It should be noted that films created with THF and MIBK were showing good repeatability and hence only these two solvents were used in the second approach.

### 3.2.2.2. FIXED SPIN SPEED, VARIABLE CONCENTRATION.

In this particular experiment the spin parameters such as spin speed, acceleration and spin time were kept constant at 3500 rpm, increase of 180 rpm per second and 45 seconds respectively. Different solutions of PMSQ with THF and MIBK were made with varying amounts of the polymer.

The amount of solute was varied from 0.125 gram to 1 gram in the case of MIBK, increasing in steps of 0.125 gram for 5 gram of MIBK. Samples were made with each of these eight solutions and their thicknesses were measured. Contrary to the previous set of experiments, we were able to see an increase in the measured thickness as the solution concentration increased. The following plot shows the increasing trend in thickness with respect to the increase in solution concentrations. Figure 3.5 shows the measured thicknesses of films deposited from the PMSQ – MIBK solution. The thicknesses varied from ~ 70 nm for a solution with 0.125 g of PMSQ and 5 g of MIBK to ~ 800 nm for the solution with 1 g of PMSQ and 5 g of MIBK.
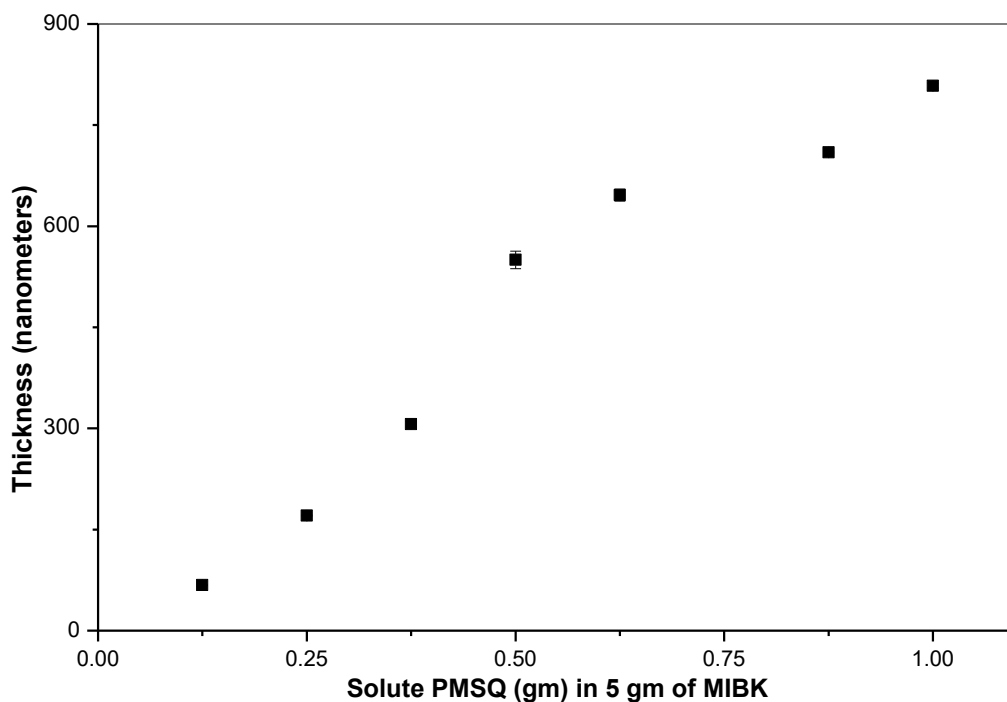
**Figure 3.3. Plot showing thickness PMSQ films from PMSQ –MIBK solutions of varying concentration with fixed spin parameters. Solution concentration increased in steps of 0.125 gm. For thickness measurements see appendix 3.5.**

The same kinds of experiments were repeated with PMSQ and THF. The solute quantities were varied from 0.125 gram to 1 gram, in 10 grams of THF. This means that these set of solutions were only half as concentrated as their MIBK counterparts. Figure 3.6 shows the plot with thickness vs concentration for the films deposited from the PMSQ – THF solution. It was observed that the thicknesses varied over a wide range. A thickness of ~ 125 nm was observed for films deposited with solution having 0.125 g of PMSQ dissolved in 10 g of THF. Films of ~ 1000 nm thickness could be deposited with solution with 1 gram of PMSQ dissolved in 10 grams of THF. For solutions with intermediate concentrations, thicknesses were in between these two values as seen in figure 3.6.

The thickness of the films produced by THF solutions were much greater than those created with the same ratio solute to solvent mixtures of MIBK. With this information in hand it is possible to develop films of the required thicknesses by adopting the corresponding solute to solvent ratios. The difference in thickness of the same ratio PMSQ - THF solution and PMSQ - MIBK solution can be attributed to the difference in the rate of dissolution of the material in solvents of different polarity, the polarity of THF being higher than that of MIBK. It was also seen that after a certain point even though the solute weight was increased the thicknesses did not increase. This can be due to the fact that the solution has reached saturation and the excess amount of solute was removed during filtration of the solution.
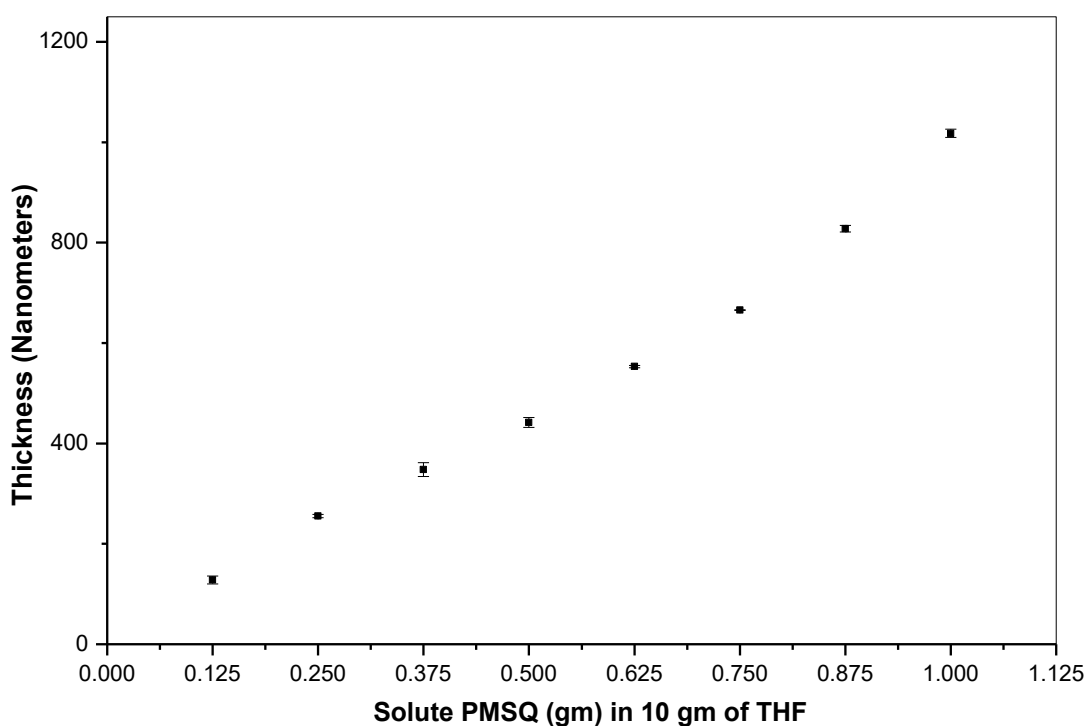


**Figure 3.4. Plot showing thickness PMSQ films from PMSQ – THF solutions of varying concentration with fixed spin parameters. Solution concentration increased in steps of 0.125 gm. For thickness measurements see appendix 3.6.**

### 3.2.3. THICKNESS MEASUREMENTS

It was necessary to make samples with step profiles to verify thicknesses with stylus profilometry. A portion of the silicon substrate onto which the solution was to be spin coated was covered with insulating tape. The substrates were then annealed, after the tape was removed, to obtain the cured film. It was seen that the profilometry measurements matched closely with the measurements made with the ellipsometer using the developed Cauchy model. Figure 3.7 shows the thicknesses from both the ellipsometry and the profilometry measurements made on the samples.
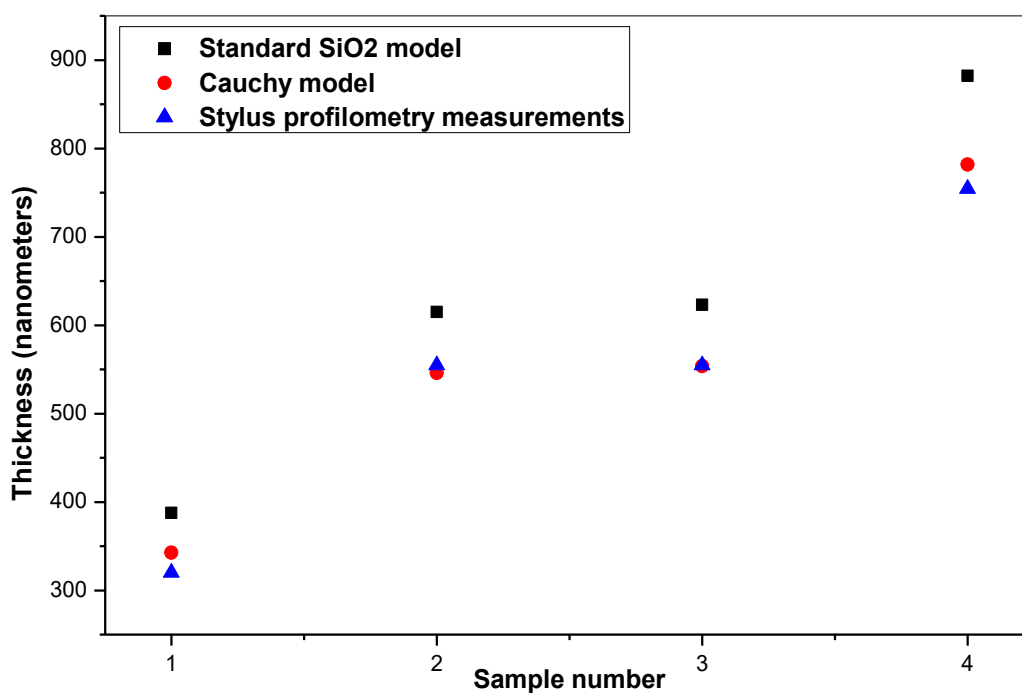


**Figure 3.5. Plot with thickness measurements of samples done by spectroscopic ellipsometry and stylus profilometry. Sample preparation technique and thickness measurements in appendix 3.7.**

It is very clear from figure that the measurement with the developed model for PMSQ gives more precise measurements than that of the $SiO_2$ over Si model, as it is in good agreement with stylus data.

66

## 3.2.4. OPTICAL MICROSCOPE IMAGES OF SPIN COATED FILMS

A good understanding of spin coating and the factors that governed the film thickness ensured the repeatability of the deposition process. Despite thoroughly cleaning the silicon, it was possible to see tiny visible spots on the surface of the spin coated film indicating the presence of particulates in the solution used for spin coating. It was possible to get good quality films that appeared better visually after the solutions were filtered with 0.2 μ PTFE syringe filters, which removed large undissolved particulates present in the spin coating solution.

An inspection of the deposited films under optical microscope revealed pin holes in films deposited from PMSQ –THF solution, while the films spin coated from PMSQ – MIBK solution appeared to have formed well during the spin coating deposition process. Images of the film surfaces obtained from optical microscope are shown in figure 3.8.



(a)                                                            (b)
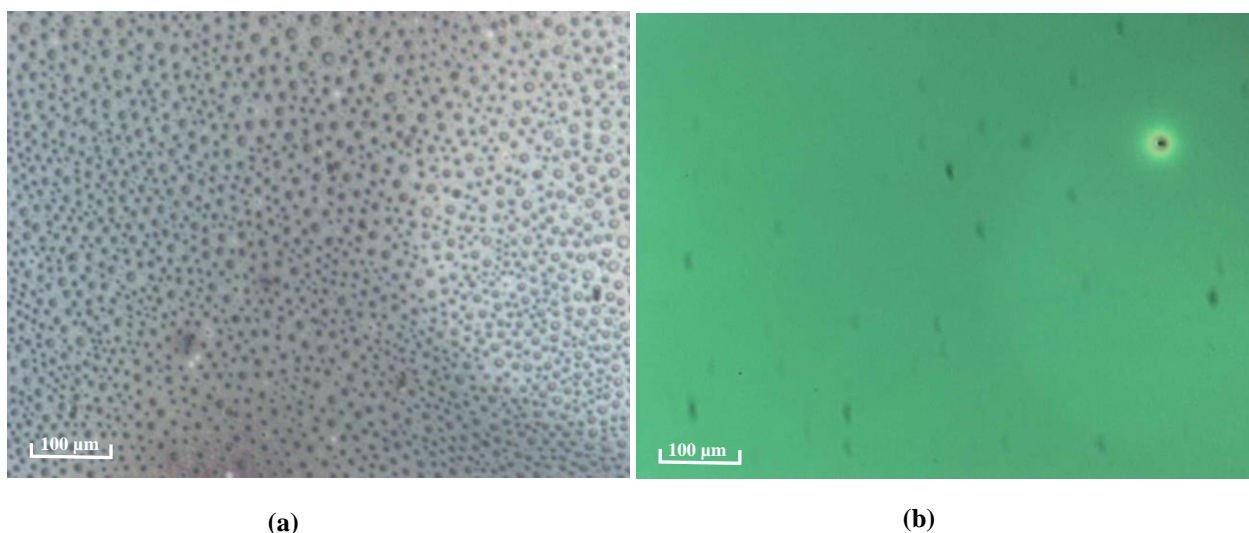
**Figure 3.6 Optical microscope images of PMSQ films in (a) THF shows pinholes on film surface after the deposition process (b) MIBK shows good quality film development during spin coating**

Deposition of polymer films from its solid form, by spin coating is a sophisticated process with a large number of parameters at play. The process was studied and the parameters were optimised to attain reproducibility. Table 3.2 summarises the key findings and process parameters employed to deposit good quality films. The same procedure was followed throughout the project for the deposition of films.

| Solution preparation parameters | |
|---|---|
| Solute weight (MSQ / PMSQ) | 1.0 / 0.75 gm |
| Solvent weight (MIBK) | 5 gm |
| Dissolution time | 1 hour |
| Solution filtration method | Using PTFE syringe filter 0.2 μm |
| **Spin coating parameters** | |
| Spin speed (maximum) | 3500 rotations per minute |
| Acceleration | 180 rotations per second |
| Spin time | 45 seconds |
| **Annealing Parameters** | |
| Annealing temperature | 400ºC |
| Anneal atmosphere | ambient |
| Time duration | 1 hour |
| Cool down period | ~ 4 hours to reach safe handling temperature |
| **Thickness parameters** | |
| Average thickness of deposited films | ~ 450 nm |

**Table 3.2. Table listing the optimised process parameters used for the solution preparation, deposition and annealing of PMSQ and MSQ films used for the experiments**

# 3.3. METHYL SILSESQUIOXANE

MSQ [$(CH_3SiO_{1.5})_n$] [71] is a material that generated great interest because of its dielectric properties and which was investigated in great detail for its use as an ILD in microelectronic manufacturing. FTIR is one of the key characterisation tools used in understanding the molecular structure of SSQs. The absorption region from 1000 – 1200cm$^{-1}$ which is the Si –O –Si stretching, is the significant feature in the spectrum that helps us to identify the material [42]. This can be used as a general characteristic to identify SSQ films as this region is the least affected by the nature of the substituent group. Figure 3.9 shows the major FTIR peaks of the MSQ polymer.
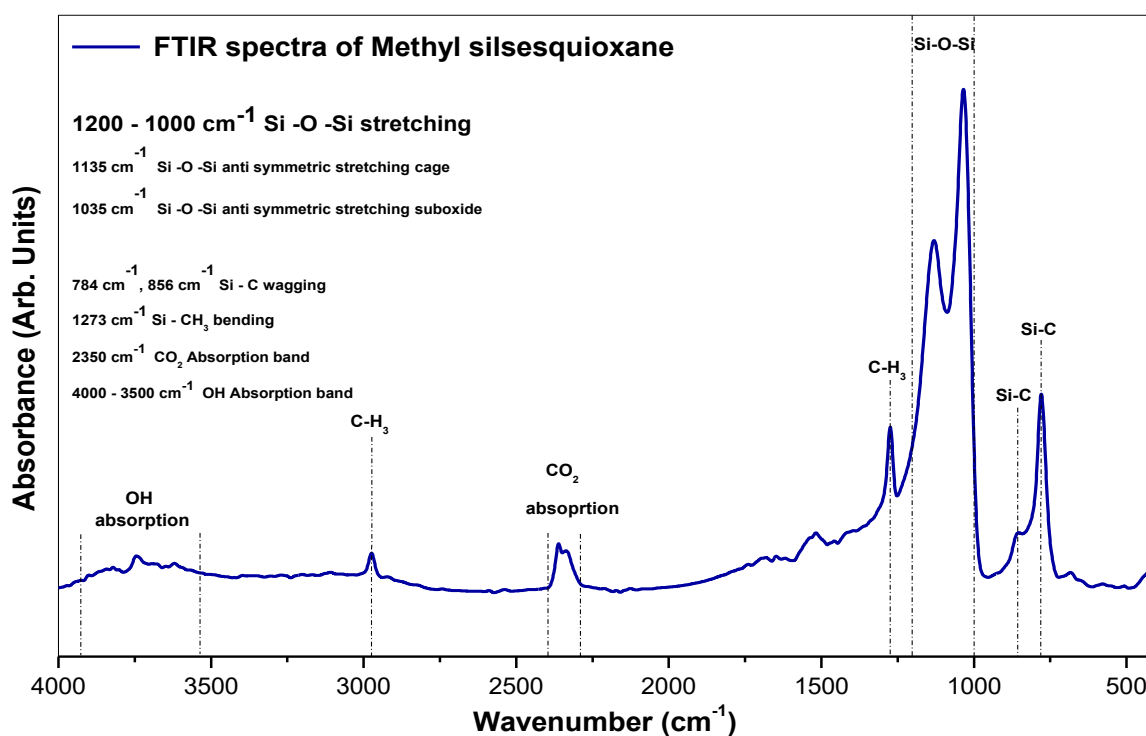


**Figure 3.7. FTIR spectra of MSQ films showing the major absorption peaks**

The broad peak stretching from 1000 – 1200 cm$^{-1}$ shows the Si – O – Si stretching of the spectrum shows the cross linking within the material. The two major peaks in this region are the Si -O -Si anti symmetric stretching cage at 1135 cm$^{-1}$ and Si -O -Si anti

69

symmetric stretching of the suboxide at 1035 cm$^{-1}$. Other peaks in the spectrum include Si - C wagging at 784 cm$^{-1}$ and 856 cm$^{-1}$. The peak at 1273 cm$^{-1}$ indicates Si - CH$_3$ bending. The CO$_2$ absorption band is seen at 2350 cm$^{-1}$. The presence of moisture can be seen in the region between 3500 cm$^{-1}$ and 4000 cm$^{-1}$ which is the OH absorption band.

Figure 3.10 show the spectrum of the MSQ material obtained during various stages of the annealing of the film. The change between the FTIR spectrum of the as deposited film and the FTIR spectrum of the film annealed at 400°C for 1 hour shows the thermal transformation happening to the film during annealing. The high temperature facilitates the cross linking of the polymer to its final form. The spectrum remains unaffected even after annealing the films in 600°C for 1 hour indicating that the material is thermally stable even at this high temperature. All annealing was done in ambient atmosphere.



**Figure 3.8. FTIR spectra of MSQ films as deposited and after being annealed at 400 °C and 600 °C for 1 hr in ambient atmosphere indicating the thermal stability of the films at high temperature.**

An increase in the annealing temperature affects the film integrity leading to degradation of the film. The change that happen in the film at this temperature is clearly evidenced in the FTIR spectrum obtained after heating the films to 700°C for a time duration of 1 hour. Figure 3.11 shows the FTIR spectrum of the MSQ films annealed at 400°C and 700°C. Many of the relevant MSQ peaks discussed in the previous section is absent in the spectrum of the material heated at 700°C signifying a change in the chemical composition of the bulk of the material. This along with the decrease in the peak intensity around the $1000 - 1200$ cm$^{-1}$ region suggests the degradation of the film at this high temperature
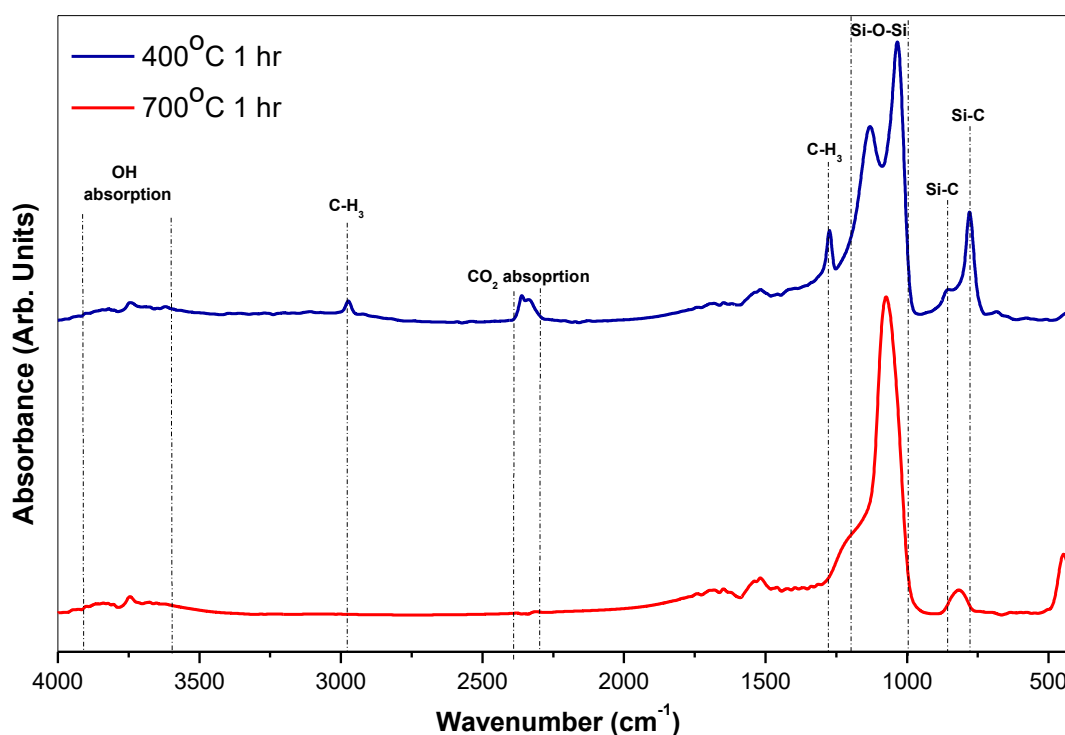


**Figure 3.9. FTIR spectra of MSQ films showing thermal degradation after being annealed for 700 °C for 1 hour in ambient atmosphere**

## 3.4.  DIELECTRIC CONSTANT MEASUREMENTS

A solution with 1.0 gm of MSQ and 5 gm of MIBK was made. The solution was stirred for 1 hour with the magnetic stirrer. The solution was then filtered using PTFE syringe filters. MIM structures were fabricated to measure dielectric constant of the films as explained previously. The dielectric values were calculated from the obtained capacitance values, and were within the range 2.5 – 2.7, well within the low 'k' regime.

## 3.5.  PLASMA EXPOSURE OF METHYL SILSESQUIOXANE FILMS

### 3.5.1. INTERACTION OF MSQ FILMS WITH $O_2$ PLASMA

Low-k films were treated with $O_2$ plasma to understand the modification happening to the films during photoresist ashing. Dielectric materials undergo extensive damage when subjected to $O_2$ plasma exposure during photoresist ashing processes. The function of the $O_2$ plasma is to remove photoresist which itself is an organic material. But when the plasma comes into contact with the ILD material it tends to chemically interact with the material removing carbon from the surface layers and inherently transforming the material to $SiO_2$ kind of structure. This eventually leads to moisture intake thereby degrading the dielectric properties of the film, which significantly increases the k value of the material.

Experiments with $O_2$ plasma were conducted in an Oxford Instruments Plasmalab 80 plus tool. The chamber pressure was set to 100 mTorr, applied forward power was 150 watts and gas flow rate was kept at a constant rate of 50 SCCM. The k value of the MSQ films used for plasma exposure experiments were measured before exposure and were found to be in the order of $2.6 \pm 0.1$.

Figure 3.12 shows the thickness measurements of the MSQ films during O₂ plasma exposure experiments. The thickness data showed no considerable variation in the thickness of the MSQ films before and after O₂ plasma exposure. Thickness measurements were done for as deposited films and after the films were exposed to 5, 10 and 15 minutes of O₂ plasmas. The sample was kept in ambient atmosphere after annealing and between each successive plasma exposures. The figure shows that the measured thicknesses were ~ 615 nm in all cases.



**Figure 3.10. Thickness measurements of MSQ films during O₂ plasma exposure (Chamber pressure: 100 mTorr, Applied forward power : 150 Watts, Gas flow rate : 50 SCCM, Exposure Interval : 5 minutes). For thickness measurements see appendix 3.12.**

Figure 3.13 shows the FTIR spectrum of the MSQ films in the as deposited state and after 5, 10 and 15 minutes of plasma exposure. The Si-O-Si peaks stretching from 1000 – 1200 $cm^{-1}$ remains unaffected even after 15 minutes of plasma treatment. This indicates



**Figure 3.113. FTIR spectra of MSQ films during O₂ plasma exposure (Chamber pressure: 100 mTorr, Applied forward power : 150 Watts, Gas flow rate : 50 SCCM, Exposure Interval : 5 minutes)**

that removal of the material is not happening during $O_2$ plasma treatment of the film. A closer inspection of the spectrum reveals the appearance of a new broad peak from ~ $3500 cm^{-1}$ to ~ 4000 $cm^{-1}$ which is the OH absorption region.

Figure 3.14. gives a better view of the FTIR spectrum of the as deposited MSQ film and the film after 15 minutes of $O_2$ plasma exposure. The appearance of the new OH absorption peak is clearly visible in the figure stretching from around ~ 3500 - ~ 4000 $cm^{-1}$ of the FTIR spectrum.
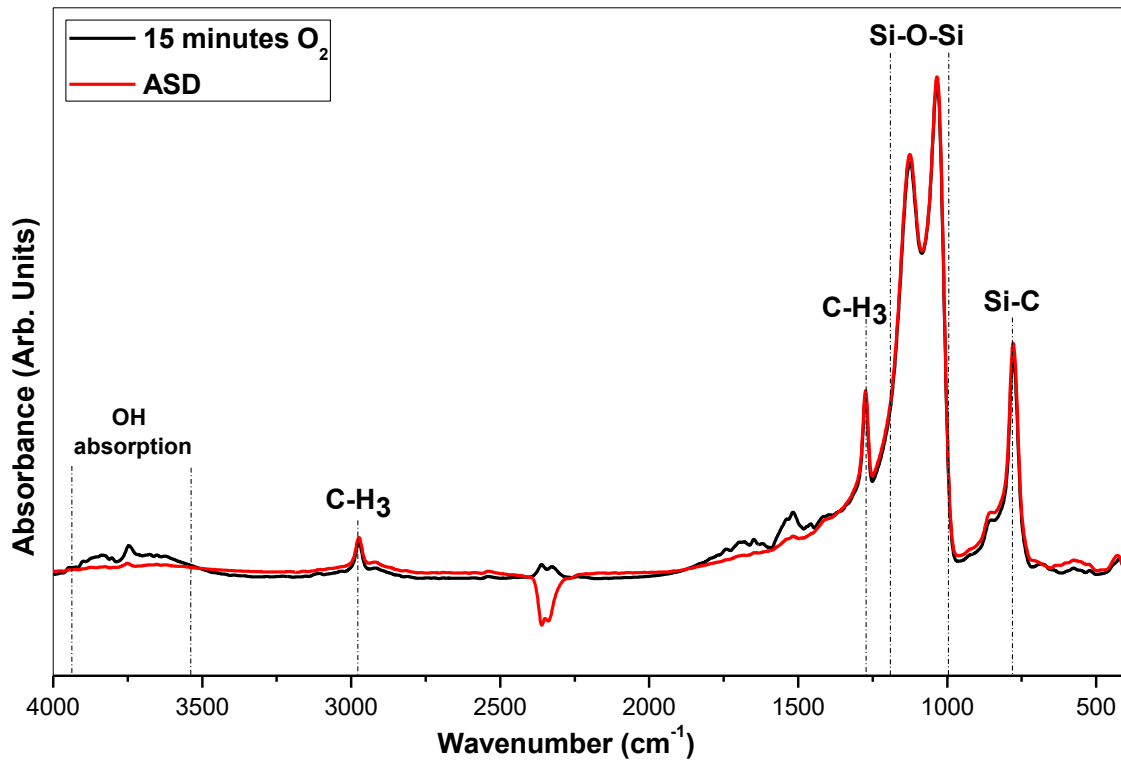
**Figure 3.12. Comparison of FTIR spectra of the as deposited MSQ film and MSQ film after 15 minutes of O₂ plasma exposure. (Chamber pressure: 100 mTorr, Applied forward power : 150 Watts, Gas flow rate : 50 SCCM)**

The $\kappa$ - variation of MSQ films as a function of oxygen plasma treatment time is shown in figure 3.15. The $\kappa$ - value of the as deposited films before plasma exposure was measured to be ~2.6. The $\kappa$ - value increased post plasma treatment as seen in the plot. The duration of plasma exposure also seemed to have an effect on the $\kappa$ - value of MSQ films. The films treated for 5 minutes with oxygen plasma showed a $\kappa$ – value of ~ 3.2 and the films that were treated for 10 minutes showed a slightly higher value of ~ 3.4.

Oxygen plasma removes carbon from the film and transforms the material to a $SiO_2$ like structure. The removal of lesser polarisable C-H and C-C bonds will increase

the κ– value of the film. Again plasma treatment creates dangling bonds on the surface of the material which eventually absorbs moisture [54,72]. This SiOH will in turn increase the κ - value of the film. This moisture absorption can be clearly seen figure 3.15 which shows the FTIR spectrum of the MSQ films pre and post oxygen plasma treatment.
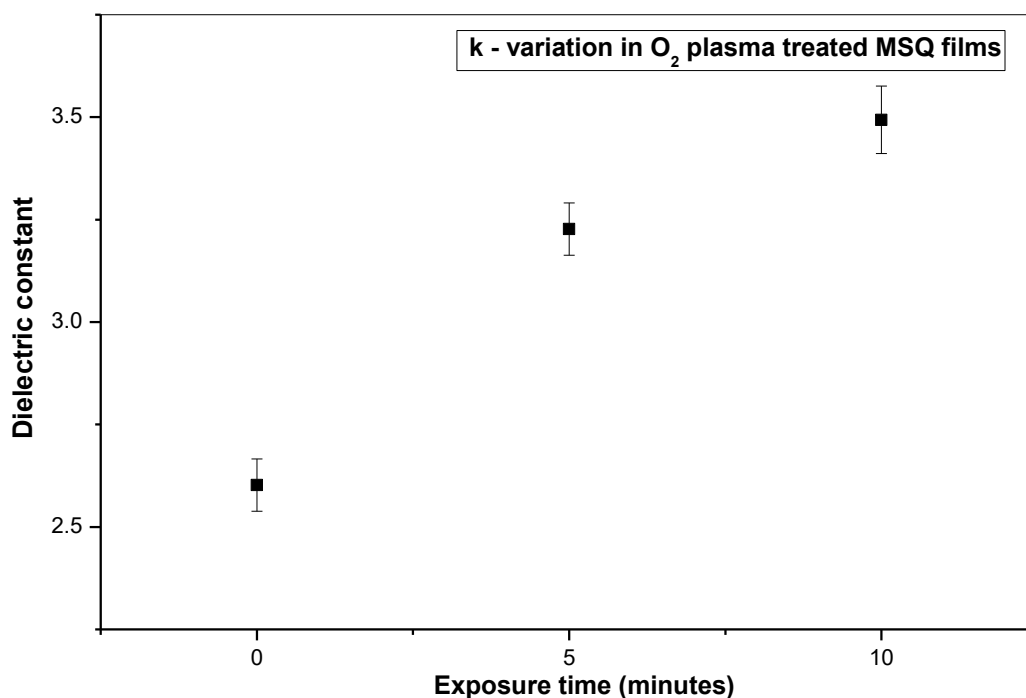


**Figure 3.13. Variation in k-value of the MSQ films during oxygen plasma treatment. (Chamber pressure: 100 mTorr, Applied forward power : 150 Watts, Gas flow rate : 50 SCCM, Exposure Interval : 5 minutes). For thickness measurements, capacitance measurements and k- value calculations see appendix 3.15.**

## 3.5.2. INTERACTION OF MSQ FILMS WITH SF$_6$ PLASMA

As the industry started using copper as the material for interconnects, the dual damascene process became the standard procedure for deposition of interconnects. SF$_6$ plasma plays a crucial role in patterning the ILD material in this process. SF$_6$ is used widely for etching dielectric material, particularly SiO$_2$ and materials with similar chemical composition. This is because F radicals react with Si creating gaseous by

products and thereby etching the material. Even though MSQ is an organic polymer, it is very similar to $SiO_2$ in composition.

Experiments with $SF_6$ plasma were conducted in the Oxford Instruments Plasmalab 80 plus tool using similar parameters to that of the $O_2$ plasma exposure experiments. The chamber pressure was set at 200 mTorr, applied forward power was 150 watts and the $SF_6$ gas flow rate was kept at a constant rate of 50 SCCM. The $\kappa$ - value of the MSQ films used for plasma exposure experiments were measure before exposure and were found to be in the order of $2.6 \pm 0.1$.

Figure 3.16 shows the variation in thickness of MSQ films during $SF_6$ plasma etch. The thickness of the film used for the etching experiments was around ~ 615 nm. The



**Figure 3.14 Thickness variation of MSQ films during SF₆ plasma etch. (Chamber pressure: 200 mTorr, Applied forward power : 150 Watts, Gas flow rate : 50 SCCM, Exposure Interval : 1 minute). For thickness measurements see appendix 3.16.**

thickness was reduced to around ~ 170 nm after etching for 3 minutes in pure $SF_6$ plasma signifying removal of the material during the etching process.

Figure 3.17 shows the FTIR spectrum of the MSQ films that were subjected to $SF_6$ plasma etch. FTIR was done after samples were repeatedly etched at 1 minute intervals. The spectrum shows consistent decrease in the intensity of peaks (figure 3.18) showing the breaking of bonds and removal of material from the film surface, as Fluorine radicals can effectively remove Si and related groups[72]. This is observed by the reduction in the area under the peaks from 1000 – 1200 cm-1 of the spectrum, the Si – O - Si stretching, which is the film backbone.



**Figure 3.157. FTIR spectra of MSQ films during $SF_6$ plasma etching. (Chamber pressure: 200 mTorr, Applied forward power : 150 Watts, Gas flow rate : 50 SCCM, Exposure Interval : 1 minute).**

Figure 3.18 shows a comparison between the spectra of MSQ films after annealing and film after etching with $SF_6$ plasma for 3 minutes. The formation of peak can be seen around ~ 3500 – 4000 cm$^{-1}$ indicating the presence of moisture in the processed film.

The κ variation of MSQ films as a result of plasma processing shown in figure 3.19. It can be seen that the κ – value of the material increased from its original value of ~ 2.65 to ~ 3.1 post plasma treatment.
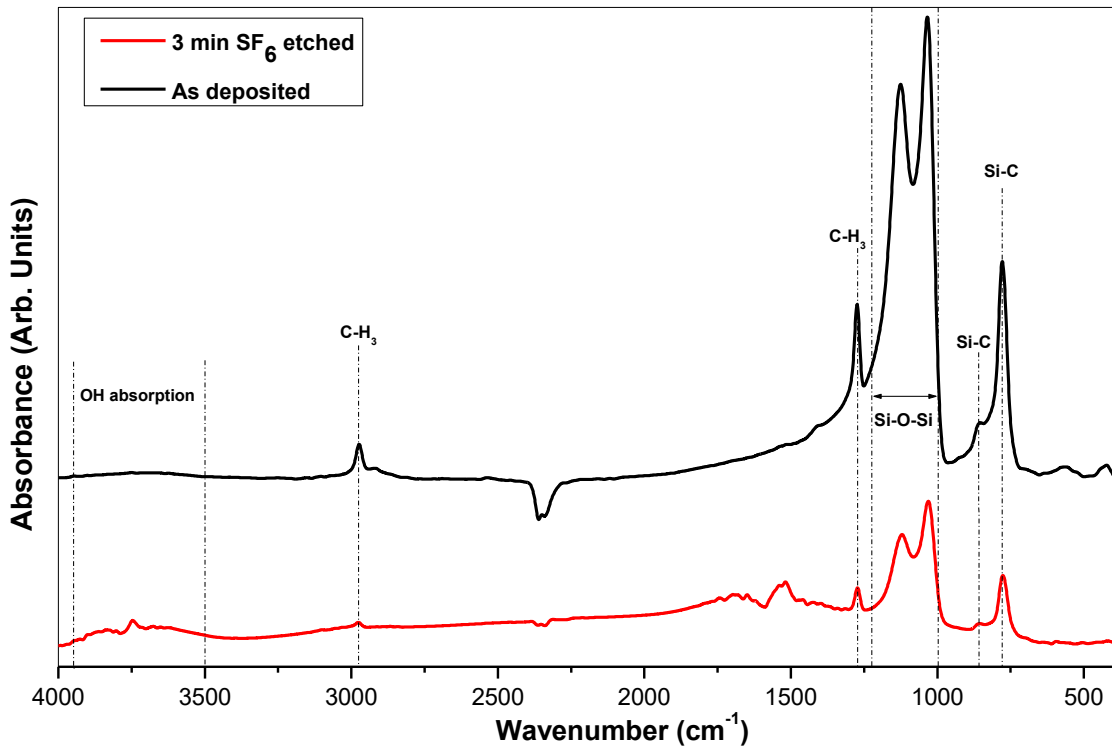


**Figure 3.16. FTIR spectra of MSQ films as deposited and after 3 minutes of SF$_6$ plasma etching. (Chamber pressure: 200 mTorr, Applied forward power : 150 Watts, Gas flow rate : 50 SCCM).**

SF$_6$ plasma treatment leads to fluorine insertion into the film. This results in the formation of a SiOF rich surface, which adsorbs moisture because of the hydrophilic behaviour of fluorine as reported by Treichel et al, [25]. This is also seen in the post processing FTIR spectra of the MSQ films. This moisture absorption leads to the increase in κ - value of the material.



**Figure 3.17. k variation of MSQ films after SF$_6$ plasma etch. (Chamber pressure: 200 mTorr, Applied forward power : 150 Watts, Gas flow rate : 50 SCCM, Exposure Interval : 1 minute). For thickness measurements, capacitance measurements and k- value calculations see appendix 3.19.**

# 3.6. POLY PHENYL METHYL SILSESQUIOXANE

Brown et. al. studied the properties of PhSSQ and reported on the good thermal stability of the material. PhSSQ combines with MSQ namely PMSQ is an SSQ material used as barrier layers in copper chloride based device fabrication [49,50]. The reports explain the use of the material as barrier layers but their dielectric properties and the response of this material to plasma is not studied in detail. Hence it would be interesting to understand the properties of this material in more detail.

## 3.6.1. THERMAL TRANSFORMATION AND FTIR ABSORPTION SPECTRUM OF PMSQ

PMSQ films were deposited using spin coating technique from a solution of the polymer in MIBK. The films were then annealed at $400^o$ C for 1 hr. Thermal annealing is an important step in the formation of the films, which determines the physical, mechanical and electrical properties of the film.

The film structure consists of a mix of cage structure and network structure. A transformation of the material from cage to network structure happens during thermal curing. Figure 3.20 shows the FTIR spectrum of PMSQ films obtained at different temperatures. During the annealing process, solvent loss happens from room temperature up to $200^o$ C. Network redistribution happens between 300 and $400^o$C. The structural transformation of the films is complete after being annealed at this temperature for some time. The films were found stable even after heating at $600^o$ C for 1 hour as none of the peaks in the spectrum show any variation as seen in figure 3.20.
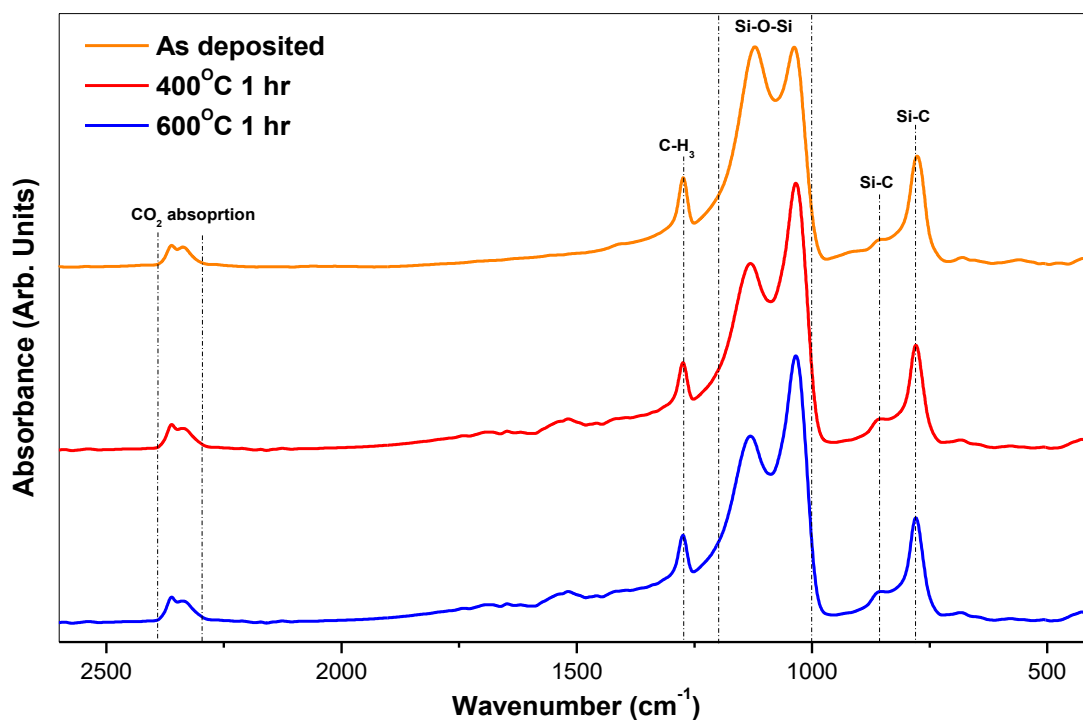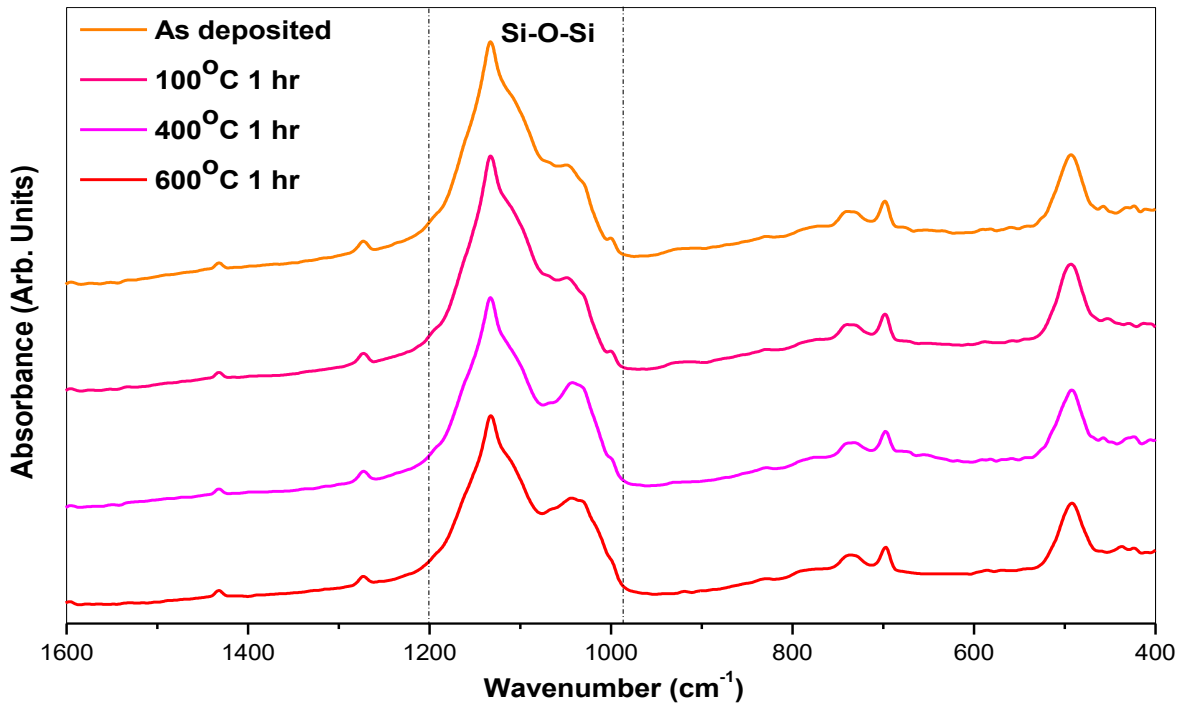
**Figure 3.180 FTIR spectra of PMSQ films as deposited and after being annealed at 100 ºC, 400 ºC and 600 ºC for 1 hr in ambient atmosphere indicating the thermal stability of the films at high temperature.**

The films were annealed at $700\,^{\circ}$C for an hour. It was found that the film degrades at this high temperature as seen in the FTIR spectrum shown in figure 3.21.
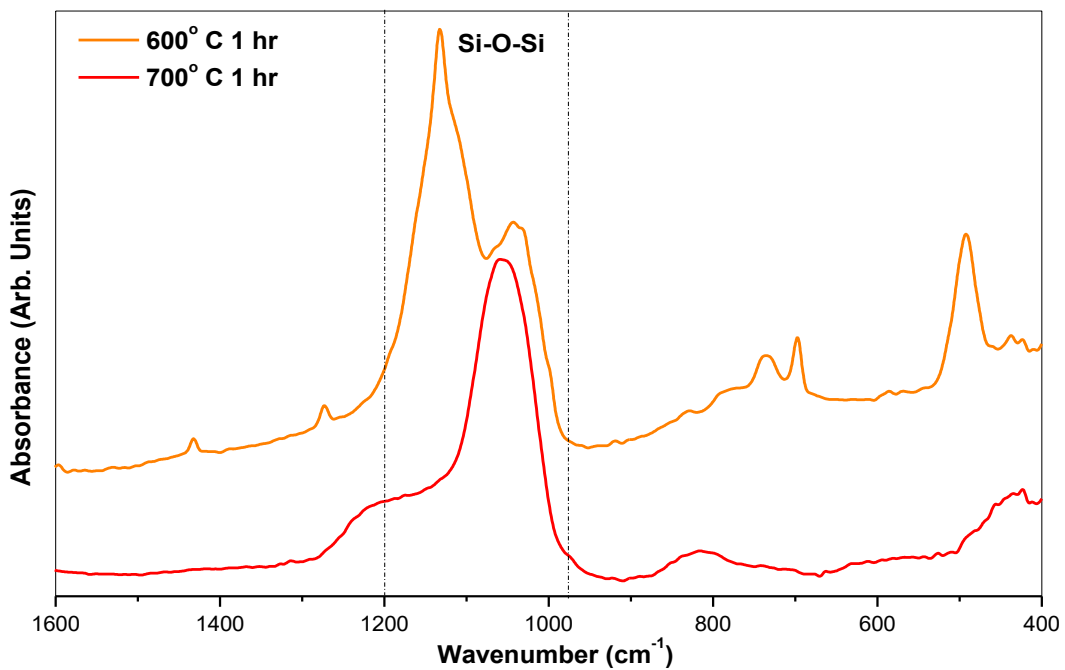


**Figure 3.19. Thermal degradation of PMSQ films after being annealed for 700 ⁰C for 1 hour in ambient atmosphere**

The spectra indicate that there is significant variation in the structure of the material, especially for the Si-O-Si backbone of the film after being heated at 700° C for 1 hour. Figure 3.22 shows the FTIR absorption spectrum of PMSQ films. The total area denotes the sum total of both cage and network structures that are present in the annealed film. The spectra indicate the existence of a sharp band at around 1133 cm$^{-1}$ ($\nu$ ring-asym band)[73] and a broad shoulder in the film cured at 100°C. As the curing temperature increases, the peak around 1043 cm-1 becomes better resolved, which indicates the formation of Si-O-Si bonding involved in low symmetry structures. The film structure consists of a mix of cage and network structures [74] and slight transformation from the cage to network structure happens as the curing temperature increases. The total area denotes the sum of both cage and network structures that are present in the cured film and the structure transformation can be identified by the variation of the area under the peaks at 1132 and 1045 cm$^{-1}$.
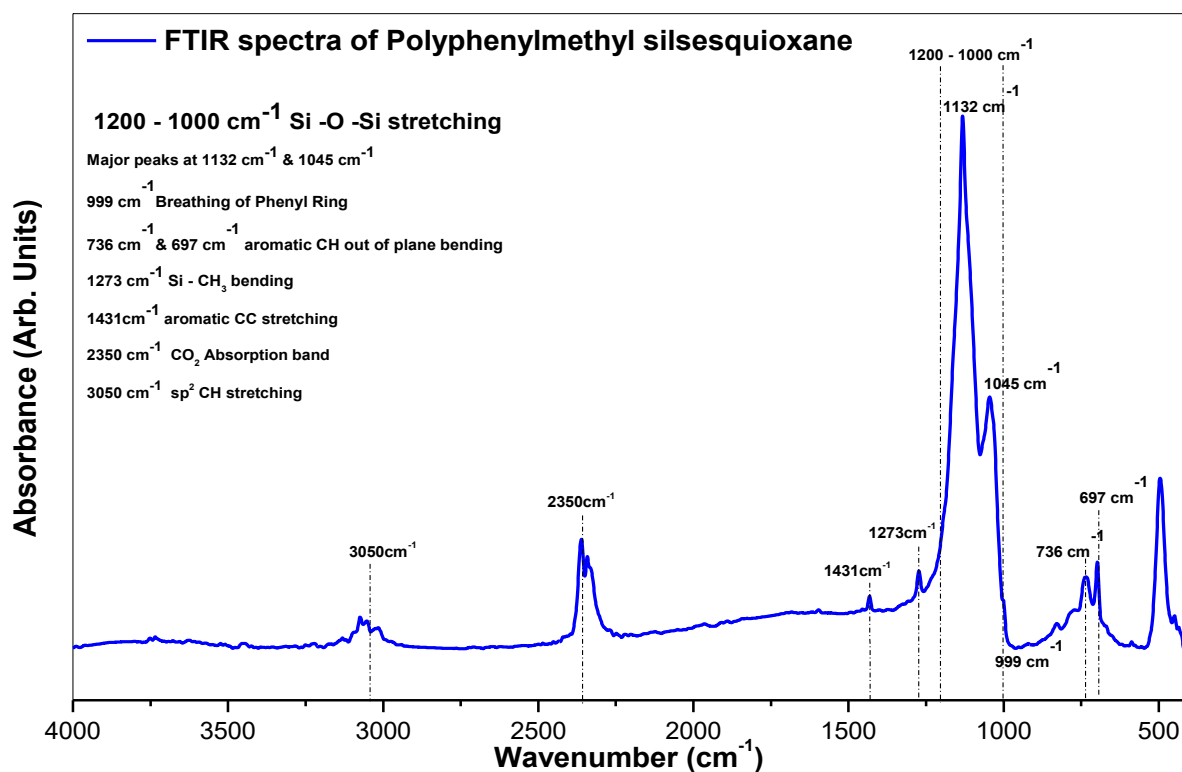


**Figure 3.20. FTIR spectra of PMSQ films showing the major absorption peaks**

It was observed that relatively lower percentage of transformation happens in the PMSQ materials compared to other SSQ materials cured at similar temperatures. Retention of high fractions of the structure without transformation imparts superior thermal withstanding capabilities to the material as reported by Brown et al [43]. The films were found stable even up to 600°C and the FTIR spectrum obtained at this temperature matched with that obtained for films cured at 400°C. This is much greater than the temperatures required for porogen integration and the temperatures that material has to sustain during fabrication.

Other prominent peaks appear in the FTIR spectrum at around 1431 cm$^{-1}$, 736 cm$^{-1}$ and 697 cm$^{-1}$ represent aromatic CC stretching, aromatic CH out of plane bending and phenyl ring out of plane deformation, respectively[75,76]. There is a small broad absorption at around 3050 cm-1 which correspond to the aromatic sp2 C-H stretching vibration.

## 3.6.2. EDX ANALYSIS

EDX analysis of the samples was done after curing. The spectrum in figure 3.23 shows the elemental composition of the film. From the spectrum it can be seen that the major constituents of the films are silicon, carbon and oxygen.
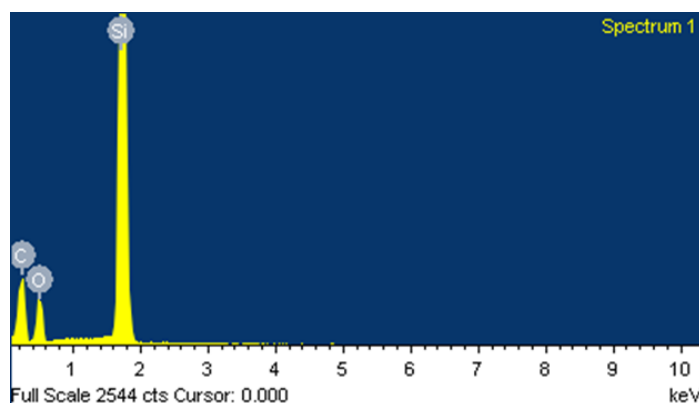


**Figure 3.21. EDX analysis of PMSQ thin films indicating presence of Si, C & O**

# 3.7.  PLASMA EXPOSURE OF PMSQ FILMS

The films were subjected to plasma exposure to investigate the effects of plasma on the films. The effects of $O_2$ plasma and $SF_6$ plasma on the film were studied.

## 3.7.1. INTERACTION OF PMSQ FILMS WITH $O_2$ PLASMAS

Experiments with $O_2$ plasma were also conducted in the Oxford Instruments Plasmalab 80 plus tool. The chamber pressure was set to a very low pressure of 200 mTorr, applied forward power was 150 Watts and gas flow rate was kept at a constant 50 SCCM throughout the experiment.

No significant reduction in thickness of the films were observed during the $O_2$ plasma etch experiments. Thickness measurements were made for as deposited films and for films exposed to 1, 2, 4, 6 and 10 minutes $O_2$ plasmas. The results are plotted in figure 3.24. It was observed that the measured thicknesses were ~ 622 nm in all cases.

Figure 3.25. show the FTIR spectra of PMSQ films pre and post plasma exposure. Pre and post plasma treatment FTIR of the films did not show significant variation in the intensity of peaks indicating no material erosion is happening during oxygen plasma exposure.

The variation of κ - values with respect to oxygen plasma exposure is plotted in figure 3.26. The κ-value of the as-deposited film used was of the order of 2.7±0.2 and no significant variation of κ-values as a result of $O_2$ ash experiments was observed.

Oxygen plasma treatment did not affect the thickness of PMSQ films as evidenced from the spectroscopic ellipsometry measurements. A comparison of the pre and post plasma exposure FTIR spectra did not show any intake of moisture into the material post plasma treatment. There was also no significant variation in the dielectric constant of the material. This is a key advantage of the PMSQ material when compared to so many other
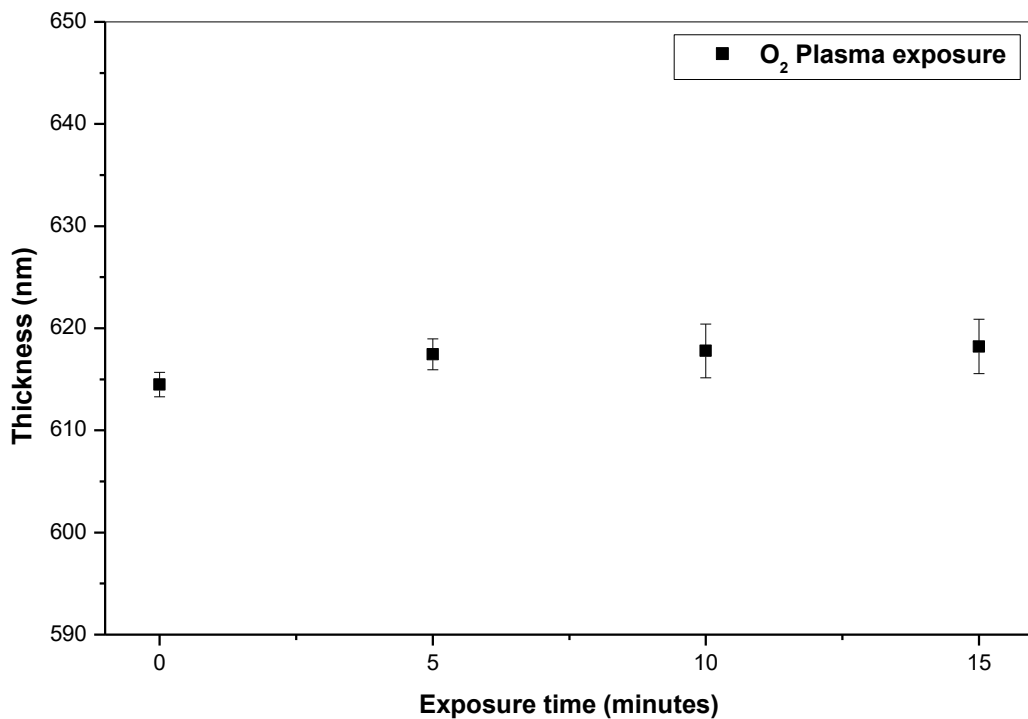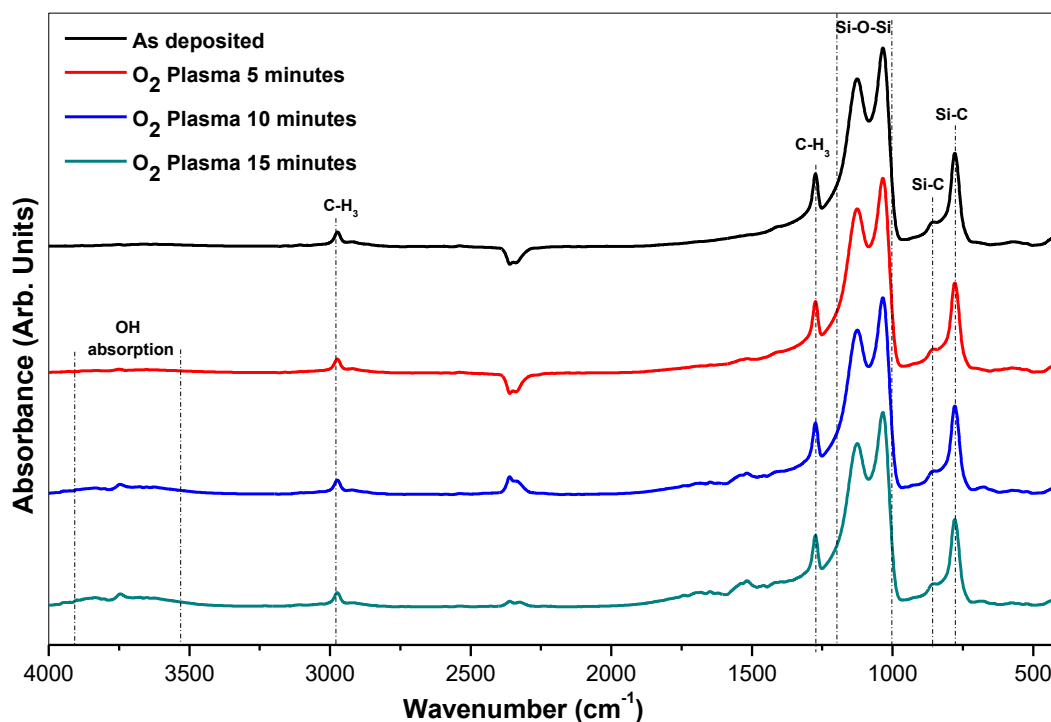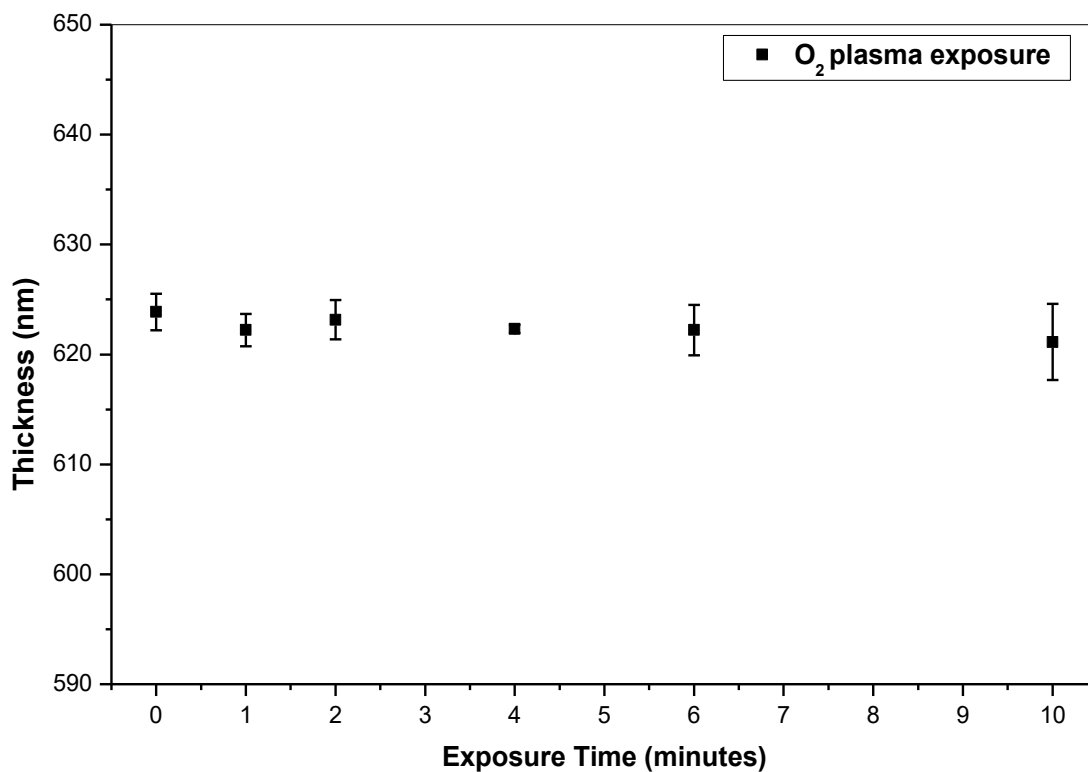
**Figure 3.224. Thickness measurements of PMSQ films during O₂ plasma exposure. (Chamber pressure: 200 mTorr, Applied forward power : 150 Watts, Gas flow rate : 50 SCCM, sample exposed for 1,2, 4, 6 &10 minutes). For thickness measurements see appendix 3.24.**
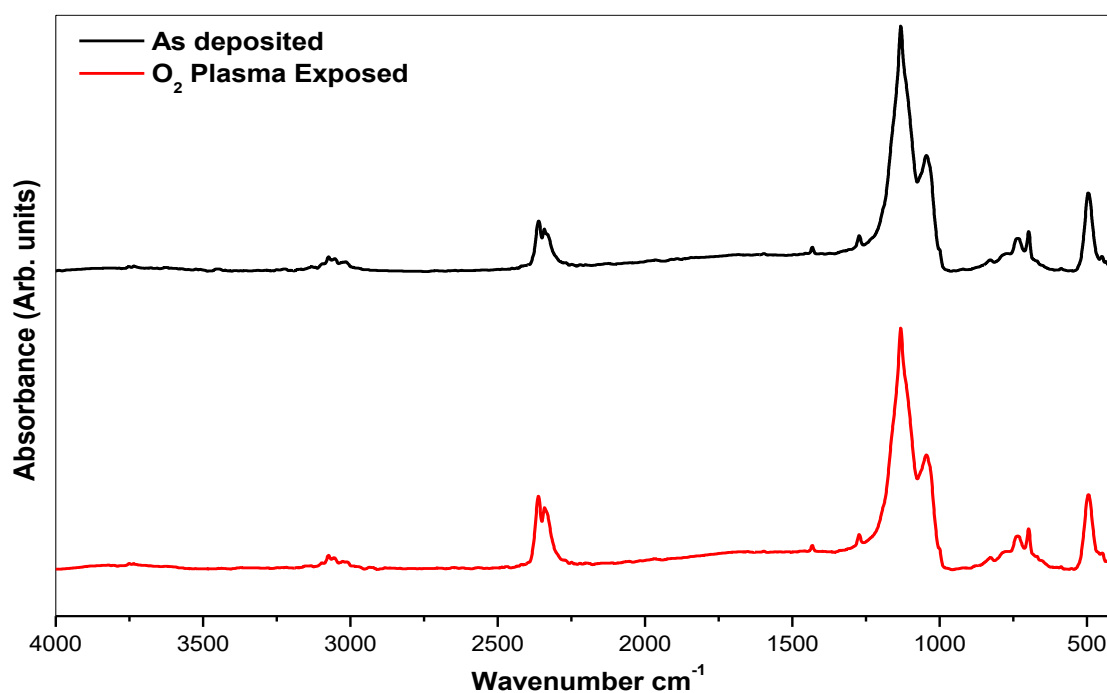


**Figure 3. 25. FTIR spectrum of PMSQ films pre and post O₂ plasma exposure ( Chamber pressure: 200 mTorr, Applied forward power : 150 Watts, Gas flow rate : 50 SCCM, sample exposed for 10 minutes).**

dielectric materials chemically similar to SSQs, as reports show increase in κ - value of these materials after exposure to oxygen plasma. The reported increase in the dielectric constant of some of these materials is shown in figure 6.1. The increase in the dielectric constant of the low-k films after ashing is reported as a major limitation for ILD materials. The higher plasma damage resistance of the PMSQ films could be explained by the inherent stability of the phenyl ring as well as its $d_\pi$-$p_\pi$ contribution in the Si-C bond, which would increase the strength of siloxane polymer [80, 81]
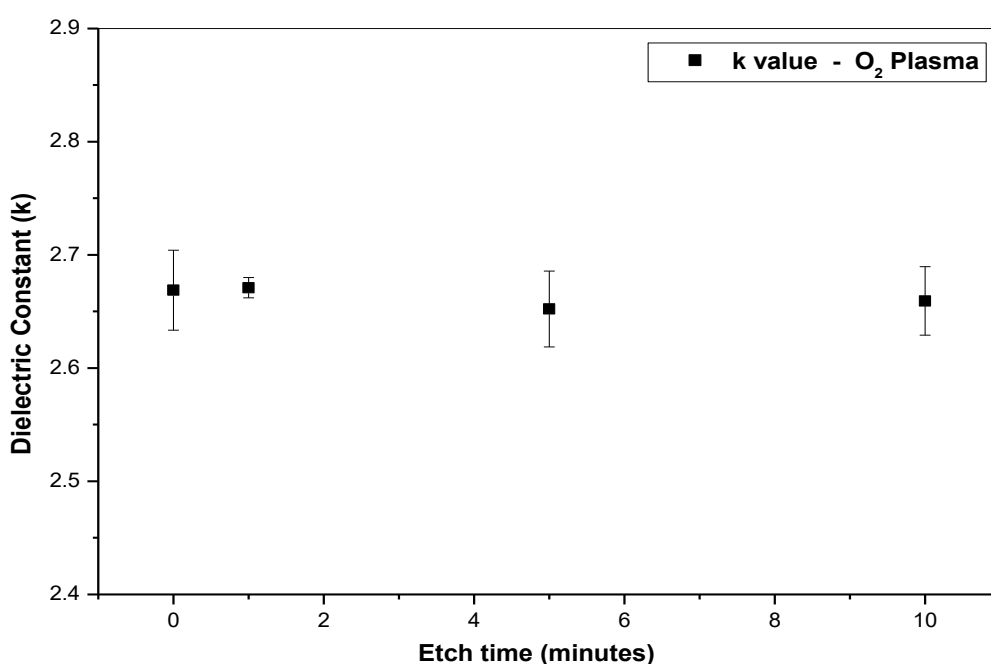


**Figure 3.23. κ – value of films during O2 plasma exposure (Chamber pressure: 200 mTorr, Applied forward power : 150 Watts, Gas flow rate : 50 SCCM, Sample exposed at 1, 5 & 10 minutes). For thickness measurements, capacitance measurements and k- value calculations see appendix 3.26.**

## 3.7.2. INTERACTION OF PMSQ FILMS WITH SF6 PLASMAS

Low-κ films were etched using $SF_6$ Plasma, using Oxford Instruments Plasmalab 80 plus. The κ - value of the pristine films used for $SF_6$ etch experiments were in the order of $2.9 \pm 0.2$. The chamber pressure was maintained at 200 mTorr and the applied forward

power was 150 Watts. The gas flow was kept at constant flow rate of 50 SCCM. Variation in the film thickness, FTIR spectrum and $\kappa$ - values were investigated after plasma exposure of the films.

Figure 3.27 plots the variation in thickness of the PMSQ films as a function of $SF_6$ plasma exposure time. The films were etched for a total of 5 minutes in steps. Thickness measurements were done before etch and after each etching step to determine the etch rate. It was found that the thickness was reduced from its initial value of ~600 nm to ~125 nm after 5 minutes of $SF_6$ plasma exposure. The thickness of the films was falling at a rate of ~ 60 nm/minute and was consistent in all the experiments for the above mentioned plasma parameters.
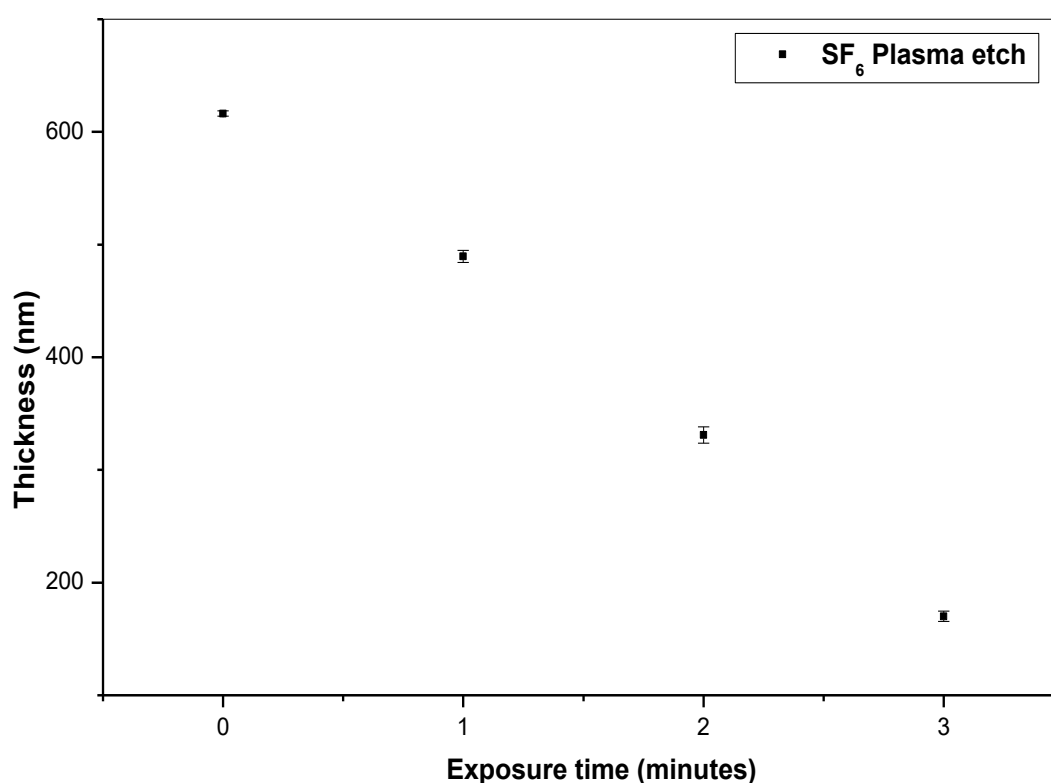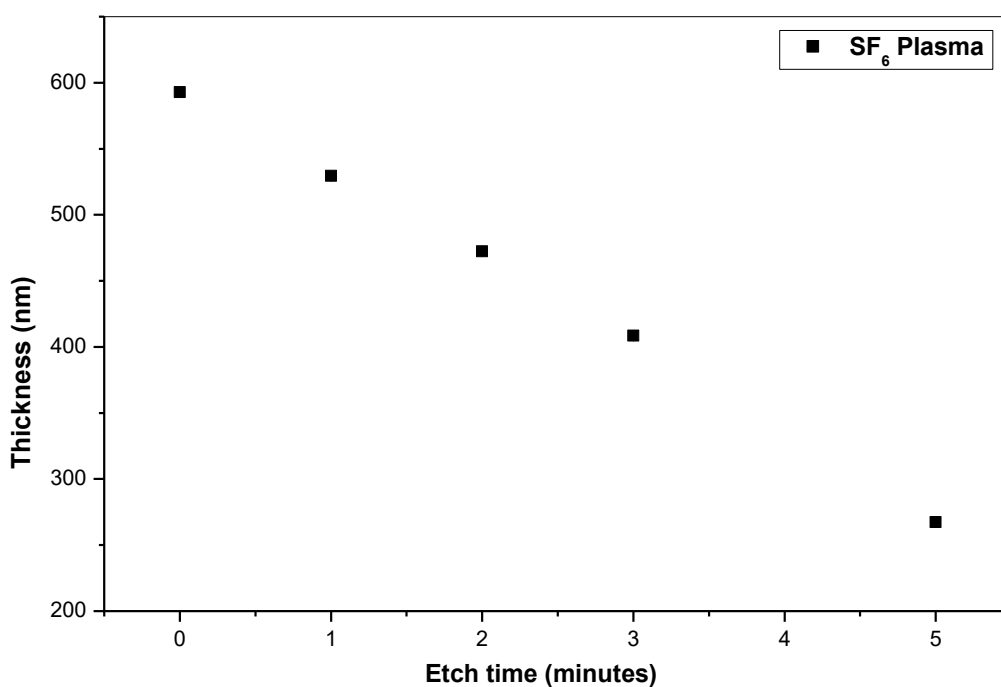


**Figure 3.24. Thickness variation of PMSQ films in $SF_6$ plasma etch. (Chamber pressure: 200 mTorr, Applied forward power : 150 Watts, Gas flow rate : 50 SCCM, sample exposed at 1,2, 3 &5 minutes). For thickness measurements see appendix 3.27.**

FTIR spectra of the PMSQ films were obtained after samples were repeatedly etched for 2 minute intervals with SF$_6$ plasma and the results are presented in figure 3.28. It is clearly seen in the post etch FTIR spectrum that all the dominant peaks are still present, which suggests that the chemical bonding in the material has not undergone significant transformation as a result of plasma exposure. The spectrum shows progressive decrease in the intensity of the peaks showing the breaking of bonds and removal of material from the film surface, as Fluorine radicals can effectively remove Si and related groups [72]. This is observed by the reduction in the area under the peaks from 1000 – 1200 cm-1 of the spectrum, the Si – O - Si stretching, which is the film backbone.
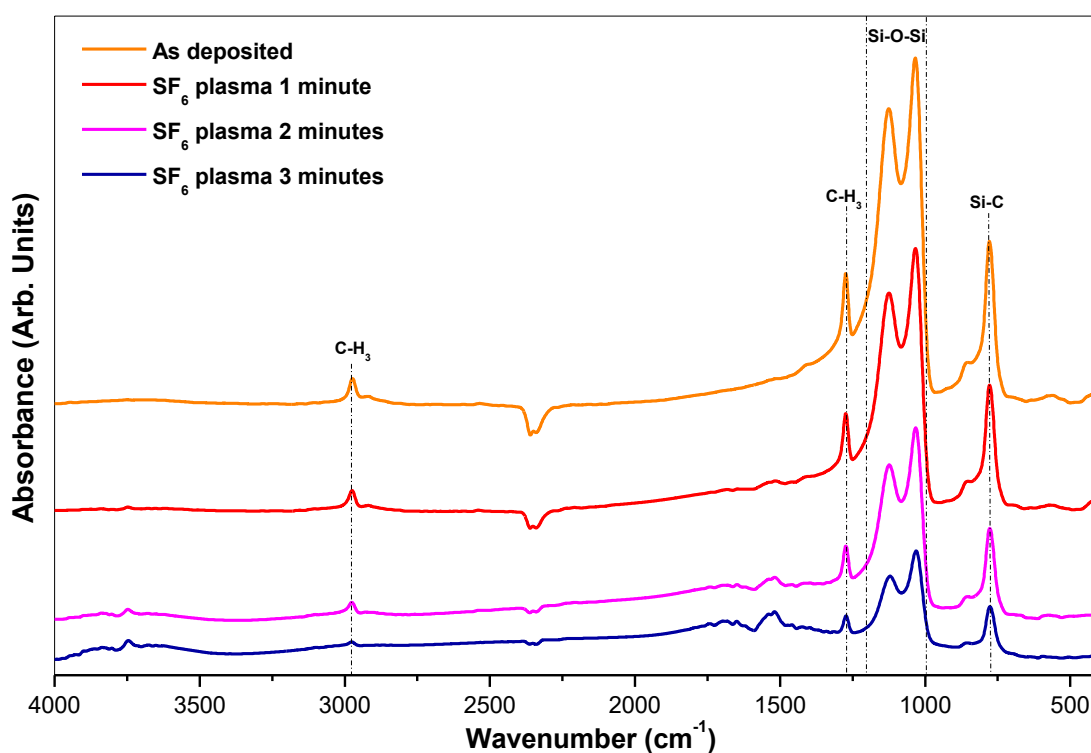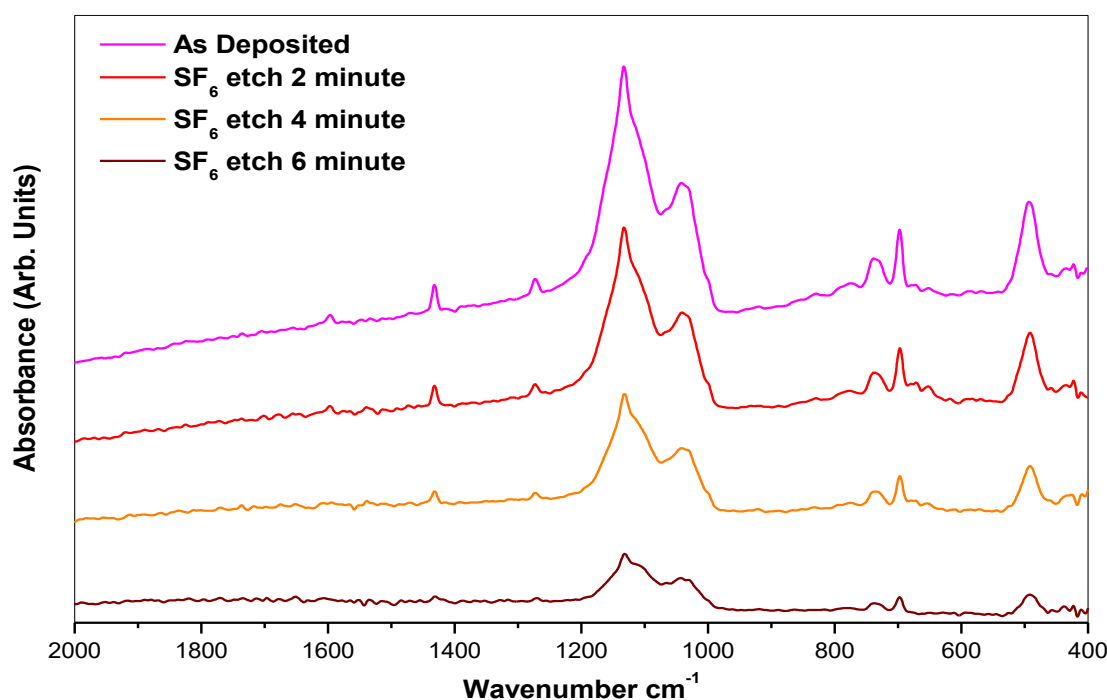


**Figure 3.25. FTIR spectrum of PMSQ films during SF6 etch experiments. (Chamber pressure: 200 mTorr, Applied forward power : 150 Watts, Gas flow rate : 50 SCCM, sample etched at 2 minute intervals).**

κ-values were measured before and after plasma exposures. The κ-values of the as-deposited films (before plasma exposure) were of the order of 2.7±0.2. Figure 3.29 shows the variation of k-value of the films due to $SF_6$ plasma exposure, showing a gradual reducing trend with the subsequent etching steps. The k-value of the as-deposited film decreased from 2.9 to 2.86 after 1 min SF6 etching and then falls to 2.64 after 2 min etch. Variations in the dielectric value of the films were also observed. Measurements showed a gradual reducing trend with the subsequent etching steps. This can be attributed to the introduction of atomic fluorine into the material which is known to reduce the dielectric constant of the material. Similar results has been published by Prado et al. [77]



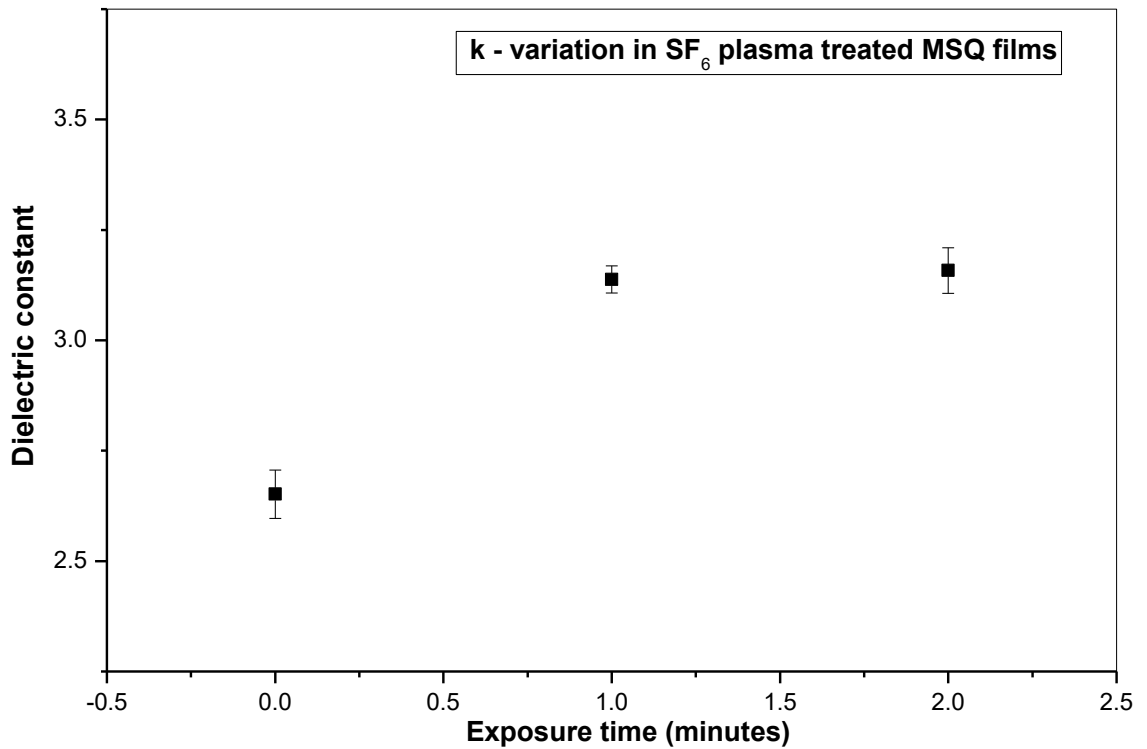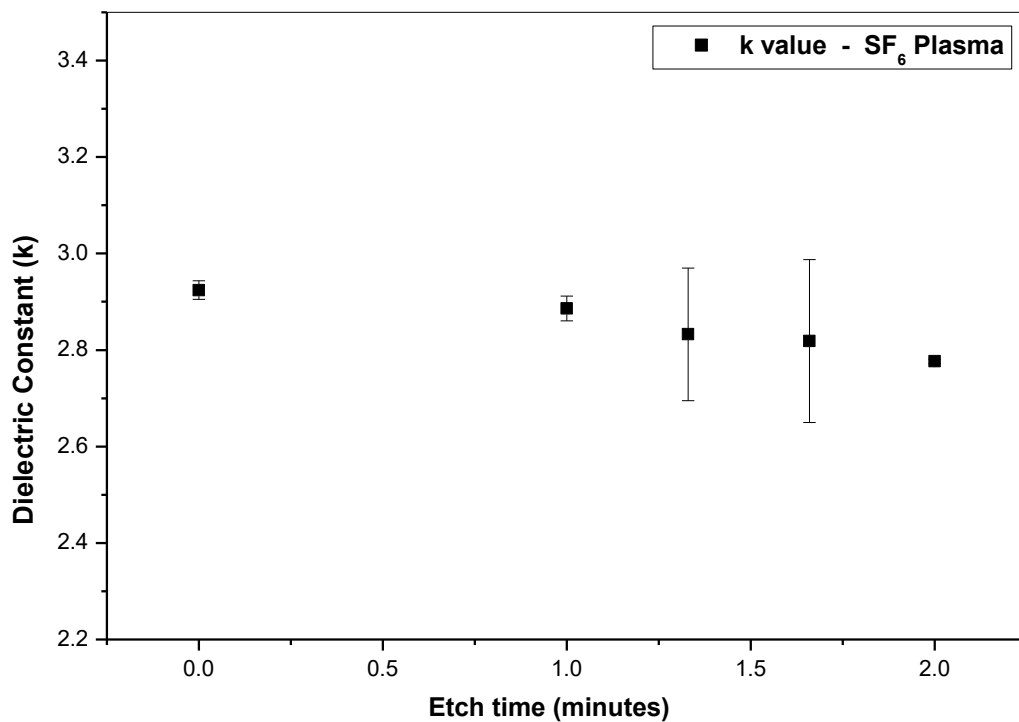**Figure 3.26. k variation of films during SF6 plasma etch. (Chamber pressure: 200 mTorr, Applied forward power : 150 Watts, Gas flow rate : 50 SCCM,  sample etched for a maximum of 2 minutes). For thickness measurements see appendix 3.29.**

### 3.7.3. XPS ANALYSIS OF PRISTINE AND PLASMA TREATED FILMS

Surface modifications of the films due to plasma exposure were studied using XPS. XPS is an ideal characterisation tool, to probe the top few nanometres of the film and to get a precise understanding of the mechanism happening on the surface as a result of plasma exposure. The XPS analysis was carried out using a VG Microtech electron spectrometer at a base pressure of $1 \times 10^{-9}$ mbar. The photoelectrons were excited with a conventional Mg K$\alpha$ (h$\nu$ = 1253.6 eV) x-ray source and an electron energy analyser operating at a 20 eV pass energy, yielding an overall resolution of 1.2 eV. All peaks in the C1s spectra were fitted with a 3:1 ratio of Gaussian and Lorentzian profiles using a Shirely-Sherwood type background. Binding energy positions were consistent with previous studies of C1s peak profiles [78].

XPS measurements were carried out on the samples in order to gain information on the chemical elements present in the sample and the bonding environments for each element. Three samples were studied using XPS, an as deposited film, oxygen plasma exposed film and a $SF_6$ plasma exposed film.

Figure 3.30 shows a series of survey scans from 0 to 1000 eV for each sample under investigation. All three samples show the presence carbon, oxygen and silicon. It can be seen that upon exposure to oxygen plasma, the O1s photoelectron peak grows in integrated area and the C1s peak decreases in area relative to the as deposited film, suggesting that the oxygen plasma has mainly removed the carbon within the top surface of the film. Upon exposure to $SF_6$ plasma, it can be seen that a large fluorine peak emerges in the survey spectra. with an additional change in the C1s bonding state relative to the as deposited film. The presence of fluorine was seen only in the $SF_6$ plasma exposed film.
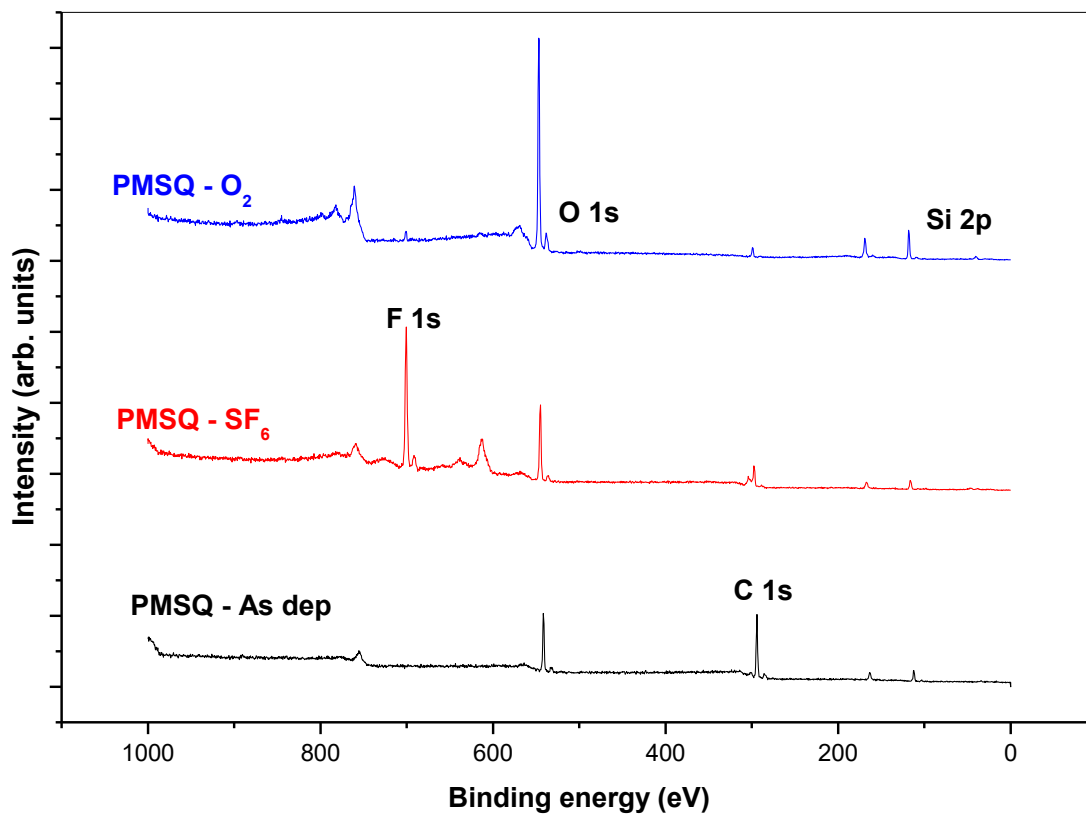
**Figure 3.27. XPS Survey spectra for As Deposited, Oxygen Plasma and SF$_6$ Plasma exposed films showing relative elemental composition of each sample**

Since this is not present in the scan of the as deposited film it is evident that fluorine was incorporated into the films during plasma processing of the films.

Figure 3.31 and 3.32 show O1s, Si2p and C1s peaks respectively, from the XPS spectra of as-deposited and plasma treated films. Both plasma treatments reduce the surface carbon content, implying the removal carbon from the film surface. The Si 2p and O 1s peak profiles remained largely unchanged after both treatments, suggesting the overall Si-O structure remained in-tact as seen in figure 3.31.
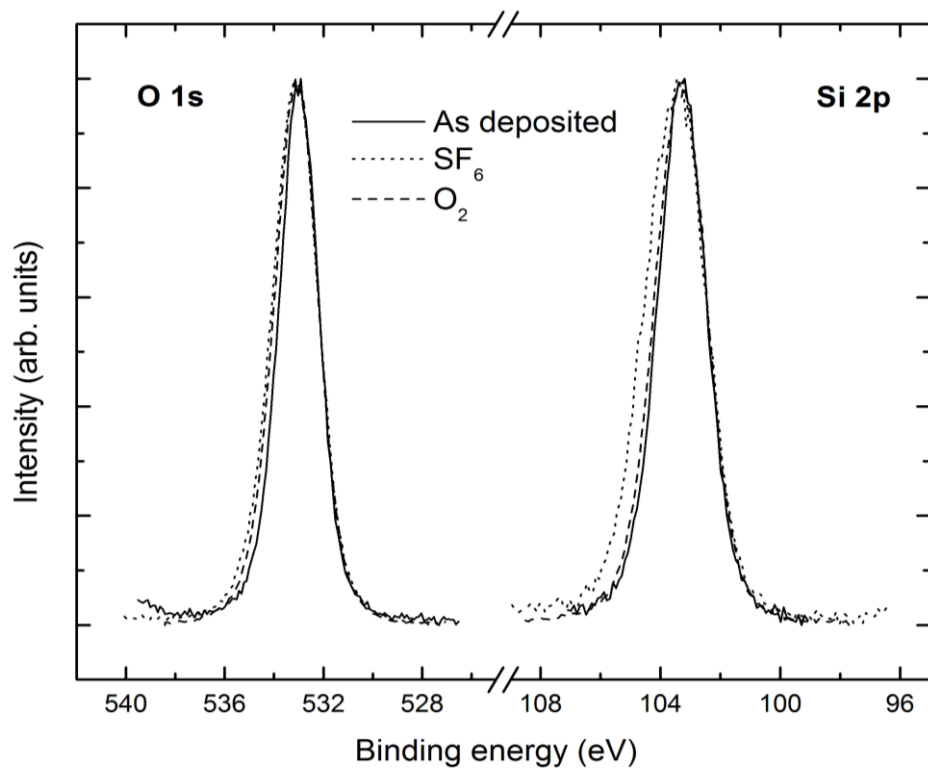
**Figure 3.31. XPS spectra showing O 1s and Si 2p peaks of pristine, SF6 plasma treated and O2 plasma treated Poly phenyl – methyl silsesquioxane films**
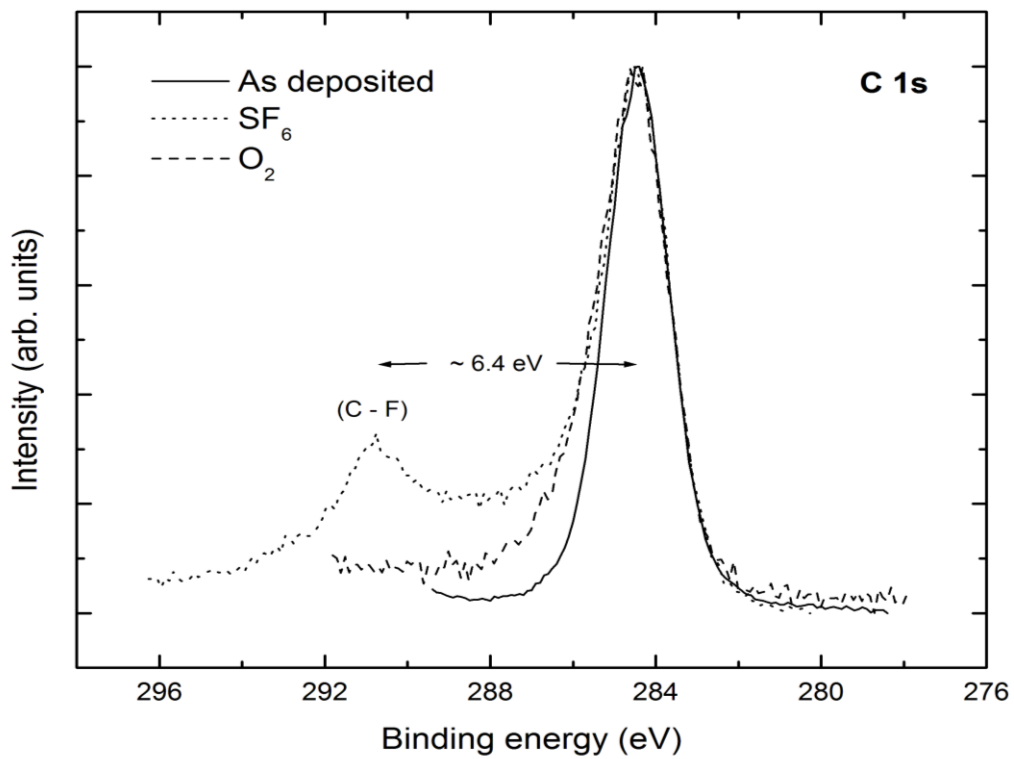


**Figure 3.28. XPS spectra showing C 1s peak of pristine, SF6 plasma treated and O2 plasma treated Poly phenyl – methyl silsesquioxane films**

Any chemical changes that did occur, appear to involve the limited amount of remaining surface carbon, as evidenced by the growth of additional component peaks on the higher binding energy side of the C 1s as seen in figure 3.32. One of these peaks emerges at a binding energy separation of ~ 6.4 eV which is consistent with the formation of C - F bonds due to the significant difference in electronegativity values between H (2.2) and F (3.98).The second, more subtle additional C 1s component peak arises at a binding energy separation of ~ 1 eV, again on the higher binding energy side which may suggest the potential growth of a limited amount of surface carbonate (C - O) species.

## 3.8. EXPOSURE OF PMSQ SAMPLES TO ATMOSPHERE DURING PROCESSING

Samples were annealed in open atmosphere. After an hour of annealing at $400^{\circ}$ C, the oven is turned off. The samples are left in the oven to cool down to ambient temperature as sudden cooling made lead to cracking of the films. This takes 4 hours. During this period the samples are still exposed to open atmosphere. The samples are then taken to perform ellipsometry measurements, which takes another half an hour. Samples are then loaded into the Aluminium evaporator for top contact deposition where κ - measurements are to be made. The samples are usually left overnight in the evaporator in vacuum since the previous steps usually takes up most of the day to reach this far. The subsequent day the contacts are deposited and k- measurements are made. The samples are again in open atmosphere once they come out of the evaporator and all during κ - value measurements. The samples are then plasma treated, thickness measurements done and loaded again into the aluminium evaporator for top contact deposition. Upon deposition post exposure k-value measurement is made. The samples are again out in the open for another 2 hours

maximum between these processing times. From the above description of time delay between successive steps we can see that the sample is exposed to open atmosphere for significant amounts of time. There is a chance moisture from the atmosphere can affect the quality of the films. Hence we need to know how the film properties vary when kept in the open for long periods of time.

## 3.9. AGEING STUDIES OF PLASMA ETCHED FILMS

Ageing studies were conducted on pristine and plasma treated samples, mainly to observe the moisture intake of the films. Fig 3.33 indicates the FTIR spectra of the as deposited and $O_2$ plasma treated PMSQ films as well as those of films aged for 1, 2, 3, and 4 days in ambient atmosphere after plasma exposure, which does not show any significant variation in the $4000 – 3500$ cm$^{-1}$ range which denotes the presence of OH [79] bonds in the material.
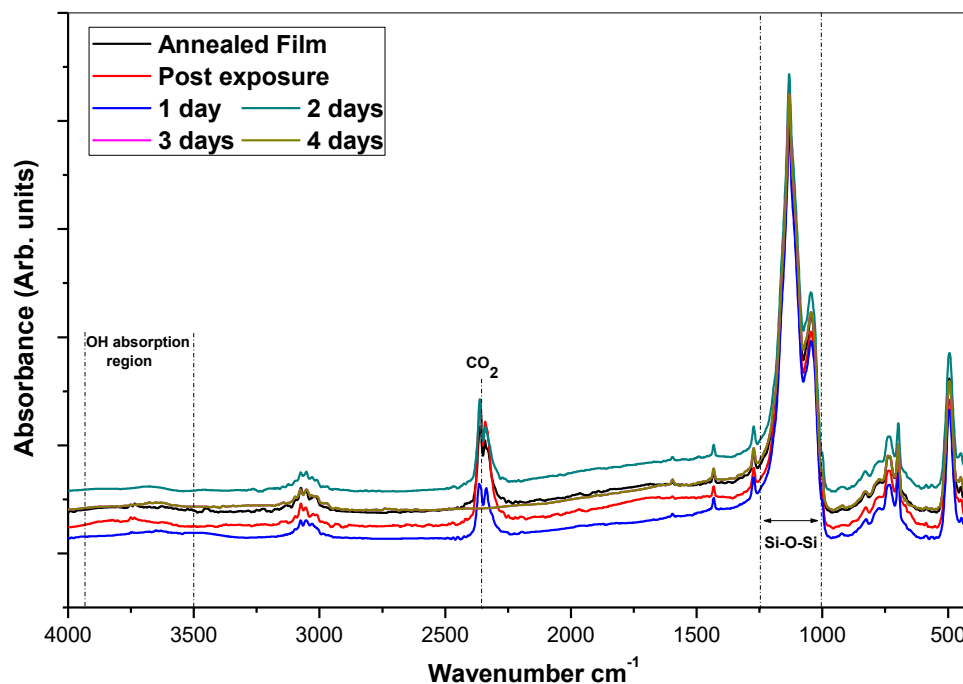


**Figure 3.29. Variation in water contact angle of PMSQ films over a 7 day period**

# 3.10.  SUMMARY

Deposition of polymer films from its solid form, by spin coating was achieved.  It is a sophisticated process with a large number of parameters at play. The process was studied and the parameters were optimised to attain reproducibility. Table 3.2 summarises the key findings and process parameters employed to deposit good quality films. The same procedure was followed throughout the project for the deposition of films.

The deposited MSQ thin films had a $\kappa$ - value of $\sim 2.6 \pm 1$. Significant increase in the $\kappa$ - value was observed upon exposure of these films to $SF_6$ and $O_2$ plasmas due to the deteriorating effect of the plasma on the films. The results from the studies done on MSQ films are in good agreement with the results widely reported. The studies conducted on MSQ films served as a benchmark standard for conducting studies on PMSQ films.

Deposited PMSQ thin films had a $\kappa$ - value of $\sim 2.7 \pm 1$ and they did not show any considerable variation in their $\kappa$ - value upon exposure to $SF_6$ and $O_2$ plasmas, even though significant erosion of the PMSQ film was observed during the exposure of the film to $SF_6$ plasma as it was seen from the thickness measurements and FTIR spectrum post plasma exposure. The FTIR and XPS analysis also did not show any significant change in the chemical state of the PMSQ material at the bulk level or at the surface level. Hence it can be concluded from these experiments that PMSQ has good resistance against the deteriorating effects of the above mentioned plasmas.

# CHAPTER 4

# DEPOSITION, CHARACTERISATION AND PLASMA INTERACTION STUDIES OF POROUS PMSQ THIN FILMS

## 4.1. INTRODUCTION

Incorporation of nano pores filled with air (k = 1.01) [82,83] into the polymer matrix of the thin films is a widely used technique to reduce the k value of thin films This is achieved by the use of thermally labile materials known as porogens, which are removed at high temperatures leaving behind pores within the material [17]. Because of the way in which the pores are integrated into the thin film, this approach is also known as the sacrificial porogen approach.

Introduction of pores within a film will essentially change the characteristics of the film. The ratio of the amount of voids within the material, to that of the total solid volume is known as porosity of the material. Porosity inherently reduces the density of the material. This leads to a corresponding decrease in the total number of dipoles with in the material and hence a corresponding reduction the dielectric constant of the material [13].

For this technique to work either in CVD or in spin coating, the film material and the porogen material should be compatible so that they will form a solution or colloidal dispersion to develop uniform films during deposition. The most important criteria is that the polymer matrix has to harden and strengthen itself sufficiently during annealing

before the decomposition of the porogen material so that the cured matrix will be able to withstand the capillary forces that will arise during the decomposition of the porogen material. Insufficient strengthening will cause pore collapse as the porogen material gets removed during its thermal decomposition [13].

# 4.2. DIFFERENT APPROACHES IN THE SACRIFICIAL POROGEN TECHNIQUE

In the sacrificial porogen approach the morphology of the hybrid film before annealing dictates to a large extent how the final pores morphology would be. The hybrid film morphology may arise because of nucleation and growth, by self-assembly or by templating.

## 4.2.1. NUCLEATION AND GROWTH PROCESS

In nucleation and growth process, the miscibility is promoted by the solvent before, during spin coating and after spin coating soft bake. At this stage much of the solvent is evaporated and miscibility is favoured by the low molecular weight of the porogens as well as the matrix resin. On further heating the matrix resin stiffens due to increase in their molecular weight as a result of condensations and other reactions happening to the resin matrix. The changes within the resin and the accompanying forces during the film curing will lead to a phase separation of the porogen material from the vitrifying resin matrix. This leads to localised formation of porogen clusters within the film. Upon further heating of the film to the decomposition temperature of the porogen, it will result in the formation of the final porous film.

### 4.2.2. SELF-ASSEMBLY TECHNIQUE

Self-assembly technique, as the name implies, makes use of the property of material systems to form spontaneous ordered arrangement of the matrix resin and the porogen material to form the hybrid morphology. Calcination results in the development of ordered and porous films. Both these techniques use both the polymer and porogen that are completely miscible in solvent which can then be deposited as a thin film. The thermally labile material self assembles or nucleates as the solvent removal begins in the film.

### 4.2.3. TEMPLATING

In the self-assembly technique and nucleation & growth technique the porogen has to nucleate or self-assemble during the solvent removal phase or the thermal curing phase of the deposited film. An alternate approach to these techniques is templating, where a fully formed nanoparticulate which is not soluble in the solvent is used as a template for the creation of pores within the film. Cross- linked organic nano particles such as styrene, acrylate, methacrylate derivatives etc., are commonly employed for templating purposes. The polymerisation occurs around these suspended particulates and upon heating to the decomposition temperature; pores are created within the film. The pores in this case will closely resemble the initial structure of the nanoparticulate used.

## 4.3. ISSUES WITH POROGEN INTEGRATION DURING FABRICATION

The reduction in density due to pore generation also affects the integrity of fabricated structures during processing. The reduced mechanical strength can result in increased cracking, tearing and delamination of the film during CMP, reduced adhesion of the dielectric layer, higher penetration of metal ions into ILDs, increase in leakage current

after plasma processing etc., [13,16] . All these issues need to be addressed before porous materials can be used as ILDs for the fabrication of reliable devices.

## 4.4.  POST INTEGRATION POROGEN REMOVAL APPROACH

Many of the detrimental effects that arise due to porosity integration during ILD deposition can be reduced to a large extent by the post integration porogen removal approach.

Figure 4.1 details the post integration porogen removal approach. In the initial stage as shown in 4.1 (a) spin coating and annealing is done to complete the formation of the ILD layer. Because of the use of high temperature porogens, the porogen material remains unaffected during the anneal step. This if followed by fluorine plasma etch to pattern the vias as seen in (b) followed by barrier layer deposition as shown in (c). Deposition of the interconnect metal is the next stage and then followed by CMP. The ILD has a higher mechanical strength during this time since being in the non-porous state. As a final stage of the integration process the porogen is removed by heating the substrate to a high temperature creating porosity within the thin films [84, 85]. A large variety of materials are available that can be used as high temperature pore templates for the introduction of porosity in thin films [40, 41, 86 - 89].
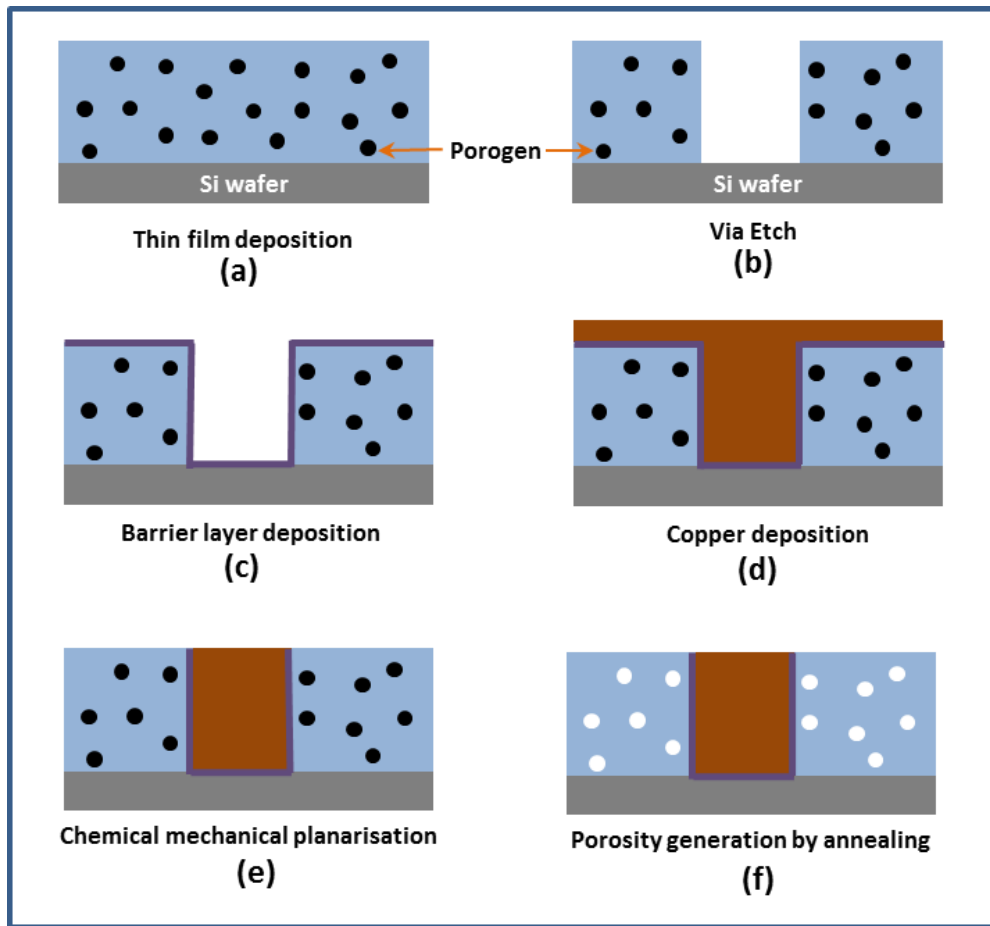
Figure 4.1.Schematic showing post integration porogen removal

# 4.5. INTRODUCTION POROSITY INTO PMSQ THIN FILMS

Spin coating is the deposition technique used in this project. Hence the best suited method of porogen integration into the film would be to introduce it into the film by making it a component of the spin coating solution. This way the porogen material can be spin coated along with the polymer precursor. Figure 4.2 explains the deposition of the hybrid films and generation of porosity within. The first phase would be to create a solution of the polymer with the porogen material in a suitable solvent. This would follow spin coating of the solution on silicon substrates to create the hybrid thin films followed by the final step which would be the thermal annealing of the films beyond the

decomposition temperature of the porogen material for creating pores within the PMSQ thin films.

It is imperative to have a good understanding about SBS and tCD materials to use them as porogens in the project. We will have an in - depth look at the thermal properties and film preparation with these materials.
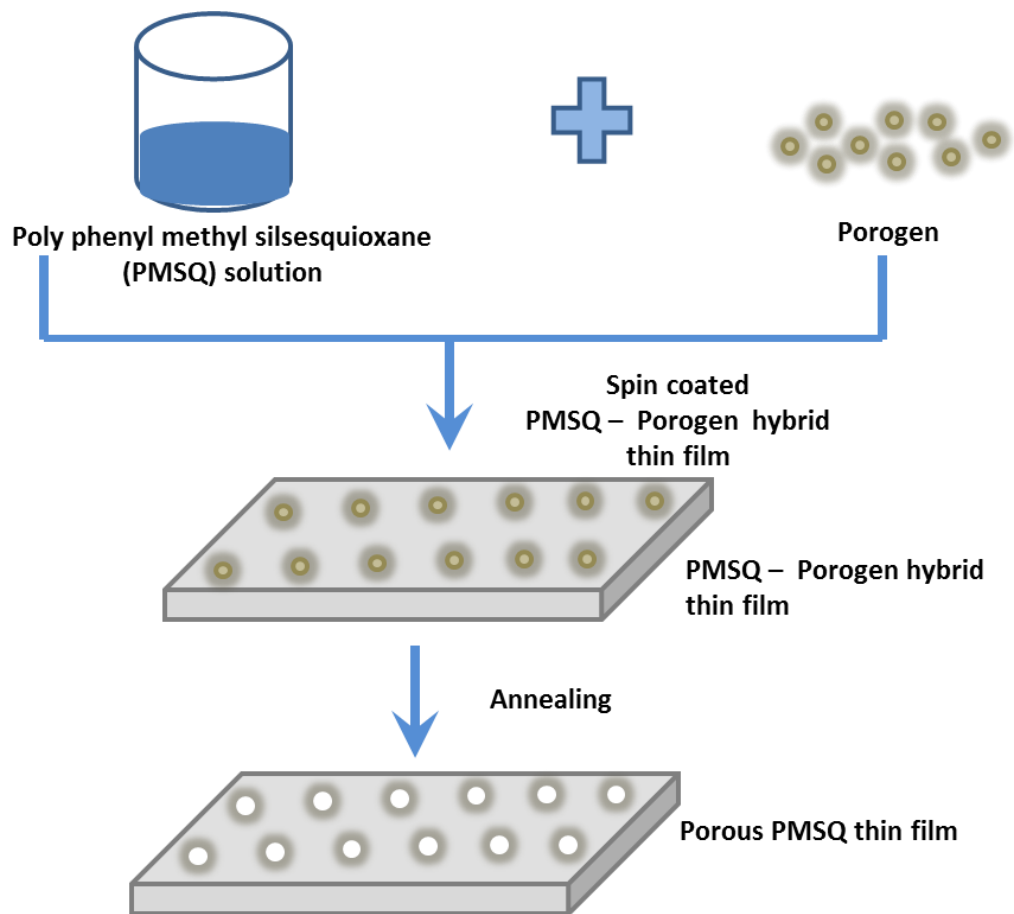


**Figure 4.2. Schematic showing deposition of porous PMSQ thin films**

## 4.5.1. EXPERIMENTS WITH STYRENE-B-BUTADIENE-B-STYRENE AS POROGEN

SBS is a tri block co – polymer with a decomposition temperature of ~ 450$^O$ C. SBS is reported to have good miscibility with MSQ because of its amphiphilic property and thereby avoiding phase separation prior to decomposition during annealing of the hybrid film [70]. Figure 4.3 shows the TGA curve of SBS. It is seen that majority weight loss of the material happens around 450$^o$ C.
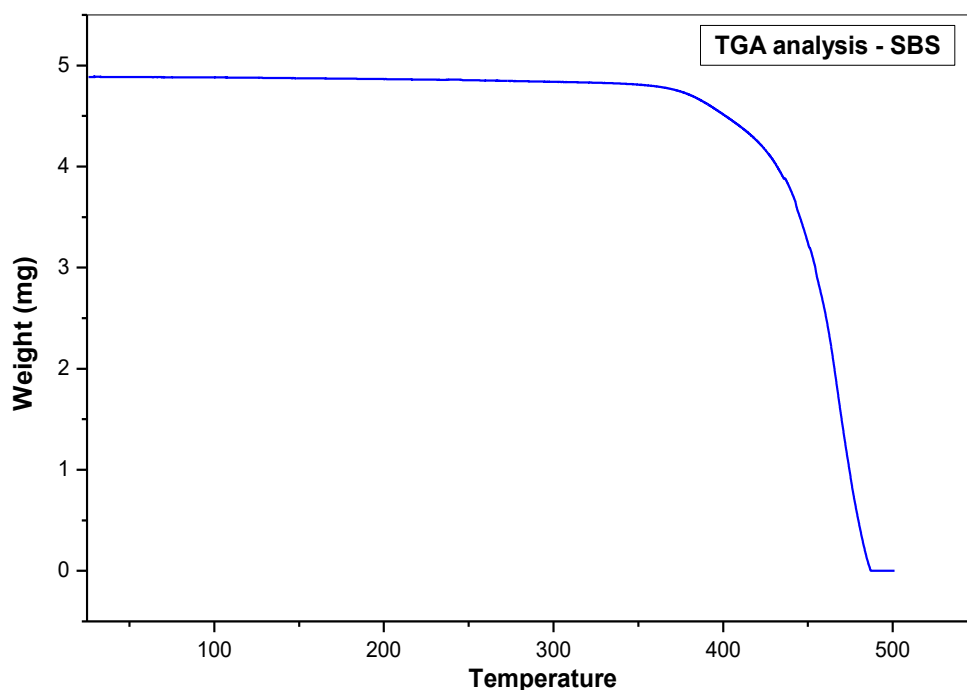


**Figure 4.3. TGA analysis of SBS**

Even though SBS was an ideal candidate for porosity generation in theory, there were solubility issues for the material in MIBK. A solution with 0.75 gm PMSQ in 5 gm of MIBK with 5 % by weight of porogen loading was made. Attempts to filter the solution using 0.2 μ PTFE filter to remove any particulates in the solution failed. It was not possible obtain the filtered solution since the filter got clogged. Hence the solution was

103

spin coated onto silicon wafer without filtering. Figure 4.4 shows an SEM image of the film surface spin coated with the solution. It is possible to see large chunks of SBS spread throughout the spin coated film. This would create macro pores upon annealing which would affect the integrity of the fabricated structure. Since the spin coated film was not of the expected quality, further experiments with SBS were not pursued.
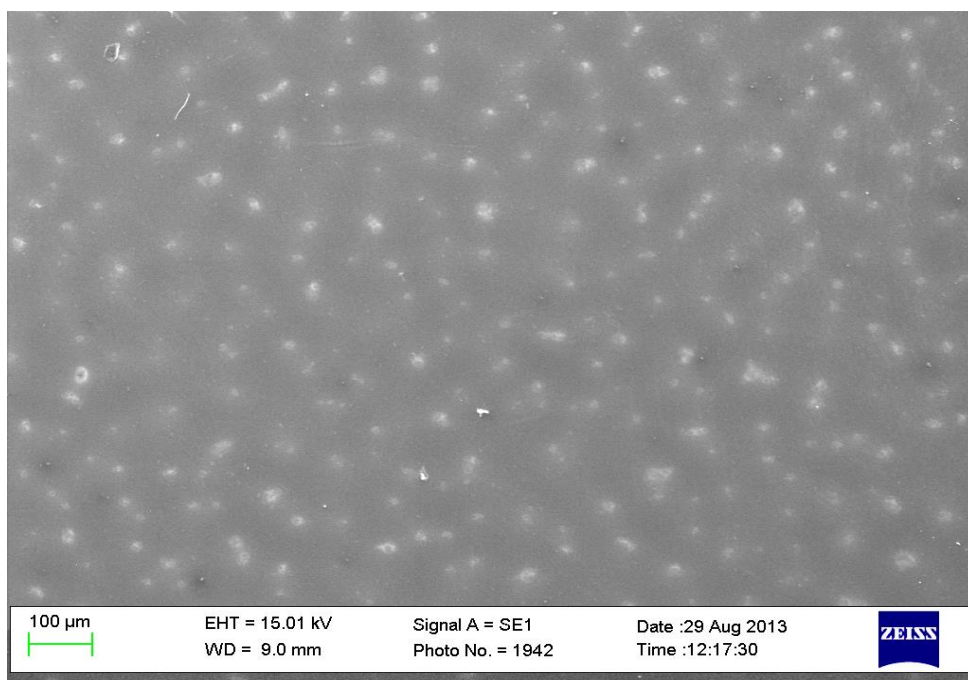


**Figure 4.4. SEM image of PMSQ SBS hybrid film surface**

## 4.5.2. EXPERIMENTS WITH CYCLODEXTRINS AS POROGEN

Cyclodextrins are cyclic oligosaccharides. They were discovered by Villiers in 1891while observing the decomposition reactions of starch by bacteria [90]. There are three well known variants of cyclodextrins. The first one namely α- cyclodextrin contain six glucopyranose units whereas β – cyclodextrin contains 7 glucopyranose units and ϒ – cyclodextrin contains 8 glucopyranose units within their cyclic structure [69,91]. Figure 4.5 shows the structure of cyclic structure of β – cyclodextrin.
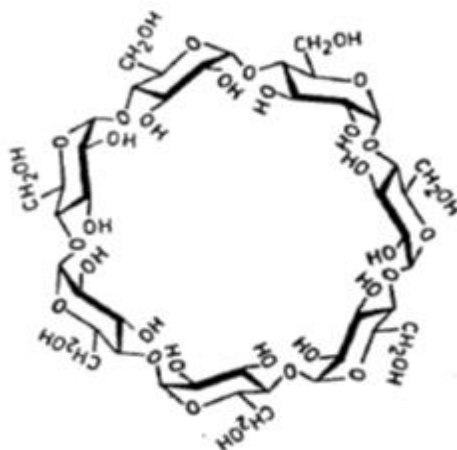
**Figure 4.5. Structure of β – cyclodextrin**

Cyclodextrin compounds can be easily functionalized by modification of their reactive hydroxyl groups [92] . Heptakis(2,3,6-tri-O-methyl)-β-cyclodextrin (tCD) was used as pore template in our experiments as they were reported to compatible with the SSQ matrix resulting in homogenous distribution of pores within the films.[93,94]. Figure 4.6 shows the molecular structure of tCD from Sigma Aldrich that was used as porogen material for introducing porosity into the PMSQ thin films.
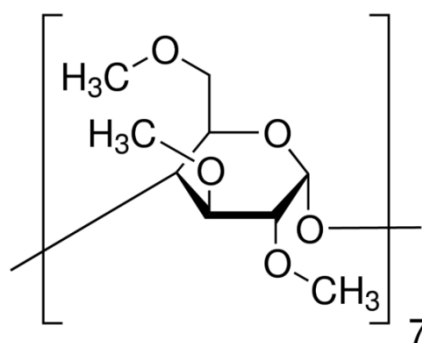


**Figure 4.6. Structure of Heptakis(2,3,6-tri-O-methyl)-β-cyclodextrin (tCD)**

Let us look at some of the key properties of cyclodextrins.

1.      They have a three-dimensional structure and have a small molecular size of ~ 14 – 17 Å [93] .

2.      Cyclodextrins therefore are capable of creating mesopores with pore size of 20Å. They have a narrow decomposition window ($<100^O$ C) with majority weight loss happening between 400 – 425º C [93] as seen in Figure 4.7. The figure shows the TGA of tCD heated to 500ºC at a constant ramp of 20ºC per minute.

3.      This high decomposition temperature ensures that the film maintains its structural integrity during the thermal cross linking of the polymer matrix.

Because of these key properties tCD was considered as pore templates for creation of pores by the sacrificial porogen technique in this study instead of SBS. Again, no published reports are available on the PMSQ - tCD hybrid system, thus making this a novel work.
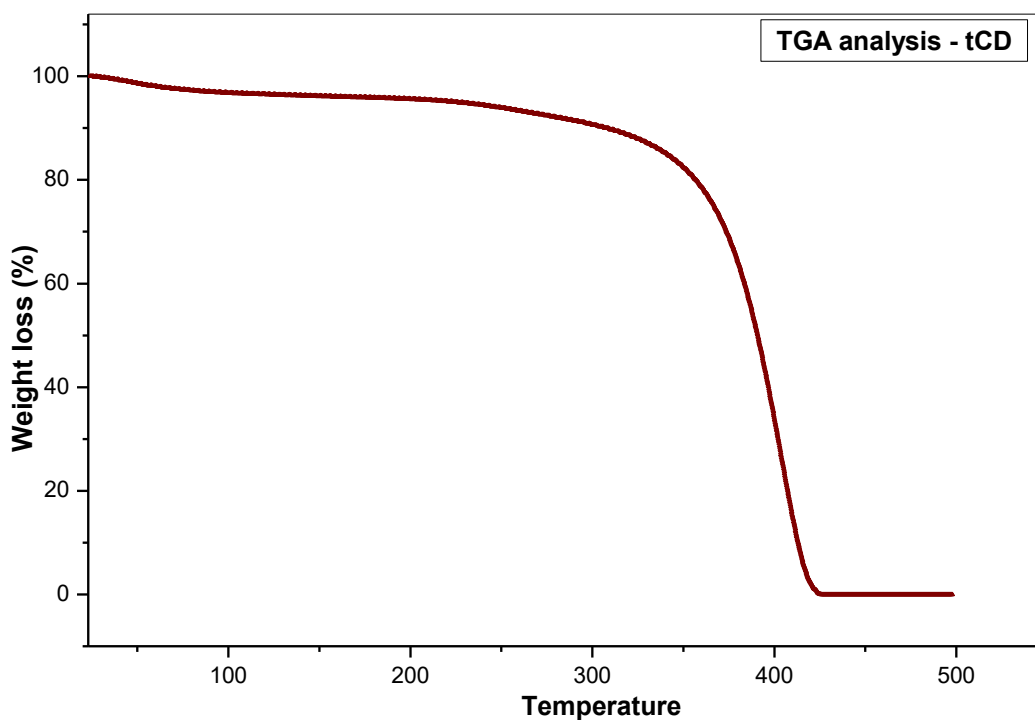


**Figure 4.7. TGA analysis of tCD**

To have a better understanding about the chemical structure of the tCD material and the changes upon anneal, a solution of 0.1 gm of the material in 1 gm MIBK was made and spin coated on piranha etched silicon wafer. The FTIR spectrum of the material obtained post deposition is shown in figure 4.8. Two dominant peaks were observed from 2800 - 3000 cm^{-1} and from 1000-1250 cm^{-1} which are the C-H aliphatic stretching peaks and the C-O-C linkages of the tCD material respectively [93]. Annealing was done in ambient atmosphere.
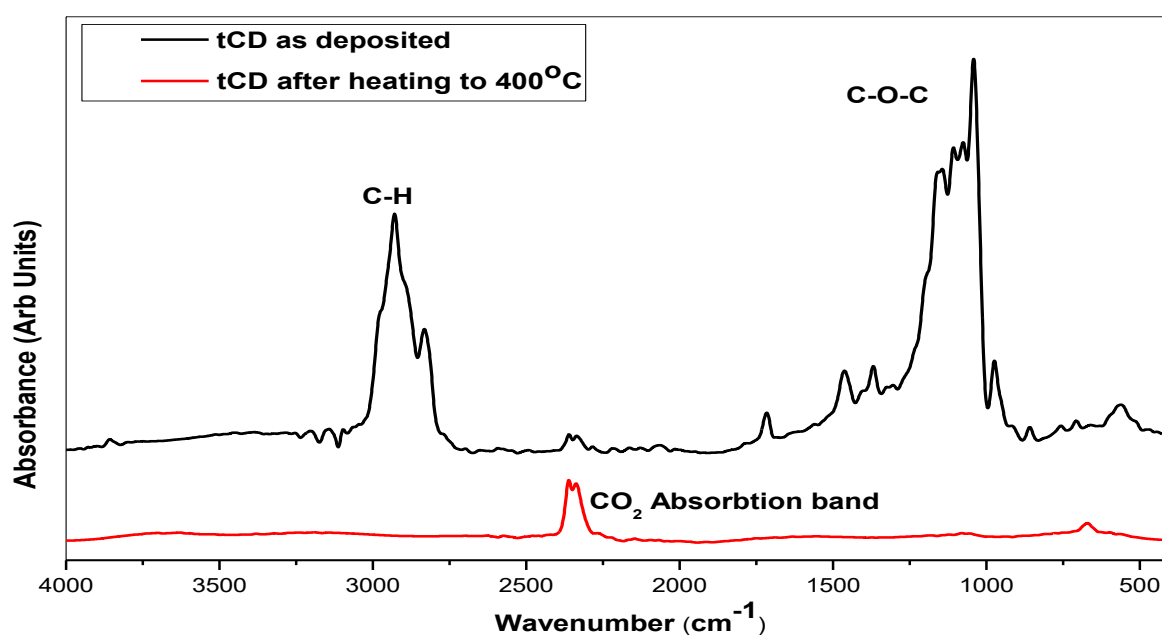


**Figure 4.8 FTIR spectrum of tCD films on silicon as deposited and after heating to 400°C**

The peaks reduce in intensity upon heating and disappear when heated to 400°C indicating the removal of the material from the silicon substrate at this temperature. A small peak present around 2350 cm^{-1} indicates the $CO_2$ absorption band [95].

A polymer solution with porogen (0.75gm PMSQ in 5 gm MIBK with 30 % by wt tCD) was made and spin coated on silicon substrate after filtering.

Figure 4.9 shows the SEM image of spin coated PMSQ - tCD hybrid films. The image does not show any visible agglomeration of the porogen material on the film surface as seen in the case of SBS- PMSQ films. This is an indication of good quality dispersion of the porogen material within the hybrid film. At first look figure 4.8 will look like a blank image, but it appears clear because the film of superior quality.
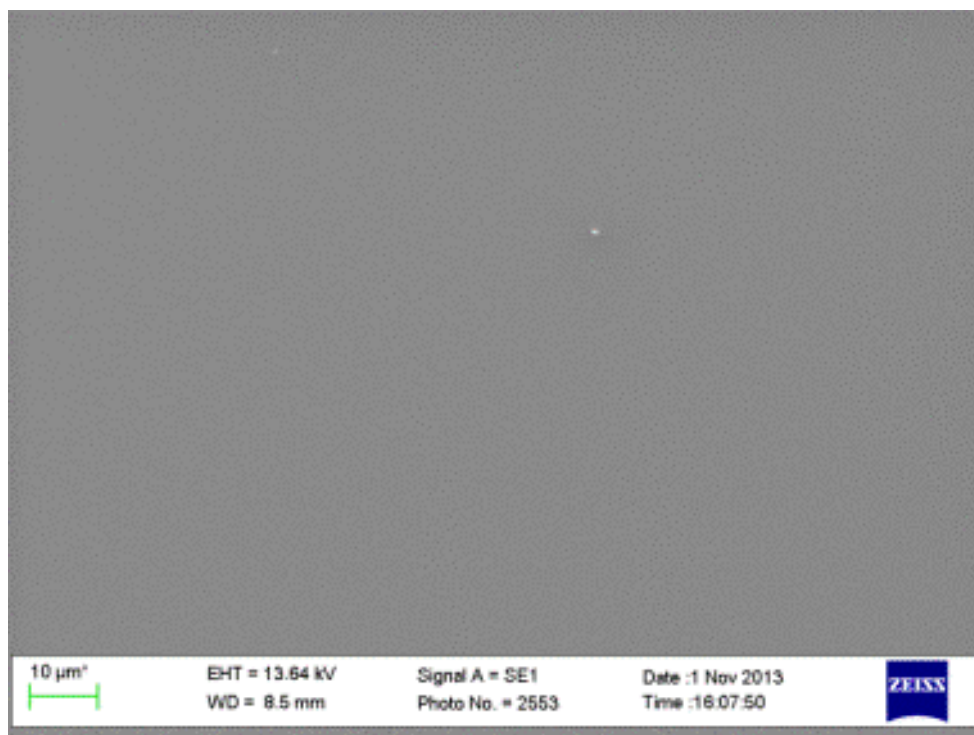


**Figure 4.9. SEM of spin coated PMSQ – tCD hybrid film surface. Compare with figure 4.4. to see the difference in deposited film quality.**

Since there was good repeatability in the film deposition with the PMSQ-MIBK-tCD chemistry all further experiments requiring porous films were done using this particular material chemistry.

# 4.6. THERMAL TRANSFORMATION OF PMSQ-tCD THIN FILMS

A solution of the PMSQ polymer (90% phenyl and 10% methyl) was obtained by dissolving the polymer in methyl isobutyl ketone (MIBK) to deposit the non-porous (normal) films. For the preparation of tCD – PMSQ hybrid samples, tCD was added to the solution mixture, with weight ranging from 0% to 45% of the polymer weight. The solution was stirred overnight and filtered by PTFE syringe filters before being spin coated onto piranha etched silicon substrates. The coated substrates were then annealed in argon at different stages, starting at a temperature $200^{o}C$ for 10 minutes for solvent evaporation. The temperature was held at $380^{o}C$ for 10 minutes to facilitate cross linking of the material upon which the temperature was ramped up to $450^{o}C$ and held for 1 hour for porogen removal in Ar ambient.

Figures 4.10 shows the FTIR spectrum of the pre - and post - annealed PMSQ - tCD hybrid films. The C –H aliphatic stretching bands of tCD were observed from 2800-3000
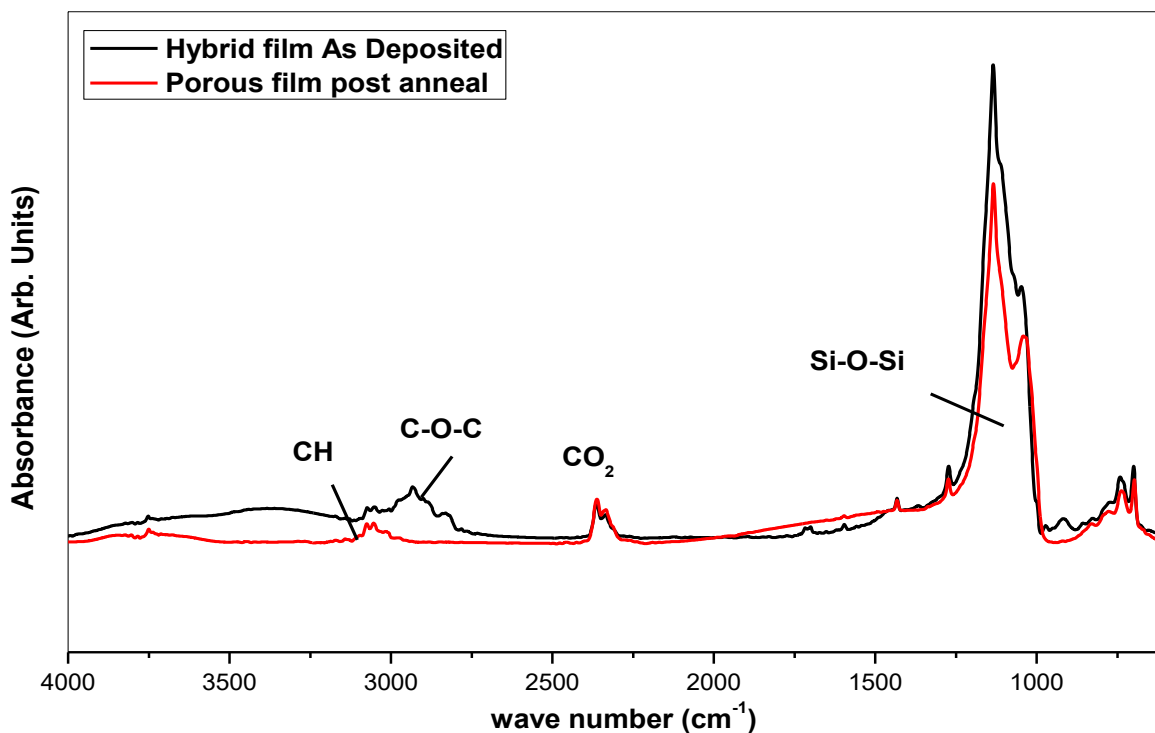


**Figure 4.10. FTIR spectrum of hybrid PMSQ – tCD as deposited and after annealing**

cm[-1] in the spectrum for the hybrid film[96]. The C-O-C linkages were not observed as such as they overlap with the Si – O –Si stretching of the PMSQ material which is seen from 1000 – 1200 cm^{-1} [42]. A reduction in these peak intensities along with the disappearance of the aliphatic stretching peaks in the post-annealed films clearly indicates the removal of the tCD material from the hybrid film after annealing. The spectrum also shows the overall variation in the area under the peaks from 1133cm^{-1} and 1043 cm^{-1} showing the transformation of the PMSQ matrix to its final cage and network structure during thermal annealing [43,74,97]

TGA data of both normal and PMSQ – tCD hybrid films (30 % porogen w.r.t polymer weight).are shown in Figure 4.11. It is seen that there was no considerable weight loss for the PMSQ thin films upon annealing. A slight drop in the weight of the PMSQ- tCD hybrid films relative to that of the normal PMSQ thin films indicates the evaporation of the porogen material. The temperature at which the weight loss happens exactly coincides
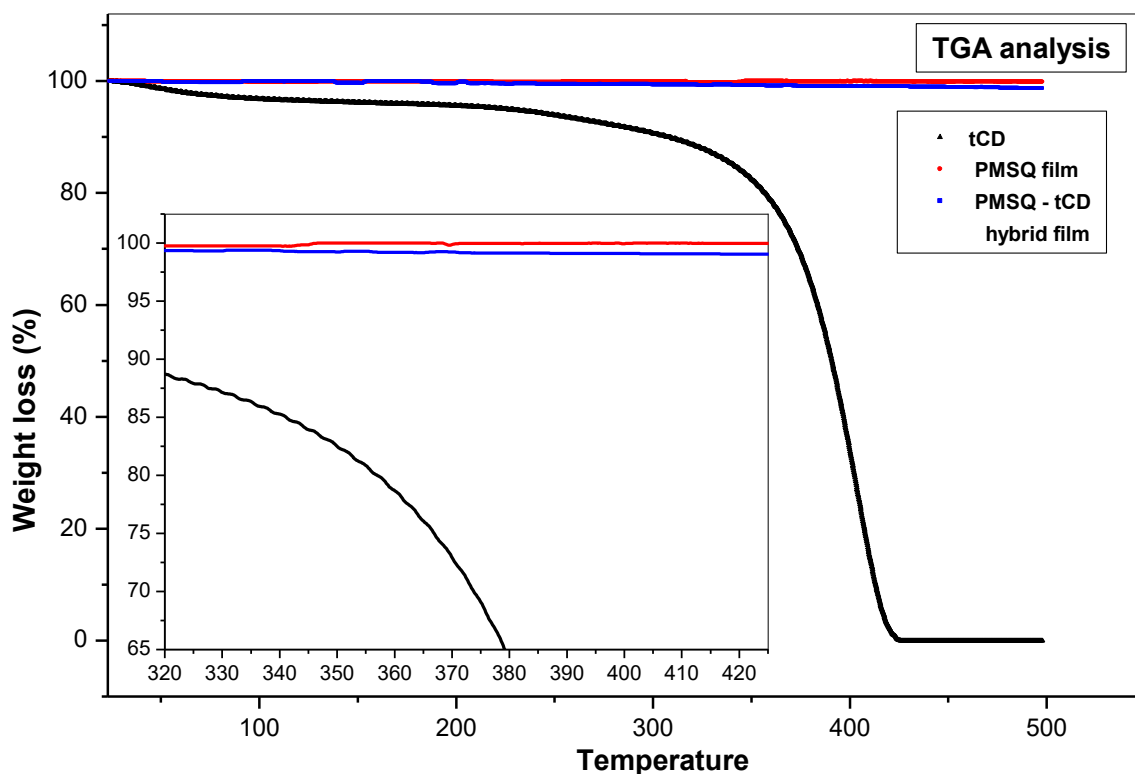


**Figure 4.11 Comparison of TGA data for tCD, PMSQ films and PMSQ –tCD hybrid films.**

with the temperature where the majority weight loss happens for the tCD as seen from the tCD TGA data in figure 4.7.

Figure 4.12 shows the thermal transformation of the films from the as - deposited state to the final annealed state. Other relevant peaks include the Si – C stretching at 1273 cm^{-1} [73], in plane bending of C–H at 1423 cm^{-1} and out of plane bending of C-H at 743 cm^{-1} [76]. The phenyl ring C-C out of plane deformation is seen at 697 cm^{-1} [75]. The films were stable at 500°C for 1 hour. The porous films therefore show a lower thermal stability than that of non-porous PMSQ films which were found to be stable up to 600°C [97].
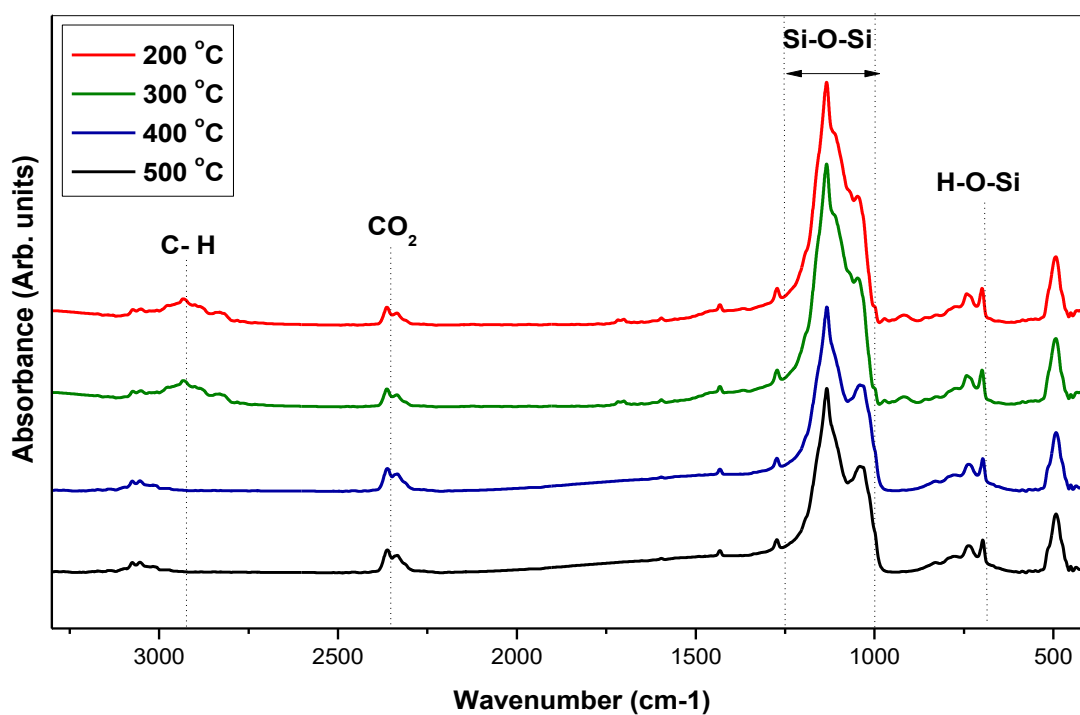


**Figure 4.12. FTIR spectra indicating structural transformation of PMSQ – tCD hybrid films as a function of annealing temperature, indicating thermal stability of the material up to 500°C**

# 4.7. VARIATION IN DENSITY AND K – VALUE OF PMSQ THIN FILMS

XRR measurements were used to study the change in density of the films as a result of introduction of porosity into the films. The studies were carried out on the films using a triple-axis Jordan Valley Bede-D1 X-ray system using a monochromatic Cu-Kα1 (λ = 1.5405Å) radiation source operated at 45 kV and 40 mA. Figure 4.13 shows fringes obtained during the XRR analysis porous PMSQ thin films.
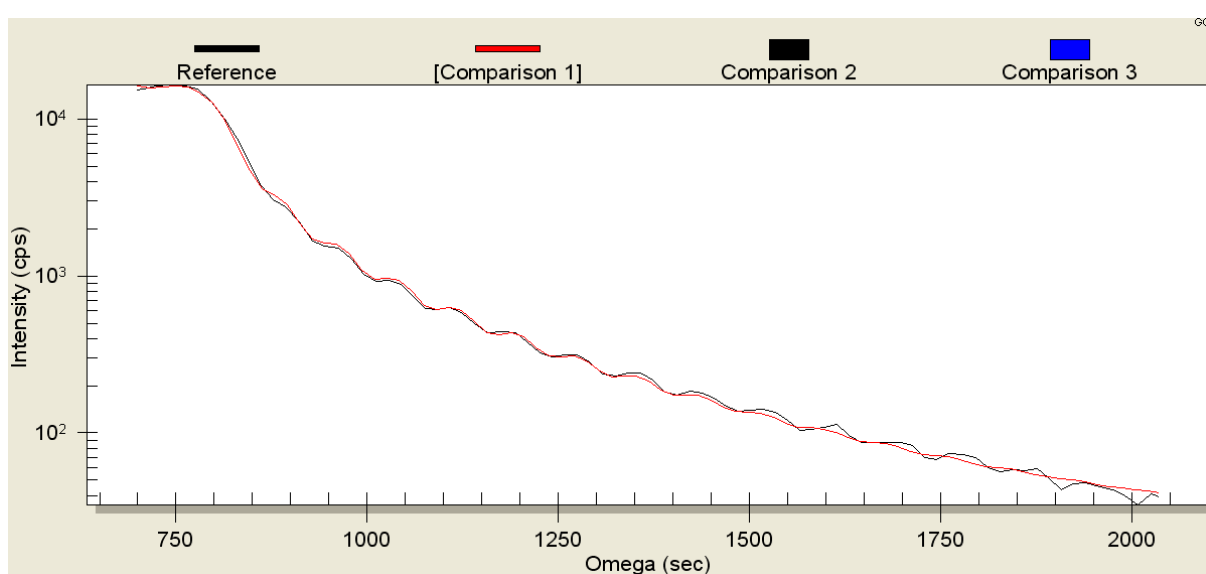


**Figure 4.13. Fringes obtained during XRR studies**

Table 4.1 shows the density data obtained from the XRR measurements. Measurement done on same sample used in thickness measurements. See figure 3.2 and appendix 3.2. for solution concentration.

| Porogen loading (% wt wrt to polymer wt) | Density Data | Density (%) |
|---|---|---|
| 0 | 1.11 | 70 |
| 15 | 0.94 | 59 |
| 30 | 0.78 | 49 |
| 45 | 0.84 | 53 |

**Table 4.1. Density data obtained from XRR measurements**

112

The density obtained from the fitted model for the normal films (70 % from table 4.1) was considered as 100 % for ease of analysis. It was possible to see a decrease in the density of the films with increase in porogen loading. A reduction of ~ 15% in film density was observed for films with 15 % porogen loading when compared to films with no porogen. Similar reducing trend in density was also observed for films with 30 % porogen loading. At higher concentration of porogen loading i.e., at 45 % the linear trend was not observed even though there was a reduction in the density as seen in figure 4.14.
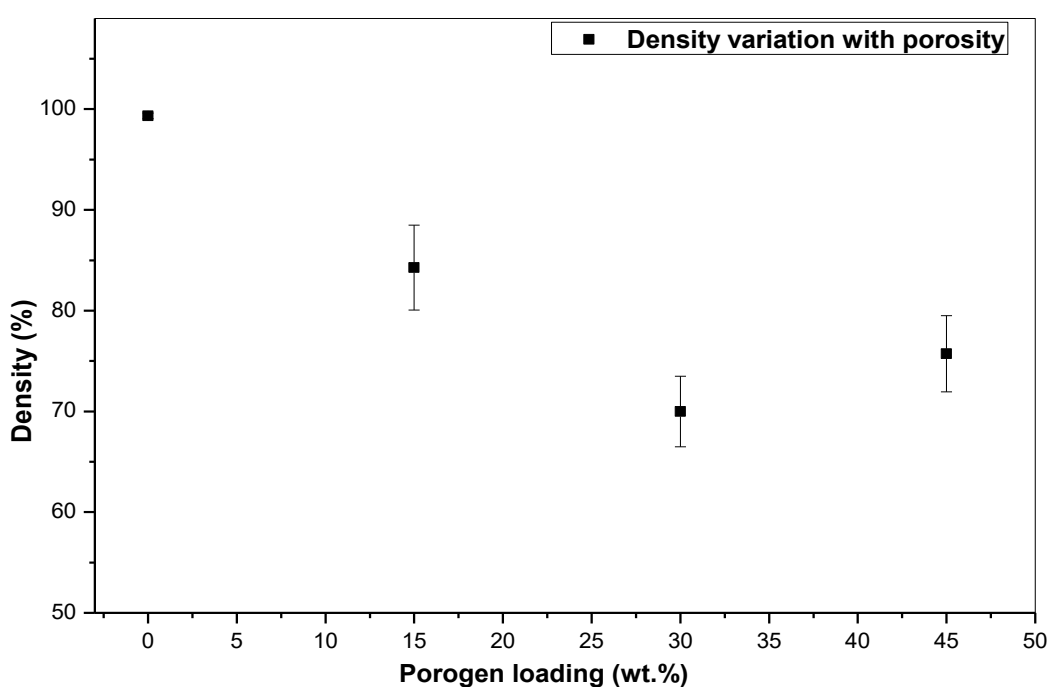


**Figure 4.14. Variation of density in porous PMSQ thin films as a function of porogen loading. Porogen concentration increased in steps of 15 % by wt of solute. See appendix 4.14 for density measurements.**

The variation in the $\kappa$ – value as a function of the porogen loading is shown in figure 4.15 which follows the similar trend with the density variation of figure 4.14. The $\kappa$- value of the normal films was successfully reduced by ~ 20% from $\kappa = 2.7 \pm 0.1$ to $\kappa = 2.2 \pm 0.1$ by the introduction of porosity of around 30 % within the PMSQ thin films.
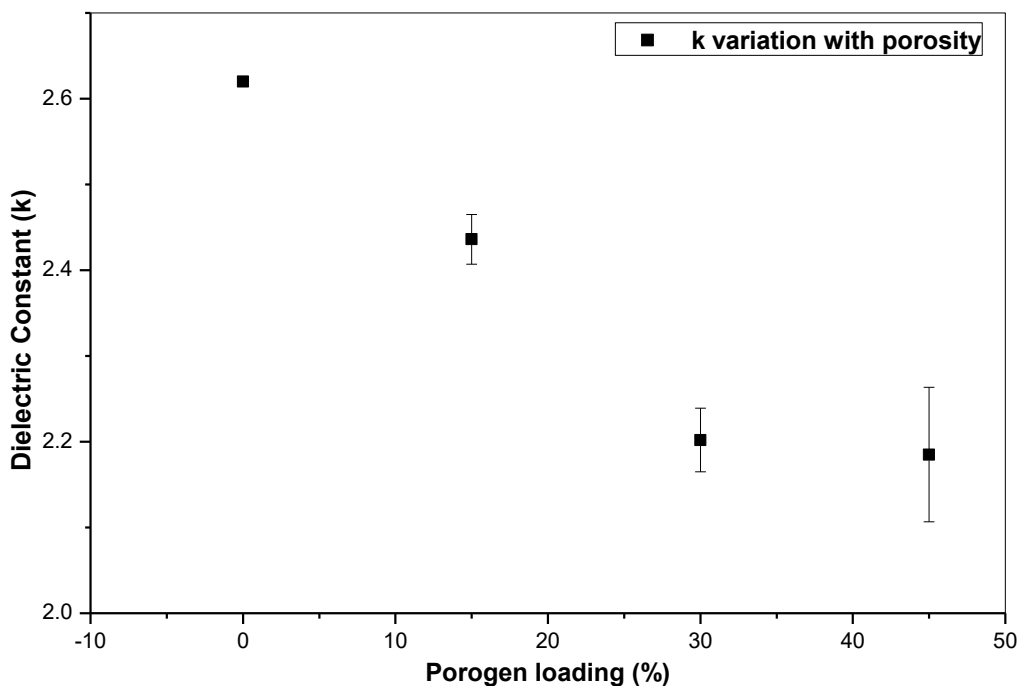
**Figure 4.15. κ – variation as a function of porogen loading. Thickness measurements, capacitance measurements and 'k' – value calculations presented in appendix 4.15.**

# 4.8. PLASMA EXPOSURE OF POROUS PHENYL METHYL SILSESQUIOXANE FILMS

The effect of plasma interaction on the porous films was studied by exposing the films to pure $SF_6$ and $O_2$ plasmas (Oxford Instruments Plasma Lab 80 plus). The chamber pressure was maintained at 200 mTorr and the applied forward power was 150 W. The gas flow rate was kept at a constant of 50 sccm.

## 4.8.1. INTERACTION OF POROUS PMSQ FILMS WITH $O_2$ PLASMA

PMSQ porous thin films were also exposed to pure $O_2$ plasma to study the effect the plasma has on the porous material. Figure 4.16 shows variation of the thicknesses of the films before plasma exposure and after 1, 2 and 8 minutes plasma exposure.
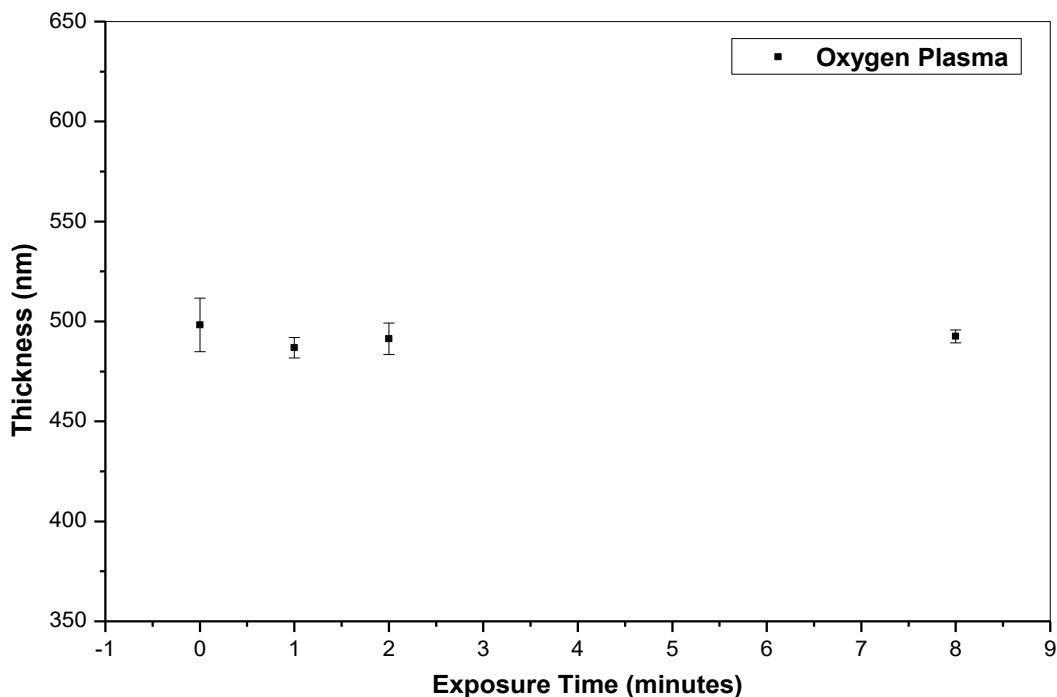
**Figure 4.16. Thickness measurements on porous PMSQ thin films as a function of exposure time to O2 plasma. (Chamber pressure: 200 mTorr, Applied forward power : 150 Watts, Gas flow rate : 50 SCCM, sample exposed for 1,2 and 8 minutes). For thickness measurements see appendix 4.16.**

Figure 4.17 shows the corresponding FTIR spectrum obtained from the film after each exposure stage.
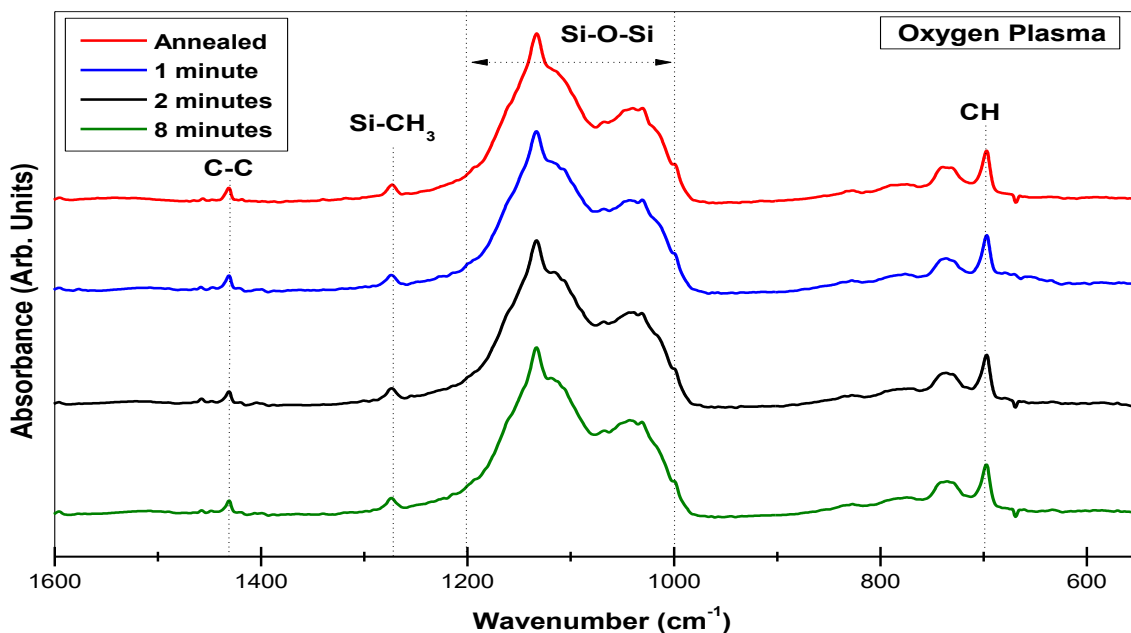


**Figure 4.16. FTIR spectrum of porous PMSQ thin films after subsequent O2 plasma exposure steps showing no change in the bonding peak intensities of the material**

The initial thickness of the film was ~ 500 nm and there were no significant changes in either the thickness or the FTIR spectra of the films even after 8 minutes of exposure to pure $O_2$ plasma. The FTIR spectra show no reduction in the peak intensities and the area under the peaks remained unchanged indicating there was no material erosion during the process.

Another set of samples were exposed to pure $O_2$ plasma for 5 to 15 minutes at 5 minute intervals to investigate the variation in dielectric constant of the porous material when subjected to oxygen plasma expsoure. Capaciatnce measurements done on the films post plasma exposure show an increase in the measured values post plasma exposure. The values were seen to increase with increase in exposure time as seen in figure 4.18.
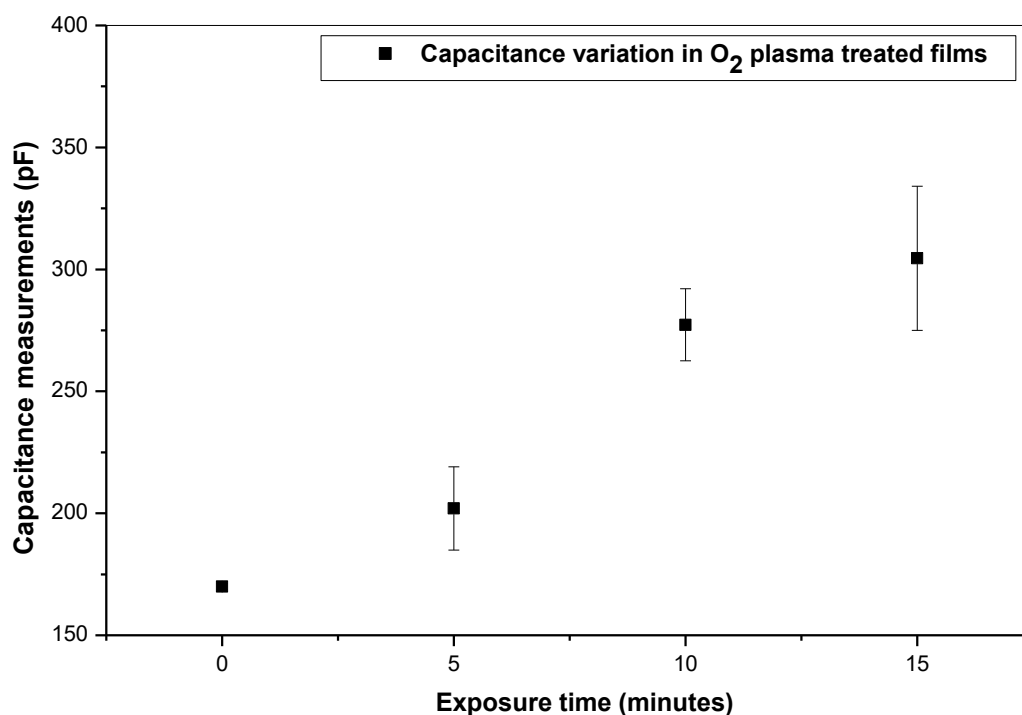


**Figure 4.17. Variation of capacitance of porous PMSQ thin films as a function of time during O2 plasma exposure. (Chamber pressure: 200 mTorr, Applied forward power : 150 Watts, Gas flow rate : 50 SCCM, Exposure Interval : 5 minutes). For thickness measurements, capacitance measurements and 'k' – value calculations see appendix 4.18.**

Figure 4.19 shows the change in the κ - value of the porous PMSQ films during $O_2$ plasma exposure. The κ - value of the as deposited film used for the experiment was of the order of κ = 2.4 ± 0.1.Even though the thickness of the films and their FTIR spectra remained unchanged during $O_2$ plasma treatment there was an increase in κ – value of the porous films.
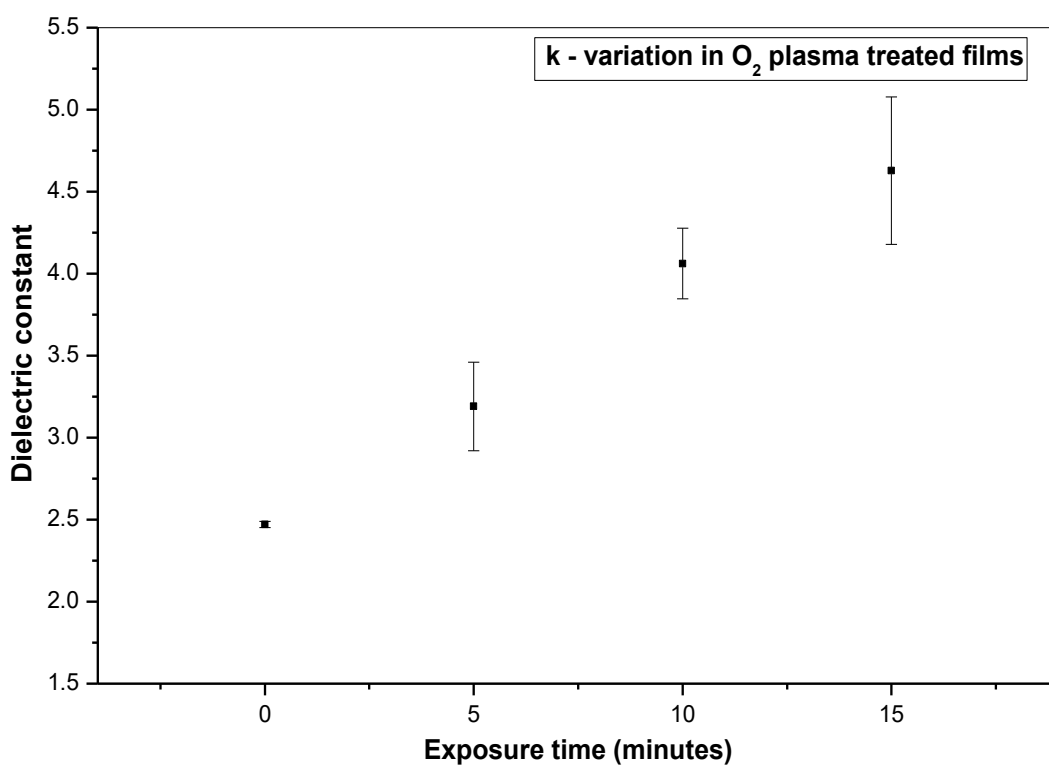


**Figure 4.18. Variation of dielectric constant of porous PMSQ thin films as a function of time during O2 plasma exposure. (Chamber pressure: 200 mTorr, Applied forward power : 150 Watts, Gas flow rate : 50 SCCM, Exposure Interval : 5 minutes).  For thickness measurements, capacitance measurements and 'k' – value calculations see appendix 4.18  & 4.19.**

## 4.8.2. INTERACTION OF POROUS PMSQ FILMS WITH SF$_6$ PLASMA

Fluorine is required to etch Si based structures as it is removed by the formation of volatile SiF$_x$ compounds [33,98]. The films thickness was reduced from an initial thickness of ~480 nm to ~125 nm with a total exposure time of 5 minutes. Thickness measurements and FTIR spectra of the films were obtained after 1, 2 and 5 minutes of plasma exposure. Figure 4.20 shows the thickness values after pure SF$_6$ plasma treatment of the porous PMSQ film. The chamber pressure was maintained at 200 mTorr and the applied forward power was 150 Watts. The gas flow was kept at constant flow rate of 50 SCCM.
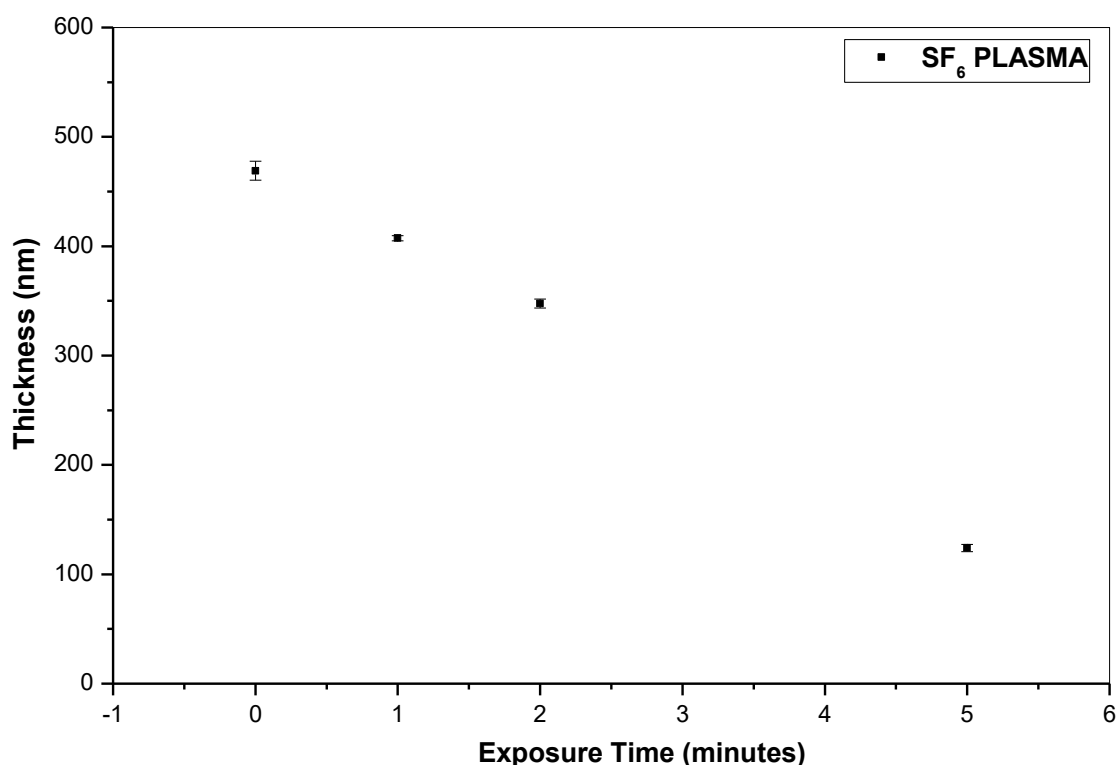


**Figure 4.19. Thickness variation of porous PMSQ thin films as a function of exposure time to SF6 plasma. (Chamber pressure: 200 mTorr, Applied forward power : 150 Watts, Gas flow rate : 50 SCCM, Samples etched for 1, 2 and 5 minutes). For thickness measurements see appendix 4.20.**

Figure 4.21 shows the FTIR spectra of the films pre and post $SF_6$ plasma exposure. It can be seen from the spectrum that the intensity of peaks are reduced, especially in the 1000 to 1200 cm$^{-1}$ region of the spectrum, as the etching progresses, indicating removal of the material.
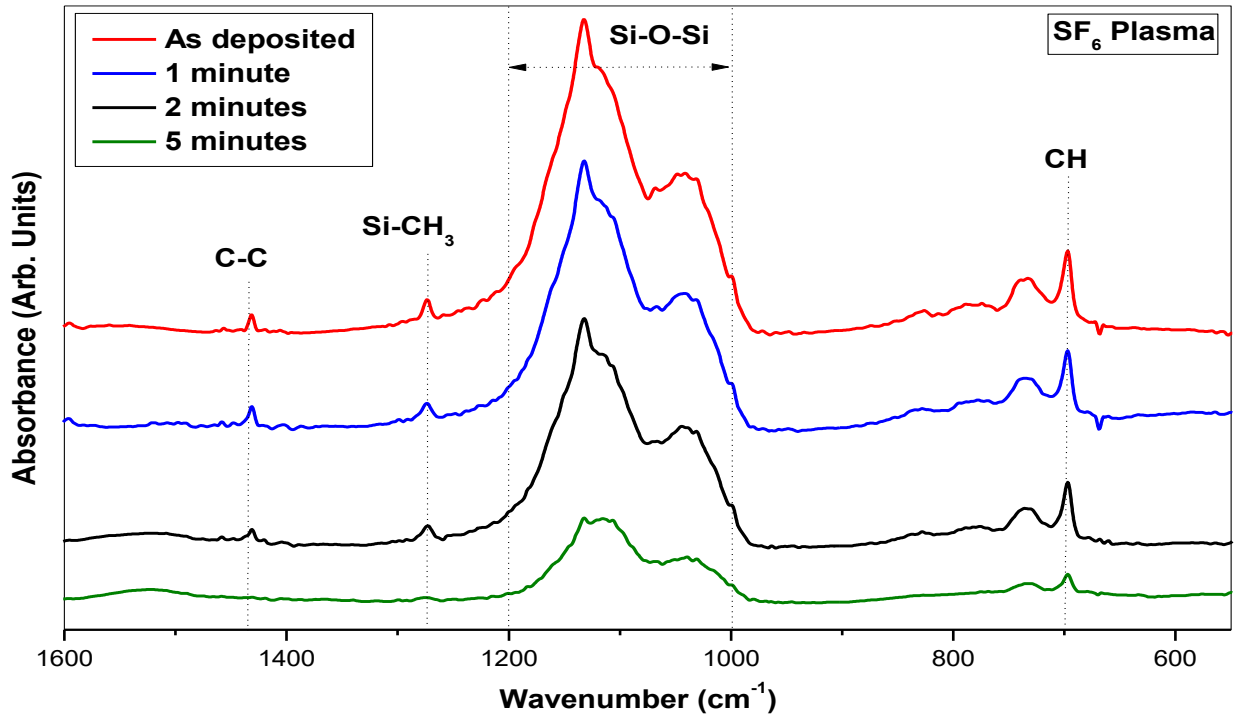


**Figure 4.20. FTIR spectrum of porous PMSQ thin films after subsequent SF6 plasma etch steps indicating the removal of the material during the etch process.**

Porous PMSQ films were exposed for 20, 40 and 60 seconds in the $SF_6$ plasma to study the variation in their κ - values as a result of plasma interaction. The average κ - value of the film prior to the plasma exposure was κ = 2.3 ± 0.1 Figure 4.22 shows the capacitance measurements obtained from the films after plasma etching. Figure 4.23 shows the variation in κ - value of the films as a function of $SF_6$ plasma exposure time. It was observed that as the plasma exposure time increases the κ - value of the films also increases.
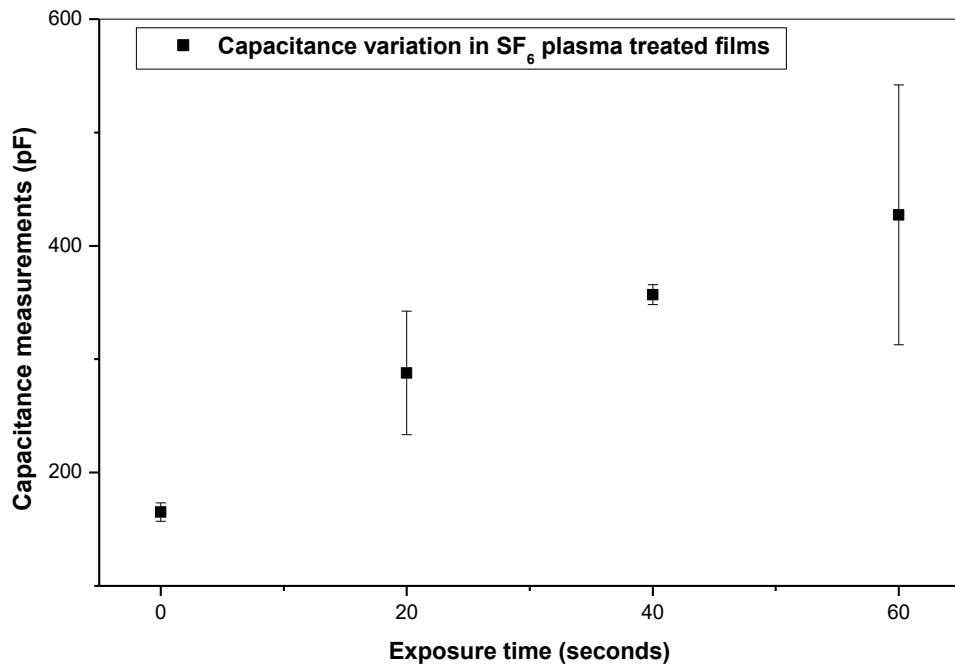
**Figure 4.22. Variation capacitance of porous PMSQ thin films as a function of time during SF6 plasma exposure. (Chamber pressure: 200 mTorr, Applied forward power : 150 Watts, Gas flow rate : 50 SCCM, Samples etched for 20, 40 and 60 seconds). For thickness measurements, capacitance measurements and 'k' – value calculations see appendix 4.22.**
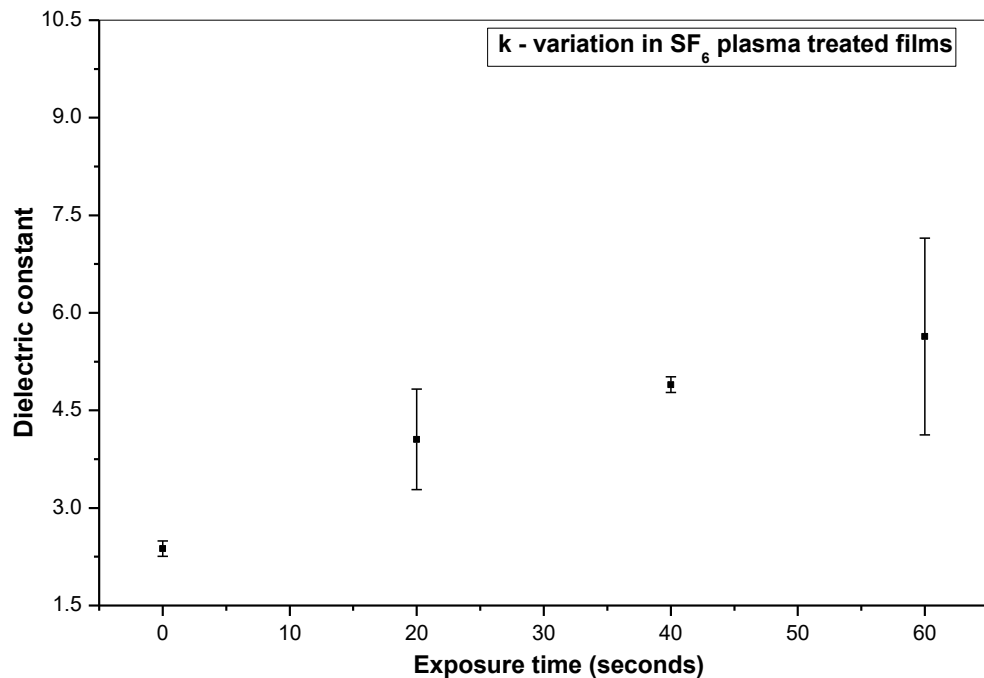


**Figure 4.21.  Variation of dielectric constant of porous PMSQ thin films as a function of time during SF6 plasma exposure. . (Chamber pressure: 200 mTorr, Applied forward power : 150 Watts, Gas flow rate : 50 SCCM, Samples etched for 20, 40 and 60 seconds). For thickness measurements, capacitance measurements and 'k' – value calculations see appendix 4.22 & 4.23.**

## 4.8.3. XPS ANALYSIS OF PRISTINE AND PLASMA TREATED POROUS PMSQ FILMS

Surface analysis of the porous PMSQ thin films were performed by XPS. Figure 4.24 shows a series of survey scans from 0 to 1000 eV for each sample under investigation. For all three samples, carbon, oxygen and silicon are present with the addition of fluorine for the $SF_6$ plasma exposed film. It is evident from the survey spectra that upon exposure to oxygen plasma, the O1s photoelectron peak grows in integrated area and the C1s peak decreases in area relative to the as deposited film, suggesting that the oxygen plasma has mainly removed the carbon within the top surface of the film. Upon exposure to $SF_6$ plasma, it can be seen that a large fluorine peak emerges in the survey spectra with an additional change in the C1s bonding state relative to the as deposited film. Peak area calculations show that upon oxygen exposure, the integrated
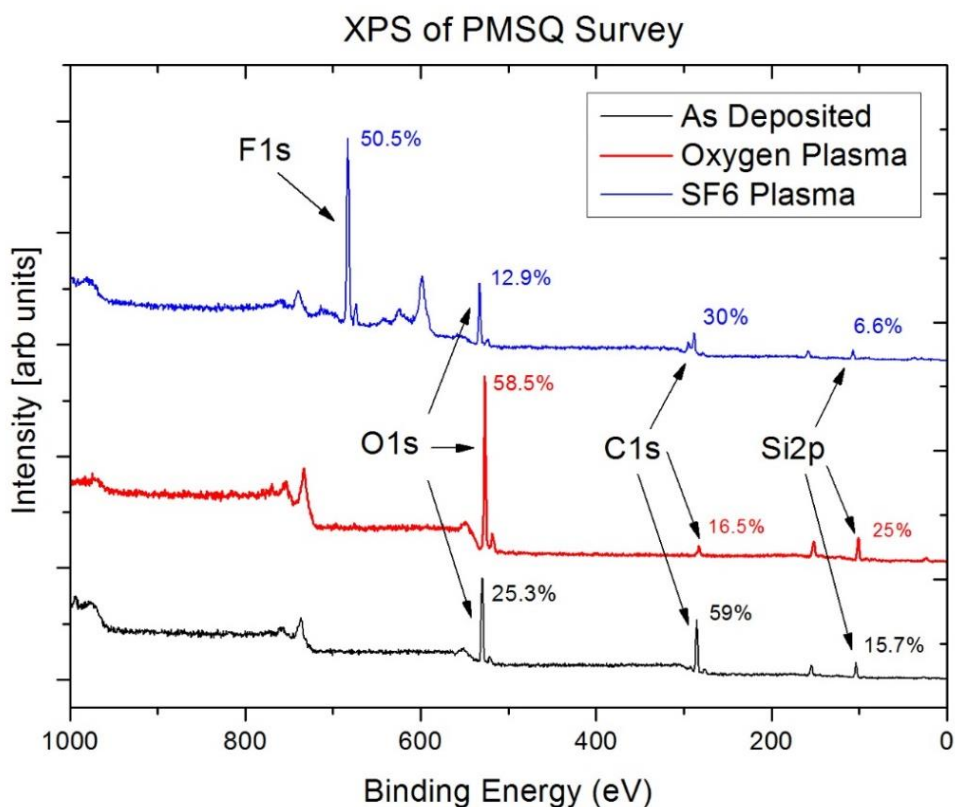


**Figure 4.22 XPS survey spectra for As Deposited, Oxygen Plasma and SF6 Plasma exposed films showing relative elemental composition of each sample.**

area of the C1s peak falls to ~ 25% relative to the as deposited film area and the C1s peak for the SF6 plasma exposed film falls to ~ 80% relative to the as deposited film area.

The Si2p and O1s photoelectron peaks are displayed in figure 4.25. The Si2p spectra show both the broadening and shifting of the overall peak to higher binding energies as a result of exposure to oxygen plasma and $SF_6$ plasma. This is consistent with Si bonding to higher electronegative elements such as oxygen in the case of oxygen plasma and fluorine in the case of $SF_6$ plasma. O1s spectra show both the shifting of the O1s peak relative to the as deposited film when exposed to oxygen plasma or $SF_6$ plasma and the increase in integrated area due to the exposure to oxygen plasma.
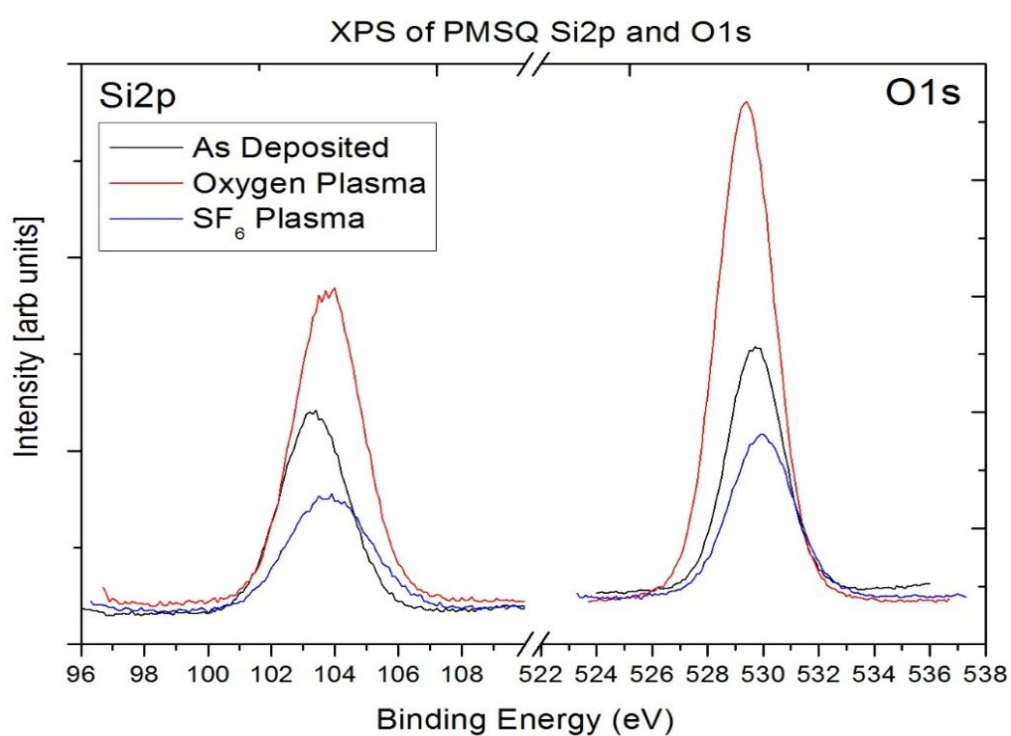


**Figure 4.23. XPS spectra showing Si2p and O1s spectra for As Deposited, Oxygen Plasma and SF6 Plasma exposed films**

Figure 4.26 displays C1s spectra for all three samples. As can be seen from the C1s spectra of the as deposited film, the carbon within the dielectric appears to be in a single bonding state within the resolution of the system used. Upon oxygen plasma exposure C-O and C=O bonds appear in the C1s spectra. The presence of C-O and C=O bonds is most likely a direct result of the exposure to oxygen plasma. When the C1s spectra for the $SF_6$ plasma exposed film is examined, it is seen that higher binding energy peaks emerge relative to the as deposited film which have been attributed to C-F bonds as evident in the survey spectra.
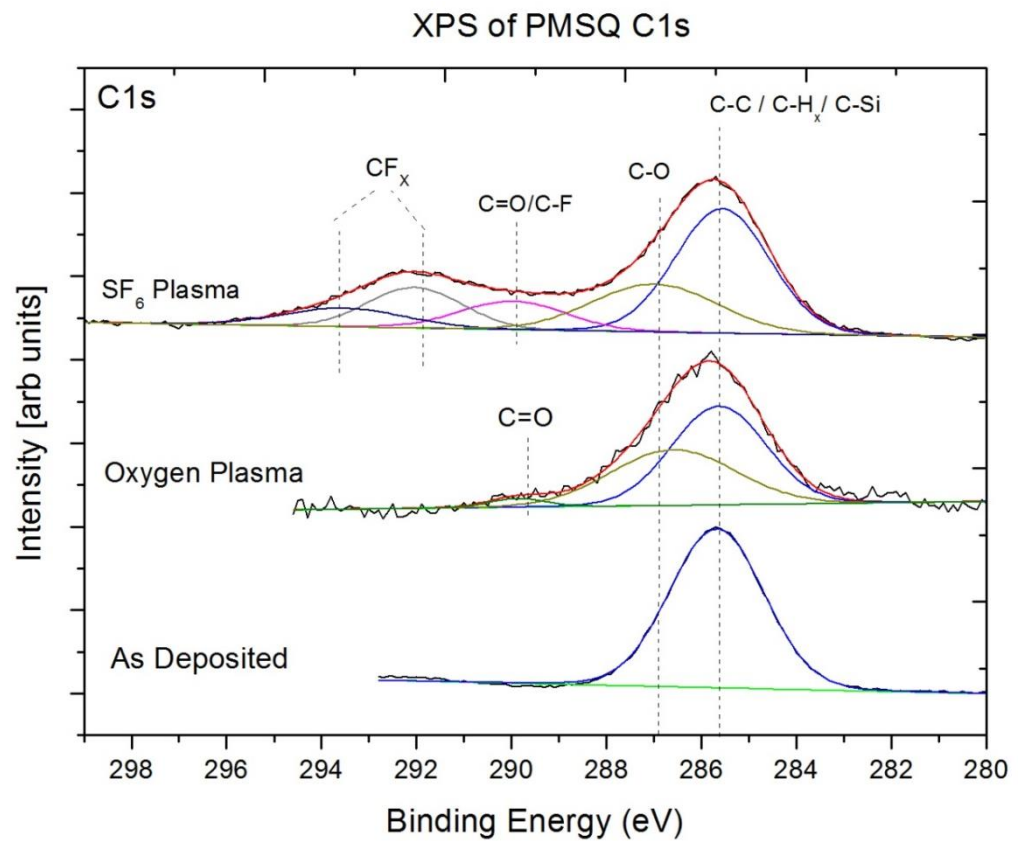


**Figure 4.24. XPS spectra showing C1s spectra for As Deposited, Oxygen Plasma and SF6 Plasma exposed films**

# 4.9. SUMMARY

The work presented in this chapter explains how the κ – value of the PMSQ material was further reduced by the sacrificial porogen technique. To attain this objective, SBS and tCD were investigated as two viable materials to be used as sacrificial porogens for creating porosity in PMSQ thin films. Even though SBS was soluble as such in MIBK, it was rendered insoluble when introduced into PMSQ solution in MIBK. tCD readily gave solution with PMSQ and MIBK. The process optimised process parameters used for the deposition of the tCD- PMSQ hybrid films and for the development of the porous PMSQ films by annealing are presented in Table 4.1.

The introduction of porosity changed the bulk properties of the film as seen from the reduction in κ- value of the film and the density of the film. An increase in the κ- value of the porous films was observed post plasma exposure of the films. A large amount of carbon is present in the phenyl and methyl substituent groups of the PMSQ material. The removal of significant amounts of carbon from the film surface during oxygen plasma exposure is evident from the XPS spectra, along with the formation of new bonds such as C-O and C=O. Oxygen plasma removes carbon from the film and transforms the material to a $SiO_2$ like structure. The removal of lesser polarisable C-H and C-C bonds increases the κ - value of the film. Again, plasma treatment creates dangling bonds on the surface of the material which eventually absorbs moisture [54,72]. This SiOH will in turn increase the κ - value of the film. All the aforementioned surface modifications contribute towards the change in the dielectric constant of the porous PMSQ material upon plasma treatment.

The exposure to $SF_6$ plasma also results in the formation of new bonds as seen in the XPS analysis. F insertion into the material results in the formation of SiOF rich surface. The hydrophilic behaviour of fluorine leads to moisture adsorption which results in the increase in the κ - value of the material [25].

| Solution preparation parameters | |
|---|---|
| Solute weight (MSQ / PMSQ / tCD) | 0.75 / 1.0 gm / loading done by % weight of the PMSQ polymer) |
| Solvent weight (MIBK) | 5 gm |
| Dissolution time | 1 hour |
| Solution filtration method | Using PTFE syringe filter 0.2 μm |
| **Spin coating parameters** | |
| Spin speed (maximum) | 3500 rotations per minute |
| Acceleration setting - 2 | ~ 180 rotations per second increment |
| Spin time | 45 seconds |
| **Annealing Parameters – Multi stage anneal** | |
| Stage 1 - 200ºC for 10 minutes | For Solvent Evaporation |
| Stage 2 - 380ºC for 10 minutes | To facilitate cross linking |
| Stage 3 - 450ºC for 60 minutes | For porogen removal |
| Anneal atmosphere | Argon |
| Cool down period | ~ 4 hours to reach safe handling temperature |
| **Thickness parameters** | |
| Average thickness of deposited films | ~ 510 nm |

**Table 4.2. Table listing the optimised process parameters used for the solution preparation, deposition and annealing of PMSQ and MSQ films used for the experiments**

# CHAPTER 5
# ANALYSIS OF THE FILM MORPHOLOGY AND PATTERNING OF FILMS BY NANOSPHERE LITHOGRAPHY

Introduction of porosity makes significant modification in the film morphology and changes it properties to a large extent as seen in the case of normal and porous PMSQ films. Even though the reduced $\kappa$ – value of the material is a desired trait, there are certain limiting factors that prevent the reduction of the $\kappa$ – value beyond a certain value. In this section we will take a look at the critical factors and mechanisms that constrict the reduction of density and also the factors that contribute to the increased interaction of the porous films with the plasma.

Thin films are patterned throughout the manufacturing process for various reasons using conventional lithography techniques. This section also presents a novel patterning technique, namely nanosphere lithography. This technique can be pursued as an alternative to conventional photolithographic techniques for the creation of periodic arrays. Deposition of polystyrene nanospheres can be done with relative ease by spin coating. The spheres get deposited evenly on surfaces by self – assembly. Self – assembly is the spontaneous organisation of components due to intermolecular forces to form a larger functional unit.

# 5.1. DEVIATION OF ACTUAL POROSITY FROM EXPECTED POROSITY

Dielectric constant is a property of the bulk of the material. We saw in chapter 4 that porosity reduces the density of the material. The $\kappa$- value of the dielectric material is be also reduced by the introduction of porosity within the material since the porosity results in the reduction of the total number of polarisable dipoles within the material. Porosity is generated by engineering the material to have a constituting component within the material that can be thermally removed by annealing at the decomposition temperature of the pore generating material as demonstrated in the sacrificial porogen technique. In this section let us analyse in detail porogen loading, pore generation and its effect on the density, $\kappa$ – value and surface area of the material

## 5.1.1. THEORETICAL ESTIMATION OF INTEGRATED AIR VOLUME

Let us consider V as the total volume of the porous dielectric film. Let $V_a$ be the constituent air volume within the material and $V_d$ be the dielectric volume so that the total volume of the material would be

$$V = V_a + V_d \qquad\qquad \text{Equation 5.1}$$

When expressed in percentage the total volume V can be expressed 100%, or we can say

$$V = 100 \ \% = 1 \qquad\qquad \text{Equation 5.2}$$

Combining the above two equations, they can be reduced to the following expression

$$V_d = 1 - V_a \qquad\qquad \text{Equation 5.3}$$

127

Let us assume that the dielectric constant value of the bulk of the material was reduced to $2.2 \pm 0.1$ by the introduction of air volume into the material. We know that the normal dielectric constant of the material is $2.7 \pm 0.1$. The net dielectric constant can be considered as the sum total of the individual contributions of the embedded air volume and the normal dielectric film and it can be expressed as follows

$$2.2 * 1 = 2.7V_d + (1-V_d)$$ **Equation 5.4**

Simplifying the above equation we will get the value of $V_a$ as 0.29412

When expressed in percentage this is the approximate estimation of the quantity of air that needs to be incorporated into the bulk material to bring down its effective $\kappa$ – value from 2.7 to 2.2. Figure 5.1 shows the expected reduction in $\kappa$ – value of the material by reducing the density of material through the generation of pores and the resulting incorporation of air volume.
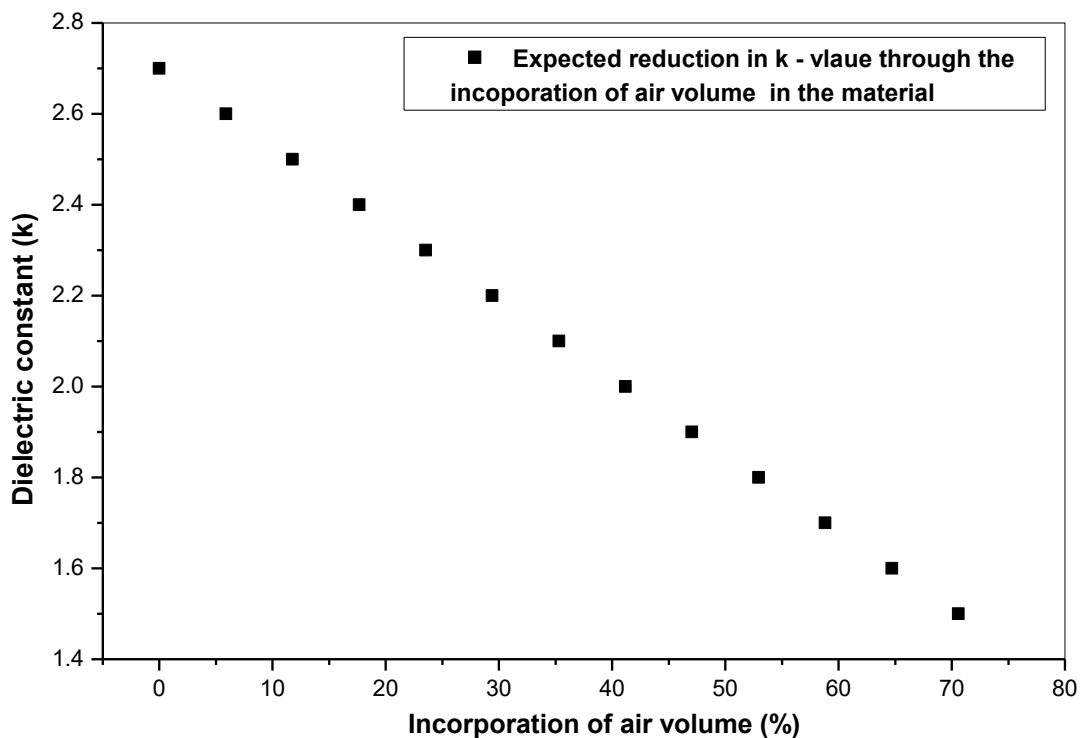


**Figure 5.1. Expected reduction in k – value by the incorporation of air volume**

## 5.1.2. MEASURED FILM DENSITIES AND DEVIATION FROM EXPECTED DENSITY

Figure 5.2 shows the measured densities of the film with various levels of porogen loading. It also shows the amount of air that would have been incorporated in the material during this process.
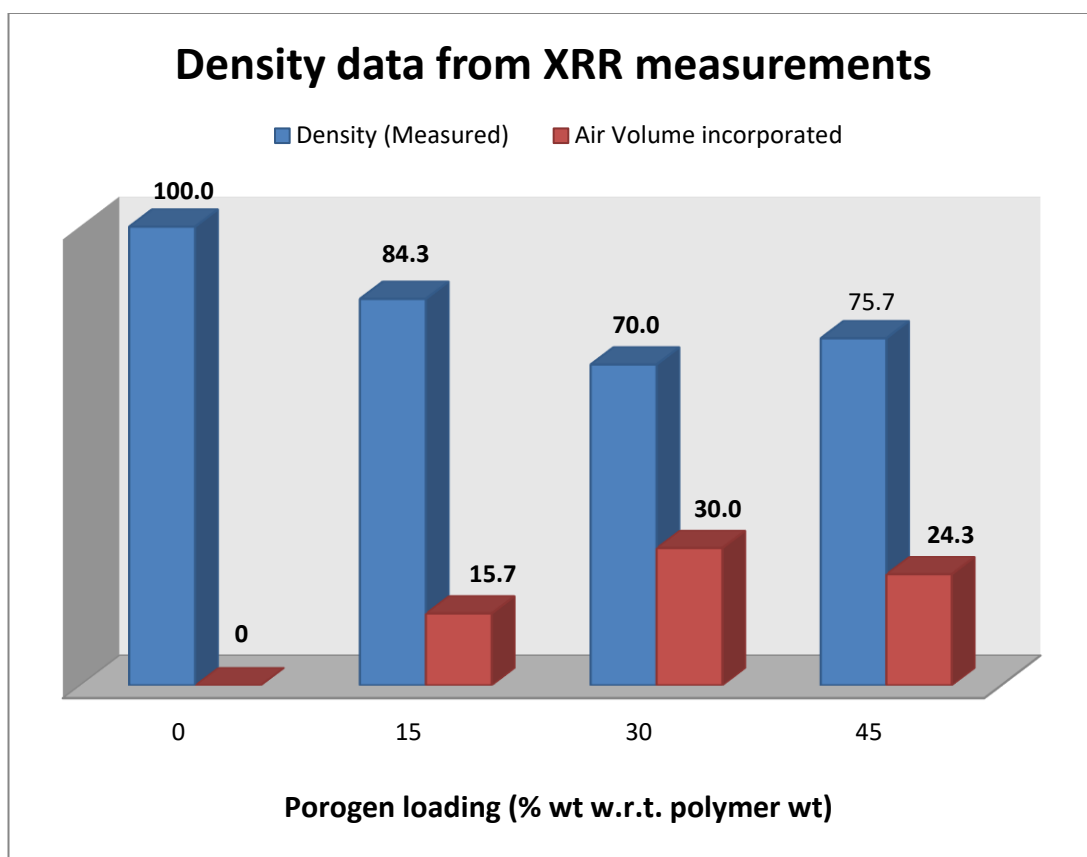


**Figure 5.2. Graph showing the measured density and incorporated air volume in PMSQ films from XRR measurements**

The addition of 15 % and 30 % of porogen loading successfully incorporated almost 15 % and 30 % of porosity into the material. But when the porogen loading was increased to 45 % it failed to incorporate similar amounts of air volume in the material. Measured values show the incorporated porosity was only ~ 25 %. Figure 5.3 show the difference in the actual values of measured density from the expected trend in calculations.
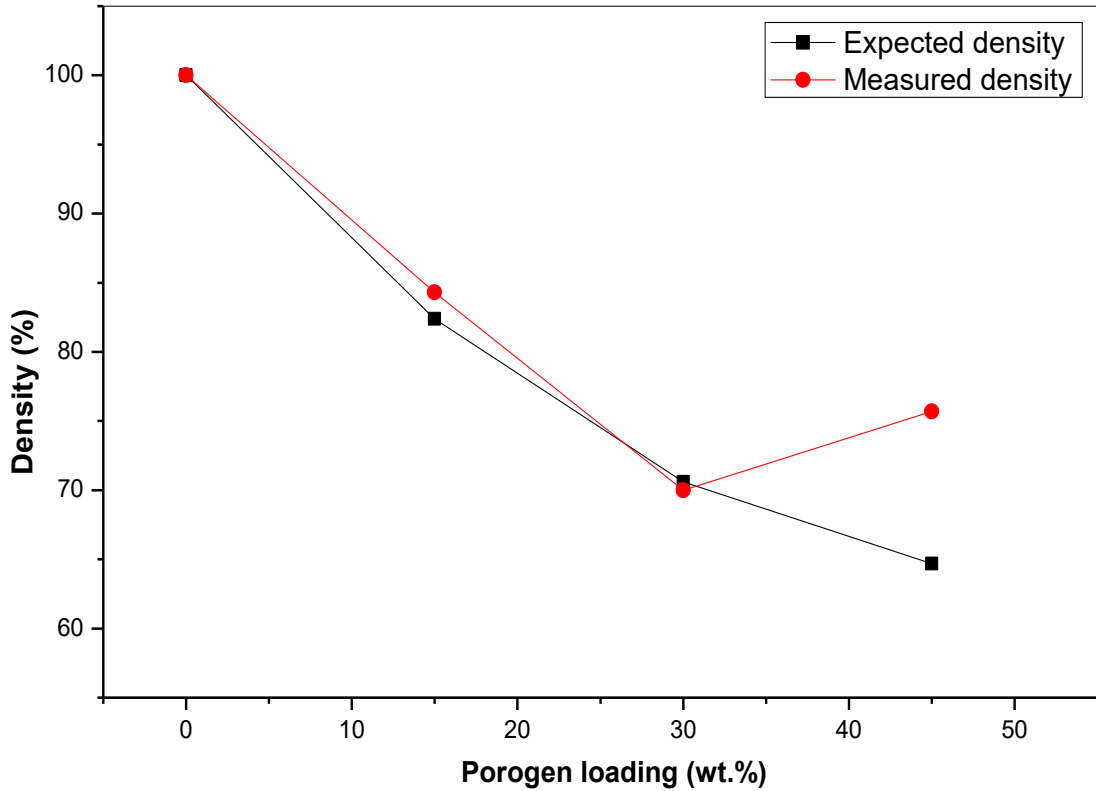
**Figure 5.3. Plot showing the deviation of measured density from expected density**

From our results it was demonstrated that at lower concentrations of porogen loading (< 30%), there is a direct correlation between the amounts of the porogen precursor in the solution to the amount of porosity introduced into the material. A further increase in the porogen concentration does not yield a similar result. This difference in the actual measured density from the expected density at higher levels of porogen loading can be due to pore collapse happening within the material at high porogen concentrations.

We know that the density of material has a direct effect on the dielectric constant of the material. The trend observed in density of the films in the experiments is also mirrored in the κ – value of the material. Figure 5.4 shows the deviation of the measured dielectric constant of the porous films from the expected value.
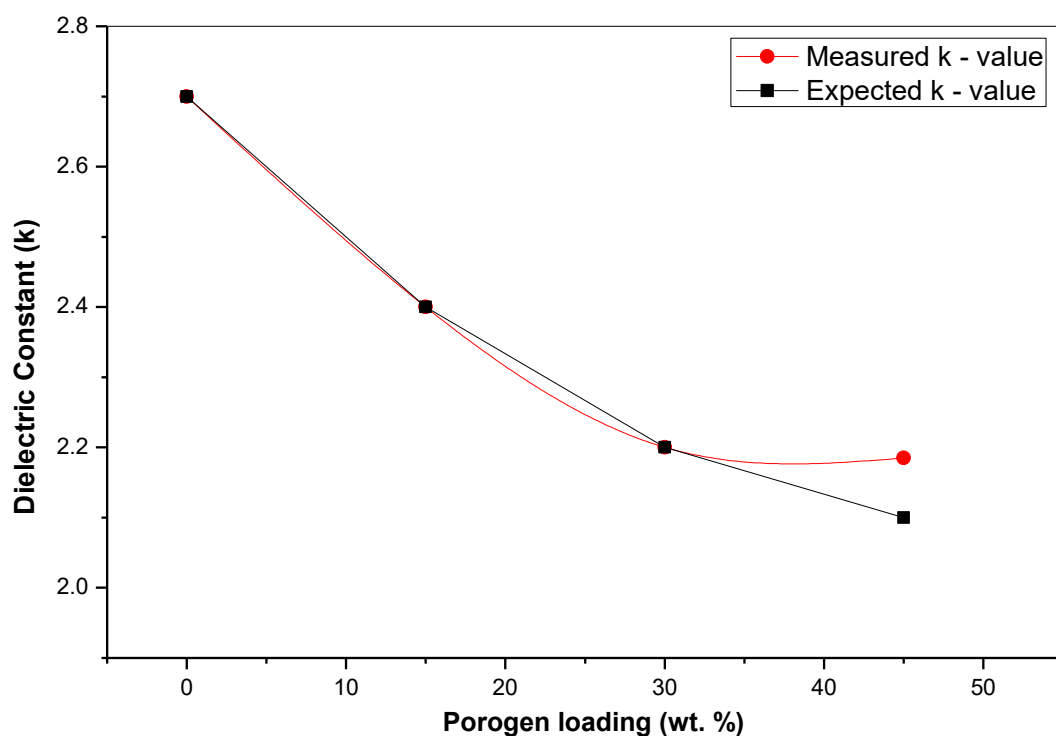


**Figure 5.4. Plot showing the deviation of measured κ - value from expected κ - value**

### 5.1.3. PERCOLATION THRESHOLD AND PORE COLLAPSE

When trying to introduce porosity into materials, the phenomenon where the change in porosity is lower than the expected porosity is a widely observed phenomenon. It has been reported in studies of cyclodextrin (tCD) /cyclic silsesquioxane (CSSQ) hybrid film system, that at high porogen loading of >30 %, the thin film porosity generated was much lower than the amount of tCD in the coating precursor [99].

At lower concentrations tCD are more evenly dispersed within the film. Hence they act as a single nano particles within the film matrix. When heated to the decomposition temperature of the porogen the molecule will decompose to leave behind a void that has almost the same dimensions of the actual tCD molecule. Because of this, the engineered porosity is usually very close to the expected value. But as we increase the concentration of the porogen beyond a certain point known as the percolation threshold (> 30% in our case), the cyclodextrin (tCD) interacts more favourably with each other leading to agglomeration of material within the deposited hybrid film as shown in figure 5.5.
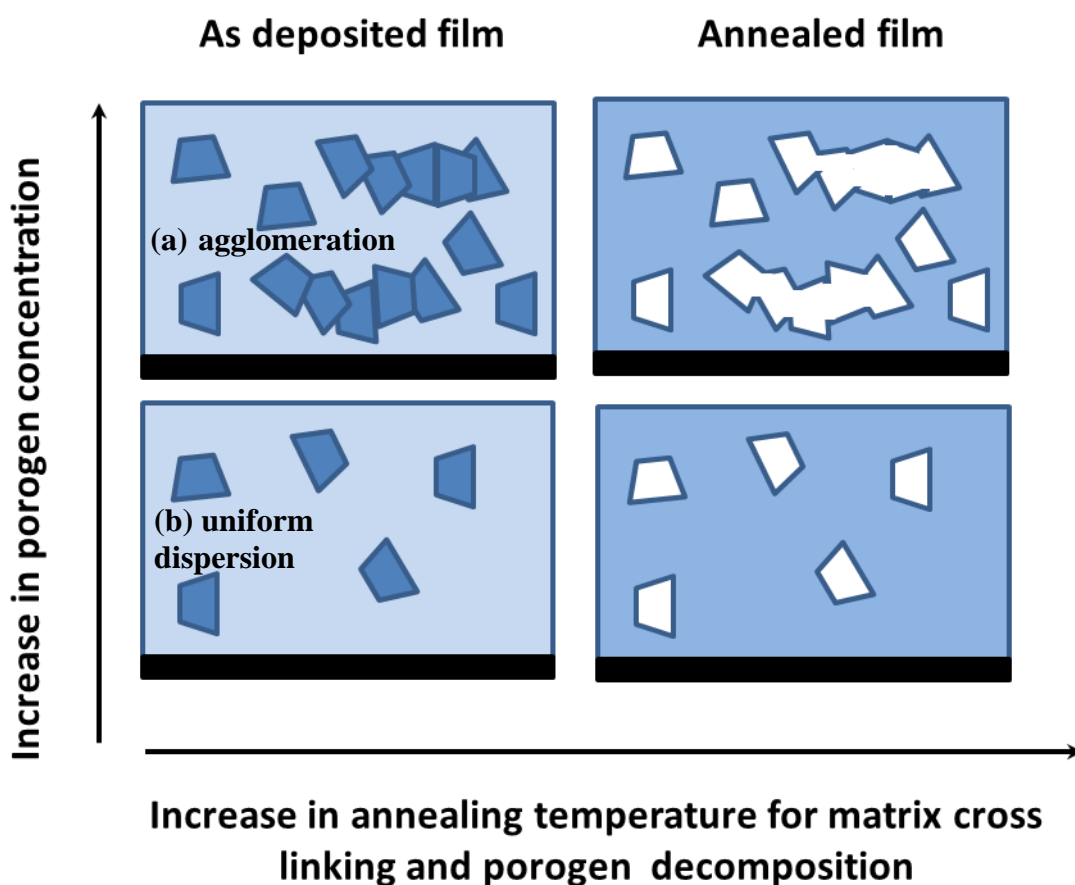


**Figure 5.5. Schematic showing porogen dispersion on deposition, and pore dispersion post annealing. (a) agglomeration and (b) uniform dispersion**

Hence on burnout the agglomerated porogen material creates worm like pore systems leading to pore collapse and thereby deviating away from the expected porosity [93,99].

## 5.2. HIGHER IMPACT OF PLASMA ON POROUS DIELECTRIC FILMS

When porosity is introduced in a film the pores generated are not just confined to the insides of the film. The location of the pores is determined by the manner in which the porogen molecules are dispersed within the film before burnout of the thermally labile material. The molecules positioned along the film surface can lead to the formation of open pores on the surface of the film. The formation of pores on the surface changes the surface morphology, particularly changes the exposed surface area of the film. To get a rough estimate about the change happening in surface area as a result of the presence of open pores on the surface of the film let consider a deposited sample as seen in figure 5.5.
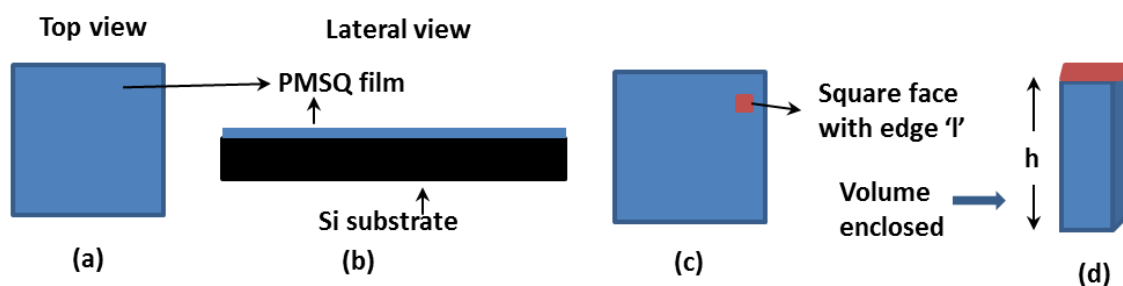


**Figure 5.6. Schematic showing (a & b ) deposited porous PMSQ film (c) a small square area on the surface of a deposited porous film with 'l' as edge length of the square face (d) volume enclosed under the square face and 'h' being the height of the enclosed volume**

The figure 5.6 (a) shows the top view of the deposited sample and (b) shows the lateral view of a PMSQ-tCD hybrid film sample deposited on silicon substrate. Let us

consider a small square section of the film with edge length 'l' as shown in figure (c) and the thickness of the film is 'h'.

The area of the square face, the initial area '$A_I$' is given by

$$A_I = l^2$$
**Equation 5.5**

The enclosed volume '$V_{tot}$', figure 5.6.(d), under the square face would be

$$V_{tot} = l^2 h$$
**Equation 5.6**

If 'p' is the amount of porogen loaded into the film in %, then the amount of air volume incorporated (in low porogen loading conditions, >30%) after the removal of the porogen '$V_{air}$' would be

$$V_{air} = p \, V_{tot} \, \%$$
**Equation 5.7**

Let us once again consider the porogen material used, which is tCD. Let 'D' be the diameter of the tCD molecule, then the volume of the molecule '$V_{tCD}$' assuming a spherical shape for the molecule is

$$V_{tCD} = \frac{4}{3} \pi \left(\frac{D}{2}\right)^3$$
**Equation 5.8**

Hence the number of molecules '$n_{tCD}$' required to constitute the amount of air volume can be calculated as

$$n_{tCD} = \frac{V_{air}}{V_{tCD}}$$
**Equation 5.9**

134

If 'D' is the diameter of the tCD molecule and 'h' is the thickness of the film then the number of layers '$n_L$' that can be linearly arranged each with a perfect arrangement of a mono-layer of porogen molecules would be

$$n_L = \frac{h}{D}$$  Equation 5.10

This can be seen in figure 5.7. (a).
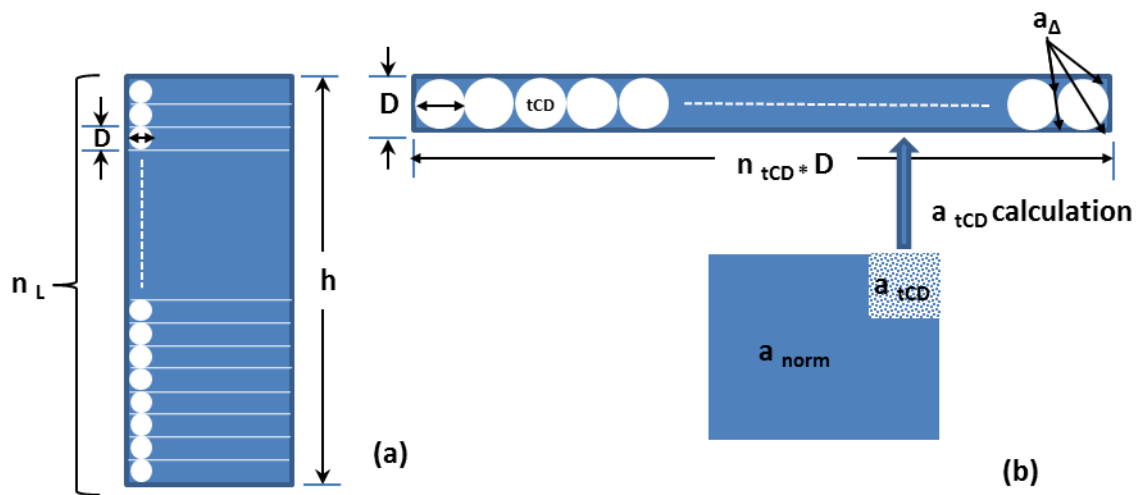


**Figure 5.7. Schematic showing assumed distribution of tCD molecules in the region under consideration for the purpose of theoretical calculation**

If the tCD molecules are evenly distributed among the layers the number of tCD molecules in each layer 'n' would be dividing the total number of tCD molecules (Eq 5.9) by the number of layers of linear arrangement (Eq 5.10)

$$n = \frac{n_{tCD}}{n_L} = \frac{6pl^2}{100\pi D^2}$$  Equation 5.11

Let us consider figure 5.7.(b). The figure shows the total area of the as deposited film surface. The surface will have two kinds of regions. First would be the area with the

normal PMSQ film ($a_{norm}$) and the other is the area occupied by the tCD molecules ($a_{tCD}$). Since the change in area happens in the region with tCD we can ignore '$a_{norm}$'. For the ease of calculation let us bring together these two areas even though they are intermixed throughout in the actual deposited film. Now each layer has 'n' number of tCD molecules per layer, the area occupied by all the spheres on the square face of the layer '$a_{tCD}$' would be

$$a_{tCD} = n\, D^2 + a_\Delta \qquad \textbf{Equation 5.12}$$

This area calculation is done by taking into consideration the total number of assumed molecules in the layer to be linearly arranged as shown in the figure. We will also account for the area not covered by the molecules but still included in the area calculation and quantify it as $a_\Delta$.

We assumed that the porogen molecules are spherical in shape. This means that the voids left behind by each tCD molecule on burn out would be a sphere. The outer surface area of the porogen molecule would hence be the inner surface area of the pores generated. But on the surface of the film, there can be open pores of different shapes. For the sake of easy calculations let us assume that on an average, all the molecules present in the surface are in the form of open pores that are perfect hemispheres as seen in figure 5.8.



**Figure 5.8. (a) actual pore formation on surface (b) pore formation considered for calculation**

The surface area changes when the burn out of the porogen takes place during the porogen removal stage. The new area thus created can be expressed as

$$a_{new} = n\ 2\pi \left(\frac{D}{2}\right)^2 + a_\Delta$$

This change is only happening in the area which was earlier quantified as $a_{tCD}$, and there is no change happening to $a_\Delta$

At this point we can calculate the difference in the area because of porosity integration '$\Delta A$'

$$\Delta A = a_{new} - a_{tCD} = 0.5714\ n\ D^2$$

So we can denote the new area after the burnout of the porogen material as the final area $A_F$

$$A_F = A_I + \Delta A$$

Knowing the initial area as deposited and the final area after porogen integration, the percentage change in area can be calculated by the equation

$$\left(\frac{A_F - A_I}{A_I}\right) 100\ \%$$

Substituting the terms for $A_F$ and $A_I$ in the above equation (equations 5.5, 5.14 & 5.15 in 5.16), it is reduced as

$$\frac{0.5714\ n\ D^2}{l^2} * 100$$

Substituting for 'n' the above expression (5.11 in 5.17), the percentage increase in surface area can be expressed as

137

$$1.0919 \, p \, \%$$

So based on our two assumptions

(i)    homogeneous distribution of porogen within the material and

(ii)   hemisphere shaped open pores on the surface

the increase in surface area upon burnout of the porogen material is directly related to the amount of porogen loaded into the sample. From the density measurement we saw there was linear reduction in porosity till ~30 % porogen loading. From the calculations done above we were able to see that an increase of up to ~ 32 % can happen in the surface of the film by the introduction of porosity. Figure 5.9 shows the expected increase in surface area of the material with porogen loading till 30 % loading which is also the observed percolation threshold of the material.
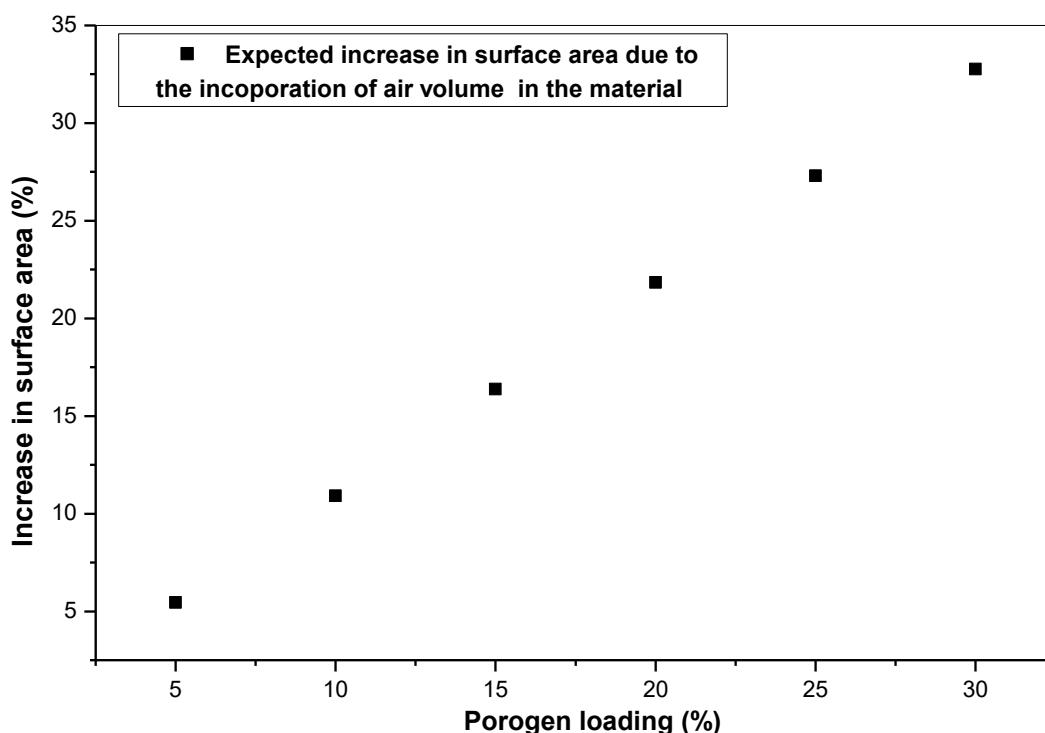


**Figure 5.9. Plot showing expected increase in surface area with incorporated porosity**

Figure 5.10 shows the AFM images of the surface of normal and porous PMSQ films. The scan was done on an area of 10 μm².
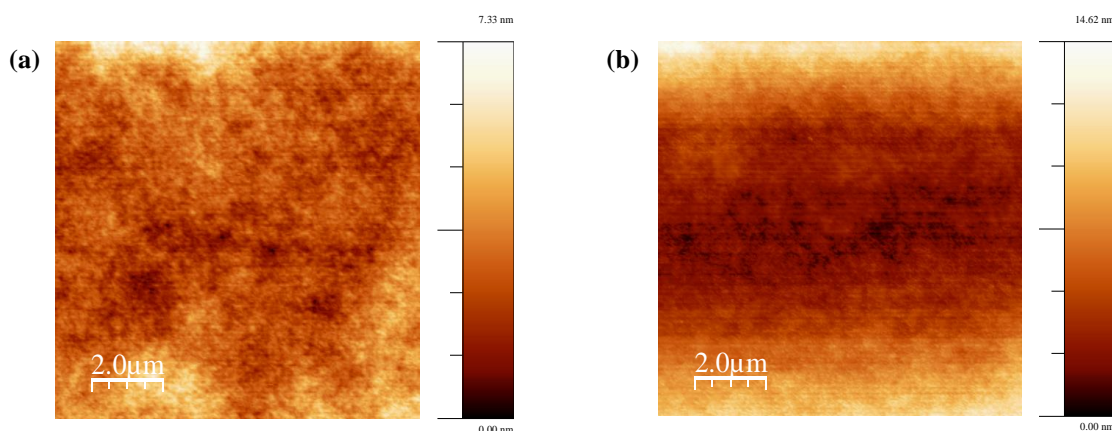


**Figure 5.10. AFM images of (a) normal film (b) porous film**

Roughness analysis done on figure 5.10.(a) which is the image of the surface of a normal PMSQ sample gave an RMS roughness of 0.98 nm. The roughness measurement increased to 2.91 nm, was obtained for the surface of the porous PMSQ film shown in figure 5.10.(b). This increase in the surface roughness of the porous film can be attributed to the creation of open pores on the surface during the decomposition of the porogen material.

The increase in surface area provides greater opportunity for the reactant species in the plasma to interact with the dielectric material. The presence of open pores further aids the plasma to penetrate deeper into the porous material when compared to normal density films, thereby causing higher degradation of the porous material when subjected to plasma exposure. This was evidenced in the increased κ – value of porous PMSQ films post plasma exposure, indicating significant damage happening during plasma exposure of the porous films.

# 5.3. PATTERNING OF DIELECTRIC USING NANOSPHERE LITHOGRAPHY

Patterning of dielectric is an important aspect of fabrication of integrated circuits. Patterning of low-k materials is a complicated process. Conventional lithographic techniques such as photolithography, X - ray lithography, scanning electron beam lithography etc. are expensive and time consuming processes. Industry processes include application of low-k layer, followed by the application of a metal to serve as hard mask. On top of the metal an antireflection coating (ARC) is applied followed by the photoresist layer. The photoresist is patterned by photolithographic techniques. The patterned photoresist is used to pattern the ARC and the metal hardmask. After that pattern transfer is done the photoresist layer and the ARC layer are stripped and the low-k material is patterned using the metal hard mask.

Nanosphere lithography [100 - 104] is a cost effective alternative to these techniques and can be successfully used to create ordered nanostructures. In this technique polystyrene nanospheres are organised on the surface to be patterned through self – assembly to get a single monolayer. These nanospheres are used as hard masks for further processing of the underlying dielectric layer. The idea is to deposit a periodic particle array (PPA) on the surface of the PMSQ film by PVD and use the deposited metal PPA to further etch patterns on the dielectric film. Figure 5.11 shows the schematic of NSL process.

Experiments were conducted to try and pattern the dielectric material using nanosphere lithography technique. Polystyrene nanospheres are commercially available as a suspension in water. It is easy to coat the spheres on a hydrophilic surface hence we need to determine the affinity of PMSQ films to water.
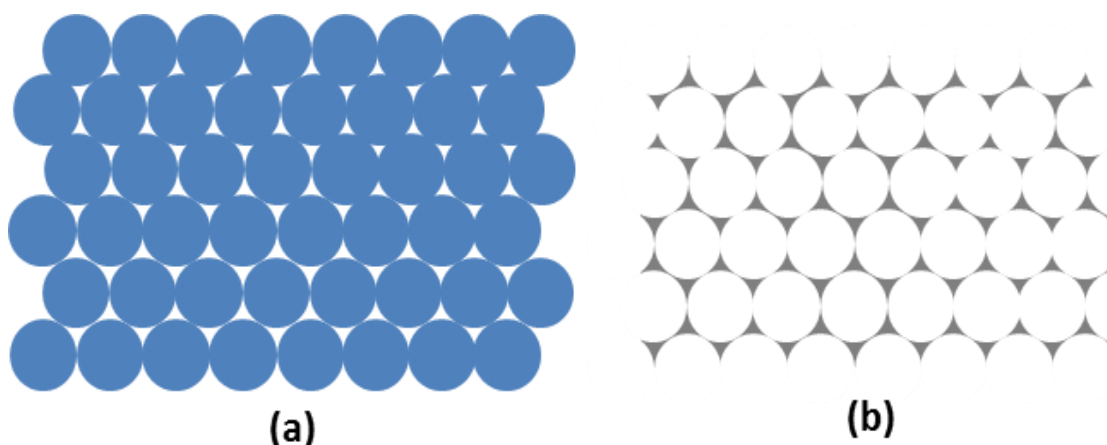
**Figure 5.11. Schematic showing the patterning using nanosphere lithography. (a) Self-assembled monolayer of nanospheres (b)figure showing the metal periodic particle array deposited using the nanospheres as hard mask through PVD after removal of nanospheres**

## 5.3.1. WATER CONTACT ANGLE MEASUREMENTS ON NORMAL AND PLASMA TREATED PMSQ FILMS

Contact angle measurements were made on the film after deposition to determine its affinity towards water. The films exhibit hydrophobic character, with a water contact angle of 91.11 degrees. Figure 5.12.(a) shows a snapshot of the water contact angle measurement for annealed PMSQ film. As the PMSQ films are hydrophobic in nature, direct application of the nanospheres onto the surface was not possible as it did not allow any water droplets with nanospheres to stick on to the surface.

Contact angle measurements were performed on plasma treated samples. Oxygen plasma treatment rendered the surface totally hydrophilic as seen in figure 5.12.(b). Figure 5.12.(c).shows a PMSQ film exposed to $SF_6$ plasma It was seen that the contact angle of the film surface reduced from around 91.11° to 42.18° as a result of 2 minutes of plasma exposure. The hydrophobic nature of the PMSQ surface was completely changed to hydrophobic after for 15 seconds of Ar plasma treatment as seen in figure 5.12.(d).

**Results: 56H.mdb**

| | |
|---|---|
| Contact Angle (deg) | 91.11 |
| Contact Angle Left (deg) | 90.22 |
| Contact Angle Right (deg) | 92.01 |
| Wetting Tension (dy/cm) | -1.420 |
| Wetting Tension Left (dy/cm) | -0.2841 |
| Wetting Tension Right (dy/cm) | -2.557 |
| Base Tilt Angle (deg) | 0.00 |
| Base (mm) | 2.7300 |
| Base Area (mm2) | 5.8535 |
| Height (mm) | 1.2200 |
| Tip Width (mm) | 0.6090 |
| Wetted Tip Width (mm) | 0.5989 |
| Sessile Volume (ul) | 4.9041 |
| Sessile Surface Area (mm2) | 10.974 |

**(a)**

**Results: 56F post.mdb**

| | |
|---|---|
| Contact Angle (deg) | 7.94 |
| Wetting Tension (dy/cm) | 72.30 |
| Wetting Tension Left (dy/cm) | 39.44 |
| Wetting Tension Right (dy/cm) | 39.44 |
| Base Tilt Angle (deg) | 0.00 |
| Base (mm) | 1.3321 |
| Base Area (mm2) | 1.3937 |
| Height (mm) | 4.623E-2 |
| Tip Width (mm) | 0.6106 |
| Wetted Tip Width (mm) | 0.5993 |
| Sessile Volume (ul) | 3.227E-2 |
| Sessile Surface Area (mm2) | 1.4004 |
| Contrast (cts) | 239 |
| Sharpness (cts) | 167 |

**(b)**

**Results: 56E post.mdb**

| | |
|---|---|
| Contact Angle (deg) | 42.18 |
| Wetting Tension (dy/cm) | 54.10 |
| Wetting Tension Left (dy/cm) | 39.44 |
| Wetting Tension Right (dy/cm) | 39.44 |
| Base Tilt Angle (deg) | 0.00 |
| Base (mm) | 4.1011 |
| Base Area (mm2) | 13.210 |
| Height (mm) | 0.7908 |
| Tip Width (mm) | 0.6103 |
| Wetted Tip Width (mm) | 0.5978 |
| Sessile Volume (ul) | 5.4823 |
| Sessile Surface Area (mm2) | 15.175 |
| Contrast (cts) | 249 |
| Sharpness (cts) | 174 |

**(c)**

**Results: 56G post.mdb**

| | |
|---|---|
| Contact Angle (deg) | 6.05 |
| Wetting Tension (dy/cm) | 72.59 |
| Wetting Tension Left (dy/cm) | 39.44 |
| Wetting Tension Right (dy/cm) | 39.44 |
| Base Tilt Angle (deg) | 0.00 |
| Base (mm) | 2.7635 |
| Base Area (mm2) | 5.9979 |
| Height (mm) | 7.306E-2 |
| Tip Width (mm) | 0.6105 |
| Wetted Tip Width (mm) | 0.5010 |
| Sessile Volume (ul) | 0.2193 |
| Sessile Surface Area (mm2) | 6.0147 |
| Contrast (cts) | 247 |
| Sharpness (cts) | 169 |

**(d)**

**Figure 5.12. Water contact angle measurement of PMSQ film (a) as deposited (b) $O_2$ plasma treated (c) $SF_6$ plasma treated (d) Ar plasma treated**

From these measurements performed we can see that a surface treatment with either with either $O_2$ or Ar plasma will produce the desired result by making the film surface hydrophilic and thereby making it ready for the coating of nanospheres on the film surface. From the studies presented in section 3.7, we know that oxygen plasma did not create any significant variation in the thickness of either the normal or the PMSQ films. But there was significant change in the κ – value of porous PMSQ films post $O_2$ plasma exposure. Hence Ar plasma treatment was selected for surface pre – treatment of PMSQ films to make it hydrophilic before coating nanospheres on the films.

## 5.3.2. ARGON PLASMA INTERACTION WITH PMSQ FILMS

To ensure that no etching or chemical modification was happening to the bulk of the film during Ar plasma exposure, thickness measurements were made on PMSQ films after 5 and 10 minutes of exposure. Figure 5.13. shows the measurements made during the exposure experiments. Figure 5.14 shows the FTIR spectrum of PMSQ films as deposited and after being exposed to Ar plasma for 15 minutes. The spectrum do not show any change in the intensities before and after exposure.
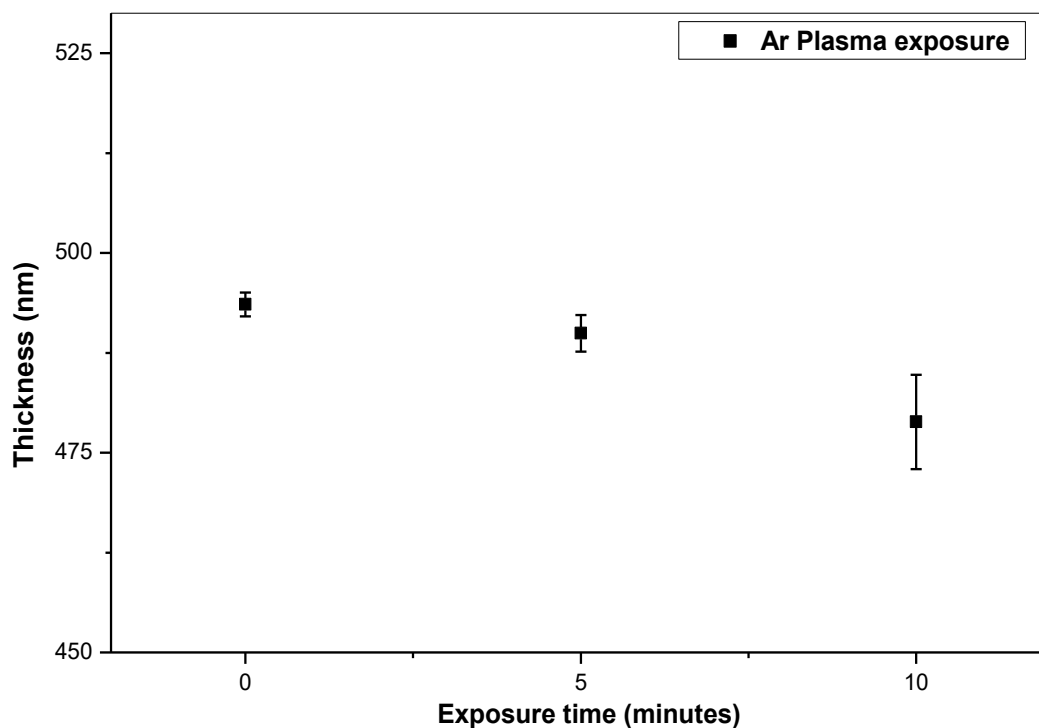


**Figure. 5.13. Thickness measurements done on PMSQ polymer during Ar plasma exposure (Chamber pressure: 200 mTorr, Applied forward power : 150 Watts, Gas flow rate : 50 SCCM, samples exposed at 5 minute intervals)**
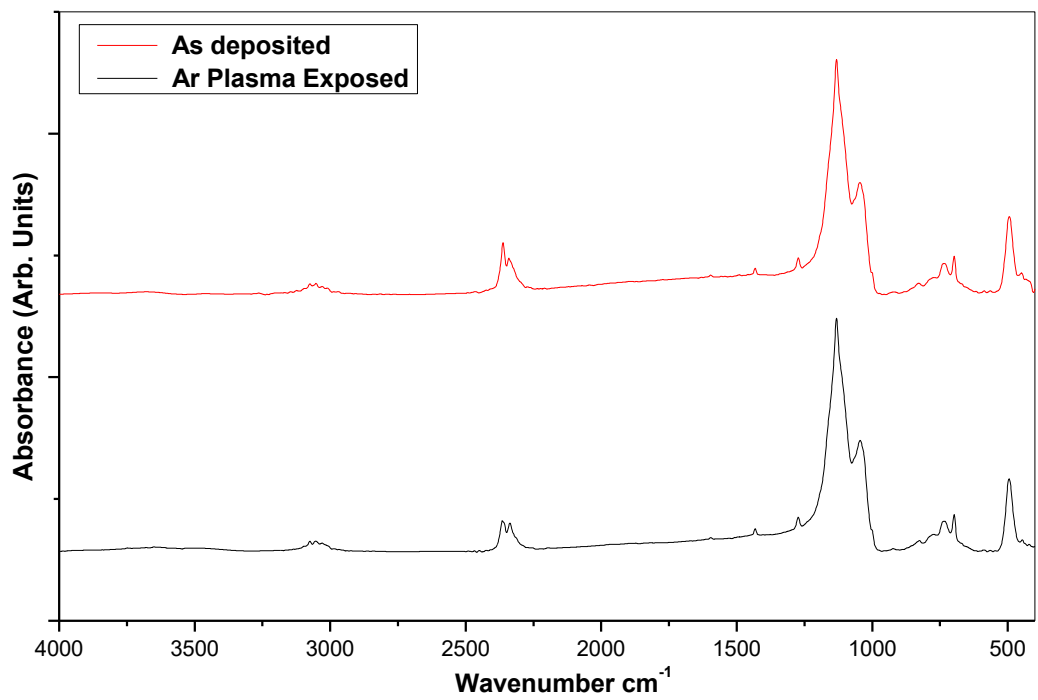
**Figure 5.14 SEM image showing nanospheres spin coated on the surface of PMSQ polymer**

## 5.3.3. AFM IMAGES OF PMSQ FILM SURFACE EXPOSED TO $O_2$ & ARGON PLASMAS

Since no significant changes in the thickness or chemical structure was observed for $O_2$ and Ar plasma treated samples, surface roughness measurements were performed on PMSQ films exposed to these plasmas to understand the effect of plasma exposure on the film surface. Figure 5.15 shows 10 $\mu m^2$ scans of PMSQ films exposed to (a) Ar plasma for a duration 1 min and (b) to $O_2$ plasma for 1 min. The RMS roughness measurement showed a value of 4.8 for Ar plasma treated sample and roughness measurement of 3.1 for $O_2$ plasm treated film. This increase in surface roughness can be due to the sputtering effect that happens on the film surface when exposed to plasmas. This large increase in surface roughness may be the reason for the variation in contact angle of PMSQ films after plasma exposure.
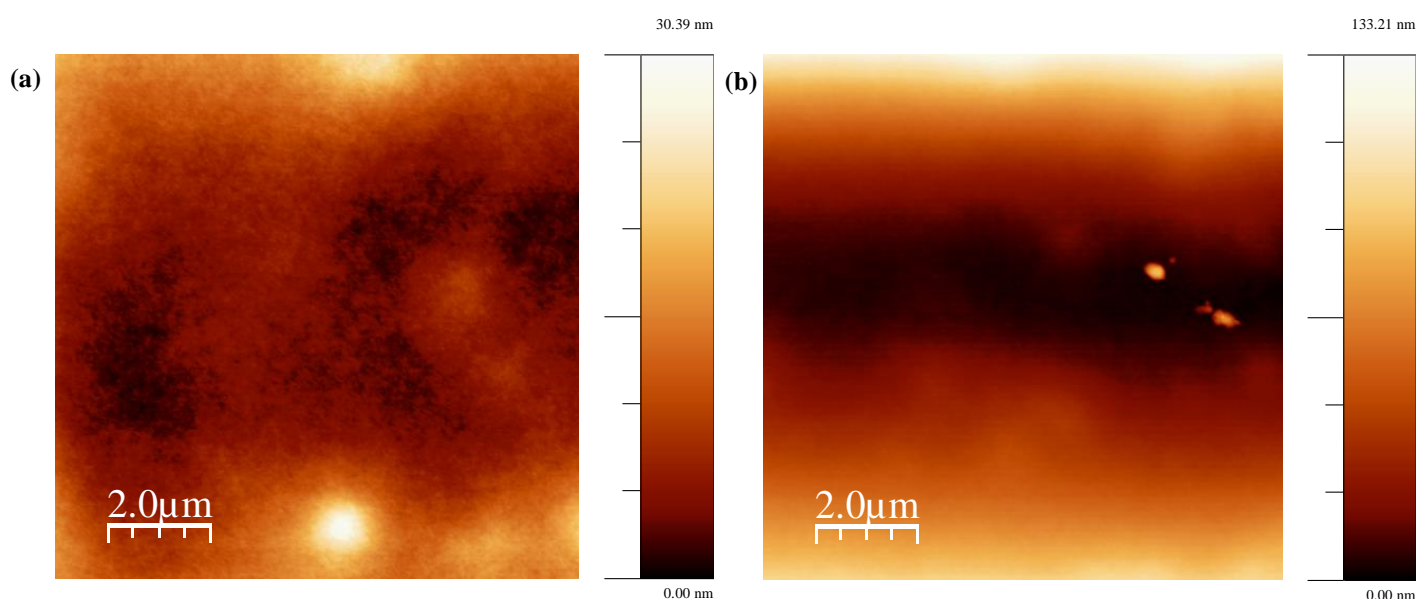


**Figure. 5.15. AFM images of PMSQ films exposed to (a) Ar plasma (b) $O_2$ plasma**

## 5.3.4. INTERACTION OF FILMS WITH $SF_6$ - $O_2$ PLASMAS

Material erosion was not observed for pure oxygen plasma exposed films where as pure $SF_6$ plasma etched the film at an approximate rate of ~ 60 nm/minute as seen in

section 3.7. It was observed that the use of a mixture of $SF_6$ and $O_2$ gases at various concentrations can significantly alter the etch rate. Figure 5.16 shows the variation in etch rate of PMSQ films with the variation in feed gas ratio. The chamber pressure was maintained at 200 mTorr and the applied forward power was 150 W. The gas flow rate was kept at a constant net flow rate of 50 sccm. A mixture of 45 SCCM $O_2$ and 5 SCCM $SF_6$ gave an etch rate of ~ 260 nm/minute and the etch rate peaked at 40 SCCM $O_2$ and 10 SCCM $SF_6$ at ~ 280 nm/minute. The rate falls down with further increase in the percentage of $O_2$ and reaches approximately ~ 60 nm/s for pure $SF_6$ plasma.

The experiment gave a good understanding of the plasma with different gas ratios which proved helpful in etching patterns on PMSQ thin films using nanosphere lithography technique
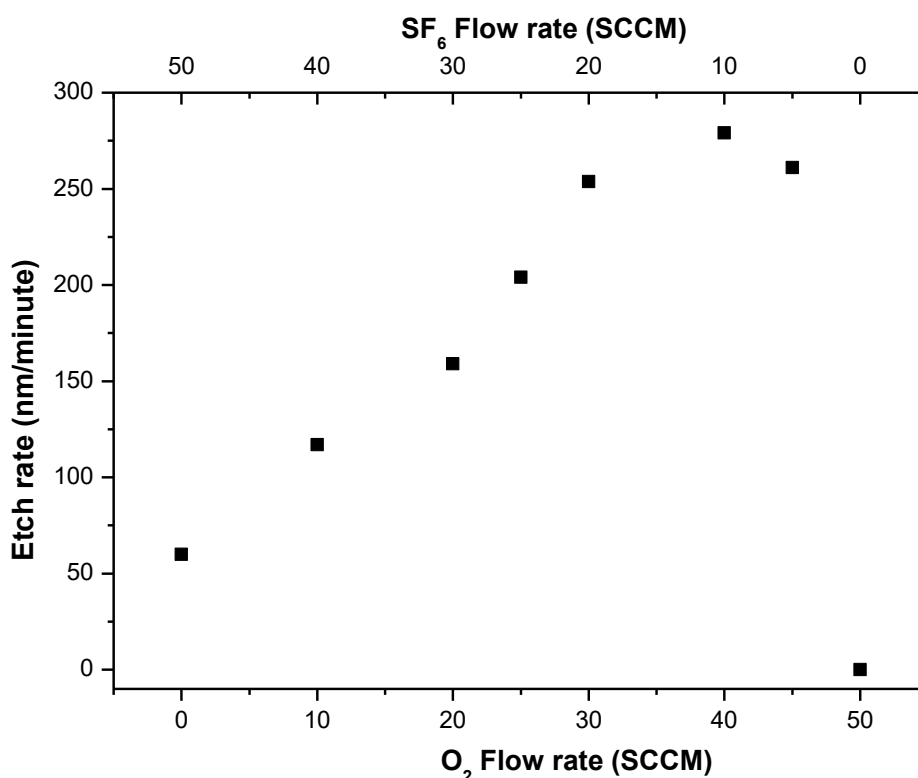


**Figure 5.16. Etch rate of PMSQ films in SF6 - O2 plasma exposure (Chamber pressure: 200 mTorr, Applied forward power : 150 Watts, combined $O_2$ & $SF_6$ gas flow rate : 50 SCCM, samples exposed for 1 minute)**

## 5.3.5. DEPOSITION OF NANOSPHERES BY SPIN COATING

Polystyrene nanospheres.(Fisher Scientific) were obtained as a suspension in water. The suspension can settle down and get aggregated at the bottom of the bottle after a period of time. It is possible to get them back into the suspended state by sonication them for 15 – 20 minutes in an ultrasonic bath.

The nanospheres were the applied to the films by a multi stage spin coating process [105] after plasma treating the PMSQ films with Ar plasma and creating a hydrophilic surface for the spheres to disperse. The substrates coated with nanosphere were spun at 400 rpm around 10 seconds for the even spreading off of the solution. The spin speed was increased to 800 rpm for 120 seconds to remove the excess solution from the surface and then finally ramped up to 1400 rpm for 10 seconds to help the spheres for uniform assembly. An SEM image of the spin coated spheres on top the low-k PMSQ material is shown in the figure 5.17.
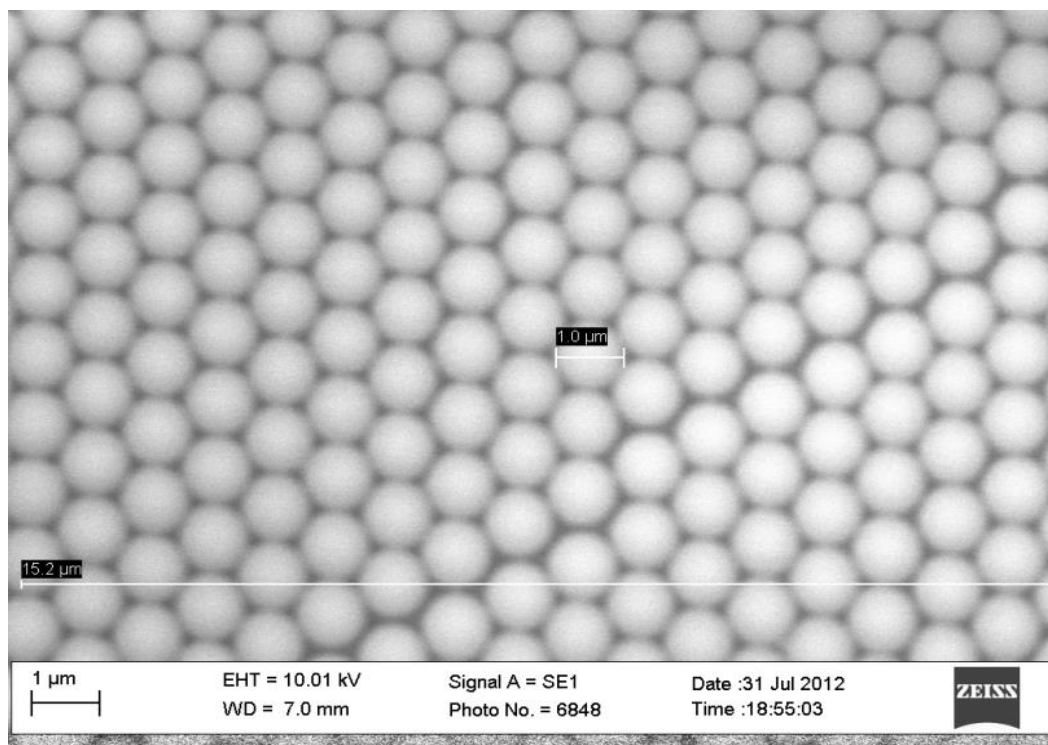


**Figure 5.17. SEM image showing nanospheres spin coated on the surface of PMSQ polymer**

SEM images of self-assembled nanospheres were taken at an EHT of ~ 10 KV and that of deposited aluminium patterns and plasma etched patterns were taken at EHT of ~ 13 – 14 KV.

## 5.3.6. DEPOSITION OF METAL PATTERN ON THE PMSQ FILMS USING NANOSPHERE LAYER AS THE HARDMASK

The nanosphere coated substrate was loaded into an evaporator. The evaporator was pumped down to high vacuum and aluminium metal was deposited on the substrates through evaporation. The spheres were then removed by sonication in ethanol for 3 minutes. Figure 5.18. shows the metal patterns deposited on the PMSQ film surface by using the deposited nanospheres as the deposition mask.
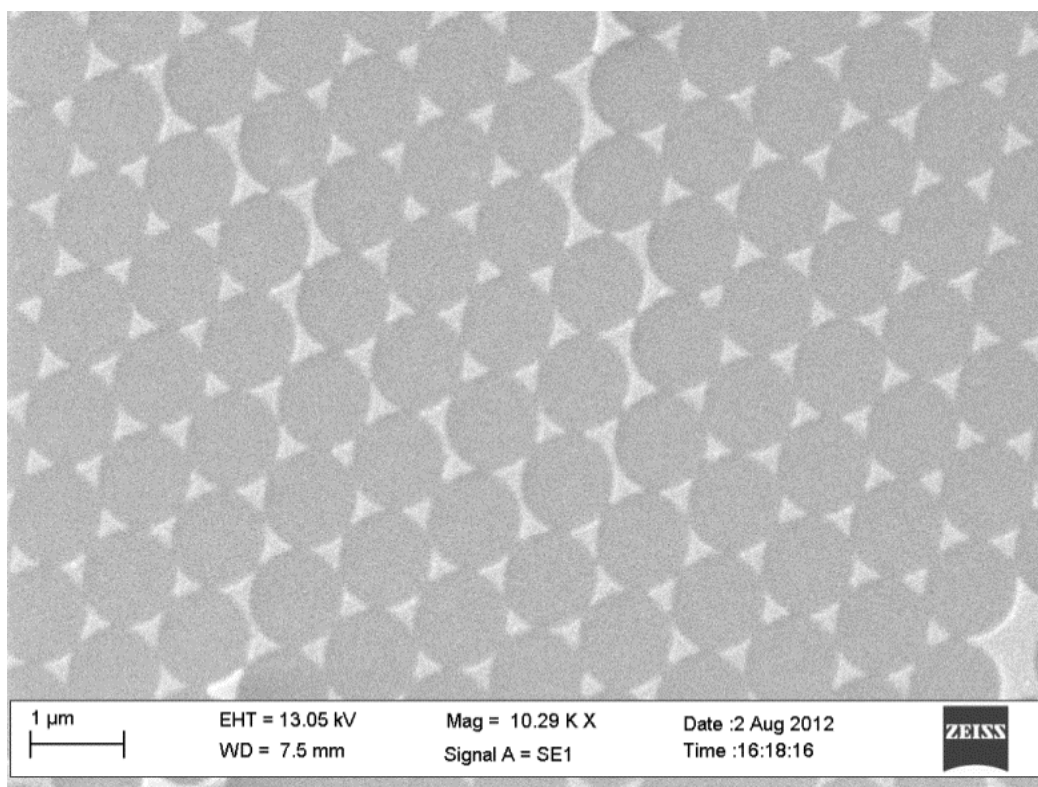


**Figure 5.18. Metal pattern left behind after removal of the nanospheres by sonication**

## 5.3.7. SF$_6$ - O$_2$ ETCH OF PMSQ FILMS USING DEPOSITED AL PATTERN AS METAL HARD MASK

Attempts were made to create periodic structures on top of dielectric films by etching in SF$_6$ - O$_2$ plasma (SF$_6$ 40SCCM O$_2$ 10 SCCM, 100mTorr, 150 Watts) for two minutes. This particular gas mixture was giving the most etch rate in previous etching experiments as described in section 5.3.4. The etched patterns were imaged by SEM after the etch process as seen in figures 5.19 and 5.20..
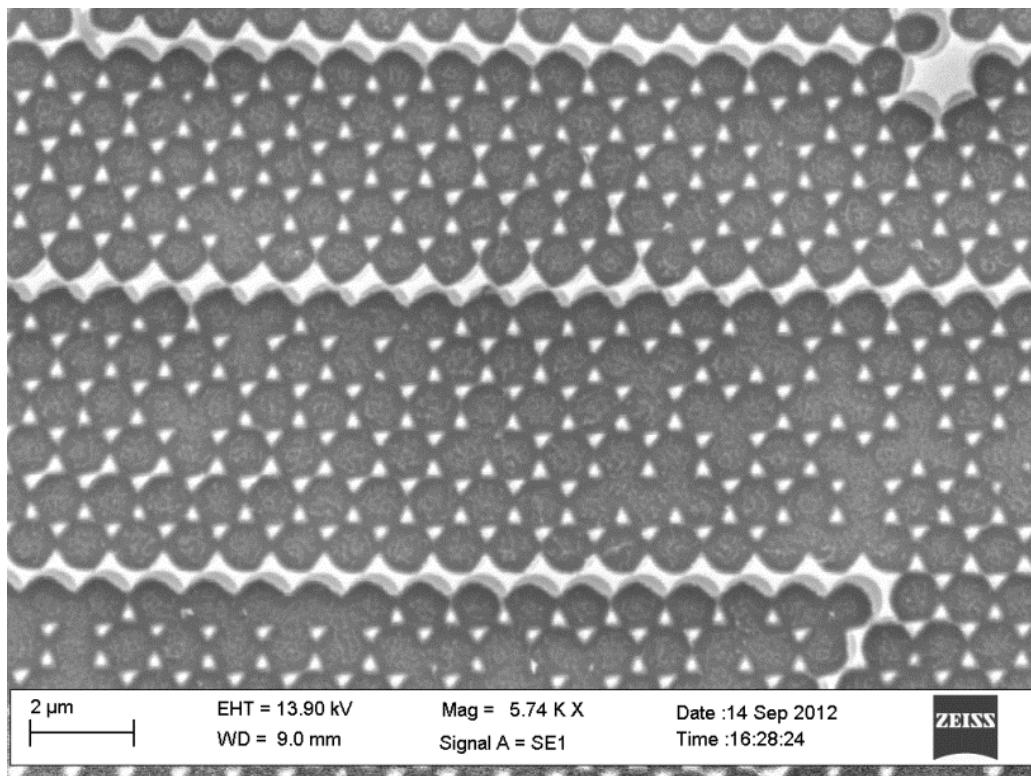


**Figure 5.19. Plasma etched patterns - top view. exposure (Chamber pressure: 200 mTorr, Applied forward power : 150 Watts, Gas flow rate : SF$_6$ 40 SCCM & O$_2$ 10 SCCM, samples exposed for 2 minutes)**
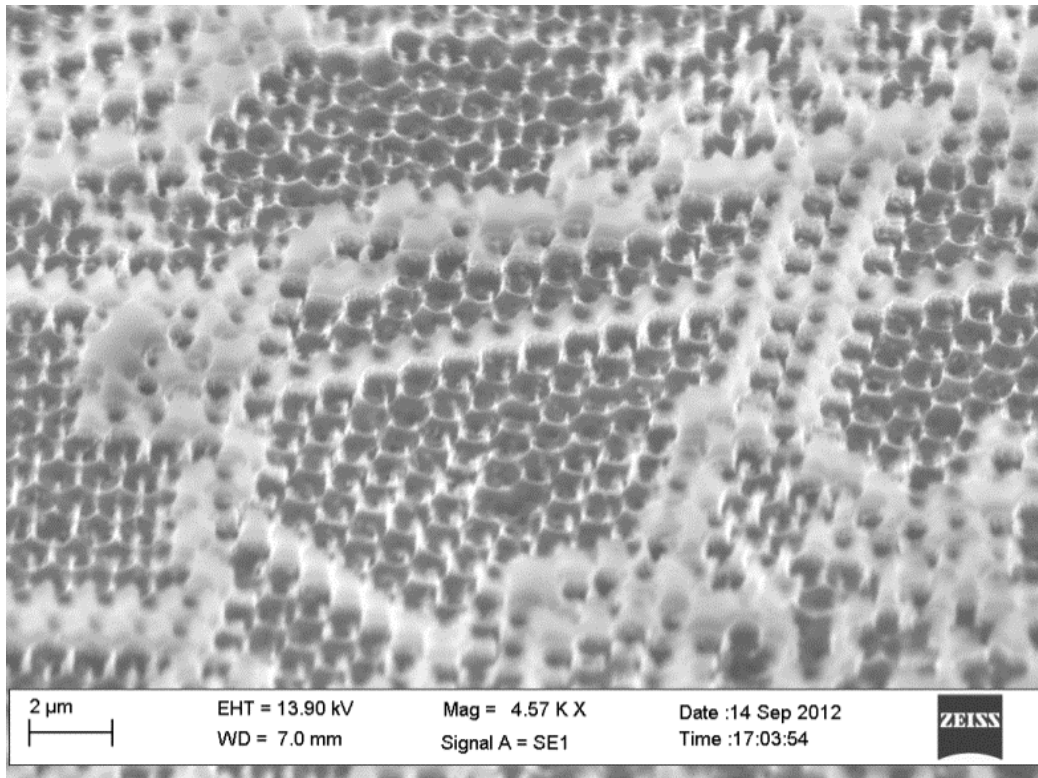
**Figure 5.20. Plasma etched patterns – side view , tilted at 60 degrees. (Chamber pressure: 200 mTorr, Applied forward power : 150 Watts, Gas flow rate : SF$_6$ 40 SCCM & O$_2$ 10 SCCM, samples exposed for 2 minutes)**

The SEM image in figure 5.19. shows a top down view of the etched film. The picture clearly gives us a sense of depth indicating that the material surrounding the deposited metal was removed during the etch process. Figure 5.20. shows the same substrate titled at an angle of 60 °. The image shows tiny pointed structures surrounded with crater like regions. This shows that the dielectric material directly beneath the deposited metal hard mask remains intact whereas the film surrounding the metal is etched in an isotropic fashion.

The images lack clarity as there is the problem of the dielectric film, being an electrical insulator, charging during the imaging process due to the accumulation of electrons.

# 5.4. SUMMARY

Incorporation of air volume into the PMSQ films reduces the density and subsequently the $\kappa$ – value of the material. But the measured densities at different levels of incorporated porosity show that the amount of air volume incorporated into the material deviates from the expected level. Even though we could see a direct correlation between the porogen loading and incorporated porosity at lower concentrations, there a visible deviation from this correlation beyond the percolation threshold after which agglomeration of porogen molecules leads to pore collapse. The integration of pores into the material also increases the surface area of the film as seen from the calculations and the AFM data which can be the reason for the increased interaction of the plasma with the porous material resulting in the increase in the dielectric constant of the material post exposure.

NSL is a promising cost effective technology to deposit periodic patterns as seen from the SEM images. Nanospheres were successfully deposited on the PMSQ thin films after priming the surface with Ar plasma. The process parameters for deposition and removal of nanospheres post metal hard mask deposition is listed in summarised in table 5.1.

| Re – Dispersion of nanospheres in water | |
| --- | --- |
| Sonication of the container in a water bath for 10 minutes | |
| **Spin coating parameters** | |
| 400 rpm for 10 seconds | For even spreading of the solution |
| 800 rpm for 120 seconds | For removal of excess solution |
| 1400 rpm for 10 seconds | To facilitate uniform assembly of spheres |
| Acceleration setting – 15 | ~ 1500 rotations per second increment |
| **Removal of nanospheres** | |
| By sonication of nanospheres in ethanol for 3 minutes and by rinsing in DI water thereafter. | |

**Table 5.1. Table listing the optimised process parameters used NSL**

# CHAPTER 6
# CONCLUSIONS AND FUTURE WORK

## 6.1. THESIS CONCLUSIONS

SSQ class of materials are good candidates for ILD applications. My studies focused on PMSQ which was a material that was not previously investigated for use as an ILD.

A process to successfully deposit SSQ thin films was developed and optimised to obtain good quality films. It was seen that the spin speed did not have any significant effect on the thickness of the deposited films. This is due to the low viscosity of the polymer solution in MIBK. The thickness of the deposited films had direct relation with the solute concentration in the solution. This correlation was observed only till a critical concentration beyond which the solution gets saturated. Further increase of solute ratio in the solution did not increase the thickness of the deposited film accordingly. The evaporation rate of the solvent also affects the film formation. Rapid evaporation of the solvent led to pinhole formation with solutions from solvents such as THF. Solutions from solvents with lower evaporation rate such as MIBK gave good quality films. Filtering the solution prior to spin coating improved the film quality considerably. Both MSQ and PMSQ films undergo crosslinking transformation at ~ 400° C.

MSQ films were successfully deposited and the thermal transformation of the films was studied. The crosslinking of the polymer happens at 400° C which was observed by the variation in the peak intensities of the dominant peaks seen in the 1000 – 1200 cm$^{-1}$ region of the FTIR spectrum of the material. The dielectric constant of the films was determined to be ~ 2.6 ±0.1 which is in good agreement with reported κ - value of the

material. Oxygen plasma exposure did not affect the thickness of MSQ films but there was an increase in the κ - value of the films as a result of plasma exposure. This is due to the intake of moisture resulting from plasms exposure, as seen from the post oxygen plasma exposure FTIR of the MSQ film. The films were etched when subjected to $SF_6$ plasma exposure. F radicals present in the plasma play a key role in etching the films. Moisture absorption observed in films post plasma exposure resulted in increased κ – value for the films.

Successful deposition of PMSQ were done employing identical techniques as in the case of MSQ films. Comparing the post anneal FTIR spectra of MSQ and PMSQ films it can be seen that film backbone in both films extent from ~ 1000 - 1200 cm $^{-1}$, but the dominant peak in this region are different for both materials. For MSQ film the dominant peak lies at ~ 1035 cm$^{-1}$which is the anti- symmetric stretching of the suboxide and for PMSQ and the dominant peak for PMSQ film is at ~ 1132 cm$^{-1}$. These indicate that there is structural difference between these two materials even though they are chemically similar. The dominant suboxide peaks in the Si-O-Si region indicate that the annealed MSQ films have a network structure whereas the PMSQ films have cage structure. The films showed good thermal stability as the films were stable of the stable even at $600^{\circ}$ C. This is of great advantage as this material can withstand the high temperatures encountered during the rapid thermal annealing of copper in IC manufacturing which is an important requirement for a good ILD material.

Oxygen plasma treatment did not affect the thickness of PMSQ films as evidenced from the spectroscopic ellipsometry measurements. A comparison of the pre and post plasma exposure FTIR spectra did not show any intake of moisture into the material post plasma treatment. There was also no significant variation in the dielectric constant of the material. This is a key advantage of the PMSQ material when compared to so many other

dielectric materials chemically similar to SSQs, as reports show increase in κ - value of these materials after exposure to oxygen plasma. The reported increase in the dielectric constant of some of these materials is shown in figure 6.1. The increase in the dielectric constant of the low-k films after ashing is reported as a major limitation for ILD materials. The higher plasma damage resistance of the PMSQ films could be explained by the inherent stability of the phenyl ring as well as its $d_\pi$-$p_\pi$ contribution in the Si-C bond, which would increase the strength of siloxane polymer [80, 81]
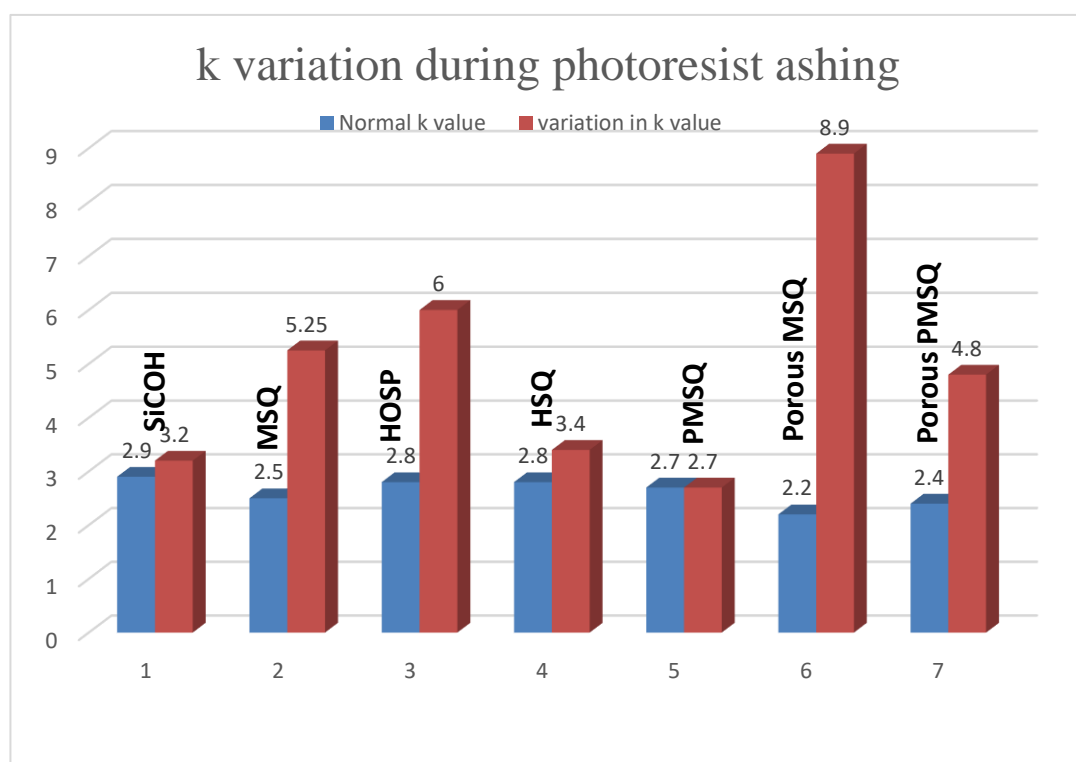


**Figure 6.1. Graph showing the variation in κ – value of different materials during O₂ plasma treatment**

PMSQ films were etched when processed with SF₆ plasma. This is evident from the reduction in thickness and decrease in peak intensities of FTIR spectra of the films after plasma treatment. The κ – value of the films showed a slight decrease following SF₆

plasma etch This is due to the insertion of F into the material as a result of plasma exposure, as F incorporation can reduce the dielectric constant of the material.

A deposition process was developed to deposit tCD –PMSQ hybrid films and the annealing conditions were modified to facilitate the proper burn out of the porogen material when heated to its decomposition temperature. The process was optimised to ensure repeatability and to ensure the generation of pores within the films to obtain porous PMSQ thin films. TGA analysis showed that tCd had decomposition temperature of ~ $400^{\circ}$C with a narrow decomposition temperature of $> 100^{O}$ C. This is evidenced from the disappearance of the two dominant peaks from 2800 - 3000 cm$^{-1}$ (C-H aliphatic stretching peaks) and from 1000-1250 cm$^{-1}$ (C-O-C linkages) from the FTIR spectra of the tCD material when heated to $400^{O}$ C.

The successful introduction of porosity into the PMSQ material was substantiated by the density and $\kappa$ – value measurements done of the films. Data obtained from XRR measurements showed that the density of the films decreased ~ 25 % with addition of 30 % of tCD by weight to the weight of polymer. This generation of porosity reduced the net dielectric constant of the bulk of the material. The $\kappa$- value of the normal films was successfully reduced by ~ 20% from $\kappa = 2.7 \pm 0.1$ to $\kappa = 2.2 \pm 0.1$ by the introduction of ~ 25% porosity.

Exposure to oxygen plasma did not result in erosion of the material as evidenced from the thickness measurements and from the comparison of FTIR spectrum of the films pre and post plasma exposure. But there was substantial increase in the $\kappa$- value of the material. This is in contrast to the behaviour of the PMSQ material in its normal state with no porosity present within the films.

The porous PMSQ films were successfully etched when subjected to $SF_6$ plasma exposure as it was in the case of the normal films as seen from the thickness measurements and from the FTIR spectra of the films post plasma exposure.

The introduction of porosity into thin films changes key properties of the film such as density, dielectric constant, surface area etc. At lower concentrations of porogen loading, below a certain critical limit known as the percolation threshold, there is an observed correlation between the amount of porogen loaded into the film to the amount of porosity generated as seen from the XRR measurements. Beyond the percolation threshold further porogen loading will not effectively reduce the density of the films further. This is due to pore collapse happening within the material owing to the agglomeration of tCD within the films leading to the formation of worm like structures, rather than individual pores. Generation of porosity within the material also increases the area of the films. Calculations done show that this increase in the surface area also has a correlation with the amount of porogen loaded into the material up to the percolation threshold.

Even though deposited PMSQ films are hydrophilic in nature, plasma treatment changes the surface roughness and water affinity of the films. $O_2$ and Ar plasmas rendered the films totally hydrophilic. The etch rate of the films varied with the gas ratios in the feed gas. The films were etched at a higher rate with $SF_6 – O_2$ plasmas.

Nanospheres were spin coated on PMSQ film surfaces that were made hydrophilic by Ar plasma treatment by a multi stage spin coating deposition technique. Al patterns were deposited on the surface of the film using the self - assembled nanospheres as mask. The films were etched using the deposited Al pattern as hard mask after removal of the nanospheres by sonication in ethanol. SEM images showed the formation of etched

patterns on the film surface and thus it was demonstrated that NSL technique could be used as a viable technique for creating periodic structures.

A detailed understanding of PMSQ has been obtained with this work which will enable this material to be used as an ILD. The plasma interaction of the pristine and porous PMSQ films has been done and the exceptional stability of the normal films has been identified. The hydrophobic nature of the material when cast into thin films and also its superior thermal stability was also proven suggesting that this material in an ideal and cost effective material for ILD applications.

# 6.2. SUGGESTED FUTURE WORK

It will be great importance to understand the size of the pores generated within the films and their distribution to have a better understanding of the porous PMSQ material. The mechanical stability of the material needs to be tested. Porosity obviously increases the leakage current within the material. Hence it will good to do a study about the leakage current in both the porous and pristine PMSQ films and also to measure their dielectric breakdown voltage.

Several measurements were made with a wide variety of characterisation techniques. Some more additional electrical measurements can be done which would be quite interesting. Measurements can be made by changing the ac frequency. Other factors that could be varied are the electrical bias and oscillator level magnitude. It would also be interesting to see if there is any variation if we change the area of the deposited top contact.

Diffusion of metals into the dielectric material also needs to be investigated which will in turn also help to identify suitable materials to be used as diffusion barrier layers with the dielectric material. A good understanding of the adhesion between the PMSQ material and the identified barrier layer is yet another interesting study. The coefficient of thermal expansion (CTE) is another critical parameter that needs to be investigated especially PMSQ being an organic polymer. A wide variety of organic polymers tends to have CTE mismatches with Cu, the metal most widely used for interconnect wiring in the IC manufacturing industry.

# REFERENCES

1. Bardeen, J. and Brattain, W.H. 1948. The transistor, a semi-conductor triode. *Physical Review,* 74(2), pp.230.

2. Brattain, W. and Bardeen, J. 1948. Nature of the forward current in germanium point contacts. *Physical Review,* 74(2), pp.231.

3. Teal, G. 1954. Some recent developments in silicon and germanium materials and devices. *IN: National IRE Conf.,(Dayton, OH).*

4. Kilby, J.S. 1976. Invention of the integrated circuit. *IEEE Transactions on Electron Devices,* 23(7), pp.648-654.

5. Kilby, J.S.C. 2001. Turning potential into realities: The invention of the integrated circuit (Nobel lecture). *ChemPhysChem,* 2(8-9), pp.482-489.

6. Moore, G.E. 1965. Cramming more components onto integrated circuits. *Cramming More Components Onto Integrated Circuits,*

7. Petkov, M. 2003. Low-k interlevel dielectrics technology.

8. Havemann, R.H. and Hutchby, J.A. 2001. High-performance interconnects: An integration overview. *Proceedings of the IEEE,* 89(5), pp.586-601.

9. Baklanov, M., Maex, K. and Green, M. 2007. *Dielectric films for advanced microelectronics.* Wiley.

10. Andricacos, P.C. 1999. Copper on-chip interconnections. *The Electrochemical Society Interface,* 8(1), pp.6.

11. Edelstein, D., Heidenreich, J., Goldblatt, R., Cote, W., Uzoh, C., Lustig, N., Roper, P., McDevitt, T., Motsiff, W. and Simon, A. 1997. Full copper wiring in a sub-

0.25 μm CMOS ULSI technology. *IN: Electron Devices Meeting, 1997. IEDM'97. Technical Digest., International.* IEEE.

12. Edelstein, D., Rathore, H., Davis, C., Clevenger, L., Cowley, A., Nogami, T., Agarwala, B., Arai, S., Carbone, A. and Chanda, K. 2004. Comprehensive reliability evaluation of a 90 nm CMOS technology with Cu/PECVD low-k BEOL. *IN: Reliability Physics Symposium Proceedings, 2004. 42nd Annual. 2004 IEEE International.* IEEE.

13. Volksen, W., Miller, R.D. and Dubois, G. 2010. Low dielectric constant materials. *Chemical Reviews,* 110(1), pp.56.

14. Grill, A. 2009. Porous pSiCOH Ultralow-k Dielectrics for Chip Interconnects Prepared by PECVD. *Annual Review of Materials Research,* 39pp.49-69.

15. Houssa, M. 2010. *High k Gate Dielectrics.* CRC Press.

16. Beaudoin, S., Graham, S., Jaiswal, R., Kilroy, C., Kim, B.S., Kumar, G. and Smith, S. 2005. An update on low-k dielectrics. *Interface-Electrochemical Society,* 14(2), pp.35-40.

17. Miller, R.D. 1999. In Search of Low-k Dielectrics. *Science,* 286(5439), pp.421-423.

18. Treichel, H. 2001. Low dielectric constant materials. *Journal of Electronic Materials,* 30(4), pp.290-298.

19. Maex, K., Baklanov, M., Shamiryan, D., Iacopi, F., Brongersma, S. and Yanovitskaya, Z. 2003. Low dielectric constant materials for microelectronics. *Journal of Applied Physics,* 93(11), pp.8793-8841.

20. Shamiryan, D., Abell, T., Iacopi, F. and Maex, K. 2004. Low-k dielectric materials. *Materials Today,* 7(1), pp.34-39.

21. Morgen, M., Ryan, E.T., Zhao, J.H., Hu, C., Cho, T. and Ho, P.S. 2000. Low dielectric constant materials for ULSI interconnects. *Annual Review of Materials Science,* 30(1), pp.645-680.

22. Volksen, W., Lionti, K., Magbitang, T. and Dubois, G. 2013. Hybrid low dielectric constant thin films for microelectronics. *Scripta Materialia,* (0),

23. Hatton, B.D., Landskron, K., Hunks, W.J., Bennett, M.R., Shukaris, D., Perovic, D.D. and Ozin, G.A. 2006. Materials chemistry for low-k materials. *Materials Today,* 9(3), pp.22-31.

24. Homma, T. 1998. Low dielectric constant materials and methods for interlayer dielectric films in ultralarge-scale integrated circuit multilevel interconnections. *Materials Science and Engineering: R: Reports,* 23(6), pp.243-285.

25. Treichel, H., Ruhl, G., Ansmann, P., Wurl, R., Muller, C. and Dietlmeier, M. 1998. Low dielectric constant materials for interlayer dielectric. *Microelectronic Engineering,* 40(1), pp.1-19.

26. Baklanov, M., Ho, P.S. and Zschech, E. 2012. *Advanced Interconnects for ULSI Technology.* Wiley.

27. Martin, S.J., Godschalx, J.P., Mills, M.E., Shaffer, E. and Townsend, P.H. 2000. Development of a Low-Dielectric-Constant Polymer for the Fabrication of Integrated Circuit Interconnect. *Advanced Materials,* 12(23), pp.1769-1778.

28. Wu, W., Wallace, W.E., Lin, E.K., Lynn, G.W., Glinka, C.J., Ryan, E.T. and Ho, H. 2000. Properties of nanoporous silica thin films determined by high-resolution x-ray reflectivity and small-angle neutron scattering. *Journal of Applied Physics,* 87(3), pp.1193-1200.

29. Fayolle, M., Passemard, G., Louveau, O., Fusalba, F. and Cluzel, J. 2003. Challenges of back end of the line for sub 65 nm generation. *Microelectronic Engineering,* 70(2–4), pp.255-266.

30. Hoofman, R., Verheijden, G., Michelon, J., Iacopi, F., Travaly, Y., Baklanov, M., Tökei, Z. and Beyer, G. 2005. Challenges in the implementation of low-k dielectrics in the back-end of line. *Microelectronic Engineering,* 80pp.337-344.

31. Kim, C. 2011. *Electromigration in thin films and electronic devices: Materials and reliability.* Elsevier.

32. Mosig, K., Jacobs, T., Brennan, K., Rasco, M., Wolf, J. and Augur, R. 2002. Integration challenges of porous ultra low-< i> k spin-on dielectrics. *Microelectronic Engineering,* 64(1), pp.11-24.

33. Baklanov, M.R., de Marneffe, J., Shamiryan, D., Urbanowicz, A.M., Shi, H., Rakhimova, T.V., Huang, H. and Ho, P.S. 2013. Plasma processing of low-k dielectrics. *Journal of Applied Physics,* 113(4), pp.041101-041101-41.

34. Lieberman, M.A. and Lichtenberg, A.J. 1994. Principles of plasma discharges and materials processing.

35. Kaanta, C.W., Bombardier, S.G., Cote, W.J., Hill, W.R., Kerszykowski, G., Landis, H.S., Poindexter, D.J., Pollard, C.W., Ross, G.H. and Ryan, J.G. 1991. Dual damascene: a ULSI wiring technology. *IN: VLSI Multilevel Interconnection Conference, 1991, Proceedings., Eighth International IEEE.* IEEE.

36. Arden, W., Brillouët, M., Cogez, P., Graef, M., Huizing, B. and Mahnkopf, R. 2010. More-than-Moore white paper. *Version,* 2pp.14.

37. Baklanov, M.R., Urbanowicz, A., Mannaert, G. and Vanhaelemeersch, S. 2006. Low dielectric constant materials: challenges of plasma damage. *IN: Solid-State and Integrated Circuit Technology, 2006. ICSICT '06. 8th International Conference on.*

38. Tokei, Z., Baklanov, M., Ciofi, I., Li, Y. and Urbanowicz, A. 2008. Plasma-induced Low-k Modification and Its Impact on Reliability. *Semiconductor Fabtech,* 35pp.1-6.

39. H. BaneyItohSakakibara and Suzuki,1995. *Chem. Rev.***95**1409

40. Lee, B., Park, Y., Hwang, Y., Oh, W., Yoon, J. and Ree, M. 2005. Ultralow-k nanoporous organosilicate dielectric films imprinted with dendritic spheres. *Nature Materials,* 4(2), pp.147-U26.

41. Kohl, A.T., Mimna, R., Shick, R., Rhodes, L., Wang, Z.L. and Kohl, P.A. 1999. Low k, Porous Methyl Silsesquioxane and Spin-On-Glass. *Electrochemical and Solid-State Letters,* 2(2), pp.77-79.

42. Brown, J.F., Vogt, L.H. and Prescott, P.I. 1964. Preparation and characterization of the lower equilibrated phenylsilsesquioxanes. *Journal of the American Chemical Society,* 86(6), pp.1120-1125.

43. Brown Jr, J.F., Vogt Jr, L.H., Katchman, A., Eustance, J.W., Kiser, K.M. and Krantz, K.W. 1960. Double chain polymers of phenylsilsesquioxane. *Journal of the American Chemical Society,* 82(23), pp.6194-6195.

44. Yang, C. and Chen, W. 2002. The structures and properties of hydrogen silsesquioxane (HSQ) films produced by thermal curing. *Journal of Materials Chemistry,* 12(4), pp.1138-1141.

45. Penaud, J., Fruleux, F. and Dubois, E. 2006. Transformation of hydrogen silsesquioxane properties with RIE plasma treatment for advanced multiple-gate MOSFETs. *Applied Surface Science,* 253(1), pp.395-399.

46. Min, Z., Baoqin, C., Changqing, X., Ming, L. and Jiebing, N. 2010. Study of process of HSQ in electron beam lithography. *IN: Nano/Micro Engineered and Molecular Systems (NEMS), 2010 5th IEEE International Conference on.* IEEE.

47. Baek, I., Yang, J., Cho, W., Ahn, C., Im, K. and Lee, S. 2005. Electron beam lithography patterning of sub-10nm line using hydrogen silsesquioxane for nanoscale device applications. *Journal of Vacuum Science & Technology B,* 23(6), pp.3120-3123.

48. Jin, C. and Wetzel, J. 2000. Characterization and integration of porous extra low-k (XLK) dielectrics. *IN: Interconnect Technology Conference, 2000. Proceedings of the IEEE 2000 International.* IEEE.

49. Lucas, F.O. 2008. *Evaluation of the Microstructural, Electronic and Optoelectronic Properties of Y-CuCl Thin Films and their Fabrication on Si Substrates,*

50. Alam, M. 2012. *Synthesis and Characterization of Nanocrystalline CuCl Hybrid Films for Electroluminescent Device Fabrication.,*

51. Chang, T., Mor, Y., Liu, P., Tsai, T., Chen, C., Mei, Y. and Sze, S. 2002. Recovering dielectric loss of low dielectric constant organic siloxane during the photoresist removal process. *Journal of the Electrochemical Society,* 149(8), pp.F81-F84.

52. Yonekura, K., Sakamori, S., Goto, K., Matsuura, M., Fujiwara, N. and Yoneda, M. 2004. Investigation of ash damage to ultralow-$k$ inorganic materials. *Journal of Vacuum Science & Technology B: Microelectronics and Nanometer Structures,* 22(2), pp.548-553.

53. Xu, S., Qin, C., Diao, L., Gilbert, D., Hou, L., Wiesnoski, A., Busch, E., McGowan, R., White, B. and Weber, F. 2007. Study of plasma-induced damage of porous ultralow-< equation> k</equation> dielectric films during photoresist stripping. *Journal of Vacuum Science & Technology B: Microelectronics and Nanometer Structures,* 25(1), pp.156-163.

54. Liu, P., Chang, T., Sze, S., Pan, F., Mei, Y., Wu, W., Tsai, M., Dai, B., Chang, C. and Shih, F. 1998. The effects of plasma treatment for low dielectric constant hydrogen silsesquioxane (HSQ). *Thin Solid Films,* 332(1), pp.345-350.

55. Chang, T., Liu, P., Mei, Y., Mor, Y., Perng, T., Yang, Y. and Sze, S.M. 1999. Effects of H2 plasma treatment on low dielectric constant methylsilsesquioxane. *Journal of Vacuum Science & Technology B: Microelectronics and Nanometer Structures,* 17(5), pp.2325-2330.

56. Rossnagel, S. 2003. Thin film deposition with physical vapor deposition and related technologies. *Journal of Vacuum Science & Technology A,* 21(5), pp.S74-S87.

57. Seshan, K. 2012. *Handbook of thin film deposition.* William Andrew.

58. Aguilar, R.G. and Ortíz-López, J. 2011. Low cost instrumentation for spin-coating deposition of thin films in an undergraduate aboratory. *Latin-American Journal of Physics Education,* 5(2), pp.8.

59. Manos, D.M. and Flamm, D.L. 1989. Plasma Etching: an Introduction.(Retroactive Coverage). *Academic Press, Inc.(United States), 1989,* pp.476.

60. Tompkins, H.G. 1992. *A user's guide to ellipsometry.* Academic Press.

61. Günzler, H. and Gremlich, H. 2002. *IR spectroscopy: an introduction.* Wiley-vch.

62. Woodruff, D. and Delchar, T. 1986. Modern techniques of surface science.

63. Watts, J.F. and Wolstenholme, J. 2003. An introduction to surface analysis by XPS and AES. *An Introduction to Surface Analysis by XPS and AES, by John F.Watts, John Wolstenholme, Pp.224.ISBN 0-470-84713-1.Wiley-VCH, may 2003.,* 1

64. Vickerman, J.C. and Gilmore, I.S. 2009. *Surface analysis: the principal techniques.* Wiley Online Library.

65. Reimer, L. and Kohl, H. 2008. *Transmission electron microscopy: physics of image formation.* Springer Verlag.

66. Eaton, P.J. and West, P. 2010. *Atomic force microscopy.* Oxford University Press Oxford.

67. Magonov, S.N. and Whangbo, M. 2008. *Surface analysis with STM and AFM: experimental and theoretical aspects of image analysis.* John Wiley & Sons.

68. Ciofi, I., Baklanov, M.R., Tokei, Z. and Beyer, G.P. 2010. Capacitance measurements and k-value extractions of low-k films. *Microelectronic Engineering,* 87(11), pp.2391-2406.

69. Szejtli, J. 1998. Introduction and general overview of cyclodextrin chemistry. *Chemical Reviews,* 98(5), pp.1743-1754.

70. Chen, Y., Jeng, U. and Leu, J. 2011. Effect of Curing on the Porogen Size in the Low-k MSQ/SBS Hybrid Films. *Journal of the Electrochemical Society,* 158(3), pp.G52-G57.

71. Oh, W. and Ree, M. 2004. Anisotropic thermal expansion behavior of thin films of polymethylsilsesquioxane, a spin-on-glass dielectric for high-performance integrated circuits. *Langmuir,* 20(16), pp.6932-6939.

72. Silverstein, M.S., Shach-Caplan, M., Khristosov, M. and Harel, T. 2007. Effects of plasma exposure on SiCOH and methyl silsesquioxane films. *Plasma Processes and Polymers,* 4(9), pp.789-796.

73. Park, E.S., Ro, H.W., Nguyen, C.V., Jaffe, R.L. and Yoon, D.Y. 2008. Infrared Spectroscopy Study of Microstructures of poly(silsesquioxane)s. *Chem.Mater.,* 20pp.1548-1548 - 1554.

74. Liu, W., Yang, C., Chen, W., Dai, B. and Tsai, M. 2002. The structural transformation and properties of spin-on poly(silsesquioxane) films by thermal curing. *Journal of Non-Crystalline Solids,* 311(3), pp.233-240.

75. Yang, H., Cheng, Y. and Xiao, F. 2011. Thermal stable superhydrophobic polyphenylsilsesquioxane/nanosilica composite coatings. *Applied Surface Science,* 258(4), pp.1572-1580.

76. Prado, L.A.S.D.A., Radovanovic, E., Pastore, H.O., Yoshida, I.V.P. and Torriani, I.L. 2000. Poly(phenylsilsesquioxane)s: Structural and morphological characterization. *Journal of Polymer Science Part A: Polymer Chemistry,* 38(9), pp.1580-1589.

77. Maier, G. 2001. Low dielectric constant polymers for microelectronics. *Progress in Polymer Science,* 26(1), pp.3-65.

78. Kitsara, M., Nwankire, C.E., Walsh, L., Hughes, G., Somers, M., Kurzbuch, D., Zhang, X., Donohoe, G.G., O'Kennedy, R. and Ducrée, J. 2014. Spin coating of hydrophilic polymeric films for enhanced centrifugal flow control by serial siphoning. *Microfluidics and Nanofluidics,* 16(4), pp.691-699.

79. Wang, J., He, C., Lin, Y. and Chung, T.S. 2002. Studies on the thermal stability of F- and non-F-containing ladder polyepoxysilsesquioxanes by TGA–FTIR. *Thermochimica Acta,* 381(1), pp.83-92.

80. Soffer, H. and Vries, T.D. 1951. Dipole Moments of Aromatic Derivatives of Trimethylsilane. *Journal of the American Chemical Society,* 73(12), pp.5817-5819.

81. Chatt, J. and Williams, A. 1954. The nature of the co-ordinate link. Part IX. The dissociation constants of the acids p-R3M· C6H4· CO2H (M= C, Si, Ge, and Sn and R= Me and Et) and the relative strengths of dπ–pπ-bonding in the M–Car bond. *Journal of the Chemical Society (Resumed),* pp.4403-4411.

82. Xu, J., Moxom, J., Yang, S., Suzuki, R. and Ohdaira, T. 2002. Porosity in porous methyl-silsesquioxane (MSQ) films. *Applied Surface Science,* 194(1), pp.189-194.

83. Su, H. and Chen, W. 2009. Preparation of nanoporous poly (methyl silsesquioxane) films using core-shell silsesquioxane as porogen. *Materials Chemistry and Physics,* 114(2), pp.736-741.

84. Calvert, J.M. and Gallagher, M.K. 2003. A new approach to ultralow-k dielectrics. *Semiconductor International,* 26(12), pp.56-60.

85. Fayolle, M., Jousseaume, V., Assous, M., Tabouret, E., Le Cornec, C., Haumesser, P., Leduc, P., Feldis, H., Louveau, O. and Passemard, G. 2004. Cu/ULK integration using a post integration porogen removal approach. *IN: Interconnect Technology Conference, 2004. Proceedings of the IEEE 2004 International.* IEEE.

86. Che, M., Huang, C., Choang, S., Chen, Y. and Leu, J. 2010. Thermal and mechanical properties of hybrid methylsilsesquioxane/poly (styrene-b-4-vinylpyridine)

low-k dielectrics using a late porogen removal scheme. *Journal of Materials Research,* 25(06), pp.1049-1056.

87. Wilson, L.D., Mohamed, M.H. and Headley, J.V. 2011. Surface area and pore structure properties of urethane-based copolymers containing β-cyclodextrin. *Journal of Colloid and Interface Science,* 357(1), pp.215-222.

88. Li, S., Li, Z. and Yan, Y. 2003. Ultra-Low-k Pure-Silica Zeolite MFI Films Using Cyclodextrin as Porogen. *Advanced Materials,* 15(18), pp.1528-1531.

89. Ree, M., Yoon, J. and Heo, K. 2006. Imprinting well-controlled closed-nanopores in spin-on polymeric dielectric thin films. *Journal of Materials Chemistry,* 16(7), pp.685-697.

90. Villiers, A. 1891. Sur la fermentation de la fécule par l'action du ferment butyrique. *Compt.Rend.Acad.Sci,* 112pp.536-538.

91. Park, S., Shin, J., Min, S. and Rhee, H. 2006. Formation of nanoporous organosilicate films using cyclodextrins as a porogen. *Current Applied Physics,* 6(4), pp.743-746.

92. Croft, A.P. and Bartsch, R.A. 1983. Synthesis of chemically modified cyclodextrins. *Tetrahedron,* 39(9), pp.1417-1474.

93. Yim, J., Lyu, Y., Jeong, H., Song, S.A., Hwang, I., Hyeon-Lee, J., Mah, S.K., Chang, S., Park, J. and Hu, Y.F. 2003. The Preparation and Characterization of Small Mesopores in Siloxane-Based Materials That Use Cyclodextrins as Templates. *Advanced Functional Materials,* 13(5), pp.382-386.

94. Yim, J., Seon, J., Jeong, H., Pu, L.S., Baklanov, M.R. and Gidley, D.W. 2004. Morphological control of nanoporous films by the use of functionalized cyclodextrins as porogens. *Advanced Functional Materials,* 14(3), pp.277-282.

95. Nakamura, K., Nishimura, Y., Zetterlund, P., Hatakeyama, T. and Hatakeyama, H. 1996. TG-FTIR studies on biodegradable polyurethanes containing mono-and disaccharide components. *Thermochimica Acta,* 282pp.433-441.

96. King, S.W., French, M., Bielefeld, J. and Lanford, W.A. 2011. Fourier transform infrared spectroscopy investigation of chemical bonding in low-k a-SiC:H thin films. *Journal of Non-Crystalline Solids,* 357(15), pp.2970-2983.

97. Cherunilam, J., Rajani, K., McCoy, A., Heise, A. and Daniels, S. 2014. Investigation of O2 and SF6 plasma interactions on thermally stable damage resistant poly phenyl-methyl silsesquioxane low-k films. *Journal of Physics D: Applied Physics,* 47(10), pp.105204.

98. Chang, J. and Coburn, J. 2003. Plasma–surface interactions. *Journal of Vacuum Science & Technology A: Vacuum, Surfaces, and Films,* 21(5), pp.S145-S151.

99. Yim, J., Baklanov, M.R., Gidley, D.W., Peng, H., Jeong, H. and Sun Pu, L. 2004. Pore structure of modified cyclic silsesquioxane thin films made porous using a cyclodextrins-based porogen. *The Journal of Physical Chemistry B,* 108(26), pp.8953-8959.

100. Peng, K., Zhang, M., Lu, A., Wong, N., Zhang, R. and Lee, S. 2007. Ordered silicon nanowire arrays via nanosphere lithography and metal-induced etching. *Applied Physics Letters,* 90(16), pp.163123-163123-3.

101. Zhang, Y., Li, W. and Chen, K. 2008. Application of two-dimensional polystyrene arrays in the fabrication of ordered silicon pillars. *Journal of Alloys and Compounds,* 450(1), pp.512-516.

102. Li, W., Xu, L., Zhao, W., Sun, P., Huang, X. and Chen, K. 2007. Fabrication of large-scale periodic silicon nanopillar arrays for 2D nanomold using modified nanosphere lithography. *Applied Surface Science,* 253(22), pp.9035-9038.

103. Rybczynski, J., Ebels, U. and Giersig, M. 2003. Large-scale, 2D arrays of magnetic nanoparticles. *Colloids and Surfaces A: Physicochemical and Engineering Aspects,* 219(1), pp.1-6.

104. Hulteen, J.C. and Van Duyne, R.P. 1995. Nanosphere lithography: A materials general fabrication process for periodic particle array surfaces. *Journal of Vacuum Science & Technology A: Vacuum, Surfaces, and Films,* 13(3), pp.1553-1558.

105. Cheung, C.L., Nikolić, R., Reinhardt, C. and Wang, T. 2006. Fabrication of nanopillars by nanosphere lithography. *Nanotechnology,* 17(5), pp.1339.

# APPENDIX

**THICKNESS MEASUREMENT DATA FOR PLOTS – FIXED CONCENTRATION AND VARIABLE SPIN SPEED – SPIN PARAMETERS**

| SPIN PARAMETERS | |
|---|---|
| Spin Speed | Varied in steps of 1000 rpm from 2500 to 5500 |
| Acceleration | 180 rotations per second |
| Spin time | 45 seconds |

These spin parameters are used all throughout the work unless explicitly mentioned.

**THICKNESS MEASUREMENT DATA FOR PLOTS – FIXED CONCENTRATION AND VARIABLE SPIN SPEED**

**Measurement process:**

Three measurements are taken from a sample. Samples are approximately 1.5 cm x 1.5 cm in size. The mean of the measurements is taken and standard deviation calculated to show the error bars. The light shown from the instrument to the sample can be seen as a tiny spot as depicted in the diagram, from which we can see that the thickness variation across sample surface is very low.
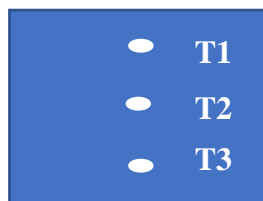
### 3.1. PMSQ – THF Solution

Solution concentration : 0.5 gm of PMSQ in 5 gm of THF

| Spin Speed | Thickness Measurement (nm) | | | Mean | Standard Deviation |
|---|---|---|---|---|---|
| | T1 | T2 | T3 | | |
| 2500 | 327.94 | 324.78 | 346.23 | 332.9833 | 11.58024 |
| 3500 | 375.2 | 362.28 | 342.11 | 359.8633 | 16.67685 |
| 4500 | 341.489 | 362.52 | 352.88 | 352.2963 | 10.52764 |
| 5500 | 357.97 | 362.66 | 351.49 | 357.3733 | 5.60885 |

### 3.2. PMSQ – MIBK Solution

Solution concentration : 0.5 gm of PMSQ in 5 gm of MIBK

| Spin Speed | Thickness Measurement (nm) | | | Mean | Standard Deviation |
|---|---|---|---|---|---|
| | T1 | T2 | T3 | | |
| 2500 | 132.04 | 130.73 | 131.83 | 131.5333 | 0.70359 |
| 3500 | 131.45 | 131.25 | 129.31 | 130.67 | 1.18203 |
| 4500 | 133.07 | 135.96 | 133.91 | 134.3133 | 1.48662 |
| 5500 | 131.1 | 129.84 | 131.62 | 130.8533 | 0.91528 |

### 3.3. PMSQ – Butanone Solution

Solution concentration : 0.5 gm of PMSQ in 5 gm of Butanone

| Spin Speed | Thickness Measurement (nm) | | | Mean | Standard Deviation |
|---|---|---|---|---|---|
| | T1 | T2 | T3 | | |
| 2500 | 262.1 | 232.05 | 238 | 244.05 | 15.91234 |
| 3500 | 229.62 | 236.49 | 230.37 | 232.16 | 3.76859 |
| 4500 | 241.98 | 227.75 | 227.82 | 232.5167 | 8.19556 |
| 5500 | 229.15 | 240.44 | 236.89 | 235.4933 | 5.77313 |

### 3.4. PMSQ – TCE Solution

Solution concentration : 0.5 gm of PMSQ in 5 gm of TCE

| Spin Speed | Thickness Measurement (nm) | | | Mean | Standard Deviation |
|---|---|---|---|---|---|
| | T1 | T2 | T3 | | |
| 2500 | 346.32 | 364.61 | 352.35 | 354.4267 | 9.32016 |
| 3500 | 351.5 | 350.98 | 351.4 | 351.2933 | 0.27592 |
| 4500 | 351.68 | 342.1 | 354.35 | 349.3767 | 6.44163 |
| 5500 | 350.4 | 352.19 | 347.68 | 350.09 | 2.27092 |

# THICKNESS MEASUREMENT DATA FOR PLOTS – FIXED SPIN SPEED AND VARIABLE CONCENTRATION

| SPIN PARAMETERS | |
|---|---|
| Spin Speed | 3500 rpm |
| Acceleration | 180 rotations per second |
| Spin time | 45 seconds |

### 3.5. PMSQ – MIBK Solution

Concentration varied from 0.125 gm to 1.0 gm in steps of 0.125 gm in 5 gm of MIBK.

| Amount of PMSQ (gm) in 5 gm of MIBK | Thickness Measurement (nm) | | | Mean | Standard Deviation |
|---|---|---|---|---|---|
| | T1 | T2 | T3 | | |
| 0.125 | 67.9 | 67.69 | 66.65 | 67.41333 | 0.66935 |
| 0.25 | 171.35 | 170.36 | 170.64 | 170.7833 | 0.51033 |
| 0.375 | 311.25 | 303.02 | 304.67 | 306.3133 | 4.35415 |
| 0.5 | 555.24 | 559.36 | 535.42 | 550.0067 | 12.79929 |
| 0.625 | 638.99 | 656.17 | 643.22 | 646.1267 | 8.95124 |
| 0.875 | 708.92 | 710.67 | 709.31 | 709.6333 | 0.91871 |
| 1 | 804.77 | 812.12 | 808.46 | 808.45 | 3.67501 |

### 3.6. PMSQ – THF Solution

Concentration varied from 0.125 gm to 1.0 gm in steps of 0.125 gm in 10 gm of THF.

| Amount of PMSQ (gm) in 10 gm of MIBK | Thickness Measurement (nm) | | | Mean | Standard Deviation |
|---|---|---|---|---|---|
| | T1 | T2 | T3 | | |
| 0.125 | 124.87 | 121.88 | 137.33 | 128.0267 | 8.19445 |
| 0.25 | 257.84 | 250.86 | 253.28 | 255.56 | 3.22441 |
| 0.375 | 348.71 | 334.1 | 361.09 | 347.9667 | 13.51035 |
| 0.5 | 448.71 | 445.9 | 430.44 | 441.6833 | 9.83786 |
| 0.625 | 552.26 | 551.33 | 556.07 | 553.22 | 2.51159 |
| 0.75 | 666.61 | 665.53 | 665.26 | 665.8 | 0.71435 |
| 0.875 | 821.74 | 835.28 | 826.66 | 827.8933 | 6.85374 |

### 3.7. Thickness measurements of samples done by spectroscopic ellipsometry using Standard SiO₂ model and Cauchy model developed for PMSQ and stylus profilometry

| Sample no: | Thickness Measurement (nm) (averaged values) | | |
|---|---|---|---|
| | SiO2 Model | Cauchy Model | Stylus Profilometry |
| 1 | 387.795 | 342.645 | 320.1 |
| 2 | 614.95 | 545.88 | 554.9 |
| 3 | 623.075 | 553.58 | 554.9 |
| 4 | 881.93 | 781.705 | 754.25 |

**Sample preparation for stylus profilometry measurements**

(a)      (b)      (c)      (d)

Si      Si / Scotch Tape      PMSQ      PMSQ / Si
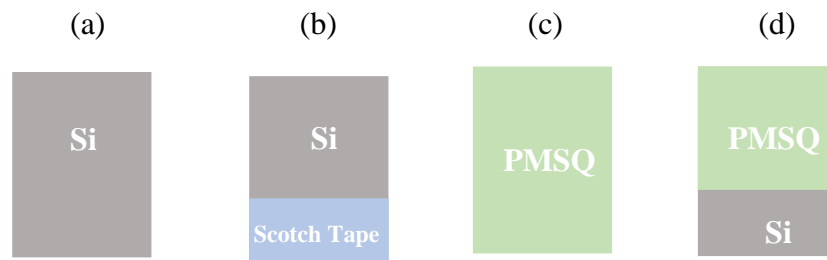
Silicon substrate was cleaned by Piranha etch method, fig (a) (Process described in page 23). A small section of the substrate was then covered with scotch tape as shown in fig (b). The prepared substrate was then spin coated with PMSQ solution, fig (c) (Process described in page 25). The scotch tape was removed to remove the deposited PMSQ material, which in turn creates a step profile as seen in fig (d) on which stylus profilometry was performed. The step height would be the thickness of the film deposited on the surface of the substrate.

### 3.12. Thickness measurements of MSQ films during O₂ plasma exposure

| Exposure Time (min) | Thickness Measurement (nm) | | | Mean | Standard Deviation |
|---|---|---|---|---|---|
| | T1 | T2 | T3 | | |
| 0 | 613.13 | 614.88 | 615.45 | 614.4867 | 1.20898 |
| 5 | 615.81 | 617.7 | 618.8 | 617.4367 | 1.51229 |
| 10 | 616.43 | 616.09 | 620.82 | 617.78 | 2.6382 |
| 15 | 615.17 | 620.11 | 619.37 | 618.2167 | 2.66431 |

### 3.15. O₂ Plasma exposure of MSQ films - Capacitance measurements and k- value calculations

Thicknesses are measured and averaged as explained before for each sample. The averaged value is used for calculating 'k' vales.

| Exposure Time | Capacitance Measured | Dielectric Thickness | Area of contact | E0 | Calculated 'k' value |
|---|---|---|---|---|---|
| Control Sample - As deposited | 188 | 448.27 | 0.00038 | 8.85E-12 | 2.50633567 |
| | 194 | 448.27 | 0.00038 | 8.85E-12 | 2.58632511 |
| | 192 | 448.27 | 0.00038 | 8.85E-12 | 2.55966196 |
| | 199 | 448.27 | 0.00038 | 8.85E-12 | 2.65298297 |
| | 201 | 448.27 | 0.00038 | 8.85E-12 | 2.67964612 |
| | 197 | 448.27 | 0.00038 | 8.85E-12 | 2.62631983 |
| 5 min O2 plasma exposure | 237 | 460.12 | 0.00038 | 8.85E-12 | 3.24310618 |
| | 239 | 460.12 | 0.00038 | 8.85E-12 | 3.27047417 |
| | 240 | 460.12 | 0.00038 | 8.85E-12 | 3.28415816 |
| | 227 | 460.12 | 0.00038 | 8.85E-12 | 3.10626626 |
| | 235 | 460.12 | 0.00038 | 8.85E-12 | 3.2157382 |
| | 237 | 460.12 | 0.00038 | 8.85E-12 | 3.24310618 |
| 10 min O2 plasma exposure | 265 | 450.65 | 0.00038 | 8.85E-12 | 3.55162382 |
| | 263 | 450.65 | 0.00038 | 8.85E-12 | 3.52481911 |
| | 269 | 450.65 | 0.00038 | 8.85E-12 | 3.60523324 |
| | 253 | 450.65 | 0.00038 | 8.85E-12 | 3.39079557 |
| | 259 | 450.65 | 0.00038 | 8.85E-12 | 3.4712097 |
| | 255 | 450.65 | 0.00038 | 8.85E-12 | 3.41760028 |

**Mean and standard deviation of 'k' values calculated for the plot**

| Exposure Time (min) | Calculated 'k' value | | | | | | Mean | Standard Deviation |
|---|---|---|---|---|---|---|---|---|
| | **k1** | **k2** | **k3** | **k4** | **k5** | **k6** | | |
| 0 | 2.50634 | 2.58633 | 2.55966 | 2.65298 | 2.67965 | 2.62632 | 2.60188 | 0.06389 |
| 5 | 3.24311 | 3.27047 | 3.28416 | 3.10627 | 3.21574 | 3.24311 | 3.22714 | 0.06384 |
| 10 | 3.55162 | 3.52482 | 3.60523 | 3.3908 | 3.47121 | 3.4176 | 3.49355 | 0.08204 |

## 3.16. Thickness measurements of MSQ films during $SF_6$ plasma etching

| Exposure Time (min) | Thickness Measurement (nm) | | | Mean | Standard Deviation |
|---|---|---|---|---|---|
| | **T1** | **T2** | **T3** | | |
| As deposited | 615.3 | 618.92 | 614.43 | 616.2167 | 2.38123 |
| 1 | 489.08 | 484.27 | 494.87 | 489.4067 | 5.30754 |
| 2 | 322.79 | 332.97 | 336.97 | 330.91 | 7.31101 |
| 3 | 173.9 | 165.04 | 171.11 | 170.0167 | 4.53006 |

## 3.19. SF₆ Plasma etch of MSQ films - Capacitance measurements and k- value calculations

Thicknesses are measured and averaged as explained before for each sample. The averaged value is used for calculating 'k' values.

| Exposure Time | Capacitance Measured | Dielectric Thickness | Area of contact | E0 | Calculated 'k' value |
|---|---|---|---|---|---|
| Control Sample - As deposited | 212 | 423.56 | 0.00037994 | 8.85E-12 | 2.670499564 |
| | 204 | 423.56 | 0.00037994 | 8.85E-12 | 2.569725996 |
| | 213 | 423.56 | 0.00037994 | 8.85E-12 | 2.683096261 |
| | 217 | 423.56 | 0.00037994 | 8.85E-12 | 2.733483045 |
| | 213 | 423.56 | 0.00037994 | 8.85E-12 | 2.683096261 |
| | 228 | 423.56 | 0.00037994 | 8.85E-12 | 2.872046701 |
| 1 min SF6 plasma etch | 246 | 426.31 | 0.00037994 | 8.85E-12 | 3.118906375 |
| | 249 | 426.31 | 0.00037994 | 8.85E-12 | 3.156941819 |
| | 251 | 426.31 | 0.00037994 | 8.85E-12 | 3.182298781 |
| | 244 | 426.31 | 0.00037994 | 8.85E-12 | 3.093549413 |
| | 247 | 426.31 | 0.00037994 | 8.85E-12 | 3.131584856 |
| | 248 | 426.31 | 0.00037994 | 8.85E-12 | 3.144263337 |
| 2 min SF6 plasma etch | 400 | 271.08 | 0.00037994 | 8.85E-12 | 3.224773225 |
| | 387 | 271.08 | 0.00037994 | 8.85E-12 | 3.119968095 |
| | 380 | 271.08 | 0.00037994 | 8.85E-12 | 3.063534563 |
| | 391 | 271.08 | 0.00037994 | 8.85E-12 | 3.152215827 |
| | 388 | 271.08 | 0.00037994 | 8.85E-12 | 3.128030028 |
| | 392 | 271.08 | 0.00037994 | 8.85E-12 | 3.16027776 |

**Mean and standard deviation of 'k' values calculated for the plot**

| Exposure Time (min) | Calculated 'k' value | | | | | | Mean | Standard Deviation |
|---|---|---|---|---|---|---|---|---|
| | k1 | k2 | k3 | k4 | k5 | k6 | | |
| 0 | 2.6705 | 2.56973 | 2.6831 | 2.73348 | 2.6831 | 2.87205 | 2.6516 | 0.05491 |
| 1 | 3.11891 | 3.15694 | 3.1823 | 3.09355 | 3.13158 | 3.14426 | 3.13792 | 0.0308 |
| 2 | 3.22477 | 3.11997 | 3.06353 | 3.15222 | 3.12803 | 3.16339 | 3.14199 | 0.05339 |

**3.24. Thickness measurements of PMSQ films during O₂ plasma exposure**

| Exposure Time (min) | Thickness Measurement (nm) | | | Mean | Standard Deviation |
|---|---|---|---|---|---|
| | T1 | T2 | T3 | | |
| As deposited | 625.5 | 623.9 | 622.18 | 623.86 | 1.66036 |
| 1 | 623.61 | 620.68 | 622.39 | 622.2267 | 1.47181 |
| 2 | 621.62 | 622.73 | 625.12 | 623.1567 | 1.78858 |
| 4 | 622.38 | 621.93 | 622.69 | 622.3333 | 0.38214 |
| 6 | 619.78 | 622.56 | 624.32 | 622.22 | 2.28902 |
| 10 | 624.96 | 618.22 | 620.21 | 621.13 | 3.4629 |

**3.26. O₂ Plasma exposure of PMSQ films -  Thickness & Capacitance measurements and k- value calculations**

Thicknesses are measured and averaged as explained before for each sample.

| Exposure time (min) | Thickness Measurements | | | |
|---|---|---|---|---|
| | 1 | 2 | 3 | Mean |
| ASD | 606.03 | 594.85 | 604.03 | 601.6367 |
| 1 | 576.29 | 579.1 | 577.58 | 577.6567 |
| 5 | 587.7 | 581.63 | 581.24 | 583.5233 |
| 10 | 578.93 | 578.34 | 578.84 | 578.7033 |

**The averaged value is used for calculating 'k' values.**

| Exposure Time | Capacitance Measured | Dielectric Thickness | Area of contact | E0 | Calculated 'k' value |
|---|---|---|---|---|---|
| As deposited | 150.35 | 601.64 | 0.00037994 | 8.85E-12 | 2.690183136 |
|  | 150.24 | 601.64 | 0.00037994 | 8.85E-12 | 2.688214928 |
|  | 146.87 | 601.64 | 0.00037994 | 8.85E-12 | 2.627916177 |
| 1 min O2 exposure | 155.21 | 577.66 | 0.00037994 | 8.85E-12 | 2.666451604 |
|  | 156.07 | 577.66 | 0.00037994 | 8.85E-12 | 2.681226093 |
|  | 155.15 | 577.66 | 0.00037994 | 8.85E-12 | 2.665420826 |
| 5 mins O2 exposure | 150.64 | 583.52 | 0.00037994 | 8.85E-12 | 2.614193701 |
|  | 153.54 | 583.52 | 0.00037994 | 8.85E-12 | 2.664520054 |
|  | 154.3 | 583.52 | 0.00037994 | 8.85E-12 | 2.677709029 |
| 10 mins O2 exposure | 155.38 | 578.37 | 0.00037994 | 8.85E-12 | 2.672653059 |
|  | 155.84 | 578.37 | 0.00037994 | 8.85E-12 | 2.680565406 |
|  | 152.6 | 578.37 | 0.00037994 | 8.85E-12 | 2.624834965 |

**Mean and standard deviation calculated for plots.**

| Exposure Time (min) | Calculated 'k' value | | | Mean | Standard Deviation |
|---|---|---|---|---|---|
|  | k1 | k2 | k3 |  |  |
| 0 | 2.69018 | 2.68821 | 2.62792 | 2.66877 | 0.03539 |
| 1 | 2.66645 | 2.68123 | 2.66542 | 2.67103 | 0.00885 |
| 5 | 2.61419 | 2.66452 | 2.67771 | 2.65214 | 0.03352 |
| 10 | 2.67265 | 2.68057 | 2.62483 | 2.65935 | 0.03016 |

**3.27. Thickness variation of PMSQ films in SF₆ plasma etch**

| Exposure time (min) | Thickness Measurements | | | | Standard Deviation |
|---|---|---|---|---|---|
| | T1 | T2 | T3 | Mean | |
| 0 | 595.12 | 590.19 | 593 | 592.77 | 2.47303 |
| 1 | 531.04 | 529.04 | 528.05 | 529.37667 | 1.52317 |
| 2 | 473.22 | 472.37 | 471.65 | 472.41333 | 0.7859 |
| 3 | 411.95 | 404.55 | 409.27 | 408.59 | 3.74657 |
| 5 | 268.83 | 263.63 | 269.94 | 267.46667 | 3.36868 |

**3.29. SF₆ Plasma etch of PMSQ films - Thickness & Capacitance measurements and k- value calculations**

**Thickness Measurements**

| Exposure time (min) | Thickness Measurements | | | |
|---|---|---|---|---|
| | 1 | 2 | 3 | Mean |
| ASD | 542.95 | 544.15 | 542.29 | 543.13 |
| 1 | 515.96 | 512.8 | 513.93 | 514.23 |
| 5 | 485.77 | 496.87 | 490.43 | 491.0233 |
| 10 | 462.74 | 463.46 | 463.03 | 463.0767 |

**Capacitance measurements and 'k' value computations**

| Exposure Time | Capacitance Measured | Dielectric Thickness | Area of contact | E0 | Calculated 'k' value |
|---|---|---|---|---|---|
| **ASD** | 162.389 | 604.35 | 0.00037994 | 8.85E-12 | 2.918682437 |
| | 158.25 | 604.35 | 0.00037994 | 8.85E-12 | 2.844290535 |
| | 160.33 | 604.35 | 0.00037994 | 8.85E-12 | 2.881675207 |
| | 162.53 | 604.35 | 0.00037994 | 8.85E-12 | 2.921216686 |
| | 166.47 | 604.35 | 0.00037994 | 8.85E-12 | 2.992031882 |
| **1 min** | 179.85 | 543.15 | 0.00037994 | 8.85E-12 | 2.905172583 |
| | 176.85 | 543.15 | 0.00037994 | 8.85E-12 | 2.856712657 |
| | 184.9 | 543.15 | 0.00037994 | 8.85E-12 | 2.986746792 |
| | 179.32 | 543.15 | 0.00037994 | 8.85E-12 | 2.896611329 |
| | 166.47 | 543.15 | 0.00037994 | 8.85E-12 | 2.689041312 |
| **1 min 20 secs** | 188.2 | 514.237 | 0.00037994 | 8.85E-12 | 2.878224406 |
| | 192.3 | 514.237 | 0.00037994 | 8.85E-12 | 2.940927488 |
| | 175.12 | 514.237 | 0.00037994 | 8.85E-12 | 2.67818628 |
| | 190.52 | 514.237 | 0.00037994 | 8.85E-12 | 2.913705174 |
| | 189.4 | 514.237 | 0.00037994 | 8.85E-12 | 2.896576528 |
| **1 min 40 secs** | 177.3 | 491.023 | 0.00037994 | 8.85E-12 | 2.58912061 |
| | 205 | 491.023 | 0.00037994 | 8.85E-12 | 2.993625071 |
| | 183.1 | 491.023 | 0.00037994 | 8.85E-12 | 2.673818295 |
| | 190.8 | 491.023 | 0.00037994 | 8.85E-12 | 2.786261774 |
| | 190.2 | 491.023 | 0.00037994 | 8.85E-12 | 2.777499944 |
| **2 mins** | 196.4 | 463.07 | 0.00037994 | 8.85E-12 | 2.704766884 |
| | 189.8 | 463.07 | 0.00037994 | 8.85E-12 | 2.613873496 |
| | 190.94 | 463.07 | 0.00037994 | 8.85E-12 | 2.629573263 |
| | 190.2 | 463.07 | 0.00037994 | 8.85E-12 | 2.619382186 |
| | 190.4 | 463.07 | 0.00037994 | 8.85E-12 | 2.622136531 |

**Mean and standard deviation calculated for plots.**

| Exposure Time (min) | Calculated 'k' value | | | Mean | Standard Deviation |
|---|---|---|---|---|---|
| | k1 | k2 | k3 | | |
| 0 | 2.93523 | 2.93523 | 2.90225 | 2.92424 | 0.01904 |
| 1 | 2.85661 | 2.8965 | 2.90507 | 2.88606 | 0.02586 |
| 1.33 | 2.87822 | 2.67818 | 2.94093 | 2.83244 | 0.13722 |
| 1.66 | 2.7775 | 2.67381 | 3.00385 | 2.81839 | 0.16877 |
| 2 | 2.77166 | 2.7775 | 2.78042 | 2.77653 | 0.00446 |

## 4.14. Variation in density with porogen loading

| Porogen loading (%) | Density measurements | | | Mean | Standard Deviation |
|---|---|---|---|---|---|
| | D1 | D2 | D3 | | |
| 0 | 99.5 | 99 | 99.5 | 99.33333 | 0.28868 |
| 15 | 80.07142 | 84.28571 | 88.5 | 84.28571 | 4.21429 |
| 30 | 66.5 | 70 | 73.5 | 70 | 3.5 |
| 45 | 71.92858 | 75.71429 | 79.5 | 75.71429 | 3.78571 |

## 4.15. 'k' – variation as a function of porogen loading

**Thickness measurements on annealed films with varying levels of porogen loading**

| Porosity loading (%) | Thickness Measurements | | | |
|---|---|---|---|---|
| | T1 | T2 | T3 | Mean |
| 0 | 544.35 | 548.2 | 549.4 | 547.3166667 |
| 15 | 532.85 | 529.61 | 531.4 | 531.2866667 |
| 30 | 478.54 | 477.81 | 477.99 | 478.1133333 |
| 45 | 504.75 | 507.48 | 507.88 | 506.7033333 |

**'k' value calculations from the capacitance measurements**

| Porogen Loading | Capacitance Measured | Dielectric Thickness | Area of contact | E0 | Calculated 'k' value |
|---|---|---|---|---|---|
| No Porogen | 160 | 547.31 | 0.00037994 | 8.85E-12 | 2.604324382 |
| | 161 | 547.31 | 0.00037994 | 8.85E-12 | 2.620601409 |
| | 161 | 547.31 | 0.00037994 | 8.85E-12 | 2.620601409 |
| | 161 | 547.31 | 0.00037994 | 8.85E-12 | 2.620601409 |
| 15% | 157 | 531.29 | 0.00037994 | 8.85E-12 | 2.480692908 |
| | 155 | 531.29 | 0.00037994 | 8.85E-12 | 2.449091724 |
| | 155 | 531.29 | 0.00037994 | 8.85E-12 | 2.449091724 |
| | 153 | 531.29 | 0.00037994 | 8.85E-12 | 2.41749054 |
| 30% | 153 | 478.11 | 0.00037994 | 8.85E-12 | 2.175509425 |
| | 156 | 478.11 | 0.00037994 | 8.85E-12 | 2.218166472 |
| | 156 | 478.11 | 0.00037994 | 8.85E-12 | 2.218166472 |
| | 156 | 478.11 | 0.00037994 | 8.85E-12 | 2.218166472 |
| 45% | 139 | 506.68 | 0.00037994 | 8.85E-12 | 2.094547786 |
| | 142 | 506.68 | 0.00037994 | 8.85E-12 | 2.139753853 |
| | 141 | 506.68 | 0.00037994 | 8.85E-12 | 2.124685164 |
| | 146 | 506.68 | 0.00037994 | 8.85E-12 | 2.20002861 |

**Mean and Standard deviation of measured 'k' values for plot**

| Porogen loading (%) | Dielectric constant measurements | | | | Mean | Standard Deviation |
|---|---|---|---|---|---|---|
| | k1 | k2 | k3 | k4 | | |
| 0 | 2.62 | 2.62 | 2.62 | 2.62 | 2.62 | 0 |
| 15 | 2.48 | 2.44 | 2.44 | 2.41 | 2.436 | 0.02881 |
| 30 | 2.21 | 2.21 | 2.14 | 2.21 | 2.202 | 0.03701 |
| 45 | 2.29 | 2.13 | 2.12 | 2.2 | 2.185 | 0.07853 |

**4.16. Thickness measurements on porous PMSQ thin films as a function of exposure time to O2 plasma**

| Exposure time (min) | Thickness Measurements | | | | Standard Deviation |
|---|---|---|---|---|---|
| | 1 | 2 | 3 | Mean | |
| 0 | 513.35 | 493.53 | 487.87 | 498.25 | 13.3797 |
| 1 | 482.06 | 486.16 | 492.33 | 486.85 | 5.16965 |
| 2 | 493.58 | 482.65 | 497.88 | 491.37 | 7.85183 |
| 8 | 494.92 | 488.93 | 493.77 | 492.54 | 3.17879 |

**4.18. Variation of capacitance of porous PMSQ thin films as a function of time during O2 plasma exposure**

Thickness measurements of films pre-and post plasma exposure – Different films were used for each experiment. One the set of measurements used for the plots shown here in the tables.

| Exposure time (min) | Thickness Measurements | | | |
|---|---|---|---|---|
| | 1 | 2 | 3 | Mean |
| 0 | 489.72 | 479.9 | 496.3 | 488.64 |
| 5 | 530.34 | 532.38 | 530.63 | 531.1166667 |
| 10 | 494.55 | 490.17 | 493.01 | 492.5766667 |
| 15 | 507.71 | 508.54 | 516.54 | 510.93 |

**Capacitance and 'k' value measurements**

| Exposure time (mins) | Capacitance Measured | Dielectric Thickness | Area of contact | E0 | Calculated 'k' value |
|---|---|---|---|---|---|
| As Deposited | 172 | 488.64 | 0.00037994 | 8.85E-12 | 2.499534717 |
| | 170 | 488.64 | 0.00037994 | 8.85E-12 | 2.47047036 |
| | 170 | 488.64 | 0.00037994 | 8.85E-12 | 2.47047036 |
| | 169 | 488.64 | 0.00037994 | 8.85E-12 | 2.455938181 |
| | 171 | 488.64 | 0.00037994 | 8.85E-12 | 2.485002538 |
| | 168 | 488.64 | 0.00037994 | 8.85E-12 | 2.441406003 |
| | 170 | 488.64 | 0.00037994 | 8.85E-12 | 2.47047036 |
| 5 min | 186 | 531.12 | 0.00037994 | 8.85E-12 | 2.937969688 |
| | 233 | 531.12 | 0.00037994 | 8.85E-12 | 3.680359878 |
| | 215 | 531.12 | 0.00037994 | 8.85E-12 | 3.396040231 |
| | 192 | 531.12 | 0.00037994 | 8.85E-12 | 3.032742904 |
| | 203 | 531.12 | 0.00037994 | 8.85E-12 | 3.2064938 |
| | 186 | 531.12 | 0.00037994 | 8.85E-12 | 2.937969688 |
| | 199 | 531.12 | 0.00037994 | 8.85E-12 | 3.143311656 |
| 10 min | 271 | 492.57 | 0.00037994 | 8.85E-12 | 3.969894444 |
| | 280 | 492.57 | 0.00037994 | 8.85E-12 | 4.101735957 |
| | 295 | 492.57 | 0.00037994 | 8.85E-12 | 4.321471811 |
| | 295 | 492.57 | 0.00037994 | 8.85E-12 | 4.321471811 |
| | 266 | 492.57 | 0.00037994 | 8.85E-12 | 3.896649159 |
| | 255 | 492.57 | 0.00037994 | 8.85E-12 | 3.735509532 |
| | 279 | 492.57 | 0.00037994 | 8.85E-12 | 4.0870869 |
| 15 min | 269 | 510.93 | 0.00037994 | 8.85E-12 | 4.087477684 |
| | 288 | 510.93 | 0.00037994 | 8.85E-12 | 4.376184286 |
| | 332 | 510.93 | 0.00037994 | 8.85E-12 | 5.044767996 |
| | 273 | 510.93 | 0.00037994 | 8.85E-12 | 4.148258021 |
| | 333 | 510.93 | 0.00037994 | 8.85E-12 | 5.059963081 |
| | 299 | 510.93 | 0.00037994 | 8.85E-12 | 4.543330214 |
| | 338 | 510.93 | 0.00037994 | 8.85E-12 | 5.135938502 |

**Capacitance mean and standard deviation calculations for plot**

| Exposure time (min) | Capacitance Measurements | | | | | | | Mean | Standard Deviation |
|---|---|---|---|---|---|---|---|---|---|
| | C1 | C2 | C3 | C4 | C5 | C6 | C7 | | |
| 0 | 172 | 170 | 170 | 169 | 171 | 168 | 170 | 170 | 1.29099 |
| 5 | 186 | 233 | 215 | 192 | 203 | 186 | 199 | 202 | 17.08801 |
| 10 | 271 | 280 | 295 | 295 | 266 | 255 | 279 | 277.2857 | 14.72769 |
| 15 | 269 | 288 | 332 | 273 | 333 | 299 | 338 | 304.5714 | 29.56832 |

**6.2. Variation of dielectric constant of porous PMSQ thin films as a function of time during O2 plasma exposure**

| Exposure time (min) | Dielectric constant measurements | | | | | | | Mean | Standard Deviation |
|---|---|---|---|---|---|---|---|---|---|
| | k1 | k2 | k3 | k4 | k5 | k6 | k7 | | |
| 0 | 2.5 | 2.4705 | 2.4705 | 2.456 | 2.485 | 2.4414 | 2.4705 | 2.47047 | 0.01876 |
| 5 | 2.938 | 3.6804 | 3.396 | 3.033 | 3.206 | 2.938 | 3.1433 | 3.1907 | 0.26991 |
| 10 | 3.97 | 4.1017 | 4.3215 | 4.321 | 3.897 | 3.7355 | 4.0871 | 4.06197 | 0.21575 |
| 15 | 4.087 | 4.3762 | 5.0448 | 4.148 | 5.06 | 4.5433 | 5.1359 | 4.62799 | 0.44929 |

**6.3. Thickness variation of porous PMSQ thin films as a function of exposure time to SF6 plasma**

| Exposure time (min) | Thickness Measurements | | | | Standard Deviation |
|---|---|---|---|---|---|
| | 1 | 2 | 3 | Mean | |
| 0 | 464.99 | 463.03 | 479.05 | 469.02333 | 8.73847 |
| 1 | 404.82 | 407.62 | 409.67 | 407.37 | 2.43465 |
| 2 | 349.59 | 342.84 | 350.12 | 347.51667 | 4.05877 |
| 5 | 127.08 | 124.28 | 120.72 | 124.02667 | 3.18756 |

**6.22. Variation capacitance of porous PMSQ thin films as a function of time during SF6 plasma exposure**

**Thickness measurements**

| Exposure time (secs) | Thickness Measurements | | | |
|---|---|---|---|---|
| | 1 | 2 | 3 | Mean |
| 0 | 488 | 483.93 | 478.65 | 483.5266667 |
| 20 | 478.02 | 471.54 | 473.27 | 474.2766667 |
| 40 | 467.3 | 462.93 | 453.65 | 461.2933333 |
| 60 | 442.56 | 442.34 | 445.72 | 443.54 |

**Capacitance measurements and 'k' value calculation**

| Exposure time (secs) | Capacitance Measured | Dielectric Thickness | Area of contact | E0 | Calculated 'k' value |
|---|---|---|---|---|---|
| As Deposited | 150 | 483.7 | 0.00037994 | 8.85E-12 | 2.15778941 |
| | 166 | 483.7 | 0.00037994 | 8.85E-12 | 2.387953614 |
| | 160 | 483.7 | 0.00037994 | 8.85E-12 | 2.301642037 |
| | 166 | 483.7 | 0.00037994 | 8.85E-12 | 2.387953614 |
| | 167 | 483.7 | 0.00037994 | 8.85E-12 | 2.402338877 |
| | 165 | 483.7 | 0.00037994 | 8.85E-12 | 2.373568351 |
| | 168 | 483.7 | 0.00037994 | 8.85E-12 | 2.416724139 |
| | 179 | 483.7 | 0.00037994 | 8.85E-12 | 2.574962029 |
| 20 | 298 | 474.28 | 0.00037994 | 8.85E-12 | 4.203323213 |
| | 236 | 474.28 | 0.00037994 | 8.85E-12 | 3.328806303 |
| | 337 | 474.28 | 0.00037994 | 8.85E-12 | 4.753422559 |
| | 227 | 474.28 | 0.00037994 | 8.85E-12 | 3.2018603 |
| | 248 | 474.28 | 0.00037994 | 8.85E-12 | 3.49806764 |
| | 307 | 474.28 | 0.00037994 | 8.85E-12 | 4.330269216 |
| | 385 | 474.28 | 0.00037994 | 8.85E-12 | 5.430467909 |
| | 261 | 474.28 | 0.00037994 | 8.85E-12 | 3.681434089 |
| 40 | 358 | 461.3 | 0.00037994 | 8.85E-12 | 4.911432641 |
| | 348 | 461.3 | 0.00037994 | 8.85E-12 | 4.774241785 |
| | 367 | 461.3 | 0.00037994 | 8.85E-12 | 5.034904411 |
| | 352 | 461.3 | 0.00037994 | 8.85E-12 | 4.829118127 |
| | 355 | 461.3 | 0.00037994 | 8.85E-12 | 4.870275384 |
| | 372 | 461.3 | 0.00037994 | 8.85E-12 | 5.103499839 |
| | 356 | 461.3 | 0.00037994 | 8.85E-12 | 4.88399447 |
| | 347 | 461.3 | 0.00037994 | 8.85E-12 | 4.760522699 |
| 60 | 245 | 443.54 | 0.00037994 | 8.85E-12 | 3.231771059 |
| | 313 | 443.54 | 0.00037994 | 8.85E-12 | 4.128752414 |
| | 360 | 443.54 | 0.00037994 | 8.85E-12 | 4.748724821 |
| | 453 | 443.54 | 0.00037994 | 8.85E-12 | 5.975478733 |
| | 497 | 443.54 | 0.00037994 | 8.85E-12 | 6.555878433 |
| | 500 | 443.54 | 0.00037994 | 8.85E-12 | 6.59545114 |
| | 450 | 443.54 | 0.00037994 | 8.85E-12 | 5.935906026 |
| | 600 | 443.54 | 0.00037994 | 8.85E-12 | 7.914541368 |

**Capacitance - mean and standard deviation**

| Exposure time (min) | Capacitance Measurements | | | | | | | Mean | Standard Deviation |
|---|---|---|---|---|---|---|---|---|---|
| | C1 | C2 | C3 | C4 | C5 | C6 | C7 | | |
| 0 | 172 | 170 | 170 | 169 | 171 | 168 | 170 | 170 | 1.29099 |
| 20 | 186 | 233 | 215 | 192 | 203 | 186 | 199 | 202 | 17.08801 |
| 40 | 271 | 280 | 295 | 295 | 266 | 255 | 279 | 277.29 | 14.72769 |
| 60 | 269 | 288 | 332 | 273 | 333 | 299 | 338 | 304.57 | 29.56832 |

**6.4. Variation of dielectric constant of porous PMSQ thin films as a function of time during SF6 plasma exposure**

| Exposure time (min) | Dielectric constant measurements | | | | | | | | Mean | Standard Deviation |
|---|---|---|---|---|---|---|---|---|---|---|
| | k1 | k2 | k3 | k4 | k5 | k6 | k7 | k8 | | |
| 0 | 2.15779 | 2.38795 | 2.30164 | 2.38795 | 2.40234 | 2.37357 | 2.41672 | 2.57496 | 2.37537 | 0.11672 |
| 20 | 4.20332 | 3.32881 | 4.75342 | 3.20186 | 3.49807 | 4.33027 | 5.43047 | 3.68757 | 4.05422 | 0.77255 |
| 40 | 4.91143 | 4.77424 | 5.0349 | 4.82912 | 4.87028 | 5.1035 | 4.88399 | 4.76052 | 4.896 | 0.12015 |
| 60 | 3.23177 | 4.12875 | 4.74872 | 5.97548 | 6.55588 | 6.59545 | 5.93591 | 7.91454 | 5.63581 | 1.512 |

**5.13. Thickness measures of PMSQ during Ar plasma exposure**

| Exposure time (minutes) | Thickness Measurements | | | |
|---|---|---|---|---|
| | 1 | 2 | 3 | Mean |
| 0 | 492.32 | 493.17 | 495.22 | 493.57 |
| 5 | 487.56 | 492.16 | 490.11 | 489.9433 |
| 10 | 472.15 | 483.27 | 481.15 | 478.8567 |

**5.16. Thickness measures of PMSQ during Ar plasma exposure**

| SF6 flow rate (SCCM) | O2 flow rate (SCCM) | Thickness reduction after 1 minute | Etch rate (per second) |
|---|---|---|---|
| 50 | 0 | 60 | 1 |
| 40 | 10 | 117 | 1.95 |
| 30 | 20 | 159 | 2.65 |
| 25 | 25 | 204 | 3.4 |
| 20 | 30 | 253.8 | 4.23 |
| 10 | 40 | 279 | 4.65 |
| 5 | 45 | 261 | 4.35 |
| 0 | 50 | 0 | 0 |